Application of Infra-Red Spectroscopy to the Evaluation of Biofilm Formation and Pathogenesis of Nontypeable *Haemophilus influenzae*

by

Najla Abdullah Obaid

School of Medicine, Pharmacy

Submitted in fulfilment of the requirements for the PhD in Pharmacy

University of Tasmania September 2015

Declaration

This thesis contains no material which has been accepted for a degree or diploma by the University or any other institution, except by way of background information and duly acknowledged in the thesis, and to the best of the my knowledge and belief no material previously published or written by another person except where due acknowledgement is made in the text of the thesis, nor does the thesis contain any material that infringes copyright.

Najla Obaid

September 2015

Najla Obaid

September 2015

Publication

- Obaid, N. A., Jacobson, G. A., & Tristram, S. (2015). Relationship between clinical site of isolation and ability to form biofilms in vitro in Nontypeable Haemophilus influenzae. *Canadian Journal of Microbiology*, *61*(3), 243-245.

List of Abbreviations

2D	Two-dimensional
AOM	acute otitis media
AMX	amoxicillin
AZM	azithromycin
BHI	brain heart infusion
CaF_2	Calcium Fluoride
CAP	community acquired pneumonia
CF	cystic fibrosis
CIP	ciprofloxacin
CLSI	Clinical and Laboratory Standard Institute
CO_2	Carbon dioxide
COPD	chronic obstructive pulmonary disease
CTX	cefotaxime
EPS	Extracellular polymeric substances
FPA	Focal planer array
FTIR	Fourier Transform Infrared
h	Hours
HCA	Hierarchical Cluster analysis
Hh	*Haemophilus heamolyticus*
Hib	*Haemophilus influenzae* type b
IR	Infrared
MCT	Mercury-Cadmium-Telluride
MIC	minimum inhibitory concentration
NTHi	Nontypeable *Haemophilus influenzae*
OM	otitis media

PAO1	*Pseudomonas aeruginosa* O1
PC	principle component
PCA	Principal Component Analysis
PBS	phosphate-buffered saline
SEM	scanning electron microscope

Acknowledgment

Firstly, I would like to thank my supervisors; Dr. Glenn Jacobson (School of Medicine, Pharmacy, UTAS) for his continuous guidance, assistance and support in all aspects of this research,

Dr. Stephen Tristram (School of Human Life Sciences, UTAS) for providing the NTHi samples, his continuous support of my PhD, his patience and guidance during the research and writing of this thesis and

Dr. Thomas Rodemann (Central Science Laboratory (CSL), UTAS) for his assistance in designing the spectroscopy study, his insightful comments and for the hard question which motivated me to widen my research from various perspectives.

I am also grateful to Dr. Christian Narkowicz for his assistance in the study design and writing of this thesis.

My sincere thanks also goes to Professor Stuart McLean (School of Medicine, Pharmacy, UTAS) for his assistance in proofreading during the writing of this thesis and valuable advice in laboratory work. Dr. Peter Traill, Mrs. Heather Galloway and Mr. Anthony Whitty in their assistance in the Laboratory. Without their precious support it would not have been possible to conduct this research.

I thank my fellow PhD student, Jamuna Chhetri for the stimulating discussions and her help in preparing some of the figures for thesis preparation.

I also would like to thank Dr. Karsten Goemann (Central Science Laboratory (CSL), UTAS) for his assistance and advice in SEM sample preparation and acquisition.

I acknowledge the support of Umm Al-Qura University as a representative of the Ministry of Higher Education of Saudi Arabia who sponsored My scholarship.

I would like to thank my family, My mother as the role model in my life from her courage and perseverance through every hard matter in life. My Father who was the first person taught me how to appreciate learning and to pursue our noble goals. I would also like to thank my elder sister Awatef for always being there to support me and encourage me with her best wishes. My sisters Haifa, Lamyaa, Rania and Lama, my brothers Khaled, Abdulaziz, Sultan and Fawaz for supporting me emotionally throughout writing this thesis and my life in general. My kids, Mohammed, Mai and Mada to be in my life and being patient while I was busy to make them proud of me.

Last but not the least, My husband Hani, who was always beside me as the first person that stood to support me during my postgraduate studies and from the start of my research career and during chasing my dreams.

Table of contents

Abstract

Biofilm formation has been recognised as an aggregation of bacterial cells surrounded by extracellular polymeric substances (EPS) which are secreted from the cells. Biofilm has a significant role in chronicity of infection and cells are recalcitrant to antibacterial agents when biofilm is formed on abiotic or biotic surfaces. Nontypeable *Haemophilus influenzae* (NTHi) has been investigated previously in terms of biofilm production ability. This study examined NTHi biofilm formation using a staining assay and relationship to pathogenicity, and an assessment of the spatial distribution of the chemical components by Fourier Transform Infrared (FTIR) spectroscopy.

Firstly, a semi-quantitative microtitre plate (MTP) assay for NTHi biofilm formation was developed and validated for in vitro formation of biofilm. This assay was used to evaluate the effect of length of storage time on four fresh NTHi clinical isolates. Isolates were stored at -80C° for two, four, eight, 12, 24 and 48 weeks before measuring biofilm production. Sixty clinical isolates of NTHi from different body sites were also screened for biofilm formation ability and relationship with the body site. FTIR microspectroscopy was applied to study NTHi biofilm formation and pathogenesis by generating FTIR spectra. FTIR spectroscopy coupled with imaging of the biofilm components were assessed for untreated biofilm, as well as the effect of antibiotic treatment on new biofilm formation and treatment of mature NTHi biofilm.

The MTP showed consistent differences between the different NTHi isolates tested in first part of the project with these categorised as high and low biofilm producers. The MTP assay demonstrated that frozen storage of the isolates was not a determinant of biofilm formation. No statistically significant differences in the in vitro biofilm production were found across the clinical NTHi isolates from the nasopharynx (normal flora), ears (otitis media), lung (community acquired pneumonia and bronchiectasis in cystic fibrosis) or the isolates of *Haemophilus haemolyticus*

(oropharynx, normal flora). However, the isolates from eyes (conjunctivitis) demonstrated remarkably consistent low biofilm production compared to the isolates from other body site ($P<0.005$). In the second part of this project, FTIR spectroscopy was used to analyse the chemical constituents of the different biofilms. Unsupervised multivariate analysis (PCA) of the spectral data showed a chemical distinction between the two categories of biofilm formation (high and low). Analysis of microscopic IR hyperspectral data highlighted the spatial distribution of the different chemical components of the biofilm such as protein and carbohydrate. Analysis of antibiotic treated biofilm by FTIR showed an increase of protein bands in NTHi compared to standard *Haemophilus influenzae* isolate and untreated biofilm.

This project provides detailed information about ability of formation, pathogenesis and chemical composition of biofilms produced by NTHi isolates. Spectral information, with the effect of antibiotic on mature and newly formed NTHi biofilms provides a spatial overview of chemical differences in the bacterial biofilm.

Chapter 1

Background

1.1. Biofilm

1.1.1 Introduction

Microorganisms alter themselves to adapt to the environment of any surface. These cells combine together, responding to chemical signals and substances that help to form the cells clusters (Costerton, *et al.,* 1987 and Davies *et al.,* 1998). Communities of microorganisms colonise surfaces by producing a matrix in between the cellular components. This bacterial community slowly forms a layer around itself to protect it from the outside environment enabling it to survive on any surfaces including hostile environments. It is well established that bacterial cells in a biofilm behave differently from planktonic bacterial cells (Stewart and Franklin, 2008). A biofilm acts as a defence mechanism against chemicals and biochemical substances which otherwise would kill the microorganisms (Childs, 2008). The biofilm exhibits resistance to antibiotics, variation in nutrient utilisation and modification in the processes of expression of surfaces molecule (Hall-Stoodley and Stoodley, 2009). The following section will describe a biofilm, the involvement of various bacterial species with the capability to form biofilm on surfaces, and how to diagnose and treat biofilms.

1.1.2 Definition

A large community of bacterial cells does not itself constitute a biofilm. Micro-colonies of bacteria on an agar plate are also referred to as a bacterial cell community. A biofilm is a highly hydrated cluster of bacterial cells that secretes a matrix which is known as extracellular polymeric substances (EPS) (Stewart and Franklin, 2008). This matrix allows adaptation of the bacterial cells within itself under stressful conditions to allow their survival.

The most characteristic feature of a biofilm, as compared to planktonic bacterial cells that are the free floating cells, is the matrix. EPS keep the bacterial cells embedded inside the biofilm and determines the architecture of the bacterial film (Beloin *et al.*, 2008). There are two main roles of EPS; providing the structure of the biofilm and offering a protective role. As it keeps the cellular components inside the biofilm away from any environmental and immune defence, this matrix also offers resistance against antibacterial agents (Beloin *et al.*, 2008). It provides a viscous layer to the intracellular spaces between bacterial cells and offers channels for exchanging substances (metabolic substances and signalling chemicals) between cells. It acts as a barrier that prevents toxic material from diffusing inside the biofilm as well as preventing the leaking out of nutrients and signalling substances (Beloin *et al.*, 2008). This feature allows a favourable environment for pathogenic bacteria to be maintained and, a persist- and this may contribute to chronic infection.

The diversity of bacterial cells within a biofilm and the complexity of the chemical components both contribute to the difficulty of studying the matrix. The components of the matrix, at the present level of knowledge, are not fully understood. It is believed that 97% is composed of water with exopolysaccharide, proteins, lipids, phospholipids, nutrients, metabolites (Beloin *et al.*, 2008) and extracellular DNA comprising the balance (Whitchurch *et al.*, 2002). The constituents of this matrix have been investigated in biofilm studies, for example in Stoodley et al (2002) and Hall-Stoodley et al (2006), in which the cell populations exhibited different behaviour inside the matrix regarding nutrients and antibiotic resistance compared to outside the matrix. These differences in behaviour within the biofilm matrix imply variations in surfaces molecules, antibiotic resistance and virulence factors (Jurcisek and Bakaletz,

2007). Many factors influence the constituents of the matrix. Extrinsic factors including the microenvironment surrounding the cell aggregates, flow velocity of fluid and variation of nutrients and oxygen level (Allison, 2003). Physiological status and genetic profile of the cells also have a great effect on matrix development (Sutherland, 2001). Although there are key constituents that are recognised as important structural elements of the biofilms of some microorganisms such as polysaccharides, colanic acid (exopolysaccharide naturally produced by some bacteria) and cellulose (Beloin et al., 2008). it seems that there is a need to further identify the constituents that play roles in EPS formation which will aid the discovery treatments against biofilms.

Biofilms are able to form on any surface and their formation can be aided by many factors (Allison, 2003 and Beloin et al., 2008). Development of a biofilm on a surface involves many steps (Fig. 1). If it occurs *in vitro*, this will involve the nature of the surface and the flow velocity of the fluid that is in contact with the surfaces. There are several steps involved in the formation of a biofilm. Aggregation of cells, production of matrix, development of the EPS, maturation of the biofilm and dispersion of some cells from biofilm community are the stages of the biofilm development that have been described (Musk Jr and Hergenrother, 2006). One or more stages in this biofilm development can be accelerated by some features of the bacterial species such as type IV pilus and flagellum in *Vibrio cholera* El Tor biofilm (Watnick, P. and Kolter, R. 1999). Aggregation stage of biofilm was observed in *Pseudomonas aeruginosa* wild type with microcolonies more than the mutant strains which is defective in type IV pilli (O'Toole, G. and Kolter, R. 1998). In addition a flagella-mediated motility defective mutant was shown to be less cells attached on the surface

and suggested that motility and role of flagella has part in the initial cell-to-surface interaction (O'Toole, G. and Kolter, R. 1998).

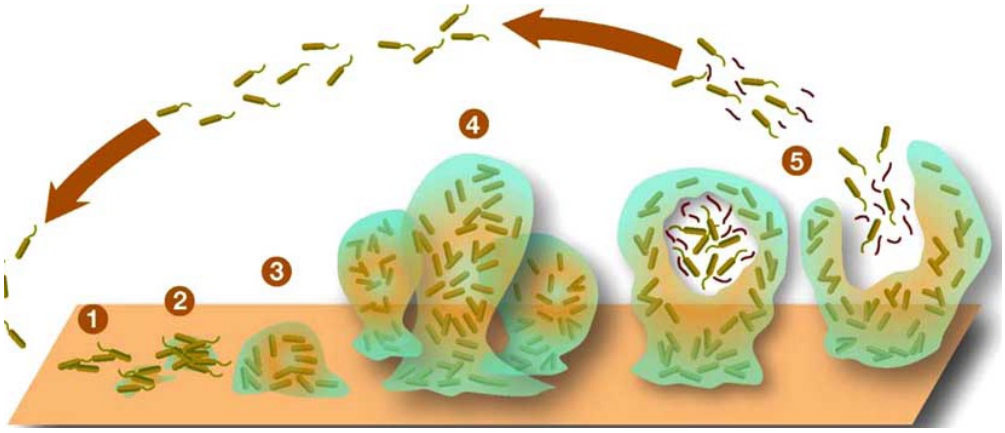

Figure 1. Stages of the formation of biofilm from freely planktonic cells to aggregates of cells surrounded by matrix and finally some cells shed from the community. Adapted from Musk Jr and Hergenrother (2006).

Resistance to antibacterial agents is the main factor of significance regarding biofilms in infectious diseases. Many clinically important pathogens now are recognised to form biofilm such as *Escherichia coli*, *Staphylococcus aureus* and *Pseudomonas aeruginosa* (Bendouah, *et al.*, 2006, Beloin, *et al.*, 2008 and Hall-Stoodley & Stoodley, 2009). According to the National Institute of Health, biofilm is responsible for 80% of chronic infections in the human body (Childs, 2008). Therefore, biofilm formation is significantly important in a clinical situation. Many researchers have investigated the occurrence of biofilm and the importance of its formation *in vitro* and *in vivo*. Numerous studies have focused on *in vitro* studies and biofilm poses significant danger to water supplies, the pharmaceutical industry and indwelling devices in a clinical setting. Biofilms can cause major problems and result in high morbidity, physical and emotional consequences for patients, and high costs for health care and the pharmaceutical industry (Mattila-Sandholm and Wirtanen, 1992, James, *et al.*, 2008 and Childs, 2008).

1.1.3 Medically important bacteria that produce a biofilm

Numbers of bacterial species have been investigated and studied intensively on genetic and pathogenic bases. These include *Pseudomonas aeruginosa* in cystic fibrosis (Bjarnsholt, *et al*., 2009); *Escherichia coli* in recurrent urinary tract infection caused by catheter biofilm (Beloin, *et al*., 2008); *Staphylococcus aureus* and *epidermidis* in chronic wound infection (Gjodsbol, *et al*., 2006); and in recent studies, Nontypeable *Haemophilus influenzae (*NTHi*)* that causes chronic otitis media in children and upper respiratory tract chronic infection in adults (Swords *et al*., 2004 and Jurcisek *et al*., 2007).

On a genetic basis, studies show that *P. aeruginosa* has distinctive features in biofilm cells different from planktonic cells. Studies have been conducted on how *P. aeruginosa* positively regulated alginate and negatively regulated flagellum in biofilm associated cells (Watnick and And Kolter, 2000). Flagella are responsible for adherence of bacteria to surfaces, and one bacterium is required to adhere in order to start to form biofilm. Alginate is involved in stabilizing the biofilm after formation. AlgC is a gene that is involved in the production of alginate. It has been shown in several studies that AlgC transcription increases within the biofilm cells about fourfold compared to planktonic cells (Watnick and And Kolter, 2000). Thus, in pulmonary isolates, *P. aeruginosa* shows mucoid due to overproduction of alginate (Hentzer, et al., 2001). Moreover, development of the flagellum is decreased as the flagellum is thought to destabilise biofilm after formation. Mucoid and non-mucoid biofilm formed by *P. aerouginosa* in cystic fibrosis have been extensively investigated with regard to the effect of innate immune response towards them. The flagella is absent in biofilm of mucoid *P. aeruginosa* frequently isolated from cystic fibrosis lung, therefore, expression of the flagellin receptor and other immune

response of neutrophils against biofilm is not established (Jensen *et al.*, 2010). Polymorphonuclear neutrophils (PMNs) encounter non-mucoid biofilm in vitro and produce bactericidal concentration of lactoferrin (Jensen *et al.*, 2010).

Bacterial cells in biofilm communicate with each other by releasing chemical substances. Bacterial products that were released are recognised as quorum sensing (QS) chemical messengers which are mediated by genetic determinants such as LuxS for Autoinducer 2 (AI-2) signalling molecule in many different bacterial species (Waters, and Bassler, 2005). Quorum systems are believed to play an important role in the adhesion of the bacterial cells to biotic and abiotic surfaces and formation of biofilm for S. aureus (Yarwood, *et al*., 2003) and maturation of the biofilm (Beenken, *et al*., 2003, Armbruster, *et al.*, 2009). In biofilm formed by Gram negative bacteria such as *P. aerouginosa*, QS occurs by substances such as acyl-homoserine lactones (acyl-HSLs) which promote the increase in density of biofilm (Stoodley, et al., 1999). Biofilm formed by *P. aerougenosa,* mutants that do not produce acyl-HSLs become loosely structured cells and are dispersed easily by detergents (Watnick and And Kolter, 2000). Also, QS can play a major role in protecting the biofilm from phagocytosis. It is found that *P. aeruginosa* produces certain signalling molecules such as (rhamnolipid B) which can kill neutrophils (Hall-Stoodley and Stoodley, 2009)A study by Bjranshlot *et al.* (2005) shows that *P. aeruginosa* biofilms which are QS deficient (lasR rhlR mutant) or blocked by a QS inhibitory drug (C-30) are readily phagocytosed by the PMNs and become more susceptible to H_2O_2 produced by PMNs (Bjarnsholt *et al.*, 2005). However, wild type biofilm is resistant and less vulnerable to PMNs by settle on top without penetrating the biofilm sub-layers.

Chronic diseases from biofilm infections are associated with interplay between the pathogen and the immune system. In cystic fibrosis, colonisation of *P. aerouginosa* occurs at a young age and is pathogenomic (Reid *et al.*, 2007). It is also believed that persistence of *P. aeruginosa* infection and formation of the biofilm in cystic fibrosis patient's lungs is related to the level of iron in the lung tissues (Reid *et al.*, 2007, Wiens, et al., 2014). *P. aerouginosa* has an efficient iron-mechanism which allows it to sequester iron from surrounding environment, and on iron-scavenging mechanisms for colonization. This may explain why the elevation of iron level in the infected lung has a major association with the *P. aeruginosa* colonisation.

Most of the studies of biofilm have been conducted on limited models of bacteria and are based mainly on genetic analyses. Bacterial biological knowledge and the majority of antibiotics susceptibility tests are based on planktonic culture of bacteria in the laboratory for many species. It is an important consideration that genetic expression in bacterial cells within biofilm is different from that of the planktonic state. About 38% of *E. coli* genome expression is affected by biofilm formation (Beloin *et al.*, 2008). It is also hypothesised that this difference in the gene expression is a consequence rather than a cause of biofilm (Beloin *et al.*, 2008).

There is much evidence from clinical specimens and animal model studies that chronic otitis media (OM) occurs due to biofilm infection (Swords et al., 2004, Jurcisek et al., 2005 and Hong et al., 2007). Nontypeable *Haemophilus influenzae* (NTHi) infection in the upper respiratory tract was identified to form a biofilm which is casually related to cause chronic infection in OM. This has been demonstrated using electron and confocal microscopy in the *Chinchilla laniger* model of OM (Hall-

Stoodley and Stoodley, 2009). However, an argument in the literature raises a point that the *in vitro* and *in vivo* NTHi biofilm is an unconfirmed hypothesis (Moxon *et al.*, 2008). Details will be discussed later in this chapter.

1.1.4 Diagnosis and Control of Biofilm

Microbiology has been developed over more than a century using many principle methods to identify bacteria in the laboratory. Diagnosis of a biofilm is different from identifying planktonic cells. To identify a biofilm from a clinical sample, it is important to study the microorganism that causes persistent infection. Researchers in the late nineties developed several phenotypic methods such as Christensen's test-tube method (CTT) and the staining agar method to discover the ability of such bacterial isolates from clinical samples to form biofilm (Ruzicka *et al.,* 2004). These methods have used dyes to stain biofilm grown overnight inside glass test tubes (Christensen *et al.*, 1982).

This method was then developed by Christensen and co-workers using the tissue culture microtitre plate (MTP) assay, with a staining method to provide quantitative measurement of biofilm (Christensen et al., 1985). These approaches are still used for detection of biofilm with other methods such as radiolabeling, microscopy and the Congo red agar plate test (Stepanović et al., 2007). Staining techniques methods such as the CTT method are focused on the degree of biofilm formation and not on the pathogenesis. These methods were developed earlier in the late nineties to examine the ability of the isolates to form biofilm. The MTP method is still the most frequently used assay for investigation of biofilm, with a number of modifications having been developed for the *in vitro* cultivation and quantification of bacterial biofilms.

Abiotic surface-associated biofilm have been highly investigated using microscopy for their structural and ultra-structural composition. Destructive and non-destructive methods have been used in recent years to investigate formation of biofilm on abiotic surfaces.

Pharmaceutical manufacturers are most concerned about biofilm formation on surfaces such as nonpolar, hydrophobic surface (plastics) and hydrophilic surfaces (metal and glass). Water is a significant part of this manufacturing process and a lot of attention is directed to the water being sterile. Monitoring of water systems against biofilm development is also important to prevent harmful consequences (Janknecht and Melo, 2004). Online non-invasive monitoring of biofilm has been applied to laboratory, industrial and research fields. Janknecht and Melo (2004) outlined several methods for analysis and online monitoring of biofilm based on electrical field, radiation, acoustic waves or heat transfer measured using specific sensors. One recent method is spectroscopy where an infrared (IR) light source on the opposite side of a transparent window measured biofilm thickness (Janknecht and Melo, 2004, Serra *et al.,* 2007, Holman *et al.,* 2009).

Microscopy is considered a powerful tool in the diagnosis of biofilm and for investigating structure-function analysis. It can provide details of the structure of biofilm as well as information about the organism that caused the biofilm. Studies using confocal microscopy have investigated the effect of mutation of a specific gene on the formation of less dense biofilm by showing the structure and number of dead and live cells (Bjarnsholt et al., 2005). The confocal image can also illustrate the contact of other cells such as PMNs with the aggregates of bacterial cells as difference

in green fluorescence signal intensity (Bjarnsholt et al., 2005). The advantage of using confocal microscopy with dead-live SYTO- stains is that it can differentiate the cells in a biofilm subpopulation. However, it is a destructive technique and demands an intense level of technical training unlike the IR vibrational spectroscopy which was recently suggested as a rapid screening method for biological diagnosis (Ellis and Goodacre, 2006). SYTO- stains using external probes interact with cells and may destroy samples removing any possibility of further investigation. For biofilm studies with discrimination between live-dead cells, Syto9 staining and confocal microscopy has been used for quantification of cells and for routine quantification of biofilm biomass (Peeter et al, 2008). Various other viability stains have been used to assess the metabolic activity of the viable cells such as 5-cyano-2,3-ditolyl tetrazolium chloride (CTC), 2,3-bis (2-methoxy-4-nitro-5-sulfophenyl)-5-[(phenylamino)carbonyl]-2H-tetrazolium hydroxide (XTT) and dye 1,9-dimethyl methylene blue (DMMB) which have been used to quantify the biofilm matrices (Peeter et al, 2008). These staining methods were used after the approach of Christensen's test tube and CTT staining for biofilm formation.

For eradication of existing biofilms from devices or abiotic surfaces, specific strategies must be taken. Antibiotic intervention to treat chronic infection caused by biofilm has had some success in eradication of biofilm and planktonic cells that are shed from the aggregates. However, there have been different degrees of success for antibiotic treatment which are dependent on the status of the biofilm and the type of microorganism that forms the biofilm (Hall-Stoodley and Stoodley, 2009). Both clinical isolates and abiotic biofilms have been extensively studied.

Bacterial biofilms formed in catheter devices tend to be a continuous source of infection and require urgent treatment. Locking of a catheter with an antibacterial agent is often used to remove and prevent reformation of biofilm (Balestrino *et al.*, 2009). *In vitro* studies have shown that 60% ethanol has a superior activity to eradicate biofilm embedded in a silicone catheter than 46.7% trisodium citrate (TSC) (Balestrino *et al.*, 2009). This study was conducted on biofilm in a silicon catheter that was formed by either *P. aerouginosa, Staphylococcus aureus*, *Staphylococcus epidermidis*, *Klebsiella pneumonia* or *Candida albicans* (Balestrino *et al.*, 2009).

Biofilm related to various chronic infections such as chronic lung infection in cystic fibrosis are acknowledged as hard to be eradicated by antibiotic treatment and this is very serious clinical issue (Donlan and Costerton, 2002). Bacterial species such as *P. aeruginosa, H. influenzae, S. pneumoniae* and *S. aureus* resist antibiotic treatment when they form biofilm even if they do not have a genetic basis for resistance (Suci, *et al*., 1994, Souli and Giamarellou, 1998, Zhang and Mah, 2008, Hall-Stoodley and Stoodley, 2009, Sword, *et al.,* 2012).

The resistance to antimicrobial agents in biofilm is multifactorial. Biofilm formation involves various stages of cell growth and subpopulations of bacteria converting to a resistant state (Patel, 2005). The subpopulations of cells contain both active and inactive cells. The variation in nutrients, slow growth cells and metabolic state of these cells may reduce the effectiveness of antibiotics (Donlan, 2000, Walters, *et al*., 2003). Mature biofilm has cells that are less activated and this attributes to less antibiotic susceptibility as conventional antibiotics are not as effective for the cells in stationary phase. When the biofilm is only hours old, bacterial cells become active and divide in a fast manner which allows antibiotics to act on cell targets more

effectively. With regard to the cells located on the superficial layer of the biofilm, antibiotics can come into contact with them, killing or altering the cells that have a greater metabolic rate than the deep layer subpopulation which has less metabolic activity. Furthermore, the biofilm provides a physical barrier thereby protecting the cells within (Patel, 2005). Some chemical metabolites released from biofilm cells may inactivate antibiotics (Patel, 2005). Altered metabolic function in biofilm is sometimes related to the signals between subpopulation cells within the biofilm matrix which decrease the efficiency of treatment agents (Patel, 2005).

Planktonic bacteria are sensitive to traditional antibiotic treatment but these same organisms when growing in a biofilm can survive antibiotic treatment. Medically significant biofilms such as P. aeruginosa biofilm leading to chronic lung infection has restricted treatment with antibiotics. Older antibiotic compounds, such as aminoglycosides, tetracycline and chloramphenicol are re-emerging as important alternatives for the treatment of infections and are more effective than the most used old synthetic antibiotics such as ampicillin, streptomycin for biofilm eradication (Liaqat et al., 2009). An in vitro study demonstrated that chloramphenicol is more effective than tetracycline in inhibiting biofilm formation of five selected isolates (*Klebsiella sp., Pseudomonas aeruginosa, Achromobacter sp., Klebsiella pneumoniae,* and *Bacillus pumilis*) on abiotic surfaces (Liaqat *et al.*, 2009). Furthermore, in recent studies, the combination of antibiotic and bacteriophage has been suggested for biofilm control (Sawhney and Berry, 2009). This new approach is believed to reduce the viscosity of EPS of the biofilm which leads to destruction of the biofilm. Destruction of the matrix by genetically engineered bacteriophage assists the removal of surrounding matrix and enhances the function of antibiotics (Sawhney

and Berry, 2009). Thus, further understanding of biofilm matrix and inner substances such as expressed proteins has the potential for controlling biofilm and for treatment of chronic infection.

1.1.5 Static method and continuous flow *in vitro* biofilm models

Biofilm studies have been conducted using *in vitro* models for several applications. The growth and analysis of biofilm has been performed by using static and flow chamber that enhances the growth by providing a favourable environment for biofilm formation. Biofilm grows in the flow chamber under hydrodynamic conditions that can be easily controlled and changed (Tolker-Nielsen and Sternberg, 2011). The flow in the chamber is a continuous flow model used to grow the biofilm under controlled conditions. It also allows addition of antibiotics at defined time points (Tolker-Nielsen and Sternberg, 2011). Essentially, biofilm is grown over a period of days and may be analysed by inspecting changes in the aggregate over time using various methods such as microscopy.

The flow chamber apparatus consists of many parts that provide appropriate conditions for growing biofilm. These parts function for inoculation of the flow chamber, running the system and disassembly and cleaning of the flow chambers (Tolker-Nielsen and Sternberg, 2011). The apparatus consists of a flow chamber, bubble trap, medium bottle, peristaltic pump, a waste container, tubing and various connectors. Inoculation of the microorganism occurs by inserting a syringe needle into the tubing close to the flow chamber inlet then resealing the tubing by silicone and resuming the medium flow (Tolker-Nielsen and Sternberg, 2011, Crusz, *et al.*,

2012) (Fig. 2). The system supports microscopic analyses by containing a glued cover slip within the channels.

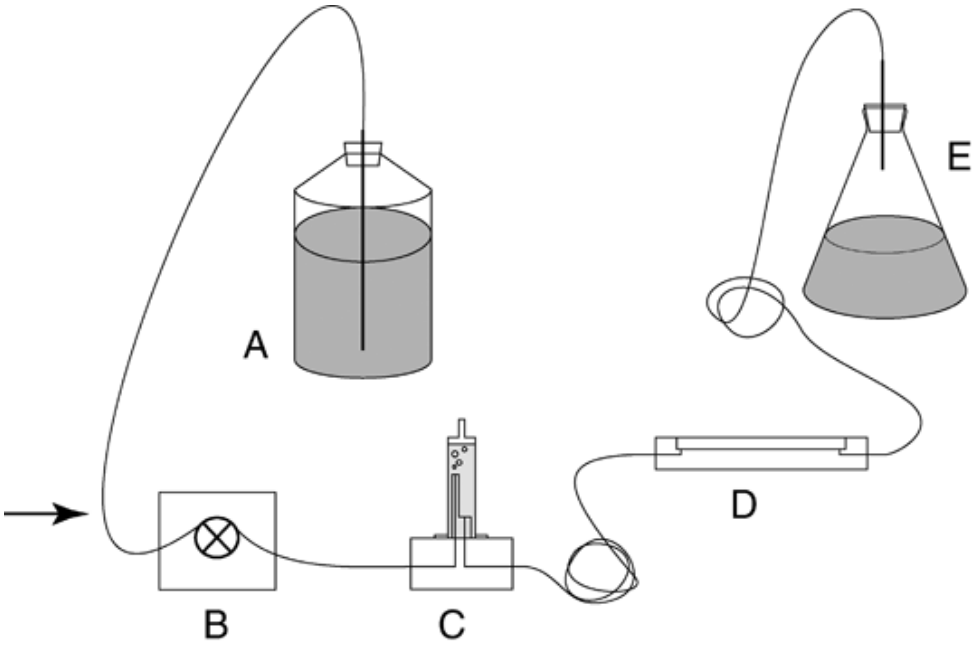

Figure 2. Flow chamber system: A medium bottle; B peristaltic pump; C bubble trap; D flow chamber; E waste container. Adapted from Tolker-Nielsen and Strenbrg (2011).

This system may run for several weeks. Maturation of the biofilm takes place within 3 to 7 days. Sterilisation and assembly of the system can take 1 or 2 days (Tolker-Nielsen and Sternberg, 2011). By contrast, the static biofilm formation assay allows the growing of biofilm over short time periods (mainly 4-48 h) depend on the growth of the organism and investigation of adhesion, aggregation and mature biofilm in a static manner. MTP assay is the most common static assay used to grow biofilm (Fig. 3). These assays were found to be easier to set up, cheap and suitable to investigate the *in-situ* characteristics by staining methods in a short time (Stepanović *et al.*,

2007). Thus, the static assay is a useful tool to investigate the biofilm formation ability and analysis of other aspects of biofilm analysis *in vitro*.

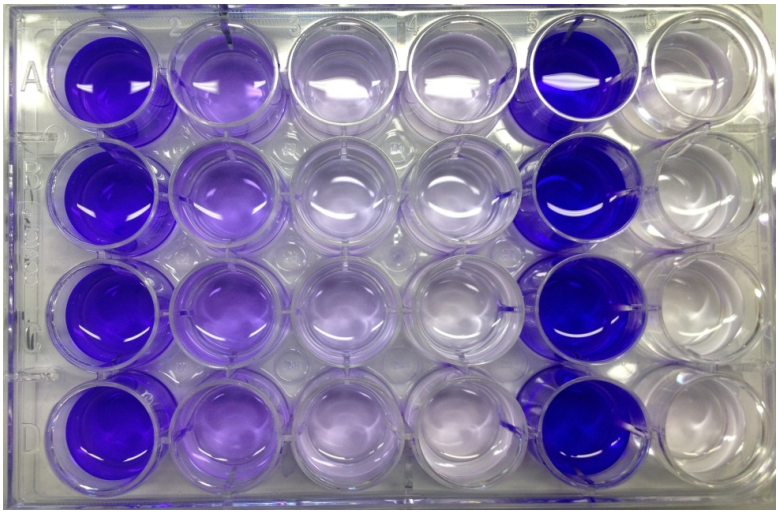

Figure. 3 Microtitre plate assay used with crystal violet to study biofilm formation in static methods. Darker wells indicate growth of biofilm indicated by retention of crystal violet stain.

1.1.6 *H. influenzae* biofilm

H. influenzae is a Gram negative bacterium and is considered as a part of the normal nasopharyngeal and upper airways flora in most healthy humans. Major studies in the last two decades have focused on *H. influenzae* serotype b which is an invasive type pathogen for respiratory tract infection in children (Erwin and Smith, 2007). In 1990, type b polysaccharide-protein conjugated vaccine was introduced to the world leading to eradication of the invasive type of *H. influenzae* in most developed countries (Erwin and Smith, 2007). After the eradication of the invasive type, most asymptomatic colonisation is from the *H. influenzae* serotype that lacks capsular polysaccharide and is known as Nontypeable *H. influenzae* (NTHi) (Erwin and Smith, 2007) and (Swords *et al.*, 2004). *H. influenzae* species require β-nicotinamide adenine dinucleotide and heme for growth in the laboratory. NTHi acquires heme from

haemoglobin complex which is facilitated by two to four *hpg* genes possessed within NTHi (Erwin and Smith, 2007). Therefore, a specific mutated NTHi 86-028NP which lacks three *hpg* genes which can delay the onset of infection to the middle ear (Erwin and Smith, 2007). Hence, not all strains of *H. influenzae* are equally virulent and resistant to host immunity.

The persistence of *H. influenzae* in host epithelial tissue such as the respiratory tract is thought to be due to many bacterial factors. Adhesion of bacteria to host is based on the cell wall composition and structures such as pilli, proteins and lipooligosaccharides (LOS) (Swords *et al.*, 2004). LOS is a low molecular weight bacterial lipopolysaccharide (LPS) which lacks the *O*-specific chain. LOS analogues of LPS play an important role in pathogenesis and are released *in vivo* as endotoxins for *Haemophilus* species (Kilár *et al.*, 2013). In many *H. influenzae* strains, LOS contain N-acetyl-neuraminic acid (NeuAc) which is added to acceptor LOS (Swords *et al.*, 2004). NeuAc is added by a cystidine monophosphate carrier to *H. influenzae* by CMP-NeuAc synthase. The oligosaccharide portion is linked by at least three sialyltransferases (Swords *et al.*, 2004). *H. influenzae* acquires NeuAc from the surrounding environment and results in sialylation of LOS. Some studies have shown that 23 NTHi strains are able to sialylate LOS (Swords *et al.*, 2004). Furthermore, NTHi strains obtain silicic acid from the host in the first stage of the infection and the process of sialylation is a major requirement for the persistence of the infection in the chinchilla model (*in vivo*) (Bouchet *et al.*, 2003). Therefore, sialylation of LOS in the NTHi cell wall promotes long duration of infection to the host.

In several studies it has been stated that sialylated LOS of NTHi is involved in the long duration of infection as well as in biofilm formation. Swords' group, by an *in vitro* model using silicone tubing, demonstrated by electron microscopy that sialylation of LOS promoted biofilm formation by NTHi (Swords *et al.*, 2004). Sialylation of LOS also contributed to the persistence of NTHi infection *in vivo* using a rat pulmonary challenge model system and a Mongolian gerbil otitis model (Swords *et al.*, 2004). It is believed that sialylation affords resistance in NTHi to the host's immune system. Immunoflurecent labelling of biofilm from the middle ear of the chinchilla model demonstrated sialylation of LOS and the duration of the biofilm formation by NTHi made no difference to immature or mature biofilm (Jurcisek and Bakaletz, 2007). Immunolabeling for LOS within NTHi biofilm was also investigated in vitro by Webster *et al.* (2006) which confirmed that LOS was secreted by the bacteria. LOS was found to be accumulated in the biofilm matrix at the base of the film which suggests that it may play an important role in initial attachment of the bacteria on the substrate as well as maintaining biofilm architecture (Webster *et al.*, 2006). In addition, NTHi biofilm formed *in vivo* contained type IV pillin protein and double stranded DNA. Double stranded DNA (dsDNA) was assumed to provide stability to the NTHi biofilm in the middle ear and formed a dense meshwork of strands that span water channels (Jurcisek and Bakaletz, 2007). The presence of DNA in the biofilm matrix has been noted to be an important part of biofilm development for many other bacteria and it appears to be important in NTHi biofilm. In a study of NTHi biofilm *in vivo* and *in vitro*, it was thought that NTHi biofilm contained an amount of dsDNA which is believed to be excreted during stages of biofilm formation and is sourced from the NTHi cells. The same study confirmed that DNA presented in the EPS of NTHi biofilm is also found with *in vitro* experiment, thus its source is

from the genetic transcription of the NTHi cells themselves as part of phenotypic changes towards the sessile form (Jurcisek and Bakaletz, 2007).

Despite literature that shows the ability of NTHi to form a biofilm *in vivo* as well as *in vitro*, Moxon and colleagues believed that this evidence is inconclusive (Moxon *et al.*, 2008). The main doubt was the matrix of the biofilm. They suggested that the bacterial component is a result of bacterial cell lysis not specific for biofilm-phenotypic gene (Moxon *et al.*, 2008). Moxon *et al.* (2008) doubted that the formation of NTHi biofilm matrix and component could be entirely or partly formed from the host cells.

The presence of exopolysaccharide or polysaccharides and proteins in the matrix are suggested to be the major components of biofilm. These components vary greatly depending on the growth conditions, the medium and nutrients and on the growth stage of the bacterial cells and maturity of the biofilm (López *et al.*, 2010). As production of biofilm is a staged process thought to occur as a result of many factors, bacterial cell metabolites and components contribute to the biofilm formation process (López *et al.*, 2010). Mechanisms of bacterial processes to form biofilm are reliant on strain attributes and the surrounding environment (López *et al.*, 2010). NTHi biofilm is understood to be formed as a consequence of aggregation, colonisation of bacterial cells and modifications of the metabolic process within the bacterial cell aggregates *in vitro* and in attachment with host material as well (Jurcisek and Bakaletz, 2007, Swords *et al.*, 2004, Langereis and Hermans, 2013). There is still insufficient knowledge about the NTHi biofilm components (proteins, polysaccharides and DNA)

and the contribution of these components to the formation of robust biofilm on endoepithelial tissues or *in vitro*.

One of the main characteristics of bacterial biofilm is its resistance to antibiotics. Therefore, NTHi biofilm in *in vitro* models is hard to remove with antibiotics. Administration of antibiotics in middle ear infection of an animal model for 96 h to 120 h showed that after treatment no biofilm appeared (Post, 2001). It is thought that eradication of NTHi biofilm may be achieved by mechanical or enzymatic disruption of the intercellular ability to form biofilm (Izano, et al., 2009). This suggests that the matrix is the main component in NTHi biofilm which plays an important role as a protective layer and in mediated resistance to antibiotic.

Electron microscopy and confocal scanning microscopy have been used to give information about the exopolysaccharide matrix but have not provided details of chemical components of the matrix to highlight that the film is formed by NTHi cells themselves (Moxon *et al.*, 2008). Thus, NTHi chronic infection of the middle ear need more investigations to understand the possible formation of biofilm and analysis of the chemical composition of its EPS.

Crystal violet (CV) is a cationic dye that binds to bacterial cell walls. That is used to bacterial Gram stain. The use of CV dye on NTHi *in vitro* biofilm has been indicated in many studies. CV assay for biofilm is a widely used method to detect the biofilm that formed by Gram negative bacteria. It was questionable whether the CV assay predicts NTHi biofilm behaviour *in vivo* precisely (Moxon *et al.*, 2008). *In vivo*, bacterial cells indeed are exposed to host immune action that is believed to affect

biofilm formation by NTHi. The evidence stated in previous studies is mainly based on ultra-structural part of *in vivo* and *in vitro* NTHi biofilm and thus observations are subjected to the nature of the microscopy which has been used (Moxon *et al.*, 2008). This does not provide accurate details of NTHi biofilm and gives no indication of the pathogenesis of the formation of biofilm by NTHi.

A mass spectrometry study of *in vitro* formed NTHi biofilm in a flow chamber showed high molecular weight glycoforms in the bacterial cells attached to biofilm, as compared with planktonic cells (Moxon *et al.*, 2008). Also, the role of sialylation of LOS has been stated by using evidence from a mutated NTHi strain. In sialylation-deficient mutants, LOS of the biofilm decreased in ability and elaborated the role of sialylation in biofilm formation (Swords *et al.*, 2004). On the other hand, Moxon's group believed that sialylation of LOS has an important role in resistance to host clearance and does not invoke biofilm for this resistance (Moxon *et al.*, 2008). In a review, Swords (2012) stated some evidences that there is a relationship between NTHi and biofilm in chronic disease.

Regarding clinical evidence, the last 15 years show there is a number of persistent infections that implicate biofilm and are caused by *H. influenzae* (Table 1.1). A range of patients with chronic infections where NTHi was confirmed as the causative agent using molecular methods, tested negative by conventional culture methods. For example, studies of OM infection showed that NTHi and other bacteria were detected using PCR-based methods (Post *et al.*, 1996, Bakaletz *et al.*, 1998, Kunthalert *et al.*, 2013). Other evidence is that clinical NTHi isolates from patients are resistant to

antibiotics. NTHi biofilms have showed some resistance/tolerance to a range of antibiotics (Slinger *et al*., 2006).

Table 1.1 Clinical isolates show evidence in the relationship between *H. influenzae* biofilm and chronic airway diseases, adapted from Swords, W. (2012).

Body site	**Finding**
Otitis media	-Bacteria and bacterial components present in culture-negative effusion fluids -Bacterial RNA found in culture-negative effusion fluids - *H. influenzae* biofilms in middle-ear chamber of experimentally infected chinchillas - *H. influenzae* surface-attached communities in patient tissues
Chronic bronchitis	-Long-term persistence as evidenced by recurrent sputum cultures -Expression of peroxiredoxins levels similar to those observed in biofilm
Rhino sinusitis	*H. influenzae* surface-attached communities in patient tissues

Surface components of NTHi bacteria may contribute to the biofilm formation process as mentioned earlier in this review. Sialylation of the bacterial surface, expression of type IV pili and nuclear DNA protein are all factors that play a role in stabilising biofilm formation (Jurcisedk and Bakaletz, 2007), and determined as evidence of the relationship between chronicity of the infection and biofilm (Post, 2001, Hall-Stoodley *et al.*, 2006). Strains that lack these factors and one of the QS responsible genes failed to form biofilm, or they formed biofilm that was susceptible to antibiotics and immune system eradication.

In conclusion, several studies provide evidence that NTHi forms biofilm. On the other hand, others argue the evidence is insufficient to demonstrate *in vivo* NTHi biofilm formation. Indeed, it seems too early to conclude definitively that NTHi forms biofilm which has a relationship with chronic disease.

1.1.7 Antibiofilm studies by static assays

Microtitre plate (MTP) assay has been used successfully to study the effect of antibiotics and antibiofilm agents on biofilm in static manner and evaluate biofilm production by NTHi strains (Kaji *et al.*, 2008, Wang *et al.*, 2009). The MTP assay method is readily adapted for diagnostics and research for *in vitro* biofilm models and can be efficiently developed (Harrison *et al.*, 2010). It is a simple, unsophisticated and well established *in vitro* method used to obtain information about antibiotic susceptibility of biofilm formed by several species such as *Klebsiella pneumoniae* (Anderl *et al.*, 2000, Anderl *et al.*, 2003). The morphology of biofilm formed inside the wells is similar to the NTHi biofilm formed in flow cells and is a useful tool for antibiotic analysis (Webster *et al*., 2006). The biofilms grown after 20-24 h of incubation in the static MTP are more stable and resistant to washing than biofilm produced in a short incubation time (≈ 4 h) (Donlan and Costerton, 2002).

1.2 Vibrational Spectroscopy

The study of molecular structure and chemical functional groups within a sample are essential for the understanding of the molecular features of the material. Vibrational spectroscopy is one of the analytical techniques that has developed constantly during the last century to investigate these features. Infrared (IR) and Raman spectroscopy are both vibrational spectroscopy methods for determination of molecular structure. Vibrational spectroscopy techniques contribute to the analysis of organic molecular structure and are useful for micro and surface analysis (Kellner, 1998). They also offer analysis of molecular systems by providing inherent information relating to functional groups; their kind, interactions and orientations of isomers from the fingerprint region (Kellner, 1998). These two spectroscopic techniques facilitate non-invasive analysis and can be used for labile compound, liquids, solids and gases as well as surfaces and interfaces between phases (Kellner, 1998). IR and Raman are complementary in regard to signal generation. IR spectra are obtained from infrared light absorption whereas Raman spectra are acquired from light scattering. Infrared and Raman spectroscopy are the most important tools to study and observe vibrational spectra (Schrader, 2008).

1.2.1 IR Spectroscopy

IR spectroscopy is a non-destructive technique for the analysis of chemical components in inorganic and organic materials. It has been developed for the analysis of organic and inorganic material in the past seventy years. IR has then been applied for the analysis of biological samples since 1951 and scientists have implemented this type of vibrational spectroscopy to analyse many aspects of biological samples (Wenning and Scherer, 2013). Traditional IR spectra are obtained by passing IR

electromagnetic radiation through the sample resulting in a transmission spectrum. The IR wavelength is scanned over a range of wavelengths and absorption of IR energy occurs at specific wavelength resulting in a spectral bands (Schrader, 2008). The vibrational mode of the molecule in a functional group after IR absorption could be one of stretching, deformation, bending or wavelength overlaps for the molecule (Ellis and Goodacre, 2006). Examples for the vibrational modes for H_2O and CO_2 molecules are illustrated in Fig. 4. The simplest example for IR spectra is illustrated in Fig. 5 which show the peak from CO_2 absorption of stretching and bending mode.

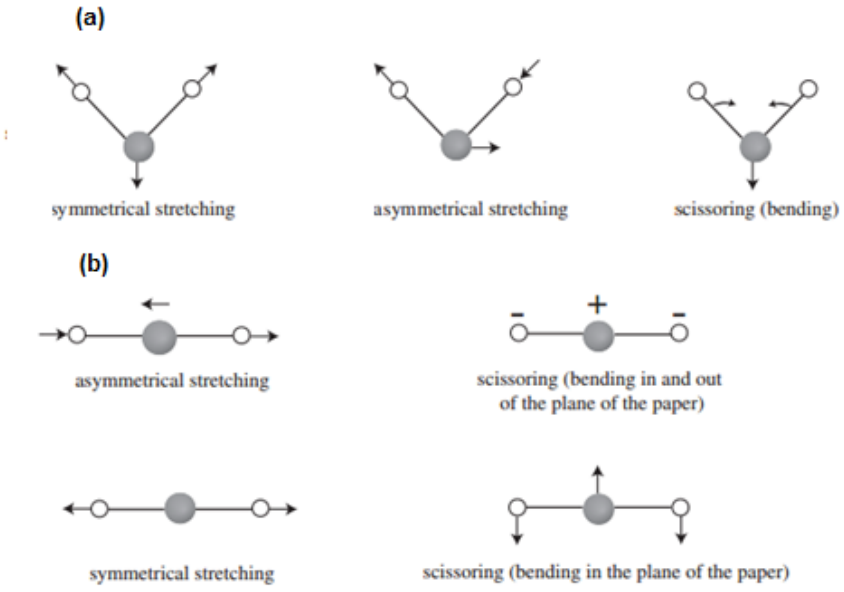

Figure 4. (a) H_2O molecule vibrational modes, stretching and bending, and (b) two CO_2 molecule visible vibrational modes, stretching and bending. Adapted from http://orgchem.colorado.edu/Spectroscopy/irtutor/IRtheory (2001).

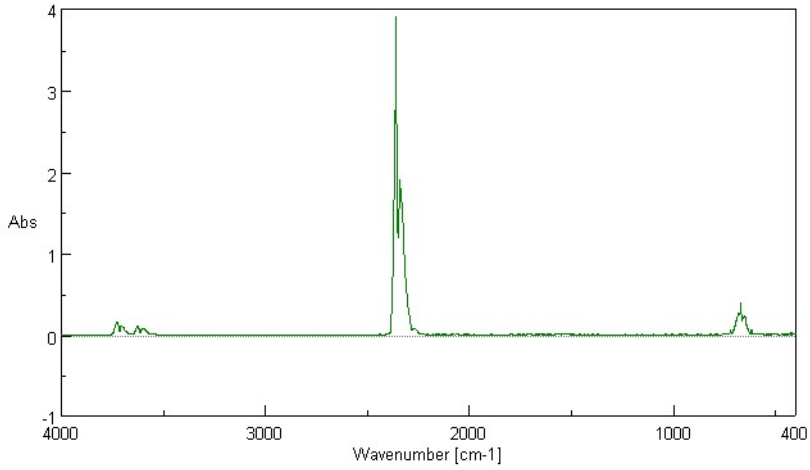

Figure 5. IR spectra of CO_2 molecule adapted from Anderson (2013).

There are three most common techniques used for the IR spectroscopy: i) transmission, ii) transflection and iii) attenuated total reflection (ATR). The first two techniques require IR transmission sample supporter and non-reflective interference support with the measurement such as IR transparent substrate ZnSe or CaF_2 (Wenning *et al*., 2008, Naumann, 2006). The transmission mode of FTIR microspectroscopy is most applicable for cellular biological samples to obtain accurate spectral data acquisition (Baker *et al*., 2014). ATR measurements are performed with direct contact at high pressure on the sample and may be suitable only for solid or dehydrated liquid samples. This type of technique provides an *in-situ* measurement with the use of an internal reflection element (IRE) that is in direct contact with the test material.

1.2.1.1 The IR Spectra Ranges

The electromagnetic spectrum of the IR region wavelength extends from 1,000 nm to 1,000,000 nm (10,000 to 10 cm^{-1} wavenumber) including near-infrared (NIR), mid-infrared (MIR) and far-infrared (Burgula *et al.*, 2007). These IR spectrum regions are illustrated in Fig. 6.

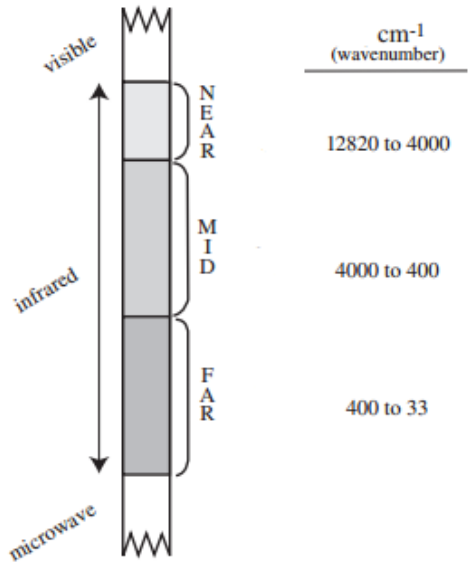

Figure 6. Electromagnetic spectrum within three IR regions. Adapted from http://orgchem.colorado.edu/Spectroscopy/irtutor/IRtheory (2001)

The biological material spectra extends within the region from 4000 to 400 cm^{-1} as the vibrations of specific functional groups related to biological structures are present within this region.

1.2.1.2 Analytical Approaches of FTIR spectroscopy

Infrared spectrum is the IR frequency itself of the sample without any processing. The Fourier transform infrared (FTIR) is measurement of infrared spectra converted mathematically and processed using Fourier transformation which allows analysis of very specific frequencies. FTIR and Raman spectroscopy, when coupled with microscopy, is a promising analytical technique (Wenning and Scherer, 2013).

1.2.1.3 Raman Spectroscopy

Raman spectroscopy measures the polarisability of a molecule by light scattering technique that allows the use of standard optics so the whole spectrum can be

collected by excitation with fixed laser wavelength (Kellner, 1998). The light hits a molecule resulting in an elastic scattering process from the laser beam polarisation which does not change the vibrational state and the scattered photon will have the same energy as the original photon and is called Rayleigh scattering (Kellner, 1998). While in 1 to 10 million photons, the vibrational state is higher than the state of original and results in inelastic scattering giving information about the vibrational modes of the material. (Schrader, 2008). Therefore, molecular structure information can be obtained from vibrational spectra by both IR and Raman spectroscopy.

1.2.1.4 Advantages and disadvantages of IR spectroscopy and Raman spectroscopy for biological samples

FTIR spectroscopy is a non-invasive and fast technique that does not require special staining methods and only requires minimal sample preparation (Ellis and Goodacre, 2006, Maquelin *et al.*, 2003). When combined with a microscopy setup, FTIR allows great spatial resolution by magnification with high numerical aperture which can identify subcellular components within a size of about 10 μm (Harz *et al.*, 2009). In contrast to Raman spectroscopy, FTIR microscopy has high sensitivity to water in wet samples and the water peaks in the IR spectra can interfere with some biological characteristic peaks (Pätzold *et al.*, 2006). Therefore, Raman microscopy could allow analysis of biological samples with fully hydrated conditions.

Generally more spectral features are identifiable in Raman spectra than FTIR spectra. The spectra generated for excitation wavelengths near the infrared laser have more intense fluorescence emissions (Harz *et al.*, 2009). However, for most biological sample near-IR lasers are usually better for fluorescence than visible lasers. Biological

sample with Raman scattering autofluorescence is a significant challenge from the Raman scattering signal in the acquired raw spectra (Zhao *et al.* 2007).

In the past decade, FTIR and Raman spectroscopy have been used to provide spectral fingerprint based on chemical information and characterisation of (cell-) biological systems at the molecular level (Naumann, 2006). They can provide great information for both chemical compositions of cells with high spectral resolution. It also has a potential role in the identification of functional groups by initiating a chemical database for each cell phenotype.

According to many studies reviewed by Harz *et al.* (2009), IR and Raman spectroscopy demonstrate significant potential in microbial cell classification. As a diagnostic tool, analysing bacterial strains has been established by the commercial sector using database such as River Diagnostic (www.river.co) (Harz *et al.*, 2009). Generally, in vibrational spectroscopy, spectra of microbial cells have similar bands (Davis and Mauer, 2010, Alvarez-Ordóñez and Prieto, 2012). However, these bands quantitatively vary in the relative amounts of chemical component such as proteins and carbohydrates in the strains and species of different bacterial cells (Harz *et al.*, 2009) which is illustrated in Fig. 7. Many statistical evaluation methods have been previously established to measure the relative changes of the components within the microbial cells including the principle component analysis method (PCA) (Samek *et al.*, 2009, Wang and Mizaikoff, 2008).

FTIR and Raman spectroscopy have been shown to be complementary techniques as FTIR could produce holistic spectral information of complex biological samples or

sections of the sample and Raman could confirm the dominant bands. FTIR microscopes allow fast acquisition of spectra of small samples to be measured as quickly and easily, or possible faster, than Raman microspectroscopy (Griffiths, 2009a).

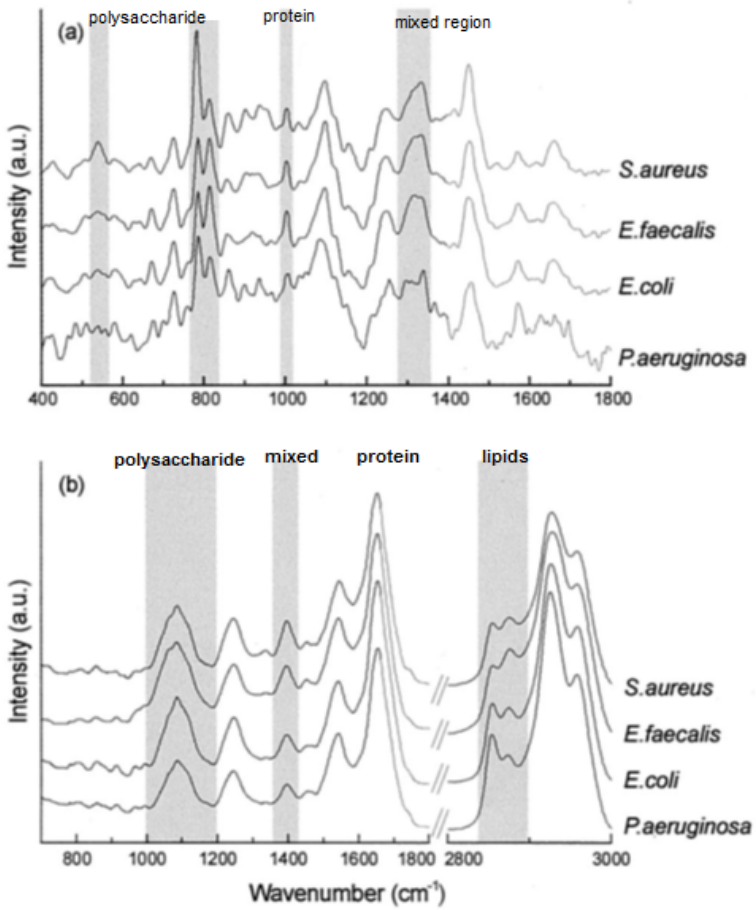

Figure 7. Spectra classifies the different bacterial species with different characteristic Raman and IR spectra with chemical fingerprints. Raman spectra (a) and FTIR spectra (b) of four microorganisms. Adapted from Maquelin *et al.* (2003).

Interpretation of the FTIR spectra for microbial cells provides an understanding of cellular and substructural composition (Huang *et al.*, 2004) (See Fig. 8). IR vibrational spectra reflect chemical composition which may give information on taxonomic differences, chemical changes during growth phase or a stressful

environment (Alvarez-Ordóñez and Prieto, 2012, Trevisan *et al.*, 2012). The vibrational bending and stretching modes of molecular bonds of functional groups for proteins, lipopolysaccharides, lipids and nucleic acids components vary from species to species (Burgula *et al.*, 2007, Wenning *et al.*, 2008) and FTIR spectroscopy can identify the characteristic spectra with the potential to be a diagnostic tool for specific species (Davis and Mauer, 2010). It also can give information about bacterial cellular structures and surface characterisation and classification of bacterial cells earlier than other techniques (Davis and Mauer, 2010). Chemical bonds presented in the IR biochemical cell fingerprint region (900-1800 cm^{-1}) provides chemical information for certain species of biological samples (Martin *et al.*, 2010, Trevisan *et al.*, 2012). Microbial IR spectra are complex and spectral pre-processing and pattern finding need to be performed to extract data. The pre-processed spectra may provide information on molecular interactions within a cell such as processes of metabolic change, cellular aging, quorum sensing, culture conditions and cell-drug interactions (Wenning *et al.*, 2008, Thi and Naumann, 2007, Alvarez-Ordonez *et al.*, 2011).

The application of bioanalytical FTIR spectroscopy and study of whole organism fingerprints has now been around for a decade (Lu *et al.*, 2011). There is considerable interest focused on applying vibrational spectroscopy, with further advances in sensitivity, selectivity, chemometric method and reductions in instrument cost which have led to the development of real-time analytical systems.

As many bacteria are unculturable and the traditional culture-base method is not suitable for distinguishing some species, techniques based on vibrational spectroscopy have been developed for this purpose. Since many bacteria are difficult to grow in

conventional culturing methods and need special media and microbial functioning tests such as special staining methods, they cannot be studied by culture-base method (Huang et al., 2004). Various studies have been reviewed the achievements of high identification accuracy for microbial identification by Raman and IR spectroscopy (Maquelin *et al.,* 2002, Ngo-Thi *et al.*, 2003, Munchberg *et al.*, 2015). There are many studies in the areas of environmental and industrial microbiology which have explored unculturable organisms with the objective of interpreting molecular information and correlating this information with bacterial composition (Kumar *et al.*, 2015). For uncategorised bacteria identification, use of spectroscopic techniques are still challenging and require a well- established biomolecular database acquired from previously studied cultivable microbes to be used as a references for unculturable organisms (Kumar *et al.*, 2015).

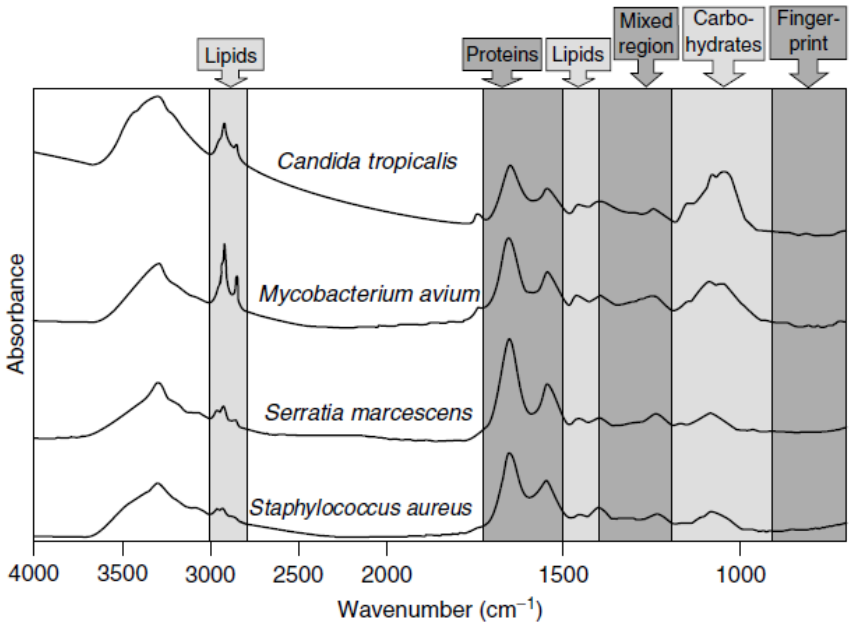

Figure 8. IR spectra for different microorganisms with characteristics absorption bands for each species adapted from Wenning *et al.* (2008).

Smears of cells and harvested colonies from microbiological samples can be measured by spectroscopy with less than 6 h incubation to give rapid and direct identification (Maquelin *et al.*, 2003, Wenning *et al.*, 2008). Therefore, there is a need to improve diagnostic techniques in general using various techniques such as spectroscopy that provide information and discrimination to microorganism *in-situ* and in their environment.

1.2.2 Application of FTIR to study the effects of antibiotics on bacterial cells

Generating chemical fingerprint for single-cells could be an approach to widen the knowledge in bacterial species and for identification *in situ* (Naumann, 2006) (Martin *et al.*, 2010). FTIR spectroscopy is believed to have the ability to provide a non-destructive and non-invasive spectroscopic technique for the analysis and provision of phenotypic classification for bacterial cells (Davis and Mauer, 2010). This application has great potential for food and pharmaceutical microbiology by studying differences in physiology within a single species (Naumann, 2006).

Metabolic changes which occur by external or internal effects on bacterial cells can be detected by observing FTIR spectra changes and also offer insights into the antibiotic effects on a bacterial cell (Maquelin *et al.*, 2002, Sockalingum *et al.*, 1997). Suci et al. group (1994) studied the effect of ciprofloxacin on bacterial growth and biofilm formation using ATR-FTIR spectroscopy and demonstrated this technique as a good approach to study the effects of antibiotics on bacterial cells. The interaction of the antibacterial drug with its target within the cell can be monitored by small changes in spectral features.

1.2.21 Sampling methods for the microbial chemical identification and spectral acquisition by FTIR spectroscopy

Microbiological samples should be handled carefully before acquisition of the IR spectra to avoid inconsistency of the IR spectra due to variable growth and sampling differences (Naumann, 2006). Solid samples or liquid suspension can be used and growth conditions of the microorganisms must be optimised to obtain consistent IR acquisition. Growth conditions of the cultures prior to IR measurement can influence the chemical composition. Major changes in chemical composition and therefore spectra can be influenced by the culture conditions and may impact on the quality and characteristics of the peaks (Maquelin *et al.*, 2002, Naumann, 2006). Culturing conditions such as temperature, culture media and incubation time are all factors that influence the microbial cell's growth and these factors should be standardised to reduce the influence on spectra prior the FTIR spectral acquisition. Incubation time is also an important determinant of heterogeneity of the molecular and metabolic composition of the microbial cells (Maquelin *et al.*, 2002, Maquelin *et al.*, 2003, Wenning *et al.*, 2008). For example, solid microcolonies of *S. aureus*, *E. coli* and *C. albicans* grown on culture plate exhibited active molecular and metabolic processes in a stationary phase. There is less variability of the metabolic composition such as glycogen levels during early stages of culture time for the microcolony (6 or 8 h) (Choo-Smith *et al.*, 2001).

Two methods have been used for preparation of microbiological samples for FTIR and Raman spectroscopy. The microbial colonies can be collected directly from the solid culture media and transferred onto substrate. The solid sample slice can then be mounted on infrared transparent disc such as ZnSe or CaF_2 with a certain diameter and thickness suitable for the sample investigation (Naumann, 2006). One sampling

method called special stamping devices has been used by spotting bacterial colonies onto microarrays and transferring the colonies onto IR crystal (Mossoba *et al.*, 2005). The other method is to prepare the sample from liquid nutrient media which requires drying of the aqueous solution to avoid FTIR sensitivity to aqueous media. The liquid media can be prepared from standardised number of colony forming units (CFU) which contain a few hundred cells and dried to produce a thin film on the transparent slides that are applicable for IR analysis. Other samples can be applied directly without growth such as saliva or blood to detect pathological changes within these samples (Baker *et al.*, 2014). These sampling methods permit the detection, identification, analysis and differentiation of the microbiological materials within one working day. Development in these sampling methods for FTIR spectroscopy offers great potential for rapid diagnostic microbiology.

1.2.3 FTIR microspectroscopy

The sample using the FTIR microscope can be viewed using binoculars or a digital image through a video camera. This allows optimisation of the position of the sample, the aperture, and supports mapping of the sample through the use of a motorised sample stage. Immersion optics are almost never used for IR spectroscopy because it has IR absorption (Griffiths, 2009b).

1.2.3.1 Hyperspectral images and spectral dataset by FTIR microspectroscopy

Vibrational microspectroscopy can be accomplished in two ways; mapping or imaging. Both are now described in turn. Mapping involves measurement of regions on the samples that are defined by an aperture which are then arranged sequentially in the xy plane. The sequential map measurement is achieved by moving each region of

the sample into the beam focus of the microscope after measuring the spectrum from previous region. The aperture size will depend on the sample features but generally range from 5-150 μm. The lower end of the aperture size is limited by the light diffraction (d) and for IR microscopy d approximately equals λ (light wavelength). In a typical IR spectrum ranging from 4000-800 cm^{-1} λ = 2.5-25.5 μm. Sensitive liquid nitrogen cooled mercury cadmium telluride (MCT) detectors are used for mapping measurements. The resulting map is called a hyperspectral map where each pixel contains the information of the IR spectrum which then can be used for highly specific chemical fingerprinting (Wenning and Scherer, 2013). Hyperspectral mapping can also be obtained by Raman spectroscopy which is a light scattering technique. Imaging requires an area of the sample to be focused onto an array detector to produce a hyperspectral image. Like sequential mapping, each pixel of the hyperspectral images contains the IR spectral information. To visualise these data sets a false colour map can be produced to highlight certain spectral features. An example of an IR image using a heat map colours to highlight specific spectral integration areas of a biological sample is illustrated in Fig. 9.

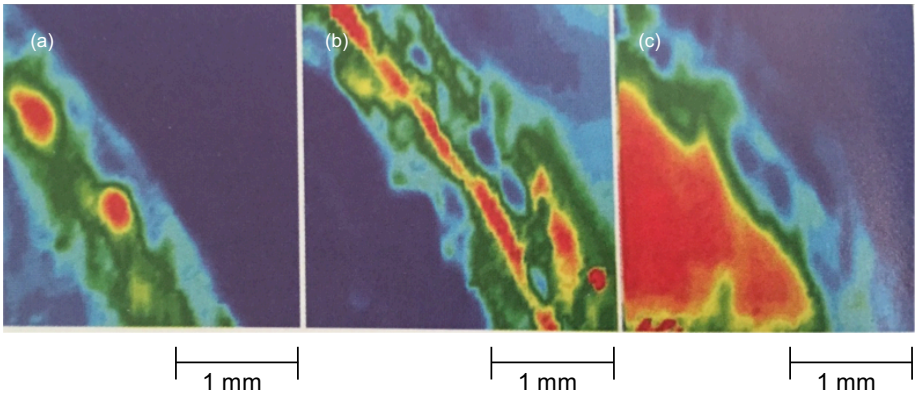

Figure 9. IR hyperspectral image for biological sample by FPA (a) amide I integration band area image; (b) & (c) carbohydrate band area. Adopted from Reeder *et al.* (1999).

FPA detectors are employed to cover pixel array between 16×16 and 128×128 pixels and are highly sensitive which provide faster scan ability. Each grid position of FPA detector displays an IR spectrum corresponding to the sample (see Fig. 9). The microscope optics and the geometry of the FPA usually predetermine the pixel size and is usually around 2.7 x 2.7 μm. The hyperspectral data can then be displayed as a false colour grid which is constructed based on the IR intensity and ratios of the functional group distribution. The example in Fig. 10 shows the protein amide I band integration.

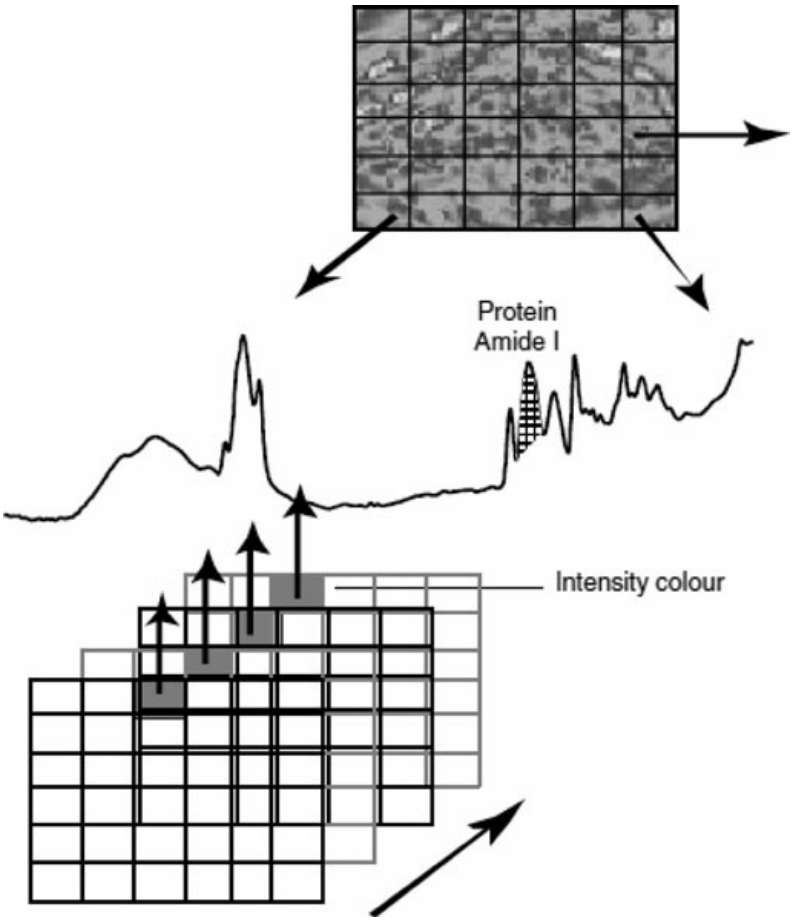

Figure 10. Focal plane array imaging that show multiple grids where each grid presents a spectrum. Adopted from Bunaciu *et al.* (2014).

Transmission and reflectance are two modes used for FTIR microspectroscopy (Wenning and Scherer, 2013, Alvarez-Ordóñez and Prieto, 2012). The development of detectors has resulted in improved signal-to-noise ratio to produce high quality spectral data and along with improved computational analysis of the spectra, the data can be used to distinguish features of microbiological samples (Wenning *et al.*, 2008). FTIR microspectroscopy is believed to be more informative than conventional FTIR spectroscopy (Wenning *et al.*, 2008). For identification of microorganisms, FTIR microspectroscopy has some advantages over conventional spectroscopy by allowing identification of microbe cells at the strain level with short incubation time and rapid discrimination of mixed samples (Ngo-Thi *et al.*, 2003, Wenning *et al.*, 2008). Sandet group (2006) used FTIR microspectroscopy to map microcolonies and claimed that Gram positives were classified with 100% accuracy and Gram negative with 80% accuracy. FTIR mapping and analysis of mixed cultures is developing toward accurate identification and classification of the microorganisms with a fully automated IR microscopic system (Wenning *et al.*, 2008). However, it is a new avenue for rapid identification in microbiological applications. FTIR spectroscopic imaging also allows the analysis of chemical components spatial distribution in the biological samples such as bacterial biofilm. This is a promising tool in studying the chemical heterogeneity across small sizes samples range from mm to μm.

1.2.3.2 Spectral pre-processing and multivariate analysis for the hyperspectral image

The analysis of FTIR spectroscopic data of biological compounds is not straightforward as the complexity of the data has a major effect on analysing and resolving specific spectra. There is significant overlap in infrared absorption peaks of the different molecular functional groups in biological samples. The hyperspectral

images result in large spectral data sets with a clear need for tools to identify spectral features and to be able to extract interpretable information. Spectral pre-processing of the hyperspectral data is a great way to resolve overlapping peaks and second derivatives are the commonly used for spectral analysis (Baker *et al.*, 2014). Second derivatives allow more specific identification of small overlapped absorption peaks that are not easily determined in original spectrum. Therefore, second derivatives offer means to increase the specificity of absorption peaks for certain molecules of the sample. On one hand, the second derivative offers a practical and more specific method for spectral analysis methods with FTIR imaging of biological samples (Rieppo *et al.*, 2012), but on the other hand it has the disadvantage that it can cause a significant loss in the signal-to-noise ratio. Consequently there is a need for high quality FTIR spectroscopic data. Many previous FTIR spectral data were not useful for image analysis due to poor signal-to-noise ratio (Mark and Workman Jr, 2003). Increasing both the spectral quality and the signal-to-noise ratio have been recent technological developments. Data normalisation is also used for chemical imaging to reduce the influence of confounding factors such as variation in thickness of the sample, and to highlight differences in biochemical structure. Vector normalisation is often used for biological sample pre-processing and it is performed after differentiation of spectra (Baker *et al.*, 2014).

1.2.4.2.1 Principal Component Analysis (PCA)

The most widely used method for multivariate analysis is principal component analysis (PCA). It involves decomposing the data matrix in order to detect and find a "pattern" or "hidden phenomena" (Esbensen *et al.*, 2002). The largest variances within the data matrix are reduced by performing PCA, and main variances are

condensed to principle components (Wehrli *et al.,* 2013). The number of principal components (PCs) needed to describe an image data set reflect the number of chemical constituents of the image and the pure spectra (de Juan *et al.,* 2009). Statistically a principle component analysis deconstructs the data into Eigenvalues and Eigenvectors. The numbers of score values (Eigenvalues) are represented by false colour pixels providing information about the spatial distribution of chemical composition where pixels that have similar score values for a given PC are shown in the same colour. Score maps for PCs provide perception at which area of the image relates to the feature. 2-D scatter plots of the scores illustrate the variation of individual spectra without spatial information where the two chosen principal components are the x and y axis. A scatter plot produced using a combination of two PCs is shown in Fig. 11.

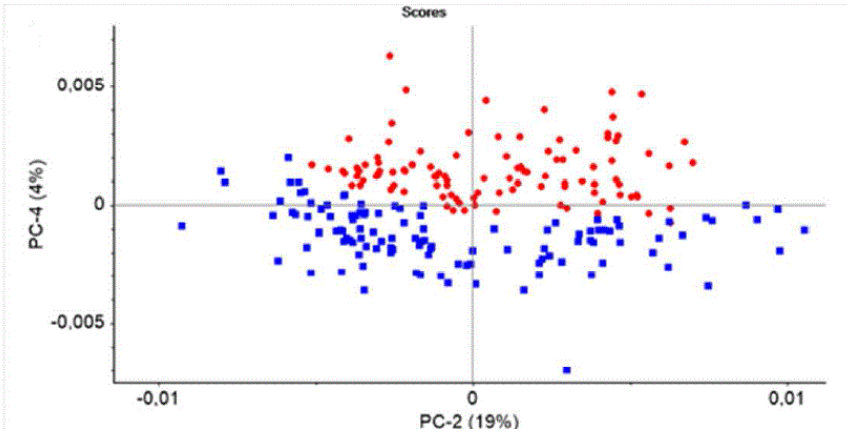

Figure 11. Score plot shows two groups of second derivatives spectra represented as two colour dots (red and blue) within two dimensional axes (PC4 and PC2) adopted from Staniszewska-Selzak *et al.* (2015).

Loading plots resulting from the PCA analysis (Eigenvectors) highlight the relevant spectral features that are responsible for the variation between the different measurement points (see Fig. 12).

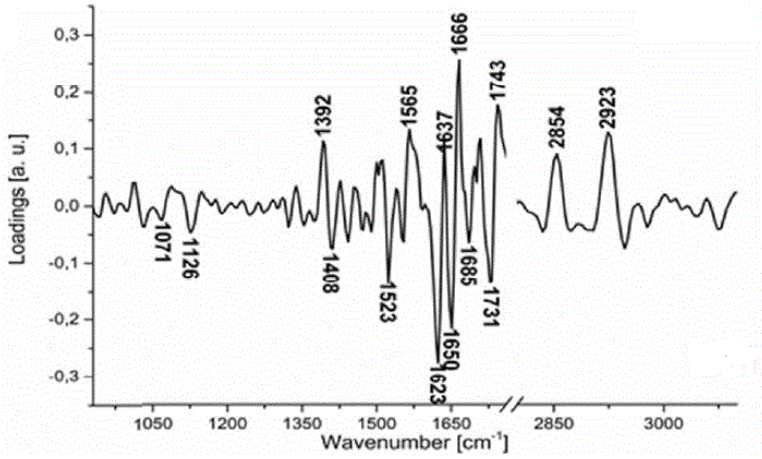

Figure 12. Loading plot corresponding to the PC4 of Figure 10. This loading plot shows the spectral features clustered by the PCA. Adopted from Staniszewska-Selzak *et al.* (2015).

1.2.3.2.2 Hierarchical Cluster Analysis (HCA)

Hierarchical Cluster Analysis (HCA) is a powerful unsupervised method of data sorting. It is based on finding the smallest distances of difference between elements present in the spectral data in hyperspectral images. The distance between the spectra data, based on local decision criteria, is presented as a dendrogram (Diem *et al.*, 2009). The term distance may imply Euclidean or correlation coefficient. This HCA does not produce an image, but it shows pseudo-colour maps of the hyperspectral data collected from the sample (Diem *et al.*, 2009). This HCA cluster map illustrates the clusters of the data according to the features identified similar to each other depending on distance of the differences. The dendrogram is used to show spectral distance differences and classify the groups into clusters. In microbiology, the HCA was used for identification and classification of bacterial species and strains level illustrated in Fig. 13.

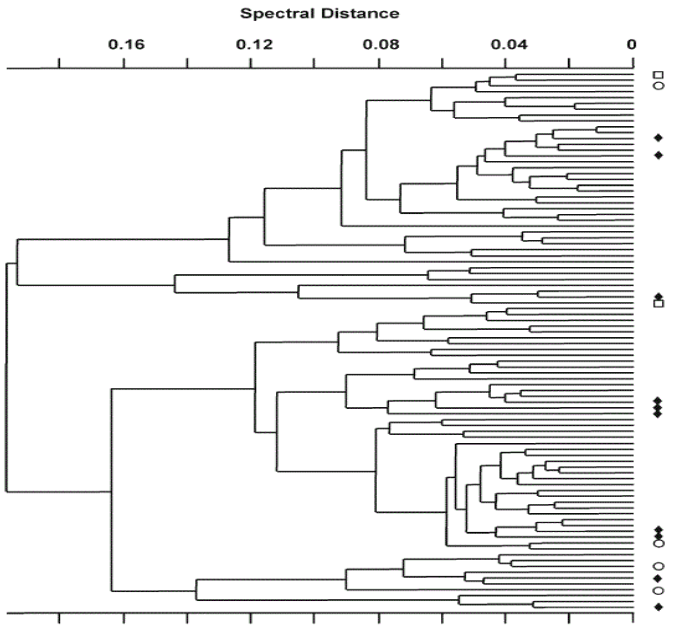

Figure 13. Dendrogram from hierarchical cluster analysis of 46 bacterial strains identified by symbols at the right side of the graph. This HCA was calculated by first derivatives and cluster of the spectra based on chemical features of these strains. This dendrogram adopted from Wenning and Scherer (2013).

1.2.4 Potential advantages of applying FTIR spectroscopy to biofilm

Studying bacterial cells at different growth phases and metabolic changes by FTIR microspectroscopy enables the determination of changes in chemical compositions. These changes reflect fluctuations in bacterial metabolite and reveal the molecular basis of biofilm formation and give an understanding of the bacterial cellular aggregation mechanisms (Huang *et al.*, 2010). Biofilm is a sessile bacterial aggregation on a surface and it can be heterogeneous or homogeneous in regards to bacterial cell species inclusion within one biofilm structure (Christensen *et al.*, 1982). The main characteristics of this organic material in EPS is polysaccharides but also substantial amount of protein, nucleic acids and lipids as shown in Table 2.1. Development of biofilm and secretion of the EPS is viewed as a staged process that expresses metabolic changes, stress response and biological activities which generate chemical gradients (Watnick and And Kolter, 2000, Stewart and Franklin, 2008).

Studying bacterial biofilm using FTIR spectroscopy could provide information on the chemical composition of the biofilm and the effect of external factors on its composition. It may identify biomarkers for diagnostic or treatment purposes. This type of investigation will be undertaken within an exploratory framework which involves both pattern finding and investigating changes in biomolecules.

Table 2.1 Chemical composition of biofilm. Adapted from Denkhaus *et al.* (2007).

Extracellular polymeric substances (EPS)

– Cationic groups in amino sugars and proteins

(e.g. $NH3^{+}$)

– Anionic groups in uronic acid, proteins, and nucleic acids

(e.g. COO^{-}; HPO_4^{-})

– Apolar groups from proteins (such as in aromatic amino acids),

phospholipids, and humic substances

Microbial cell

Outer membrane: lipopolysaccharides of Gram-negative cells

– Cell wall consisting of N-acetylglucosamine and N-acetylmuramic

acid, offering cationic and anionic sites, and the lipoteichoic acids

in Gram-positive cells

Cytoplasmic membrane, offering a lipophilic region

– Cytoplasm, as a water phase separated from the surrounding water

Minerals

– Precipitates (sulfides, carbonates, phosphates, hydroxides)

– Free and bound metals (Ca_2^{+}, Fe_3^{+}, Mg_2^{+})

Biogenic particulate materials (degradation products)

Environmentally relevant substances

– Organic pollutants (e.g. biocides, detergents, xenobiotics)

– Inorganic pollutants (e.g. heavy metals)

The most widely used FTIR approach to study whole bacterial cells and biofilm is the ATR-IR spectroscopy (Denkhaus *et al*., 2007). To characterise the structure and the chemistry of biofilms in vitro, combination of FTIR spectroscopy with microscopy has been used earlier in the field of introducing spectroscopic studies for biofilm (Suci *et al.*, 1997). From FTIR microspectroscopy, IR spectral maps of the biofilm will provide chemical information to give insights related to biological mechanisms or the metabolic processes occurring during different biofilm formation stages (Pink *et al.*, 2004, Vertes *et al.*, 2012, Holman *et al.*, 2009).

Identification of morphological changes of the biofilm may be correlated to differences in chemical makeup of the cellular component and the structural biomolecules of biofilm. These investigations can be performed without staining or labelling with probes, to reveal chemical processes within the intracellular structure (Holman *et al.*, 2009, Trevisan *et al.*, 2012). IR absorption bands correspond to lipids, proteins, nucleic acids and polysaccharides. Lipid contents can be observed mainly from the CH_2, CH_3 bands which are seen mainly at the CH stretching region from (3000-2830 cm^{-1}), protein content is seen in the area of amide I (1730-1590 cm^{-1}), amide II (1590-1490 cm^{-1}), amide III with nucleic acid bands from P=O (1280-1190), and DNA/RNA chemical compound information (1490–1000 cm^{-1}). The carbohydrate band for the polysaccharide profile can also be observed from 1140 to 950 cm^{-1} (Naumann, 2006, Burgula *et al.*, 2007).

Furthermore, some specific bands such as in the amide and polysaccharides regions can be considered as a marker for changes and intensities of protein development and modification in the sample analysed (Serra *et al.*, 2007). Pink *et al.* (2004)

investigated the region from 1500 to 1180 cm^{-1} where an excess of protein during *Pseudomonas aeruginosa* biofilm development was observed. The study concluded that amide II and III in biofilm could not be completely accounted for due to changes in the protein contents but showed an accumulation of protein near the attachment surface.

Investigating chemical components and functional groups that play important roles in biofilm construction is extremely difficult by optical microscopy and staining methods, however, FTIR and Raman spectroscopy provide a constantly developing frontier with improvements in many aspects of analysis of biofilm samples.

1.3 Rationale and Objectives

The main objective of this thesis is to understand the biofilm formation behaviour of NTHi isolates *in vitro*, to study the variations of chemical constituents, and the contribution of NTHi biofilm to pathogenicity. In order to achieve this, firstly, a semi-quantitative bacterial model of biofilm formation will be developed and validated *in vitro*. This model will be used to investigate determinants that may affect *in vitro* NTHi biofilm formation. This model will be used to investigate the biofilm forming ability of 60 strains selected from normal flora, clinical isolates from patients with otitis media (OM), from the lungs of infected cystic fibrosis (CF) patients as well as patients with lower respiratory tract infection, isolates from the eyes of patients with conjunctivitis, as well as from oropharyngeal normal flora (NF), and oropharyngeal normal flora isolates of *Haemophilus haemolyticus* (*H. haemolyticus*) .

Generating FTIR spectra coupled with hyperspectral imaging for selected biofilms will be used to produce a chemical fingerprint of biofilm composition. Characteristic FTIR spectra for high and low biofilm producing strains will be investigated. Spectral information will be used to study cells that are adhered to abiotic surfaces using this non-destructive technique for quantitative characterisation of NTHi biofilm. The spatial distribution of NTHi mature biofilm specific macromolecules and exploration of the chemical heterogeneity of biofilm has not been performed until now.

Analysis of antibiotic treated biofilm by FTIR microspectroscopy and comparison of the changes in spectral information with untreated biofilm will also be undertaken in this project. To our knowledge, NTHi biofilm treated with antibiotics has not been studied by vibrational spectroscopic approaches and will be investigate along with a MTP method for quantitation.

Biofilm chemical components are thought to be related to the variability of biofilm formation on a small scale (mm to μm) which could contribute to pathogesis and persistence of the NTHi biofilm. Biofilm research is expanding due to technological advances in spectroscopic methods yet is still in its infancy because of the complex and heterogeneous 3D properties of biofilm structure. Spectral microscopy studies on chemical distribution and biochemical composition of bacterial cells and EPS of biofilm will offer an insight into the mechanism of biofilm formation and physiochemical properties of NTHi biofilm.

1.4 References

Allison, D, G, 2003. 'The biofilm matrix'. Biofouling, 19, 139-150.

Alvarez-Ordonez, A, Mouwen, D, Lopez, M & Prieto, M, 2011. 'Fourier transform infrared spectroscopy as a tool to characterize molecular composition and stress response in foodborne pathogenic bacteria'. *Journal of Microbiological Methods,* 84**,** 369-378.

Alvarez-Ordóñez, A & Prieto, M, 2012. 'Technical and Methodological Aspects of Fourier Transform Infrared Spectroscopy in Food Microbiology Research'. *Fourier Transform Infrared Spectroscopy in Food Microbiology.* Springer.

Anderl, J N, Franklin, M J & Stewart, P S, 2000. 'Role of antibiotic penetration in Klebsiella pneumoniae biofilm resistance to ampicillin and ciprofloxacin'. *Antimicrobial Agents and Chemotherapy,* 44**,** 1818-1824.

Anderl, J N, Zahller, J, Roe, F & Stewart, P S, 2003. 'Role of nutrient and stationary-phase existence in Klebsiella pneumoniae biofilm resistance to ampicillin and ciprofloxacin'. *Antimicrobial Agents and Chemotherapy,* 47**,** 1251-1256.

Anderson, C R, 2013. 'Infrared-Absorbing Gases and the Earth's Surface Temperature:A Relatively Simple Baseline Evaluation of the Physics'. *Infrared-Absorbing Gases and the Earth's Surface Temperature* [Online]

Armbruster, C,E, Hong, W, Pang, B, Dew, K,E, Juneau, R,A,, Byrd, M,S, Love, C.F, Kock, N,D, and Swords, W,E, 2009. 'LuxS promotes biofilm maturation and persistence of nontypeable Haemophilus influenzae in vivo via modulation of lipooligosaccharides on the bacterial surface.' *Infection and immunity*, 77, 4081-4091.

Baker, M J, Trevisan, J, Bassan, P, Bhargava, R, Butler, H J, Dorling, K M, Fielden, P R, Fogarty, S W, Fullwood, N J & Heys, K A, 2014. 'Using Fourier transform IR spectroscopy to analyze biological materials'. *Nature Protocols,* 9**,** 1771-1791.

Balestrino, D, Souweine, B, Charbonnel, N, Lautrette, A, Aumeran, C, Traore, O & Forestier, C, 2009. 'Eradication of microorganisms embedded in biofilm by an ethanol-based catheter lock solution'. *Nephrology Dialysis transplantation,* 24**,** 3204-3209.

Bakaletz, L,O, White, G,J, Post, J,C, and Ehrlich, G,D, 1998. 'Blinded multiplex PCR analyses of middle ear and nasopharyngeal fluids from chinchilla models of single- and mixed-pathogen-induced otitis media.' *Clinical and Diagnostic Laboratory Immunology*, 5, 219-224.

Beenken, K, E, Blevins, J, S, & Smeltzer, M, S, 2003. 'Mutation of sarA in Staphylococcus aureus limits biofilm formation.' *Infection and Immunity*,71, 4206-4211.

Beloin, C, Roux, A. & Ghigo, J M, 2008. 'Escherichia Coli Biofilm' *Current Topic in Microbiology and Immunology*, 322, 249-289.

Bendouah, Z, Barbeau, J, Hamad, W, A, & Desrosiers, M, 2006. 'Biofilm formation by Staphylococcus aureus and Pseudomonas aeruginosa is associated with an unfavorable evolution after surgery for chronic sinusitis and nasal polyposis.' *Otolaryngology Head and Neck Surgery*, 134, 991-996.

Bjarnsholt, T, Jensen, P Ø, Burmølle, M, Hentzer, M, Haagensen, J J, Hougen, H P, Calum, H, Madsen, K G, Moser, C & Molin, S, 2005. 'Pseudomonas aeruginosa

tolerance to tobramycin, hydrogen peroxide and polymorphonuclear leukocytes is quorum-sensing dependent'. *Microbiology,* 151**,** 373-383.

Bjarnsholt, T, Jensen, P, Ø, Fiandaca, M, J, Pedersen, J, Hansen, C, R, Andersen, C, B, & Høiby, N, 2009. 'Pseudomonas aeruginosa biofilms in the respiratory tract of cystic fibrosis patients.' *Pediatric pulmonology*, 44, 547-558.

Bouchet, V, D W , Hood, J, Li, J R, Brisson, G A, Randle, A, Martin, Z, Li, R, Goldstein, E K, Schweda, S I, Pelton, J C & Richards, A, 2003. 'Host-derived sialic acid is incorporated into Haemophilus influenzae lipopolysaccharide and is a major virulence factor in experimental otitis media'. *National Academy of Sciences in USA,* 100**,** 8898–8903.

Bunaciu, A A, Fleschin, S & Aboul-Enein, H Y, 2014. 'Biomedical Investigations Using Fourier Transform-Infrared Microspectroscopy'. *Critical Reviews in Analytical Chemistry,* 44**,** 270-276.

Burgula, Y, Khali, D, Kim, S, Krishnan, S, Cousin, M, Gore, J, Reuhs, B & Mauer, L, 2007. 'Review Of Mid-Infrared Fourier Transform Infrared Spectroscopy Applications For Bacterial Detection'. *Journal of Rapid Methods & Automation in Microbiology,* 15**,** 146-175.

Childs, S G, 2008. 'Biofilm: Pathogenesis of Slime Glycocalyx'. *Orthopedic Nursing,* 27**,** 361-369.

Choo-Smith, L P, Maquelin, K ,.Van Vreeswijk, T., Bruining, H, Puppels, G, Thi, N N, Kirschner, C, Naumann, D, Ami, D & Villa, A, 2001. 'Investigating microbial (micro) colony heterogeneity by vibrational spectroscopy'. *Applied and Environmental Microbiology,* 67**,** 1461-1469.

Christensen, G, Simpson, W A, Bisno, A L & Beachey, E, 1982. 'Adherence of slime-producing strains of Staphylococcus epidermidis to smooth surfaces'. *Infection and Immunity,* 37**,** 318-326.

Christensen, G D, Simpson, W, Younger, J, Baddour, L, Barrett, F ,.Melton, D & Beachey, E, 1985. 'Adherence of coagulase-negative staphylococci to plastic tissue culture plates: a quantitative model for the adherence of staphylococci to medical devices'. *Journal of Clinical Microbiology,* 22**,** 996-1006.

Costerton, J, W, Cheng, K, J, Geesey, G, G, Ladd, T, I, Nickel, J, C, Dasgupta, M, & Marrie, T, J, 1987. 'Bacterial biofilms in nature and disease.' *Annual Reviews in Microbiology*, 41, 435-464.

Costerton, W, Veeh, R, Shirtliff, M, Pasmore, M, Post, C & Ehrlich, G, 2003. 'The application of biofilm science to the study and control of chronic bacterial infections'. *Journal of Clinical Investigation,* 112**,** 1466.

Crusz, S,A, Popat, R, Rybtke, M,T, Cámara, M, Givskov, M, Tolker-Nielsen, T, Diggle, S,P, and Williams, P, 2012. 'Bursting the bubble on bacterial biofilms: a flow cell methodology.' *Biofouling*, 28, 835-842.

Davies, D, G, Parsek, M, R, Pearson, J, P, Iglewski, B, H, Costerton, J, W, & Greenberg, E, P, 1998. 'The involvement of cell-to-cell signals in the development of a bacterial biofilm.' *Science*, 280, 295-298.

Davis, R & Mauer, L, 2010. 'Fourier transform infrared (FT-IR) spectroscopy: a rapid tool for detection and analysis of foodborne pathogenic bacteria'. *Current Research, Technology and Education Topics in Applied Microbiology and Microbial Biotechnology***,** 1582-1594.

De Jaun, A, Maeder, M, Hancewicz, T, Duponchel, L, And & Tauler, R A, 2009. 'Chemometric Tools for Image Analysis. *In:* Salzer, R. & Siesler, H. W. (eds.) *Infrared and Raman Spectroscopic Imaging.* Wiley Online Library.

Denkhaus ,E, Meisen, S, Telgheder, U & Wingender, J, 2007. 'Chemical and physical methods for characterisation of biofilms'. *Microchimica Acta,* 158**,** 1-27.

Diem, M, Matthaus, C, Chernenko, T, Romeo, M J, Miljkovic, M, Bird, B, Schubert, J, Papamarkais, K & Laver, N (eds.) 2009. *Infrared and Raman Spectroscopy and Spectral Imaging of Individual Cells,* Weinheim, Germany: Wiley-VCH Verlag GmbH & Co .

Donlan, R, M, 2000. 'Role of biofilms in antimicrobial resistance'. Asaio Journal, 46, S47-S52.

Donlan, R M & Costerton, J W, 2002. 'Biofilms: survival mechanisms of clinically relevant microorganisms'. *Clinical Microbiology Reviews,* 15**,** 167-193.

Ellis, D I & Goodacre, R, 2006. 'Metabolic fingerprinting in disease diagnosis: biomedical applications of infrared and Raman spectroscopy'. *Analyst,* 131**,** 875-885.

Erwin, A L & Smith, A L, 2007. 'Nontypeable Haemophilus influenzae: understanding virulence and commensal behavior'. *Trends in Microbiology,* 15**,** 355-362.

Esbensen, K H, Guyot, D, Westad, F & Houmoller, L P, 2002. 'Multivariate data analysis-in practice: an introduction to multivariate data analysis and experimental design'. *Multivariate Data Analysis*, 5th edition.

Flemming, H C & Wingender, J, 2010. 'The biofilm matrix'. *Nature Reviews Microbiology,* 8**,** 623-633.

Gjødsbøl, K, Christensen, J, J, Karlsmark, T, Jørgensen, B, Klein, B, M, & Krogfelt, K, A, 2006. 'Multiple bacterial species reside in chronic wounds: a longitudinal study.' *International wound journal*, 3, 225-231.

Griffiths, P R (ed.) 2009. *Infrared and Raman Instrumentation for Mapping and Imaging,* Weinheim, Germany: Wiley-VCH Verlag GmbH & Co.

Hall-Stoodley, L & Stoodley, P, 2009. 'Evolving Concepts in Biofilm Infections'. *Cellular Microbiology,* 11**,** 1034-1043.

Hall-Stoodley, L, Hu, F, Z,, Gieseke, A, Nistico, L, Nguyen, D, Hayes, J, Forbes, M, Greenberg, D, P, Dice, B, & Burrows, A. 2006.' Direct detection of bacterial biofilms on the middle-ear mucosa of children with chronic otitis media'. *The Journal of the American Medical Associaion*, 296, 202-211.

Harrison, J J, Stremick, C A, Turner, R J, Allan, N D, Olson ,M E & Ceri, H, 2010. 'Microtiter susceptibility testing of microbes growing on peg lids: a miniaturized biofilm model for high-throughput screening'. *Nature Protocols,* 5**,** 1236-1254.

Hentzer, M, Teitzel, G, M, Balzer, G, J, Heydorn, A, Molin, S, Givskov, M, & Parsek, M, R, 2001. 'Alginate overproduction affects Pseudomonas aeruginosa biofilm structure and function.' *Journal of bacteriology*, 183, 5395-5401.

Harz, M, Ro¨Sch, P & Popp, J, 2009. 'Vibrational Spectroscopy: Powerful Tool for the Rapid Identification of Microbial Cells at the Single-Cell Level'. *Cytometry,* 75**,** 104-113.

Holman, H , Miles, R, Hao, Z, Wozei, E, Anderson, L M & Yang, H, 2009. 'Real-time chemical imaging of bacterial activity in biofilms using open-channel microfluidics and synchrotron FTIR spectromicroscopy'. *Analytical Chemistry,* 81**,** 8564-8570.

Huang, W E, Griffiths, R I, Thompson, I P, Bailey, M J & Whiteley, A S, 2004. 'Raman microscopic analysis of single microbial cells'. *Analytical Chemistry,* 76**,** 4452-4458.

Huang, W E, Li, M, Jarvis, R M, Goodacre, R & Banwart, S A, 2010. 'Shining Light on the Microbial World: The Application of Raman Microspectroscopy'. *Advances in Applied Microbiology,* 70**,** 153-186.

Izano, E,A, Shah, S,M, and Kaplan, J,B, 2009. 'Intercellular adhesion and biocide resistance in nontypeable Haemophilus influenzae biofilms.' *Microbial pathogenesis*, 46, 207-213.

James, G, A, Swogger, E, Wolcott, R, Secor, P, Sestrich, J, Costerton, J, W, & Stewart, P, S, 2008. 'Biofilms in chronic wounds.' *Wound Repair and regeneration,* 16, 37-44.

Janknecht, P & Melo, L F, 2004. 'Online biofilm monitoring'. *Reviews in Environmental Science and Bio/Technology*, 2, 269-283.

Jensen, P Ø, Givskov, M, Bjarnsholt, T & Moser, C, 2010. 'The immune system vs. Pseudomonas aeruginosa biofilms'. *FEMS Immunology & Medical Microbiology*, 59, 292-305.

Jurcisek, J A & Bakaletz, L O, 2007. 'Biofilms Formed by Nontypeable *Haemophilus influenzae In Vivo* Contain both Double-Stranded DNA and Type IV Pilin Protein'. *Journal of Bacteriology*, 189, 3868-3874.

Kaji, C, Watanabe, K, Apicella, M A & Watanabe, H, 2008. 'Antimicrobial effect of fluoroquinolones for the eradication of nontypeable Haemophilus influenzae isolates within biofilms'. *The Tohoku Journal of Experimental Medicine*, 214, 121-128.

Kellner, R (ed.) 1998. *Infrared and Raman Sectroscopy*: Wiley-VCH.

Kilár, A, Dörnyei, Á & Kocsis, B, 2013. 'Structural characterization of bacterial lipopolysaccharides with mass spectrometry and on-and off-line separation techniques'. *Mass Spectrometry Reviews,* 32**,** 90-117.

Kunthalert, D, Henghiranyawong, K, Sistayanarain, A, and Khoothiam, K, 2013. 'A single-step polymerase chain reaction for simultaneous detection and differentiation of nontypeable and serotypeable Haemophilus influenzae, Moraxella catarrhalis and Streptococcus pneumoniae.' *International Journal of Pediatric Otorhinolaryngology,* 77, 275-280.

Kumar, V, Kampe, B, Rösch, P, & Popp, J, 2015. 'Classification and identification of pigmented cocci bacteria relevant to the soil environment via Raman spectroscopy'. Environmental Science and Pollution Research, 1-9.

Langereis, J D. & Hermans, P W, 2013. 'Novel concepts in nontypeable Haemophilus influenzae biofilm formation'. *FEMS microbiology letters*, 346, 81-89.

Liaqat, I, Sumbal, F & Sabri, A N, 2009. 'Tetracycline and Chloramphenicol Efficiency Against Selected Biofilm Forming Bacteria'. *Current Microbiology,* 59**,** 212-220.

López, D, Vlamakis, H & Kolter, R, 2010. 'Biofilms'. *Cold Spring Harbor Perspectives in Biology,* 2**,** 1-11.

Lu, X, Al-Qadiri, H M, Lin, M & Rasco, B A, 2011. 'Application of Mid-infrared and Raman Spectroscopy to the Study of Bacteria'. *Food and Bioprocess Technology***,** 16, 919-935.

Mattila-Sandholm, T, & Wirtanen, G, 1992. 'Biofilm formation in the industry: a review.' *Food Reviews International*, 8, 573-603.

Maquelin, K, Kirschner, C, Choo-Smith, L P, Ngo-Thi, N, Van Vreeswijk, T, Stämmler, M, Endtz, H, Bruining, H, Naumann, D & Puppels, G, 2003. 'Prospective study of the performance of vibrational spectroscopies for rapid identification of bacterial and fungal pathogens recovered from blood cultures'. *Journal of Clinical Microbiology,* 41**,** 324-329.

Maquelin, K, Kirschner, C, Choo-Smith, L P, Van Den Braak, N, Endtz, H P, Naumann, D & Puppels, G, 2002. 'Identification of medically relevant microorganisms by vibrational spectroscopy'. *Journal of Microbiological Methods,* 51**,** 255-271.

Mark, H & Workman Jr, J, 2003. 'Chemometrics-Derivatives in Spectroscopy: Part II--The True Derivative'. *Spectroscopy-Eugene,* 18**,** 25-28.

Martin, F L, Kelly, J G., Llabjani, V, Martin-Hirsch, P L, Patel, I I, Trevisan, J, Fullwood, N J & Walsh, M J, 2010. 'Distinguishing cell types or populations based on the computational analysis of their infrared spectra'. *Nature Protocols*, 5, 1748-1760.

Mossoba, M M, Al-Khaldi, S F, Kirkwood, J, Fry, F S, Sedman, J & Ismail, A A, 2005. 'Printing microarrays of bacteria for identification by infrared microspectroscopy'. *Vibrational Spectroscopy,* 38**,** 229-235.

Moxon, E R, Sweetman, W A, Deadman, M E, Ferguson, D J & Hood, D W, 2008.

'Haemophilus Influenzae Biofilms: Hypothesis or Fact?'. *Trends in Microbiology*, 16, 95-100.

Münchberg, U, Klob, S, Kusic, D, Meisel, S, Heinke, R, Stöckel, S, Rösch, P & Popp, J, 2015. 'IR and Raman Spectroscopy for Pathogen Detection'. Modern Techniques for Pathogen Detection, 253-294.

Musk Jr, D & Hergenrother, P, 2006. 'Chemical Countermeasures for the Control of Bacterial Biofilms: Effective Compounds and Promising Targets'. *Current Medicinal Chemistry,* 13**,** 2163-2177.

Naumann, D, 2006. 'Infrared spectroscopy in microbiology'. *Encyclopedia of Analytical Chemistry*.

Ngo-Thi, N, Kirschner, C & Naumann, D, 2003. 'Characterization and identification of microorganisms by FT-IR microspectrometry'. *Journal of Molecular Structure,* 661**,** 371-380.

O'Toole, G, A, & Kolter, R, 1998. 'Flagellar and twitching motility are necessary for Pseudomonas aeruginosa biofilm development.' *Molecular microbiology*, 30, 295-304.

Pätzold, R, Keuntje, M & Anders-Von Ahlften, A, 2006. 'A new approach to non-destructive analysis of biofilms by confocal Raman microscopy'. *Analytical and Bioanalytical Chemistry,* 386**,** 286-292.

Patel, R' 2005. 'Biofilms and antimicrobial resistance'. Clinical orthopaedics and related research, 437, 41-47.

Peeters, E, Nelis, H, J, & Coenye, T, 2008. 'Comparison of multiple methods for quantification of microbial biofilms grown in microtiter plates'. Journal of microbiological methods, 72, 157-165.

Pink, J, Smith-Palmer, T, Beveridge, T & Pink, D, 2004. 'An FTIR study of Pseudomonas aeruginosa PAO 1 biofilm growth and dispersion. An improved ATR method for studying biofilms: the C–H stretch spectral region'. *Biofilms,* 1**,** 157-163.

Post, J,C, Aul, J,J, White, G,J, Wadowsky, R,M, Zavoral, T, Tabari, R, Kerber, B, Doyle, W,J, and Ehrlich, G,D, 1996. 'PCR-based detection of bacterial DNA after antimicrobial treatment is indicative of persistent, viable bacteria in the chinchilla model of otitis media.' *American Journal of Otolaryngology*, 17, 106-111.

Post, J C, 2001. 'Direct evidence of bacterial biofilms in otitis media'. *Laryngoscope*, 111, 2083-2094.

Reeder, C, Marcott, R C, Sweat, J A & Panzer, D D W, D L, 1999. 'FTIR spectroscopy imaging microscopy of wheat kernels using a mercury-cadmium-telluride focal-plane array'. *Vibrational Spectroscopy,* 19**,** 123-9.

Reid, D W, Carroll, V, O'may, C, Champion, A & And Kirov, S M, 2007. 'Increased Airway Iron as a Potential Factor in the Persistence of Pseudomonas aeruginosa Infection in Cystic Fibrosis'. *European Respiratory Journal,* 30**,** 286-292.

Rieppo, L, Saarakkala, S, Närhi, T, Helminen, H, Jurvelin, J & Rieppo, J, 2012. 'Application of second derivative spectroscopy for increasing molecular specificity of Fourier transform infrared spectroscopic imaging of articular cartilage'. *Osteoarthritis and Cartilage,* 20**,** 451-459.

Ružicka, F ,.Holá, V, Votava, M, Tejkalová, R, Horvát, R, Heroldová, M & Woznicová, V, 2004. 'Biofilm Detection and the Clinical Significance of Staphylococcus epidermidis Isolates'. *Folia Microbiology,* 49**,** 596-600.

Samek, O, Al-Marashi, J F M & Telle, H, H, 2009. 'The potential of Raman spectroscopy for the identification of biofilm formation by Staphylococcus epidermidis'. *Laser Physics*, 7, 378-383.

Sawhney, R & Berry, V, 2009. 'Bacterial biofilm formation, pathogenisity, diagnostic and control: An overview'. *Indian Journal of Medical Sciences*, 63, 313-321.

Schrader, B, 2008. *Infrared and Raman spectroscopy: methods and applications*, John Wiley & Sons.

Serra, D, Bosch, A, Russo, D M, Rodríguez, M E, Zorreguieta, Á, Schmitt, J, Naumann, D & Yantorno, O, 2007. 'Continuous nondestructive monitoring of Bordetella pertussis biofilms by Fourier transform infrared spectroscopy and other corroborative techniques'. *Analytical and Bioanalytical Chemistry,* 387, 1759-1767.

Slinger, R, Chan, F, Ferris, W, Yeung, S,W, Denis, M,S, Gaboury, I, and Aaron, S,D, 2006. 'Multiple combination antibiotic susceptibility testing of nontypeable

Haemophilus influenzae biofilms.' *Diagnostic Microbiology and Infectious Disease,* 56, 247-253.

Sockalingum, G, Bouhedja, W, Pina, P, Allouch, P, Mandray, C, Labia, R, Millot, J & Manfait, M, 1997. 'ATR–FTIR Spectroscopic Investigation of Imipenem-Susceptible and-Resistant Pseudomonas aeruginosa Isogenic Strains'. *Biochemical and Biophysical Research Communications,* 232**,** 240-246.

Souli, M., and H. Giamarellou. 1998. 'Effects of slime produced by clinical isolates of coagulase-negative staphylococci on activities of various antimicrobial agents.' *Antimicrobial Agents Chemotherapy*. 42, 939-941.

Staniszewska-Slezak, E, Fedorowicz, A, Kramkowski, K, Leszczynska, A, Chlopicki, S, Baranska, M & Malek, K, 2015. 'Plasma biomarkers of pulmonary hypertension identified by Fourier transform infrared spectroscopy and principal component analysis'. *Analyst,* 140**,** 2273-2279.

Starner, T D, Shrout, J D, Parsek, M R, Appelbaum, P C & Kim, G, 2008. 'Subinhibitory concentrations of azithromycin decrease nontypeable Haemophilus influenzae biofilm formation and diminish established biofilms'. *Antimicrobial Agents and Chemotherapy,* 52**,** 137-145.

Stepanović, S, Vuković, D, Hola, V, Bonaventura, G D I, Djukić, S, Ćirković, I & Ruzicka, F, 2007. 'Quantification of biofilm in microtiter plates: overview of testing conditions and practical recommendations for assessment of biofilm production by staphylococci'. *Apmis,* 115**,** 891-899.

Stewart, P S & Franklin, M J, 2008. 'Physiological Heterogeneity in Biofilm'. *Nature Review,* 6**,** 199-210.

Stoodley, P, Jørgensen, F, Williams, P, & Lappin-Scott, H, M, 1999. 'The role of hydrodynamics and AHL signalling molecules as determinants of the structure of Pseudomonas aeruginosa biofilms.'

Suci, P, Mittelman, M, Yu, F & Geesey, G, 1994. 'Investigation of ciprofloxacin penetration into Pseudomonas aeruginosa biofilms'. *Antimicrobial Agents and Chemotherapy,* 38**,** 2125-2133.

Suci, P, Siedlecki, K, Palmer, R, White, D & Geesey, G, 1997. 'Combined light microscopy and attenuated total reflection fourier transform infrared spectroscopy for integration of biofilm structure, distribution, and chemistry at solid-liquid interfaces'. *Applied and environmental microbiology,* 63**,** 4600-4603.

Sutherland, I, W, 2001. 'The biofilm matrix–an immobilized but dynamic microbial environment'. Trends in microbiology, 9, 222-227.

Swords, W E, 2012. 'Nontypeable Haemophilus influenzae biofilms: role in chronic airway infections'. *Frontiers in Cellular and Infection Microbiology,* 2.

Swords, W E, Moore, M L, Godzicki, L, Bukofzer, G, Mitten, M J & Voncannon, J, 2004. 'Sialylation of Lipooligosaccharides Promotes Biofilm Formation by Nontypeable Haemophilus influenzae'. *Infection and Immunity,* 72**,** 106-113.

Thi, N N & Naumann, D, 2007. 'Investigating the heterogeneity of cell growth in microbial colonies by FTIR microspectroscopy'. *Analytical and Bioanalytical Chemistry,* 387**,** 1769-1777.

Tolker-Nielsen, T & Sternberg, C, 2011. 'Growing and Analyzing Biofilms in Flow Chambers. *In:* Coico, R., Kowalik, T., Quarles, J., Stevenson, B. & Taylor, R. (eds.). *Current Protocols in Microbiology.* 21 ed.: Wiley online Library.

Trevisan, J, Angelov, P P, Carmichael, P L, Scott, A D & Martin, F L, 2012. 'Extracting biological information with computational analysis of Fourier-transform infrared (FTIR) biospectroscopy datasets: current practices to future perspectives'. *Analyst*, 137, 3202-3215.

Vertes, A, Hitchins, V & Phillips, K S, 2012. 'Analytical challenges of microbial biofilms on medical devices'. *Analytical Chemistry*, 84, 3858-3866.

Walters, M,C, Roe, F, Bugnicourt, A, Franklin, M,J, and Stewart, P,S, 2003. 'Contributions of antibiotic penetration, oxygen limitation, and low metabolic activity to tolerance of Pseudomonas aeruginosa biofilms to ciprofloxacin and tobramycin.' *Antimicrobial Agents and Chemotherapy*, 47, 317-323.

Wang, D, Wang, Y & Liu, Y N, 2009. 'Activity of ciprofloxacin and azithromycin on biofilms produced in vitro by Haemophilus influenzae'. *Chinese Medical Journal,* 122**,** 1305-1310.

Wang, L & Mizaikoff, B, 2008. 'Application of multivariate data-analysis techniques to biomedical diagnostics based on mid-infrared spectroscopy'. *Analytical and Bioanalytical Chemistry,* 391**,** 1641-1654.

Waters, C,M, and Bassler, B,L, 2005. 'Quorum sensing: cell-to-cell communication in bacteria.' *Annual Review of Cell and Developmental Biology*, 21,319-346.

Watnick, P & And Kolter, R, 2000. 'Biofilm, City of Microbes'. *Journal of Bacteriology,* 128**,** 2675-2679.

Watnick, P I & Kolter, R, 1999. 'Steps in the development of a Vibrio cholera biofilm'. *Molecular Microbiology,* 34**,** 586-595.

Webster, P, Wu, S, Gomez, G, Apicella, M, Plaut, A G & Geme Iii, J W S, 2006. 'Distribution of bacterial proteins in biofilms formed by non-typeable Haemophilus influenzae'. *Journal of Histochemistry & Cytochemistry,* 54**,** 829-842.

Wenning, M & Scherer, S, 2013. 'Identification of microorganisms by FTIR spectroscopy: perspectives and limitations of the method'. *Applied Microbiology and Biotechnology,* 97**,** 7111-7120.

Wenning, M, Scherer, S & Naumann, D, 2008. 'Infrared spectroscopy in the identification of microorganisms'. *Handbook of Vibrational Spectroscopy*.

Whitchurch, C B, Tolker-Nielsen, T, Ragas, P C & Mattick, J S, 2002. 'Extracellular DNA Required for Bacterial Biofilm Formation'. *Science,* 295**,** 1487.

Wiens, J,R, Vasil, A,I, Schurr, M,J, and Vasil, M,L, 2014. 'Iron-regulated expression of alginate production, mucoid phenotype, and biofilm formation by Pseudomonas aeruginosa.' MBio, 5(1), pp.e01010-13.

Yarwood, J, M, and Schlievert, P, M, 2003. 'Quorum sensing in Staphylococcus infections.' *Journal of Clinical Investigation.* 112, 1620–1625

Zhang, L, and Mah, T,F, 2008. 'Involvement of a novel efflux system in biofilm-specific resistance to antibiotics.' *Journal of Bacteriology.* 190, 4447–4452.

Chapter 2

Reliability of *Haemophilus influenzae* biofilm measurement via static method and determinants of in vitro biofilm production.

Abstract

Microtitre plate (MTP) assays used to measure biofilm are generally poorly described with regard to precision. This study investigated the precision of an MTP assay for biofilm production by Nontypeable *Haemophilus influenzae* (NTHi) and the effects of frozen storage and inoculation technique on biofilm production. The density of bacterial final growth (FG) was determined by absorbance after 18-20 hours incubation and biofilm production (BF) was then measured by absorbance after crystal violet staining. Biofilm formation was categorised as high and low for each strain. For the high biofilm producing strains of NTHi, inter-day reproducibility of NTHi biofilm formation measured using the MTP assay was excellent and met the acceptance criteria but higher variability was observed in low biofilm producers. Method of inoculum preparation was a determinant of biofilm formation with inoculum prepared directly from solid media showing increased biofilm production for at least one of the high producing strains. In general, storage of NTHi cultures at -80°C for up to 48 weeks did not have any major effect on their ability to produce biofilm.

2.1 Introduction

When planktonic bacteria aggregate and become part of a protected cellular community, they are termed a biofilm. Biofilm formation is a staged and circular process that is an inherent behavioural mechanism of some bacterial species (Costerton *et al.*, 1999, Hall-Stoodley and Stoodley, 2009).

Nontypeable *Haemophilus influenzae* bacteria (NTHi) are obligate commensals of the human upper respiratory tract from where they frequently act as opportunistic pathogens. Biofilm production by NTHi may be responsible for chronicity and recurrence of some acute infections, such as otitis media (OM) and exacerbation of chronic obstructive pulmonary disease (COPD), conditions that have provided most of the NTHi strains used for biofilm investigations (Hall-Stoodley and Stoodley, 2009, Murphy *et al.*, 2004, Murphy and Kirkham, 2002, Swords, 2012, Moriyama *et al.*, 2009).

In vitro assays of biofilms, based on microtitre plate (MTP) methods, have been developed over the past few decades (Christensen *et al.*, 1985, Stepanović *et al.*, 2000, Stepanović *et al.*, 2007, Coenye and Nelis, 2010). The biofilm adhered to the MTP is quantified by staining with crystal violet, a basic dye that binds to the biofilm matrix and attached cells. By comparison with various flow systems that have been developed (Goeres *et al.*, 2005) static systems are simpler, require less specialised equipment, are more rapid and less expensive (Coenye and Nelis, 2010) with the potential for automation (Sandberg *et al.*, 2008). The American Society for Testing and Materials recently approved the first standardised biofilm disinfectant efficacy test method, based on static culture of biofilm on peg lids that sit in MTP wells

(Harrison *et al.*, 2010, Parker *et al.*, 2014). This technique has been applied to NTHi strains from acute OM cases (Takei *et al.*, 2013) and CF and COPD isolates (Starner *et al.*, 2006). However, a robust method for the quantitation of biofilm produced by NTHi is still lacking.

A lack of standardisation of inoculum, insufficient calculation methods and a lack of reporting of intra- and inter-day replicate variation of quantitative biofilm methods are typically found missing in key literature. The lack of standardised methods makes any meaningful comparison of different quantitative studies difficult. Studies have reported substantial variability in the ability of clinical isolates of NTHi to form biofilm (Murphy and Kirkham, 2002, Webster *et al.*, 2006a), but inoculum was not standardised. Other studies reported variable NTHi biofilm production in vitro from different clinical isolates using standardised inoculum (Puig *et al.*, 2014, Wu *et al.*, 2014). Other work has described the use of a ratio termed the biofilm formation index (BFI). This is the ratio of biofilm produced by an NTHi isolate to the biofilm produced by a standard *Haemophilus influenzae* strain (Moriyama *et al.*, 2009). This approach has merit but is limited by its reliance on the reproducible production of biofilm by the control, which cannot be relied upon, given the fastidious nature of NTHi (Daines *et al.*, 2005). Determination of quantitative precision and reproducibility requires a number of replicates over different days, which is more readily achieved in a static system (Goeres *et al.*, 2005). More broadly, due to the lack of a reliable reported standardised methodology there is still considerable uncertainty as to the clinical significance of biofilms in the pathogenesis of NTHi infections.

The aim of this study was to develop and validate a reproducible and robust crystal violet MTP assay for the quantitative assessment of NTHi biofilm production using a small number of representative clinical isolates and standard strains, and to use this method to measure potential determinants of biofilm production, including isolate storage and inoculum preparation techniques.

2.2 Methods

2.2.1 Strains and culture condition

Two isolates of NTHi, comprising clinical isolates (A1 and A2) and two standard strains, ATCC 10211 and RdKW20 (A3 and A4 respectively), as well as *Pseudomonas aeruginosa* PAO1 as a positive control, were used for biofilm evaluation. The strains were stored in glycerol at -80°C and recovered by overnight culture followed by an additional overnight (16 h) passage prior to use in the assay. All cultures were carried out on chocolate agar (Oxoid, Adelaide, Australia) at 37°C under 5% CO_2. Additional NTHi clinical isolates were used for the investigation of storage, as described below. All clinical isolates were epidemiologically unrelated and were identified conclusively as *H. influenzae* using 16S rRNA sequencing.

2.2.2 Baseline biofilm assay

Strains A1-A4 were preliminarily screened for their ability to form biofilm using an in vitro MTP assay adapted from published methods (Murphy and Kirkham, 2002, Webster et al., 2006b). One colony from the overnight passage culture was inoculated into 10 ml pre-warmed brain heart infusion broth (Oxoid, Adelaide, Australia) supplemented with 40 µg/ml NAD and haemin and 2% v/v Vitox (Oxoid, Adelaide, Australia) (sBHI), and incubated for 22 h. A 1.5 ml aliquot of each broth was transferred into a plastic cuvette (Kartell, Milan, Italy) and the optical density was measured at 490 nm versus fresh sBHI. Based on this reading, each inoculum was standardised by dilution with sBHI to an optical density of 0.25-0.30 (~10^7 CFU/ml) which was confirmed by producing a growth curve of the counted colonies for NTHi against OD measurement. The final inoculum was prepared by adding 100 µl of the standardised broth to 10.0 ml of fresh sBHI (1:100). Diluted inoculum (2.0 ml) was transferred to wells (2.5 ml) of a 24-well non-treated sterile, polystyrene microtitre plate (MTP) (Costar, Corning Incorporated, New York, USA). Each MTP contained 4 NTHi strains, a positive control (PAO1) and a negative control (sBHI with no inoculum) in quadruplicate wells with a single plate. Plates were incubated at 37°C under 5% CO_2 for 22 h. After incubation, MTPs were cooled to room temperature and then covered with an adhesive film (Labtek, Brendale, Australia). The optical density of each well was read at 490 nm to give a value for final growth (FG).

MTPs were inverted to empty, and then washed with tap water (3x) and air dried at room temperature for 30 min. Crystal violet solution (0.1%, 2.0 ml) was added to each well and allowed to sit at room temperature for 15 min. MTPs were inverted to empty, washed with water (3x) and air dried at room temperature. Ethanol (95%, 2.0 ml) was

added to each well to solubilise the crystal violet that had adhered to the biofilm. The optical density of each well was read at 570 nm to give a value for biofilm formation (BF).

In total, 13 MTP assays were performed (with strains A1-A4, plus positive and negative controls) over five days. On days one to four, two MTP assays were performed, and on day five, five MTP assays were performed. Unless otherwise indicated (e.g., for the determination of a particular analytical performance), the FG, BF and BF/FG for each strain within a single MTP was taken as the mean of the individual values from the four individual wells. For management of outliers (such as contamination or no growth), an *a priori* protocol for exclusion was used whereby wells with a FG value more than ±2 standard deviations from the mean of each of the quadruplicate wells within a plate were excluded.

2.2.3 Outcome measures

Final growth (FG) was measured using turbidity of the bacterial suspension in the well as a measure of overall growth of biomass, however this can often be highly variable. Biofilm formed inside the wells determined by crystal violet staining was defined as absolute biofilm (BF). The ratio (BF/FG) was then calculated and defined as relative biofilm formation, normalising for bacterial growth.

2.2.4 Precision and reproducibility

Intra-day precision was assessed using the MTP results from day 5, and comparing the mean values (BF and BF/FG) for each strain from each of 5 MTPs (n=5). Inter-day precision was assessed using the MTP results from all 5 days, and comparing the

mean values (BF and BF/FG) for each strain from each of 13 MTPs (n=13). In order to determine if strains could be reliably placed into categories based on biofilm production (e.g. high or low), the 13 means from the inter-day precision assay were compared, with an acceptance criteria of ± 20% RSD arbitrarily assigned.

2.2.5 Effect of inoculum

A non-standardised inoculum was used to evaluate the importance of inoculum standardization on biofilm quantitation. Incubations were performed in a similar manner to that described above but without adjustment of the inoculum to an optical density of 0.25-0.3 prior to 1:100 dilution and incubation of all four strains.

To evaluate the importance of inoculum pre-culture in liquid broth, the inocula was prepared from a culture off chocolate agar solid media. The inocula was standardised to an optical density of 0.25-0.3, diluted 1:100 and incubated and processed as previously described.

The effect of inoculum was assessed using two MTPs on a single day for each of the three inoculum types on five MTP assays on day five were performed comparing the variation across the plates of each day.

2.2.6 Effect of isolate storage

The effect of freezing on the ability of NTHi to form biofilm was investigated. Fresh NTHi clinical isolates (B1, B2, B3 and B4) were collected and evaluated for biofilm formation. These isolates had undergone less than four sub-cultures following initial isolation from clinical specimens. The MTP assay was performed within two days of

initial isolation, with two MTP assays performed per strain each day, to generate a single mean value for BF from eight individual wells. The same analyses were performed after freezing in glycerol on ceramic beads and storage at -80°C for two, four, eight, 12, 24 and 48 weeks.

2.2.7 Statistical analysis

For comparison of biofilm (BF) and relative biofilm formation (BF/FG) between strains and to examine the differences in biofilm production within strains, Student's t-test and one-way repeated measures ANOVA (IBM SPSS Statistics, V21.0) were used along with nonparametric tests where appropriate with $P<0.05$ considered statistically significant. For comparison of the three different inoculum methods and classification of biofilm (BF) and relative biofilm (BF/FG) production (high and low), a general linear model (GLM) and univariate analysis of variance based on individual wells was used to produce a two-way repeated measures ANOVA (IBM SPSS Statistics, V21.0) with $P<0.05$ considered statistically significant.

2.3 Results

2.3.1 Baseline biofilm assay

Biofilm formation (BF) over five different days for each of the tested strains are presented in Fig. 1. Each bar represents the mean BF on a particular day with consistency in the amount of biofilm produced between strains. It was evident that A1 and PAO1 produced a similar amount of biofilm (BF) ($P>0.05$). Strain A1 produced significantly more biofilm than strain A2 ($P<0.01$), strain A3 ($P<0.01$) and strain A4 ($P<0.01$). Strain A2 produced significantly more biofilm than A3 ($P<0.01$) and A4 ($P<0.01$) and strains A3 and A4 produced a similar amount of biofilm ($P>0.05$). Discriminatory categories of biofilm formation were calculated as; high (≥ 0.6) and low (< 0.6) producers ($P<0.05$).

Relative biofilm production (BF/FG ratio) data are presented in Fig. 2. Strain A1 gave a BF/FG ratio higher than all the other strains including PAO1 ($P<0.01$).The BF/FG ratios for all of NTHi strains gave similar relative results as for the BF data (P values were very similar).

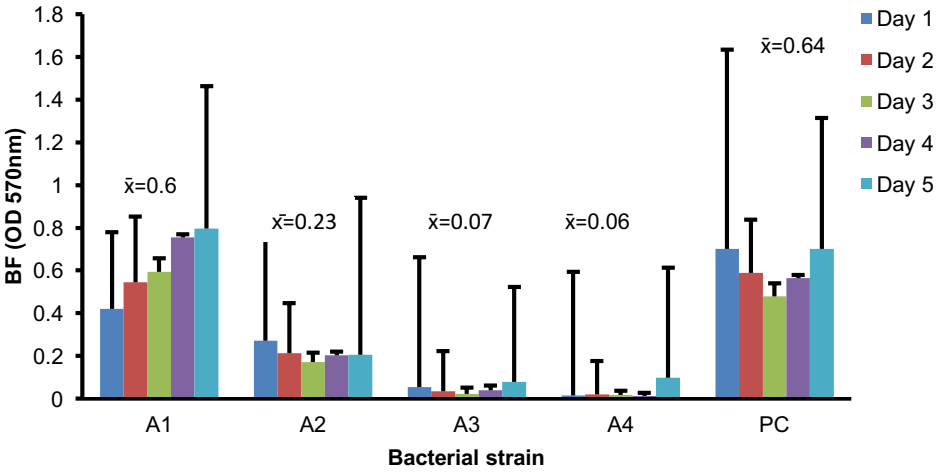

Figure 1. Biofilm production (BF) of the four NTHi strains (A1-A4) and *Pseudomonas aeruginosa* PAO1 positive control (PC) over five days. Error bars depict standard deviation.

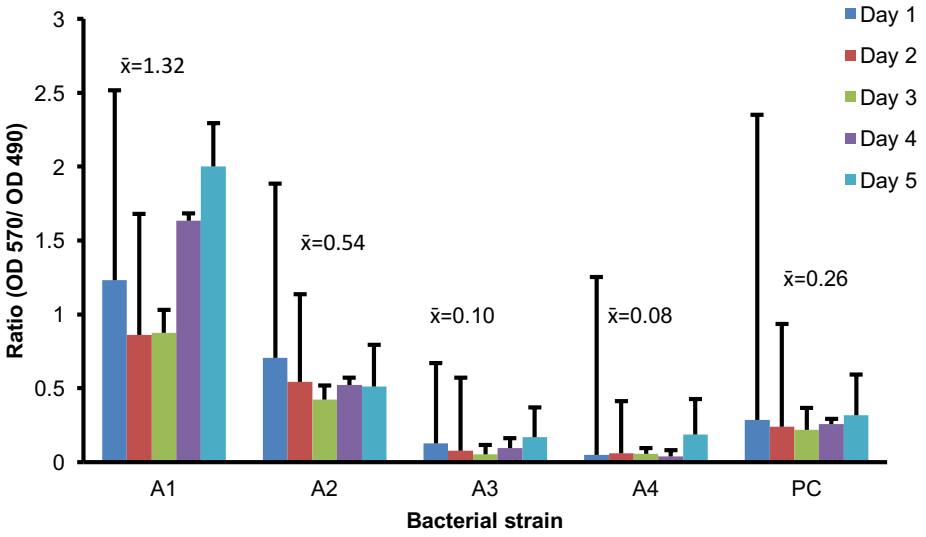

Figure 2. Relative biofilm production (BF/FG) of the four NTHi strains (A1-A4) and *Pseudomonas aeruginosa* PAO1 positive control (PC) over five days. Error bars depict standard deviation.

The percent relative standard deviation (%RSD) was calculated for each of the five days using both BF and BF/FG data which are presented in Table 1. There were no

differences in %RSD intra-day variability (P>0.05) or inter-day variability (P>0.05) between using BF/FG ratio versus BF for any of the strains.

Table 1.The percent relative deviation %RSD of the strains for each day. Nonparametric tests found no differences in the %RSD values between each strain over day 5 or within the strains across days.

	Day1		**Day 2**		**Day 3**		**Day 4**		**Day 5**	
Strain	BF	BF/FG	BF	BF/FG	BF	BF/FG	BF	BF/FG	BF	BF/FG
A1	20.67	6.04	3.49	53.51	58.96	53.70	10.74	3.74	42.86	45.48
A2	18.87	22.64	12.41	23.34	54.62	61.20	5.78	1.26	48.81	46.26
A3	30.00	34.66	34.03	31.01	13.83	20.17	-	-	9.54	11.54
A4	14.25	1.42	31.75	32.08	9.59	10.06	10.46	12.10	80.95	85.93
PAO1	6.84	3.05	10.40	12.09	4.19	12.66	10.75	12.60	28.17	29.92

2.3.2 Effects of inoculum preparation

The effect of inoculum from standardisation, non-standardisation and solid inoculum are illustrated in Fig. 3. Strains A1 and A2 demonstrated no difference in BF between inoculation techniques (P>0.05). Strain A3 and A4 increased BF measurement with solid inoculum over the other inoculum techniques (P<0.05) (see Table 2) with biofilm formation doubling in strain A3 prepared from solid inoculum compared to inoculum prepared from standardised liquid inoculum (P<0.05). Relative biofilm production BF/FG in Fig. 4 gave similar results in terms of the biofilm level production that presented in the BF value Fig. 3.

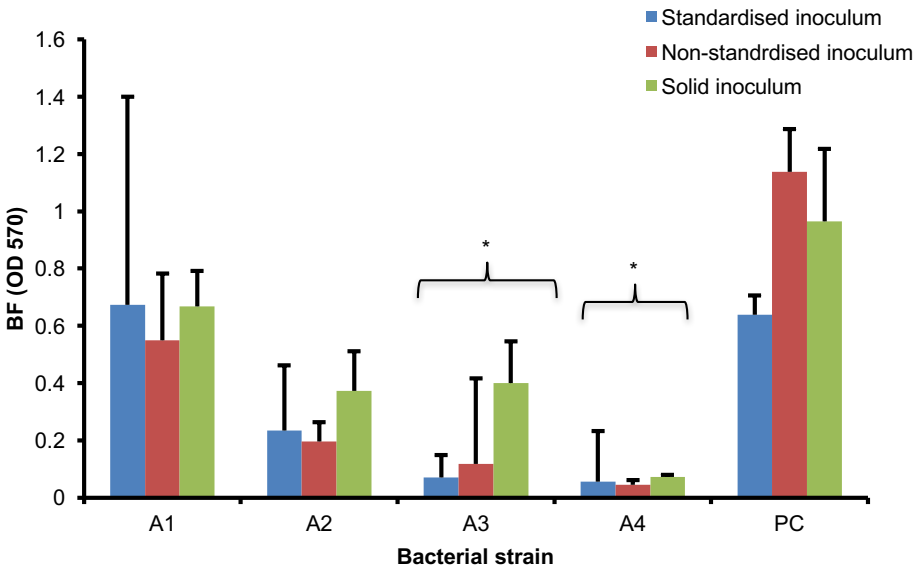

Figure 3. Robustness comparison of the standardised method, solid growth and non-standardised inoculum for NTHi strains (A1-A4) and *Pseudomonas aeruginosa* PAO1 positive control (PC) for 8 wells over 13 plates. Error bars depict standard deviation and with statistical significance P<0.05*.PC represents the positive control *Pseudomonas aeruginosa* PAO1.

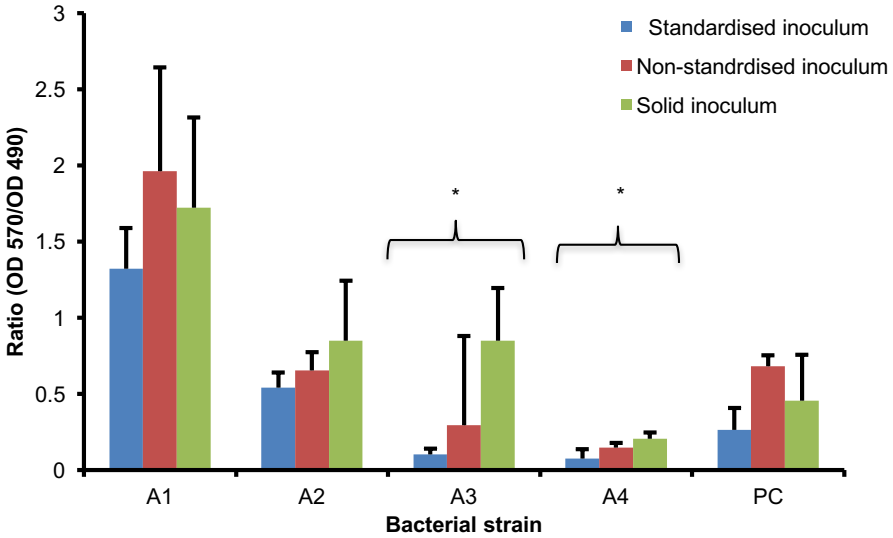

Figure 4. Robustness comparison of the standardised method, solid growth and non-standardised inoculum. Biofilm formation (BF/FG, biofilm/final growth ratio) of the four NTHi strains and *Pseudomonas aeruginosa* PAO1 positive control (PC) for 8 wells over 13 plates. Error bars depict standard deviation and with statistical significance P<0.05 (*).

Table 2 . Inter-day of %RSD for the validation of MTP assay methods. Comparison of the three methods (standardised, non-standardised and solid method). Nonparametric tests found no difference between the %RSD of the standardised method with the other methods.

	Standardised method		**Non-standardised method**		**Solid method**	
	BF	BF/FG	BF	BF/FG	BF	BF/FG
A1	24.88	37.46	39.48	30.21	32.84	34.43
A2	17.17	18.91	63.57	48.11	16.27	17.73
A3	45.37	43.41	95.16	98.87	64.96	60.11
A4	108.92	79.57	35.62	22.68	22.05	13.62
PAO1	15.59	14.42	44.67	35.24	23.96	26.83

2.3.3 Effect of isolate storage

In Fig. 5, the results of the frozen storage in -80ºC experiments demonstrated that biofilm production was not affected in most cases and that biofilm production only changed in two strain (B2 and B3) after six months ($P<0.05$). There was some fluctuation of biofilm production (BF) for B2.

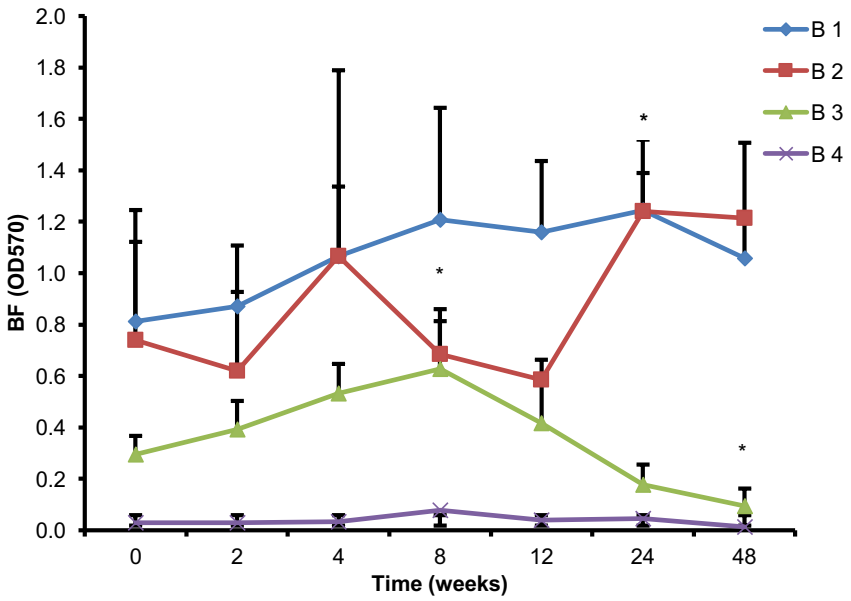

Figure 5. The mean (SD) biofilm production (BF) for four fresh NTHi strains and *Pseudomonas aeruginosa* PAO1 positive control (PC) over 48 weeks. Error bars depict standard deviation and with statistical significance $P<0.05$ (*) with B2 at week 24 and B3 at weeks 8 and 48.

2.4 Discussion

2.4.1 Baseline biofilm assay

The ability to reliably and consistently discriminate between high and low biofilm producing NTHi strains was achieved with the MTP assay method. Of the NTHi strains that were examined, strain A1 was classified as a high biofilm producer, and strains A2, A3 and A4 were low biofilm producers. A1 produced similar amounts of biofilm (BF) as the control strain (PAO1). Strain A2, although categorised as a low biofilm producer, produced around 60% of the biofilm of strain A1 but significantly more than A3 and A4 which both produced only about 10% of A1's biofilm indicating difficulty of classification of low biofilm producers. The method met acceptance criteria of precision and repeatability (±20% of %RSD) for biofilm in most of the strains measured by MTP assay.

H. influenzae strains ATCC 10211 (A3) and RdW20 (A4) were chosen in addition to unique local strains, because they are widely available and could act as reference isolates for others wishing to use or evaluate our method. ATCC 10211 was especially chosen because it is known to be particularly fastidious and is used by the Clinical Laboratory Standards Institute for quality control of susceptibility testing media (C.L.S.I, 2012). The four strains were also selected to cover a range of biofilm forming ability. In the context of this work, *P. aeruginosa* (PAO1) strain served as positive control as it has been extensively studied and confirmed as a high biofilm producer in MTP assays (Bjarnsholt *et al.*, 2005, Hall-Stoodley and Stoodley, 2009). The reason for choosing *P. aeruginosa* (PAO1) strain was that there is no NTHi strain confirmed to be a high biofilm producer to serve as positive control.

Relative biofilm production (BF/FG ratio) normalises biofilm production to the bacterial density in each well. The use of this ratio could correct for potential variations in bacterial growth in different wells. However, in the current study, the use of this ratio made no difference to the assay performance measures of intra-day and inter-day variability, compared with the use of BF alone. This indicates that bacterial growth was consistent in each well even for the known fastidious strain A3. For example, intra-day variability of final growth (FG) for strain A3 was 7.7% (%RSD) which gives a further indication of the reproducibility of the final growth. The extra step of measuring bacterial density in order to calculate this ratio cannot be justified on the basis of our results. However, there may be a benefit in using the ratio for measurement of biofilm production after treating the inoculum with antibacterial agents where variation in bacterial growth may have more experimental variability (Harrison *et al.*, 2010).

The acceptance criteria of RSD of ± 20% variability were met only for BF of strains A1 and A2. Biofilm production of strains (A3 and A4) were less reproducible and greater than the acceptance criteria. Inter-day variability tended to increase with A3 and A4, the low biofilm producers, but the correlation between BF and variability was weak. Inter-day precision of MTP biofilm measurements are not routinely described in the literature, but should be taken into account when determining the validity of biofilm quantitation using static methods. As a comparison, reproducibility of biofilm production (BF) by MTP assay for *Staphylococcus aureus* was reported as 35%, greater than that shown here for NTHi strain A1 and A2 (Sandberg *et al.* 2008).

2.4.2 Effects of inoculum preparation

Examination of the final growth measurements shows that all strains grew to a similar cell density after full incubation, regardless of the type of initial inoculum preparation. On this basis, as standardisation of the inoculum by dilution to a specified 0.25 – 0.30 OD 490 does not increase reproducibility, it is not shown to be necessary.

Solid growth inoculum made no difference for biofilm production, even after vigorously shaking the inoculum after inoculation from solid media, except for strains A3 and A4 Fig. 3. The effect of inoculum from chocolate agar was investigated because many studies do not define the source of cells for the preparation of their final inoculum. Results from solid media are not directly comparable with results of inoculum from liquid media. Stepanović *et al*. (2007) have suggested that adhesion to cell surfaces can be initiated in the first step of biofilm formation and potentially resulting in more biofilm formation from bacterial cells grown on solid medium than bacterial cells grown in liquid medium (Stepanović *et al.*, 2007).

In this study, we chose to use 24 well, flat bottom untreated well MTPs for several reasons. Plates with 24 wells have been used for MTP assays in some previous studies for other organisms as reviewed by Coenye and Nelis (2010) and specifically for NTHi biofilm studies (Murphy and Kirkham, 2002, Webster *et al.*, 2006a, Ünal *et al.*, 2012). These plates have a larger absolute surface area than other types which were used in other published studies (Stepanović *et al.*, 2007). The microtitre plates were specifically flat bottom polystyrene non-tissue culture treated wells. Non-treated wells were chosen, free of any interference from other factors that may enhance the adhesion of cells and initial biofilm formation. Tissue culture treated wells have been

reported in some papers as an enhancer of biofilm formation (Stepanović *et al.*, 2007, Murphy and Kirkham, 2002) .

2.4.3 Effect of isolate storage

These fresh clinical isolates were chosen to cover a similar range of biofilm producing ability as the strains used in the earlier study. There appeared to be some strain-specific changes in biofilm production found after frozen storage of freshly cultured cells over 48 weeks, however, these changes were within the overall inter-day variability of the MTP assay. Frozen storage affected biofilm production of strain (B2) after 24 weeks in -80ºC Fig. 5. There were also some differences in biofilm production in strain B3 which were found after eight weeks of freezing compared to fresh, and after 48 weeks. Biofilm production is the result of a complex interaction between bacterial cells and the host surfaces and there is no information on whether the ability to form biofilms is retained when the bacterial cells are removed from the host and stored for long periods. This is an important consideration as in most studies, strains are stored prior to being tested. To date, there are no studies investigating the biofilm producing ability for NTHi isolates after short or long periods of freezing. Two studies have tested the consequence of freezing; *H. influenzae* planktonic strains were stored in different types of media and repeated viability tests were undertaken after thawing/freezing cycles (Saab *et al.*, 2001, Votava and Střítecká, 2001). Viability of planktonic *Haemophilus influenzae* decreases after freezing for longer periods of time (>48 weeks) (Saab *et al.* 2001). Therefore, we can determine from our study that the ability of NTHi strains to form biofilm may be affected by freezing over a 24 week period but appears to be strain-specific as this was not observed in all NTHi strains.

2.5 Conclusion

Different strains of NTHi consistently produced different levels of biofilm. The MTP assay met precision acceptance criteria for measuring biofilm production by NTHi strains. The only determinant of variability when measuring NTHi biofilm using the MTP assay is due to the particular NTHi strain. Standardisation of the inoculum (versus non-standardised) made no difference which could be a step reserved for more fastidious strains. The source of inoculum from culture media demonstrated less precision for at least one strain. Frozen storage duration showed no major effect on the biofilm formation as the biofilm production for some strain changed but within the inter-day variability of our MTP assay. The MTP assay is a valid approach to measuring NTHi biofilm and can detect some strain-specific differences in biofilm production, was well as the effect of inoculum techniques and frozen storage duration.

2.6 References

Bjarnsholt, T, Jensen, P. Ø, Burmølle, M, Hentzer, M, Haagensen, J, Hougen, H, P, Calum, H, Madsen, K, Moser, C, & Molin, S, 2005. 'Pseudomonas aeruginosa tolerance to tobramycin, hydrogen peroxide and polymorphonuclear leukocytes is quorum-sensing dependent'. *Microbiology,* 151**,** 373-383.

C.L.S.I 2012. 'Methods for dilution antimicrobial susceptibility tests for bacteria that grow aerobically; approved standard, 9th edition *M07-A9.* Wayne, PA.

Christensen, G D, Simpson, W, Younger, J, Baddour, L, Barrett, F, Melton, D & Beachey, E 1985. 'Adherence of coagulase-negative staphylococci to plastic tissue culture plates: a quantitative model for the adherence of staphylococci to medical devices'. *Journal of Clinical Microbiology,* 22**,** 996-1006.

Coenye, T & Nelis, H J, 2010. 'In vitro and in vivo model systems to study microbial biofilm formation'. *Journal of Microbiological Methods,* 83**,** 89-105.

Costerton, J W, Stewart, P S, & Greenberg, E P 1999. 'Bacterial biofilms: a common cause of persistent infections'. *Science,* 284**,** 1318-1322.

Daines, D A, Bothwell, M., Furrer, J, Unrath, W, Nelson, K, Jarisch, J, Melrose, N, Greiner, L, Apicella, M & Smith, A L 2005. 'Haemophilus influenzae luxS mutants form a biofilm and have increased virulence'. *Microbial Pathogenesis,* 39**,** 87-96.

Goeres, D M, Loetterle, L R, Hamilton, M A, Murga, R, Kirby, D W & Donlan, R M 2005. 'Statistical assessment of a laboratory method for growing biofilms'. *Microbiology,* 151**,** 757-762.

Hall-Stoodley, L & Stoodley, P 2009. 'Evolving Concepts in Biofilm Infections'. *Cellular Microbiology,* 11**,** 1034-1043.

Harrison, J J, Stremick, C A, Turner, R J, Allan, N D, Olson, M E & Ceri, H 2010. 'Microtiter susceptibility testing of microbes growing on peg lids: a miniaturized biofilm model for high-throughput screening'. *Nature Protocols,* 5**,** 1236-1254.

Moriyama, S, Hotomi, M, Shimada, J, Billal, D S, Fujihara, K & Yamanaka, N 2009. 'Formation of biofilm by Haemophilus influenzae isolated from pediatric intractable otitis media'. *Auris Nasus Larynx,* 36**,** 525-531.

Murphy, T F, Brauer, A L, Schiffmacher, A T & Sethi, S 2004. 'Persistent colonization by Haemophilus influenzae in chronic obstructive pulmonary disease'. *American Journal of Respiratory and Critical Care Medicine,* 170**,** 266-272.

Murphy, T F & Kirkham, C 2002. 'Biofilm formation by nontypeable Haemophilus influenzae: strain variability, outer membrane antigen expression and role of pili'. *BMC microbiology,* 2**,** 7.

Parker, A, Walker, D, Goeres, D, Allan, N, Olson, M & Omar, A 2014. 'Ruggedness and reproducibility of the MBEC biofilm disinfectant efficacy test'. *Journal of Microbiological Methods,* 102**,** 55-64.

Puig, C, Domenech, A, Garmendia, J, Langereis, J D, Mayer, P, Calatayud, L, Liñares, J, Ardanuy, C & Marti, S 2014. 'Increased Biofilm Formation by Nontypeable Haemophilus influenzae Isolates from Patients with Invasive Disease or Otitis Media versus Strains Recovered from Cases of Respiratory Infections'. *Applied and Environmental Microbiology,* 80**,** 7088-7095.

Saab, O C, Castillo, M C, Ruiz Holgado, A P & Nader, O M 2001. 'A comparative study of preservation and storage of haemophilus influenzae'. *Memórias do Instituto Oswaldo Cruz,* 96**,** 583-586.

Sandberg, M, Määttänen, A, Peltonen, J, Vuorela, P M & Fallarero, A, 2008. 'Automating a 96-well microtitre plate model for Staphylococcus aureus biofilms: an

approach to screening of natural antimicrobial compounds'. *International Journal of Antimicrobial Agents,* 32**,** 233-240.

Starner, T D, Zhang, N, Kim, G, Apicella, M A & Mccray Jr, P B, 2006. 'Haemophilus influenzae forms biofilms on airway epithelia: implications in cystic fibrosis'. *American Journal of Respiratory and Critical Care Medicine,* 174**,** 213.

Stepanović, S, Vuković, D, Dakić, I, Savić, B & Švabić-Vlahović, M 2000. 'A modified microtiter-plate test for quantification of staphylococcal biofilm formation'. *Journal of Microbiological Methods,* 40**,** 175-179.

Stepanović, S, Vuković, D, Hola, V, Bonaventura, G D I, Djukić, S, Ćirković, I & Ruzicka, F 2007. 'Quantification of biofilm in microtiter plates: overview of testing conditions and practical recommendations for assessment of biofilm production by staphylococci'. *Apmis,* 115**,** 891-899.

Swords, W E 2012. 'Nontypeable Haemophilus influenzae biofilms: role in chronic airway infections'. *Frontiers in Cellular and Infection Microbiology,* 2.

Takei, S, Hotomi, M & Yamanaka, N 2013. 'Minimal biofilm eradication concentration of antimicrobial agents against nontypeable Haemophilus influenzae isolated from middle ear fluids of intractable acute otitis media'. *Journal of Infection and Chemotherapy***,** 1-6.

Ünal, C M, Singh, B, Fleury, C, Singh, K, Chávez De Paz, L, Svensäter, G & Riesbeck, K 2012. 'QseC controls biofilm formation of non-typeable Haemophilus influenzae in addition to an AI-2-dependent mechanism'. *International Journal of Medical Microbiology*.

Votava, M & StříTecká, M 2001. 'Preservation of Haemophilus influenzae and Haemophilus parainfluenzae at− 70° C'. *Cryobiology,* 43**,** 85-87.

Webster, P, Wu, S, Gomez, G, Apicella, M, Plaut, A G & Geme Iii, J W S 2006a. 'Distribution of bacterial proteins in biofilms formed by non-typeable Haemophilus influenzae'. *Journal of Histochemistry & Cytochemistry,* 54**,** 829-842.

Webster, P, Wu, S, Gomez, G., Apicella, M., Plaut, A G. & Geme Iii, J W S 2006b. 'Distribution of bacterial proteins in biofilms formed by non-typeable Haemophilus influenzae'. *Journal of Histochemistry & Cytochemistry,* 54**,** 829.

Wu, S, Baum, M M, Kerwin, J, Guerrero, D, Webster, S, Schaudinn, C, Vandervelde, D & Webster, P, 2014. 'Biofilm specific extracellular matrix proteins of nontypeable Haemophilus influenzae'. *Pathogens and Disease*. 72, 143-160.

Chapter 3

Relationship between clinical site of isolation and ability to form biofilms in vitro in Nontypeable *Haemophilus influenzae*

Abstract

Nontypeable *Haemophilus influenzae* (NTHi) is an opportunistic pathogen associated with a range of infections including various lower respiratory infections, otitis media and conjunctivitis. There is some debate as to whether or not NTHi produce biofilms and if so, whether or not this is relevant to pathogenesis. Although many studies have examined the association between *in vitro* biofilm formation and isolates from a specific infection type, few have made comparisons from isolates from a broad range of isolates grouped by clinical source. In our study, fifty NTHi from different clinical sources: otitis media, conjunctivitis, lower respiratory tract infections in both cystic fibrosis and non-cystic fibrosis patients and nasopharyngeal carriage, plus ten nasopharyngeal isolates of the commensal *H. haemolyticus* were tested for the ability to form biofilm using a static microtitre plate crystal violet assay. A high degree of variation in biofilm forming ability was observed across all isolates, with no statistically significant differences observed between the groups with the exception of the isolates from conjunctivitis. These isolates had uniformly lower biofilm forming ability compared to isolates from the other groups ($P<0.005$).

3.1 Introduction

Nontypeable *Haemophilus influenzae* (NTHi) is a commensal of the upper respiratory tract that is associated with a range of opportunistic infections such as community acquired pneumonia (CAP), exacerbations of chronic obstructive pulmonary disease (COPD), sinusitis, otitis media (OM) and conjunctivitis. (Murphy *et al.,* 2004, Homøe and Johansen, 2011, Chin *et al.,* 2005, Mizrahi *et al.,* 2014). Studying pathogenesis in NTHi is made difficult because of its extremely heterogeneous bacterial population structure and because the organism has multifaceted pathogenicity with many potential virulence attributes identified, although no single attribute has been detected in all disease associated strains (Erwin and Smith, 2007). There has been much debate as to whether NTHi actually forms biofilms, particularly *in vivo*, and if it does, whether these biofilms play a role in pathogenesis and persistence (Erwin and Smith, 2007).

Numerous studies have demonstrated the ability of NTHi to form biofilms *in vitro* and this has been shown to be highly variable amongst different strains (Murphy and Kirkham, 2002, Moxon *et al.,* 2008, Moghaddam *et al.,* 2011) but less work has been done to link biofilm formation ability with pathogenicity. Biofilm growth in other organisms has been associated with pathogenesis and particularly with chronicity of infection (Hall-Stoodley and Stoodley, 2009) and many papers have reviewed the involvement of biofilm with chronic and recurrent NTHi infection and severity of disease (Erwin and Smith, 2007). However, a limitation of many studies is that they examined strains within one or two infectious disease contexts without comparison with strains from infections at different sites. We hypothesise that if biofilm formation as demonstrated by *in vitro* assays is clinically relevant, the contribution to

pathogenesis may be different for infections at different sites because the organism will be interacting with the host at different anatomical surfaces. In this study we investigate this by testing isolates from a range of clinical sites for *in vitro* biofilm formation. A recent study compared the ability of isolates of NTHi from nasopharyngeal carriage, otitis media, non-bacteraemic community acquired pneumonia, chronic obstructive pulmonary disease and invasive disease to form biofilm (Puig *et al.,* 2014). It was found that isolates from invasive disease and otitis media produced significantly more biofilm than the isolates from other sites. In our current study we investigated this hypothesis, and within the limits of our isolate collection, attempted to replicate the findings by Puig *et al.* by testing isolates from a range of clinical sites for *in vitro* biofilm formation.

3.2 Methods

3.2.1 Bacterial isolates and growth condition

A collection of 10 clinical isolates from each of six body sites groups based on site of isolation and identity was established, consisting of NTHi isolates from otitis media (ears), conjunctivitis (eyes), lower respiratory infection from sputum sample (LRT), lower respiratory infection from cystic fibrosis patients (CF), oropharyngeal normal flora (NF) and oropharyngeal normal flora isolates of H. haemolyticus (Hh), with the latter two groups from asymptomatic volunteers. Additional specific clinical details beyond site of isolation, such as chronic or acute disease or underlying conditions such as COPD or CAP were not available for the clinical isolates listed above. Microorganisms were identified using a polymerase chain reaction (PCR) algorithm for species marker genes hpd, fucK and sodC as previously described (Witherden and Tristram, 2013). All bacterial isolates were identified by sequencing of the 16S rRNA

gene using universal primers 27F and 1492R (Weisburg, *et al,* 1991). After manual inspection of chromatograms, the sequences were trimmed to 751 bp corresponding to positions 81 to 831 of the complete 16S sequence. The isolates were then identified to species level by comparison with the GenBank nucleotide database using the blastn algorithm.

The isolates were stored in glycerol at -80ºC and recovered by overnight culture on chocolate agar (Oxoid Australia Pty, Ltd., Thebarton, SA) at 37ºC in 5% CO_2. Harvested colonies were inoculated onto chocolate agar then incubated for 18-22 h prior to use in the biofilm assay.

3.2.2 Biofilm assay

The microtitre plate assay was used to measure static biofilm formation using our laboratory protocols that validated and described in details in Chapter 2 which standardise the starting inoculum with regard to optical density.

Briefly, an overnight broth culture in supplemented brain heart infusion broth (sBHI) was adjusted to an optical density (490 nm) of 0.25-0.30. A final inoculum (~10^5 CFU/ml) was prepared by diluting this 1/100 in sBHI and 2.0 ml transferred to each of 4 wells of a 24-well non-treated 2.5 ml sterile polystyrene microtitre plate (MTP). Plates were incubated at 37°C under 5% CO_2 for 18-22 h, washed and stained with crystal violet as described in chapter 2 section 2.2.2. The average optical density at 570 nm (blanked against a no bacteria control well) of the 4 wells was determined as described in chapter 2 section 2.2.3 and the final outcome measure for biofilm formation (BF) is the average of 4 independent experiments. Individual isolates were selected randomly from all groups for testing in batches of 4 isolates per MTP to avoid any systematic bias.

3.2.3 Statistical analysis

Comparisons of BF were performed by one-way analysis of variance (ANOVA), followed by Fisher's protected least significant difference (PLSD) post hoc test to assess statistical significance between different body sites (IBM SPSS Statistics, V21.0). Results with $P<0.05$ were considered statistically significant.

3.3 Result and discussion

We chose to use the static MTP crystal violet assay for this study because it has been very widely used, is high throughput, quantitative and reproducible and therefore useful for the comparison of biofilm formation between isolates. (Murphy and Kirkham, 2002, Langereis and Hermans, 2013). A limitation of the static MTP method is that it is not standardised, with various incubation times and different outcome measures used, where some studies simply report the absorbance of the stained biofilm material at 570nm (Murphy and Kirkham, 2002, Webster *et al.,* 2006), while others calculate a ratio where the biofilm value is expressed as a ratio compared to some type of control isolate (Moriyama *et al.,* 2009). This lack of standardisation limits the ability for us to compare actual BF values between our study and previous studies.

The results are summarised in Fig. 1, and presented in full in the appendix. We found significant variation in the BF measure across the 60 isolates in our study with a range of 0.02 to 1.76 and this is very consistent with other studies (Starner *et al.,* 2006, Mizrahi *et al.,* 2014). There was no statistically significant difference in mean BF between NTHi isolates from ears, LRT, CF, NF and Hh isolates, but the BF of NTHi

isolates from eyes was consistently low and the mean BF of this group was significantly lower than the other groups (P<0.05).

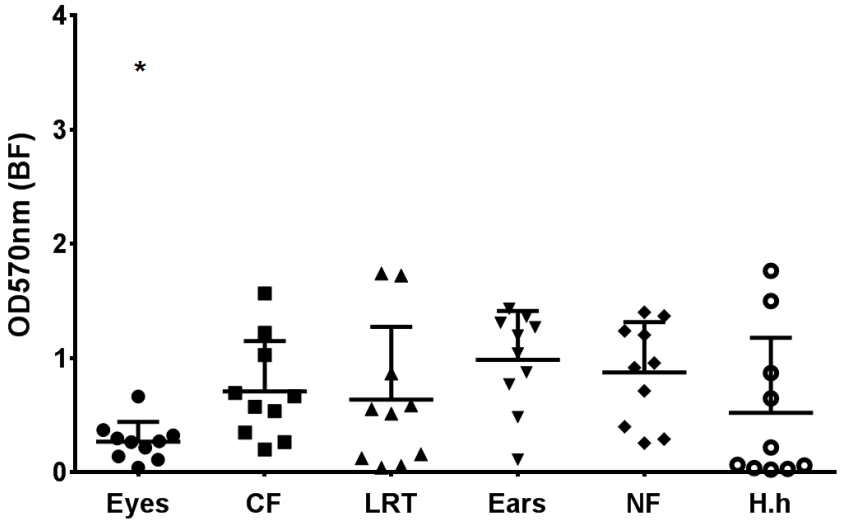

Figure 1. The mean and SD for each group of the clinical isolates by the output Biofilm formation (BF) using optical density 570nm (* P< 0.05)

These results of BF from ears, LRT, CF and NF isolates are consistent with a previous study that compared quantitative measures of biofilm formation in NTHi from; middle ear isolates with isolates from COPD (Murphy and Kirkham, 2002) and showed no association with site of isolation and biofilm formation. However, our results differ from those in the recent study by Puig *et al.* that found that isolates from OM were significantly higher biofilm producers than isolates from non-invasive respiratory infections or from the carriage state (Puig *et al.,* 2014). Significantly, the low BF for NTHi isolates from the eye group in our study is consistent with a recent study by Mizrahi *et al.* that compared middle ear isolates from patients with OM and treatment

failure, with nasopharyngeal isolates from patients with various other presentations of OM, such as first episode, recurrent episodes or with concomitant conjunctivitis. On multivariate analysis they found that only the presence of conjunctivitis was associated with low biofilm production (Mizrahi *et al.,* 2014).

While many previous studies have shown a role for biofilm formation in pathogenesis (Erwin and Smith, 2007, Vlastarakos *et al.,* 2007, Swords, 2012) our data suggest that the ability to form significant biofilm, as measured by the static method, is not a prerequisite for pathogenesis nor does it favour infection at particular anatomical niches. To our knowledge, our study is the first to demonstrate the capacity to form biofilms in the respiratory commensal *H. haemolyticus*, and although the formation of biofilms has been described previously for other non-pathogens (Langereis and Hermans, 2013), the similarity in our BF data for *H. haemolyticus* and NTHi supports the notion that the ability to form biofilms may not be a critical virulence attribute in this organism.

The observation that strains associated with eye infection have low biofilm forming capacity is difficult to explain. If we accept that isolates of NTHi associated with disease originate from the nasopharynx where isolates have demonstrated variable ability to form biofilm, then it may be that the inability to form biofilm is advantageous in the pathogenesis of conjunctivitis. A more likely explanation is that a particular sub-type of NTHi has specific but as yet unknown virulence attributes that favour infection in the eye and that these organisms have a low biofilm capacity by happenstance. A similar situation was recently described by Skaare *et al.* (2014) in the examination of the population structure of NTHi with altered penicillin-binding protein 3 (PBP3) which is associated with an ampicillin resistance phenotype. In that

study it was initially noted that isolates with altered PBP3 were more likely to cause conjunctivitis than those with normal PBP3 (Skaare *et al.,* 2014). On further examination, it was shown that multilocus sequence typing (MLST) types 385, 396 and 201 were strongly associated with eye infections, and that because sequence types 396 and 201 were also associated with altered PBP3 there was an indirect association between alt PBP3 and eye infection (Skaare *et al.,* 2014).

3.4 Conclusion

We demonstrate that the ability to form biofilms as evidenced by the static MTP method is highly variable amongst clinical isolates and does not appear to favour infection at particular anatomical niches. More work is needed to delineate the association between the ability to form biofilms, and the population structure of NTHi associated with eye infections.

3.5 References

Chin, C L, Manzel, L J, Lehman, E E, Humlicek, A L, Shi, L, Starner, T D, 2005. 'Haemophilus influenzae from patients with chronic obstructive pulmonary disease exacerbation induce more inflammation than colonizers'. *American Journal of Respiratory and Critical Care Medicine,* 172**,** 85.

Erwin, A L & Smith, A L, 2007 'Nontypeable Haemophilus influenzae: understanding virulence and commensal behavior'. *Trends in Microbiology,* 15**,** 355-362.

Hall-Stoodley, L & Stoodley, P, 2009 'Evolving concepts in biofilm infections' *Cellular microbiology,* 11**,** 1034-1043.

Homøe, P & Johansen, H K, 2011. 'The Relation of Biofilms to Chronic Otitis Media and Other Ear-Related Chronic Infections'. *Biofilm Infections***,** 25-34.

Langereis, J D & Hermans, P W, 2013. 'Novel concepts in nontypeable Haemophilus influenzae biofilm formation'. *FEMS Microbiology Letters,* 346**,** 81-89.

Mizrahi, A, Cohen, R, Varon, E, Bonacorsi, S, Bechet, S, Poyart, C, 2014. 'Non typable-Haemophilus influenzae biofilm formation and acute otitis media'. *BMC infectious diseases,* 14**,** 400.

Moghaddam, S J, Ochoa, C E, Sethi, S & Dickey, B F, 2011. 'Nontypeable Haemophilus influenzae in chronic obstructive pulmonary disease and lung cancer'. *International Journal of Chronic Obstructive Pulmonary Disease,* 6**,** 113.

Moriyama, S, Hotomi, M, Shimada, J, Billal, D S, Fujihara, K & Yamanaka, N, 2009. 'Formation of biofilm by Haemophilus influenzae isolated from pediatric intractable otitis media'. *Auris Nasus Larynx,* 36**,** 525-531.

Moxon, E R, Sweetman, W A, Deadman, M E, Ferguson, D J P & Hood, D W, 2008. 'Haemophilus Influenzae Biofilms: Hypothesis or Fact?'. *Trends in Microbiology,* 16**,** 95-100.

Murphy, T F., Brauer, A L, Schiffmacher, A T & Sethi, S, 2004. 'Persistent colonization by Haemophilus influenzae in chronic obstructive pulmonary disease'. *American Journal of Respiratory and Critical Care Medicine,* 170**,** 266-272.

Murphy, T F & Kirkham, C, 2002. 'Biofilm formation by nontypeable Haemophilus influenzae: strain variability, outer membrane antigen expression and role of pili'. *BMC Microbiology,* 2**,** 7.

Skaare, D, Anthonisen, I L, Caugant, D A, Jenkins, A, Steinbakk, M, Strand, L, 2014. 'Multilocus sequence typing and ftsI sequencing: a powerful tool for surveillance of penicillin-binding protein 3-mediated beta-lactam resistance in nontypeable Haemophilus influenzae'. *BMC Microbiology,* 14**,** 131.

Starner, T D, Zhang, N, Kim, G, Apicella, M A & Mccray Jr, P B, 2006. 'Haemophilus influenzae forms biofilms on airway epithelia: implications in cystic fibrosis'. *American Journal of Respiratory and Critical Care Medicine,* 174**,** 213.

Swords, W E, 2012. 'Nontypeable Haemophilus influenzae biofilms: role in chronic airway infections'. *Frontiers in Cellular and Infection Microbiology,* 2.

Vlastarakos, P V., Nikolopoulos, T P, Maragoudakis, P, Tzagaroulakis, A & Ferekidis, E, 2007. 'Biofilms in ear, nose, and throat infections: how important are they?'. *The Laryngoscope,* 117**,** 668-673.

Watnick, P I & Kolter, R, 2002. 'Steps in the development of a Vibrio cholerae biofilm'. *Molecular microbiology,* 34**,** 586-595.

Webster, P, Wu, S, Gomez, G, Apicella, M, Plaut, A G & Geme Iii, J W S, 2006. 'Distribution of bacterial proteins in biofilms formed by non-typeable Haemophilus influenzae'. *Journal of Histochemistry & Cytochemistry,* 54**,** 829-842.

Weisburg, W,G, Barns, S, M, Pelletier, D,A, and Lane, D,J, 1991. 16S ribosomal DNA amplification for phylogenetic study. *Journal of bacteriology*,173, 697-703.

Witherden, E A & Tristram, S G, 2013. 'Prevalence and mechanisms of β-lactam resistance in Haemophilus haemolyticus'. *Journal of Antimicrobial Chemotherapy,* 68**,** 1049-1053.

Chapter 4

Antibiotic effects on NTHi biofilm

4.1 Abstract

A range of upper and lower respiratory tract infections caused by Nontypeable *Haemophilus influenzae* (NTHi) are frequently treated with antibiotics such as amoxicillin and azithromycin. These infections may persist and antibiotic therapy may fail to eradicate the infection. The persistence of the infection may be related to biofilm formation which may not be easily managed by conventional antibiotic treatment. The laboratory measurement of antibiotic susceptibility is based on the minimum inhibitory concentrations (MICs) for particular NTHi clinical isolates in the planktonic state. The treatment with antibiotics sometimes could affect the biofilm and paradoxically may enhance the production of sessile cells. This study aims to examine the effect of four classes of antibiotics at two concentrations, on the formation of NTHi biofilm. Two isolates were used; (NTHi A1) with high biofilm formation and (RdKW20) with low biofilm formation to assess the sub-MIC and MIC of four antibiotics; β-lactams (amoxicillin;AMX and cefotaxime;CTX), macrolide (azithromycin;AZM) and flouroqunolon (ciprofloxacin;CIP). These antibiotics were applied on two stages of biofilm; adding antibiotics at the initiation of new biofilm and adding antibiotics on existing biofilms using microtitre plate assay method (MTP assay). The results showed that AMX at the MIC concentration, impacted on existing biofilm of NTHi A1 and caused formation of more biofilm material. With sub-MIC of AMX and MIC of the other antibiotics, there were no effects on new biofilm formation for NTHi A1. No changes on biofilm formation were shown by RdKW20 with addition of antibiotics compared to untreated biofilm except the increase in biofilm with sub-MIC of AMX. This MTP assay method provided a direct examination method on the impact of antibiotics for biofilm formation of an NTHi

clinical isolate and the standard isolate RdKW20 that showed an increase in biofilm after exposure to AMX.

4.2 Introduction

Nontypeable *Haemophilus influenzae* (NTHi) is an upper respiratory commensal that is also associated with a range of opportunistic infections such as community acquired pneumonia (CAP), exacerbations of chronic obstructive pulmonary disease (COPD) and otitis media (OM). These infections are often managed with antibiotic therapy although this sometimes fails to eradicate the organism and the infection may persist with/or without progression to a chronic state (Barkai *et al.*, 2009, Hall-Stoodley and Stoodley, 2009).

A classic example was from a study by Murphy et al (2004), where multiple sputum samples were collected from a cohort of patients with COPD over an extended time period (7 years). The specimens were repeatedly culture positive for the same strain of NTHi, but with significant intervening culture negative periods, although when sputum from these culture negative periods was tested using molecular methods, strain specific NTHi DNA was frequently detected. It was proposed that this may have been due to the presence of NTHi in a biofilm state, which is far less efficiently detected by traditional culture methods designed to detect planktonic growth.

A number of other studies have been able to link the inability of antibiotic therapy to clear the organisms and a tendency towards chronic infection with the ability of some strains to form biofilms (Starner *et al.*, 2006, Erwin and Smith, 2007, Hall-Stoodley and Stoodley, 2009, Vlastarakos *et al.*, 2007). It is well known that the effective concentration of antibiotic for eradicating planktonic bacteria is often ineffective in

the presence of biofilm. This is thought to be a result of altered metabolic state in the biofilm layers and the existence of persister cells, which in turn exposes the bacterial cells to sub-lethal concentrations. (Liu and Post, 2009, Vlastarakos *et al.*, 2007).

There is inconsistency between the minimum inhibitory concentrations (MICs) for organisms measured in the standard fashion using planktonic growth, and those where the measurements use growth in a biofilm state. In the case of the latter, the MIC is often considerably higher. For example, Takei *et al.* (2003) showed that the fluoroquinolone and macrolide MICs for NTHi in a biofilm state were similar to MICs (planktonic state) but for amoxicillin it was 512 times higher than when measured using a planktonic state. Similarly, amoxicillin MICs for NTHi were 4-fold higher when biofilm growth was used compared to the standard measure using planktonic growth (Slinger *et al*., 2006).

Moreover, selection and use of antibiotics based on standard MIC tests are often only capable of producing short-term therapeutic benefits for infections where biofilms are thought to be involved (Hall-Stoodley *et al.*, 2006). For example, in paediatric OM infection, 60% of infections primarily involving planktonic cells (including NTHi) were effectively eradicated using antibiotics. On the other hand, only 22% of infections where biofilms were thought to be involved were effectively eradicated by the same antibiotics (Liu and Post, 2009). However, MIC levels of amoxicillin for NTHi using biofilm growth were measured as 4- fold higher than the MIC levels for planktonic cells (Slinger *et al.*, 2006).

The poor predictive value of the traditional MIC in guiding antibiotic therapy for infections involving biofilms, has led to the development of the minimal biofilm eradication concentration (MBEC), which measures the minimum concentration of antibiotic to kill bacteria forming or existing within a biofilm (Takei *et al.*, 2013). To date, the MBEC has not been widely accepted.

Paradoxically, not only do biofilms protect the bacterial cells from the effects of antibiotics, there is now evidence which suggest that in some cases, antibiotics may stimulate the production of biofilm. This has been shown previously for *E. coli* (Sailer *et al.*, 2003) and *Pseudomonas aeruginosa* (Hoffman *et al.*, 2005), where sub-MIC levels of antibiotic stimulated biofilm production. More recently this has also been shown for NTHi, although the response was strain specific (Wu *et al.*, 2014). Thus, sub-inhibitory doses of *β*-lactams such as amoxicillin may increase the biofilm and decrease the penetration of a second course of antibiotics, this promoting recurrence of the infection (Barkai *et al.*, 2009).

In this study, we aimed to investigate the effects of two concentrations of antibiotics used for the treatment of NTHi infections on biofilm production of two clinical isolates with different levels of biofilm formation.

4.3 Methods

4.3.1 *Haemophilus influenzae* isolates used in the assay

Two isolates were selected for this study; one was a clinical isolate (A1) previously shown to be a high biofilm producer, and the other a standard strain (RdKW20) previously shown to be a low biofilm producer (reported in Chapter 2). Both isolates

were from frozen stocks that were transferred into chocolate agar, and incubated for 18-22 h at 37ºC and under 5% CO_2 for no less than three overnight passages. Both isolates were then inoculated into brain heart infusion broth supplemented and incubated as described in Chapter 2 (section 2.2.2).

4.3.2 MIC determination for planktonic cells

MICs were determined using Etest® on Mueller-Hinton agar supplemented with 5% v/v defribrinated horse blood (Oxoid, Australia) and 20 mg/L of NAD, then incubated at 37°C in 5% CO_2 for 24 h using *H. influenzae* ATCC 49247 as a control. The inoculum was prepared and applied using the EUCAST Disk Diffusion Method for Antimicrobial Susceptibility Testing (Bouchillon *et al.*, 2005, EUCAST, 2014).

The MICs were used to calculate a sub-MIC, arbitrarily determined as 20-25% of the MIC. MICs are traditionally measured in doubling dilutions. The aim was to calculate sub-MIC to be between 2 doubling dilutions (1/4 = 25%) and 3 doubling dilutions (1/8 = 12.5%).

To ensure that the sub-MIC antibiotic concentration as calculated would not inhibit growth, organisms were inoculated into paired supplemented BHI broths, one with no antibiotic and the other with a concentration equivalent to the calculated sub-MIC and incubated overnight. Growth was measured by absorbance at 490 nm.

4.3.3 Antibiotic preparations

The antibiotic solutions at MIC and sub-MIC concentrations were prepared from stock solutions previously prepared in accordance with the procedure described

(Andrews, 2001) for the following antibiotics, amoxicillin (AMX, Sigma-eldrich, Germany), ciprofloxacin (CIP, Fluka analytica, USA), azithromycin (AZM, Fluka analytica, USA) and cefotaxime (CTX, Sigma-eldrich, Germany), and aliquoted into a 2 mL sBHI broth.

4.3.4 Biofilm-antibiotic MTP assay

A modified microtitre plate (MTP) biofilm assay described in Chapter 2 (sections 2.2.2 and 2.2.3) was used to investigate the effects of antibiotics on both the production of new biofilm, and the extension of existing biofilms. To assess the effect of antibiotics on the formation of new biofilm, organisms were inoculated into the MTP using broth containing antibiotics at either the MIC or the sub-MIC concentrations (see Figure 1). For each isolate, two MTPs were prepared on the same day and incubated for 18-24 h. The two MTP replicates were repeated on three different days. Each microtitre plate contained one isolate as an untreated control and four antibiotics: (AMX, CIP, AZM and CTX) in quadruplicate along with negative control.

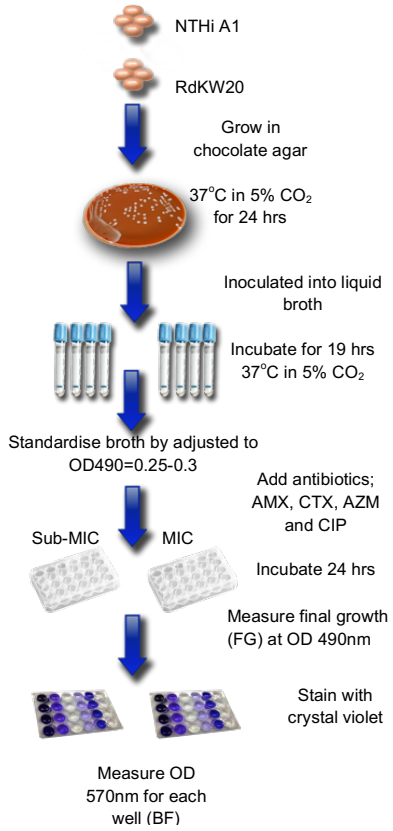

Figure 1. The steps for assessment of antibiotics used in this study (AMX,CIP,AZM and CTX) on new biofilm incubated with the antibiotics for 24 h.

The plates were incubated at 37ºC in 5% CO_2. The second approach was to measure biofilms with two levels of drug concentrations after a total of 48 h growth; to examine the extension of existing biofilm production illustrated in Figure 2. For this, two plates were prepared by inoculating the standardised inoculum ($\sim 1\times10^{-7}$) for each well, then allowing the biofilm to grow for 24 h without adding the antibiotics. The planktonic cells were then discarded aseptically and new broths with concentrations of antibiotics AMX, CIP, AZM and CTX at two different levels of antibiotic (MIC and

sub-MIC) were added into 2 mL of fresh sBHI broth. These were incubated for another 24 h.

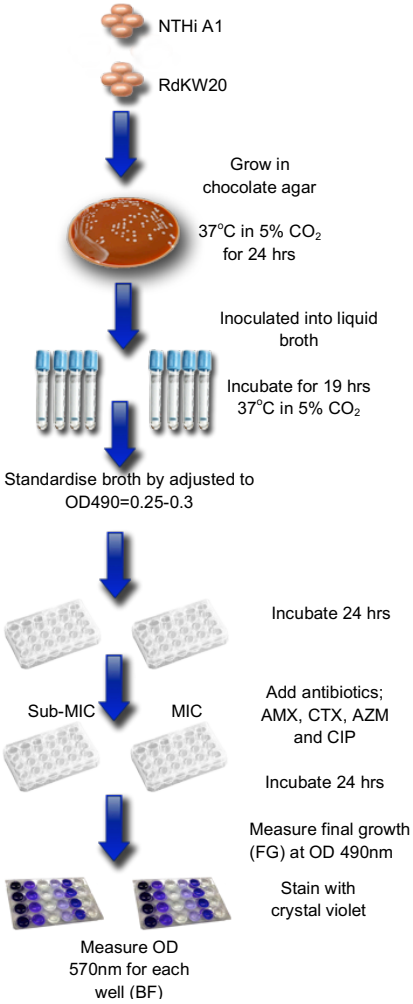

Figure 2. The steps for assessment of antibiotics used in this study (AMX,CIP,AZM and CTX) on existing incubated for 24 h then with the antibiotics for another 24 h (total incubation 48 h).

Final growth (FG) of both new biofilm and established biofilm (planktonic cells and biofilm material) was measured by reading optical density at 490 nm for the wells after incubation with antibiotics, and then the MTPs were washed with water (×3) and

stained with crystal violet for 15 min. Biofilm formation was assessed by measuring the amount of dissolved stain using 90% ethanol at OD 570 nm. This value was termed the biofilm formation (BF), a measure of the amount of biofilm grown inside the wells of the MTPs after 24 h.

4.2.5 Statistical evaluation

Data were analysed using one-way ANOVA with Bonferroni's multiple comparison test and graphed using GraphPadPrism® Version 6 software (GraphPad Software Inc, La Jolla, CA, USA). P value of <0.05 was considered statistically significant.

4.4 Results

4.4.1 Determination of the MIC and sub-MIC concentration for the isolates

The two isolates were susceptible to all the antibiotics (AMX, CIP, AZM and CTX) according to EUCAST interpretive criteria (see Table1). Both isolates were firstly evaluated by incubation with sub-MIC levels of antibiotics and the illustrated levels of growth from evaluating the optical density 490 nm are shown in Figure 4a and Figure 8a. The NTHi (A1) showed adequate growth with antibiotics at 12.5% MIC, where only AZM showed a decrease in growth (P value < 0.05) compared to the untreated control Figure 4a). The RdKW20 isolate showed adequate growth for all antibiotics at 25% MIC Figure 8a).

Table 1. The MIC level after incubation of MH with Etest® in 37c at 5% CO2 with concordance of sub-MIC level for each antibiotic agent.

(NTHi A1)	sub-MIC (µg/ml)	MIC (µg/ml)
Amoxicillin	0.5	4.0
Azithromycin	0.25	2.0
Ciprofloxacin	0.002	0.015
Cefotaxime	0.006	0.047
(RdKW20)		
Amoxicillin	0.1	0.38
Azithromycin	0.5	2.0
Ciprofloxacin	0.002	0.008
Cefotaxime	0.004	0.016

4.4.2 High biofilm producer (NTHi A1) and assessment of new biofilm formation

Fig. 3a shows that the addition of antibiotic at the MIC level inhibited the growth compared to the no-antibiotic control ($P<0.05$) and that for all antibiotics, the production of new biofilms was also inhibited with the exception of AZM ($P>0.05$) Fig. 3b. For the sub-MIC in Fig. 4a, there was no inhibition of growth with the exception of AZM ($P<0.05$), and there was no difference in biofilm production

compared to the no antibiotic control for all antibiotics Fig. 4b. Therefore, the biofilm production after incubation with sub-MIC of the antibiotics AMX, CIP, AZM and CTX illustrated no modification and the antibiotics did not increase the biofilm production.

(a)

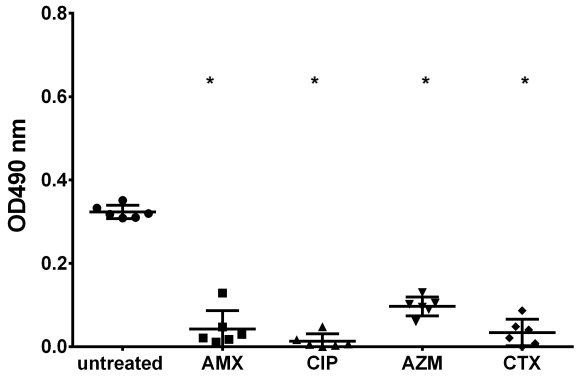

(b)

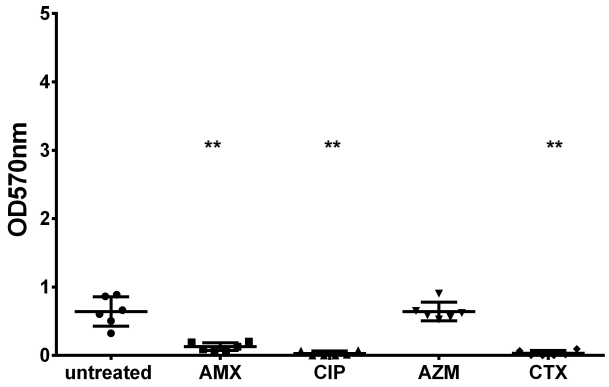

Figure 3. Effect of addition of AMX, CIP, AZM and CTX at MIC concentration to starting inoculum of NTHi A1 on (a) planktonic growth (OD490) and (b) biofilm formation (OD570) after 24 hrs incubation. (*) means $P<0.05$ and (**) $P<0.01$. Bars represent the mean (±SD) of each group.

(a)

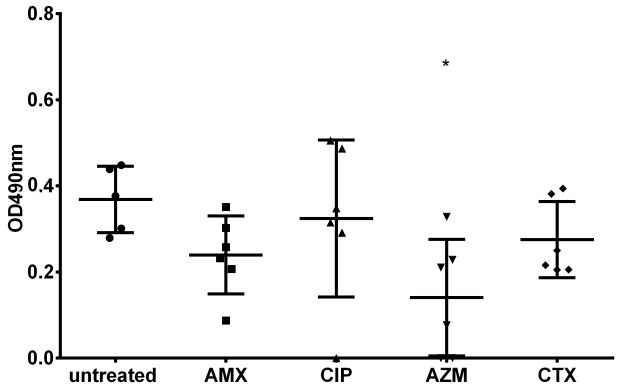

(b)

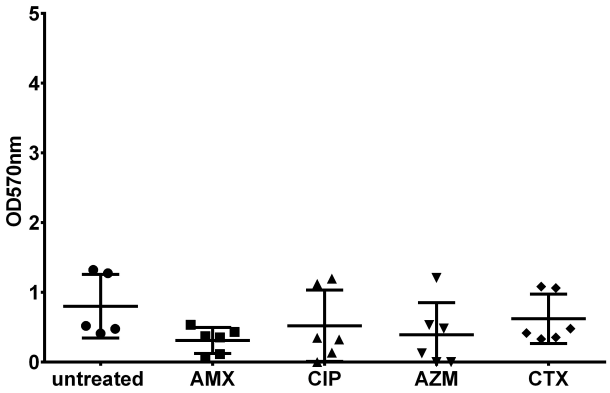

Figure 4. Effect of addition of AMX, CIP, AZM and CTX at sub- MIC concentration to starting inoculum of NTHi A1 on (a) planktonic growth (OD490) and (b) biofilm formation (OD570) after 24 hrs incubation. (*) means $P<0.05$. Bars represent the mean (±SD) of each group.

4.4.3 High biofilm producer (NTHi A1) and assessments on existing biofilm

Fig. 5a shows that the addition of antibiotic to inoculum at the MIC level has not inhibited the growth of the planktonic cells that shed from existing biofilm. The growth of bacterial cells after exposure to antibiotics compared to the no-antibiotic control was ($P<0.05$) for all antibiotics with exception of CIP ($P>0.05$). The biofilm production of MIC level of antibiotics added after biofilm establishment was also not inhibited ($P>0.05$) with exception of increase biofilm production only after AMX treatment ($P<0.05$) (Fig. 5b).

In Fig. 6a, the sub-MIC shows no inhibition of the planktonic growth with antibiotics ($P>0.05$) with exception of cells growth increase with CIP that shed from existing biofilm. Biofilm formation was found to be at the same level as the untreated biofilm ($P >0.05$); Fig. 6b.

(a)

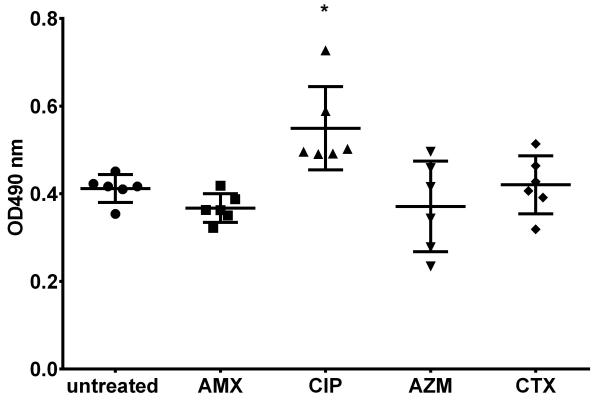

(b)

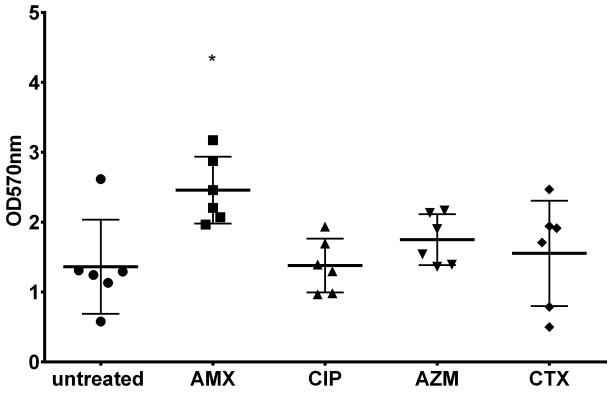

Figure 5. Effect of addition of AMX, CIP, AZM and CTX at MIC concentration to a 24 hr established biofilm of NTHi A1 on (a) additional planktonic growth (OD490) and (b) biofilm formation (OD570) after a further 24 hrs incubation. (*) means $P<0.05$. Bars represent the mean (±SD) of each group.

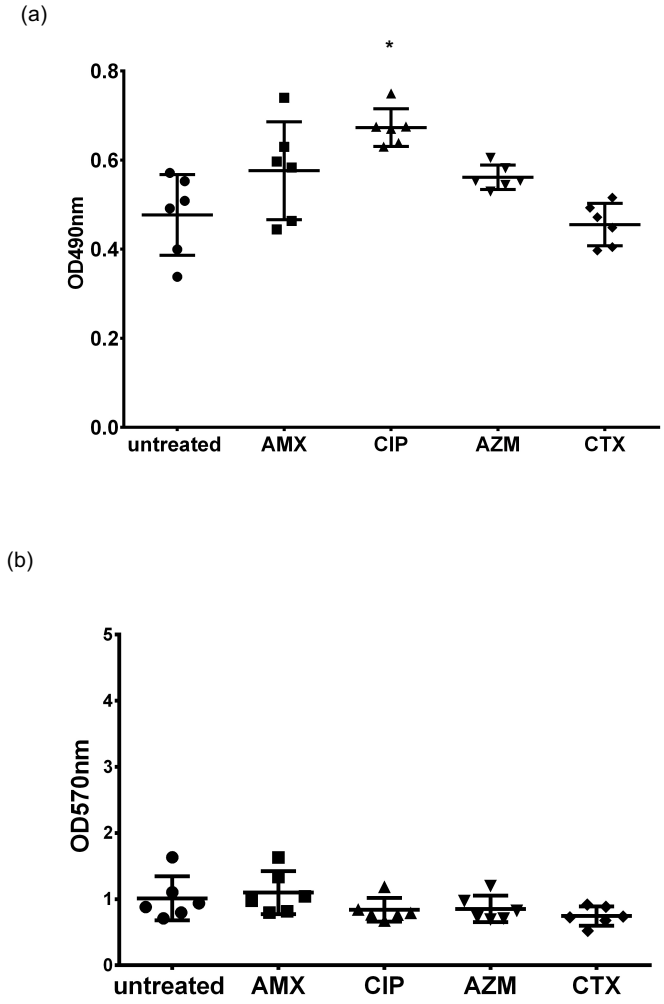

Figure 6. Effect of addition of AMX, CIP, AZM and CTX at sub-MIC concentration to a 24 hr established biofilm of NTHi A1 on (a) additional planktonic growth (OD490) and (b) biofilm formation (OD570) after a further 24 hrs incubation. (*) means $P<0.05$. Bars represent the mean (±SD) of each group.

4.4.4 Low biofilm producer (RdKW20) and assessments of new biofilm formation

In Fig. 7a, the final growth of the isolate treated by AMX, AZM and CTX at MIC was inhibited ($P<0.01$) when compared to the untreated isolate growth after incubation. The formation of biofilm after treatment with antibiotics, shown in Fig. 7b, was similar to that of the untreated isolate ($P>0.05$) and was not affected by the addition of MIC of AMX, CIP, AZM and CTX.

In Fig. 8a, sub-MIC shows no inhibition of growth of the planktonic cells that shed from existing biofilm after treatment with all the antibiotics when compared to untreated control ($P>0.05$). There was no difference in biofilm formation after treatment with the antibiotics ($P>0.05$) illustrated in Fig. 8b.

(a)

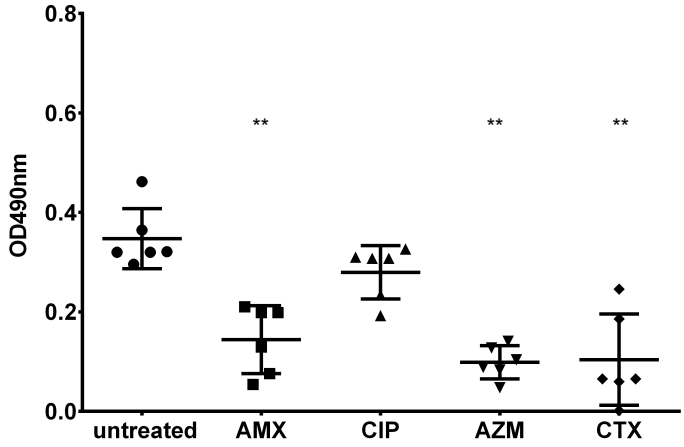

(b)

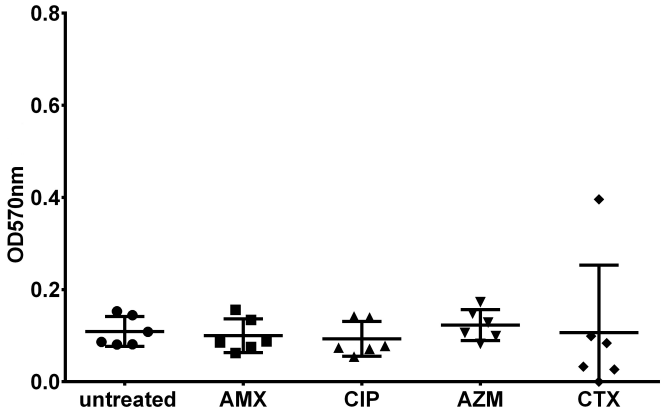

Figure 7. Effect of addition of AMX, CIP, AZM and CTX at MIC concentration to starting inoculum of RdKW20 on (a) planktonic growth (OD490) and (b) biofilm formation (OD570) after 24 hrs incubation. (*) means $P<0.05$ and (**) $P<0.01$. Bars represent the mean (±SD) of each group.

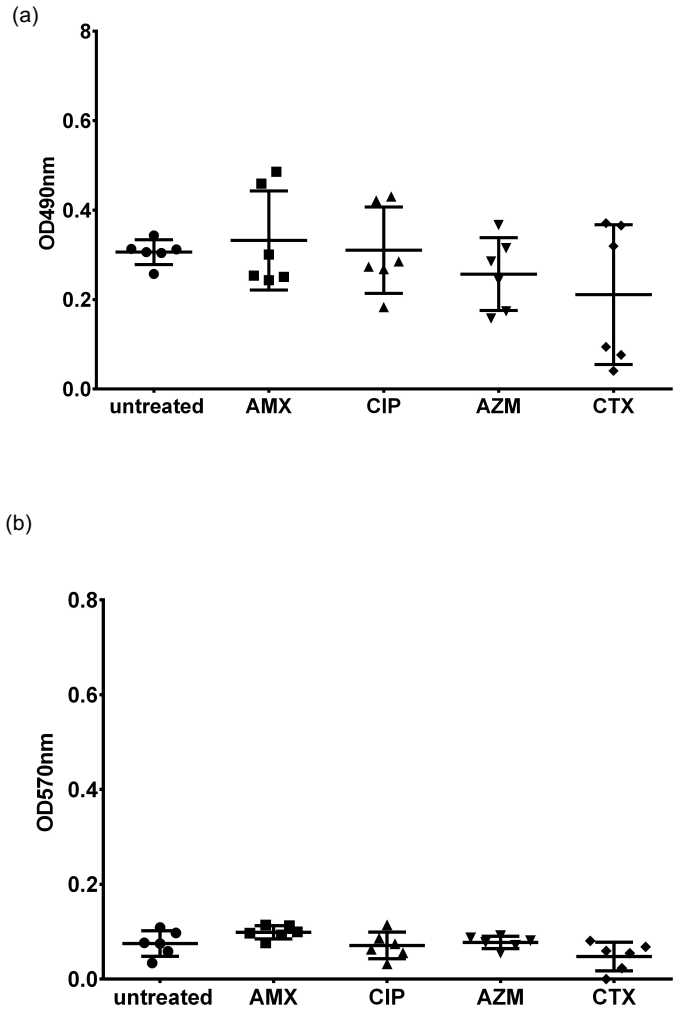

Figure 8. Effect of addition of AMX, CIP, AZM and CTX at sub-MIC concentration to starting inoculum of RdKW20 on (a) planktonic growth (OD490) and (b) biofilm formation (OD570) after 24 hrs incubation. Bars represent the mean (±SD) of each group.

4.4.5 Low biofilm producer (RdKW20) and assessments on existing biofilm

Fig. 9a shows that a MIC level of all antibiotics does not inhibit the growth of the planktonic cells that shed from established biofilm after exposure to antibiotics ($P>0.05$) with exception of CIP where growth increased ($P<0.05$) when compared to untreated inoculum. In Fig. 9b, AMX appeared to be trending towards and increase in biofilm formation when added to existing biofilm, but the effect was not significant.

In Fig. 10a, the final growth does not show inhibition of the planktonic cells that grew after exposure to antibiotics from exciting biofilm at sub-MIC level. Sub-MIC level of AMX on the existing biofilm Fig. 10b. shows an increase of biofilm ($P<0.01$) compared to the untreated isolate. The other antibiotics administered at sub-MIC did not showed any alteration in biofilm production.

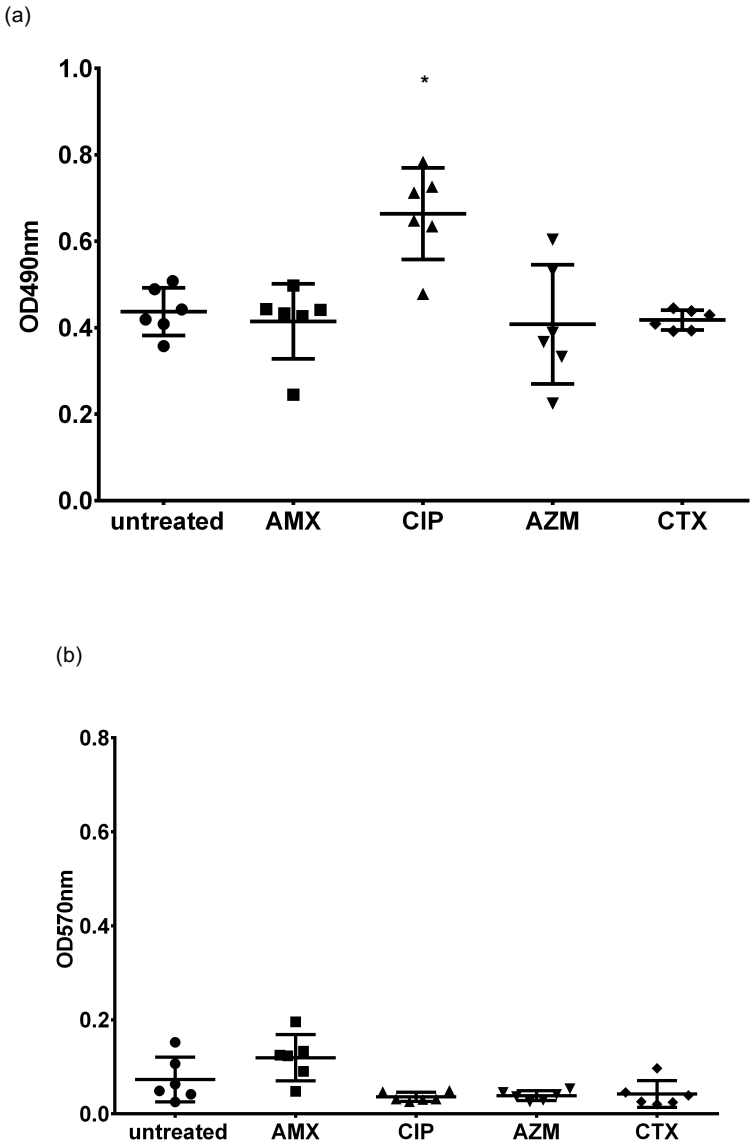

Figure 9. Effect of addition of AMX, CIP, AZM and CTX at MIC concentration to a 24 hr established biofilm of RdKW20 on (a) additional planktonic growth (OD490) and (b) biofilm formation (OD570) after a further 24 hrs incubation. (*) means $P<0.05$. Bars represent the mean (±SD) of each group.

(a)

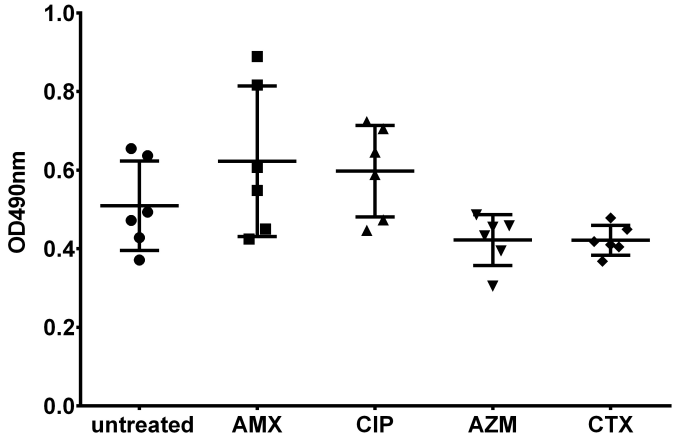

(b)

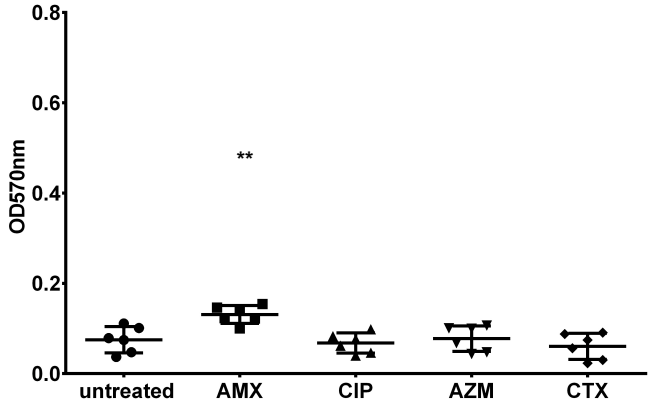

Figure 10. Effect of addition of AMX, CIP, AZM and CTX at sub-MIC concentration to a 24 hr established biofilm of RdKW20 on (a) additional planktonic growth (OD490) and (b) biofilm formation (OD570) after a further 24 hrs incubation. (*) means $P<0.05$ and (**) $P<0.01$. Bars represent the mean (±SD) of each group.

4.5 Discussion

While the Etest® is not a reference method for susceptibility testing, it is widely used and was considered appropriate for this study, as the results were only to be used to determine antibiotic levels (MIC and sub-MIC) to challenge biofilm production and not for determination of susceptibility or resistance and the guidance of clinical therapy.

In the current study, AMX was shown to produce an effect on existing biofilm. We showed that AMX stimulates additional biofilm formation upon an existing biofilms even with growth inhibition of the planktonic cells. It is clearly shown from Fig. 5b and Fig. 10b, that AMX has a significant effect on increasing existing biofilms formation at MIC levels for NTHi A1 biofilms. Although, there is limited inhibition of the growth with sub-MIC for the cells with new biofilm and growth of cells that grow from existing biofilm after treatment. This NTHi isolate was confirmed as resistant to AMX with an MIC at 4 μg/ml as defined by EUCAST breakpoints for *Haemophilus influenzae.* Bacterial responses to antibiotics here, even with resistance, raises the question of whether this biofilm induction results from a specific signal triggered by the antibiotics (Laureti *et al.*, 2013) or whether they are only the consequences of a perturbation in the cellular adhesion as a result of β-lactam antibiotics.

As shown in Fig. 4 and Fig. 6, the production of biofilm with NTHi A1 isolate was not affected after sub-MIC and remained similar to biofilm formation for untreated inoculum. In a study conducted by Wu *et al.* (2014), some β-lactam antibiotics were thought to increase and stimulate the formation of 1-day biofilm for some NTHi

clinical strains in different concentrations (Wu *et al.*, 2014). This is not quite similar to our findings which has shown NTHi A1 biofilm increase significantly after existing biofilm exposure to an MIC level of AMX (*β*-lactam antibiotic) but not with sub-MIC level of AMX.

The RdKW20 biofilms also shows an increase biofilm formation ability within sub-MIC levels on an existing biofilm even though the strain was sensitive to AMX in the planktonic cells state. However, the cells seemed to shed from existing biofilm and this is may be due to increase in the resistance to AMX. This mechanism still needs further investigation which may due to some alteration of the cells resistance mechanism to *β*-lactams, especially with AMX.

With the other antibiotics used in this study, both concentrations of CIP and CTX showed no effect of either enhancing new biofilm formation or removing the existing biofilm. However, the growth of the NTHi A1 and RdKW20 with CIP showed some resistance and cells were significantly increased in their growth when compared with the growth of untreated inoculum. This resistance of cells to CIP was not accompanied with an increase of biofilm or enhancement of biofilm formation. For the other antibiotic, AZM, there is no confirmation that AZM has any effect on biofilm production for NTHi isolates when added at MIC or sub-MIC levels. On the other hand, a study on the effect of subinhibitory concentration of AZM (macrolide) indicated a decrease of NTHi biomass in established NTHi biofilm (Starner, *et al*., 2008). Azithromycin was also found to decrease initiating NTHi biofilm as well as the established biofilm at subinhibitory MIC level (Starner *et al.*, 2008). These observations were not illustrated with the NTHi isolates in our study.

4.6 Conclusion

There was an increase of NTHi biofilm material, when the organism was incubated with amoxicillin as evident from significant increase of optical density of crystal violet. With the two concentrations of antibiotics, sub-MIC and MIC, used on NTHi biofilm, the formation of biofilm varied specifically with AMX treated biofilm. The existing NTHi biofilm confirmed an increase of biofilm formation after addition of MIC level of AMX.

Using the MTP assay for investigating biofilm formed by the clinical NTHi isolate and the standard *Haemophilus influenzae* isolate gave us a simple and direct examination of the impact of the two levels of concentration of AMX, CIP, AZM and CTX. The effect of AMX on NTHi biofilm enhancement requires further analysis to determine which part of the biofilm is stimulated to increase the biofilm biomass.

4.7 References

Andrews, J M, 2001. 'Determination of minimum inhibitory concentrations'. *Journal of Antimicrobial Chemotherapy,* 48**,** 5-16.

Barkai, G, Leibovitz, E, Givon-Lavi, N & Dagan, R, 2009. 'Potential contribution by nontypable Haemophilus influenzae in protracted and recurrent acute otitis media'. *The Pediatric Infectious Disease Journal,* 28**,** 466-471.

Bouchillon, S K, Johnson, J L, Hoban, D J, Stevens, T M & Johnson, B M, 2005. 'Impact of carbon dioxide on the susceptibility of key respiratory tract pathogens to telithromycin and azithromycin'. *Journal of Antimicrobial Chemotherapy,* 56**,** 224-227.

Erwin, A L & Smith, A L, 2007. 'Nontypeable Haemophilus influenzae: understanding virulence and commensal behavior'. *Trends in Microbiology,* 15**,** 355-362.

Eucast, 2014. 'Antimicrobial susceptibility testing'. *Disk diffusion methodology* [Online].

Hall-Stoodley, L, Hu, F Z, Gieseke, A, Nistico, L, Nguyen, D, Hayes, J, Forbes, M, Greenberg, D P, Dice, B & Burrows, A, 2006. 'Direct detection of bacterial biofilms on the middle-ear mucosa of children with chronic otitis media'. *The Journal of the American Medical Associaion,* 296**,** 202-211.

Hall-Stoodley, L & Stoodley, P 2009. 'Evolving Concepts in Biofilm Infections'. *Cellular Microbiology,* 11**,** 1034-1043.

Hoffman, L R, D'argenio, D A, Maccoss, M J, Zhang, Z, Jones, R A & Miller, S I, 2005. 'Aminoglycoside antibiotics induce bacterial biofilm formation'. *Nature,* 436**,** 1171-1175.

Laureti, L, Matic, I & Gutierrez, A, 2013. 'Bacterial responses and genome instability induced by subinhibitory concentrations of antibiotics'. *Antibiotics,* 2**,** 100-114.

Liu, Y C C & Post, J C, 2009. 'Biofilms in pediatric respiratory and related infections'. *Current Allergy and Asthma Reports,* 9**,** 449-455.

Sailer, F C, Meberg, B M & Young, K D, 2003. 'β‐Lactam induction of colanic acid gene expression in Escherichia coli'. *Federation of European Microbiological Societies Microbiology letters,* 226**,** 245-249.

Slinger, R, Chan, F, Ferris, W, Yeung, S W, St Denis, M, Gaboury, I & Aaron, S D, 2006. 'Multiple combination antibiotic susceptibility testing of nontypeable Haemophilus influenzae biofilms'. *Diagnostic Microbiology and Infectious Disease,* 56**,** 247-253.

Starner, T D, Shrout, J D, Parsek, M R, Appelbaum, P C & Kim, G, 2008. 'Subinhibitory concentrations of azithromycin decrease nontypeable Haemophilus influenzae biofilm formation and diminish established biofilms'. *Antimicrobial Agents and Chemotherapy,* 52**,** 137-145.

Starner, T D, Zhang, N, Kim, G, Apicella, M A & Mccray Jr, P B, 2006. 'Haemophilus influenzae forms biofilms on airway epithelia: implications in cystic fibrosis'. *American Journal of Respiratory and Critical Care Medicine,* 174**,** 213.

Takei, S, Hotomi, M & Yamanaka, N, 2013. 'Minimal biofilm eradication concentration of antimicrobial agents against nontypeable Haemophilus influenzae isolated from middle ear fluids of intractable acute otitis media'. *Journal of Infection and Chemotherapy,* 19**,** 504-509.

Vlastarakos, P V, Nikolopoulos, T P, Maragoudakis, P, Tzagaroulakis, A & Ferekidis, E, 2007. 'Biofilms in ear, nose, and throat infections: how important are they?'. *The Laryngoscope,* 117**,** 668-673.

Wu, S, Li, X, Gunawardana, M, Maguire, K, Guerrero-Given, D, Schaudinn, C, Wang, C, Baum, M M & Webster, P, 2014. 'Beta-Lactam Antibiotics Stimulate Biofilm Formation in Non-Typeable Haemophilus influenzae by Up-Regulating Carbohydrate Metabolism'. *Public Library of Science one,* 9**,** e99204.

Chapter 5

Exploratory approach for Nontypeable *Haemophilus influenzae* biofilm using FTIR microspectroscopy

Abstract

NTHi biofilm variability *in vitro* may also be related to differences in the chemical features of the biofilm from different strains of NTHi. Studying the conformational changes and the relative differences in some chemical functional groups, such as proteins, carbohydrates, nucleic acids and lipids, and their association with each other, will promote a better understanding of NTHi biofilms.

Fourier transform infrared spectroscopy (FTIR) is an analytical non-destructive technique requiring minimal sample preparation. It was applied to study biochemical changes over around 0.1-10 mm NTHi biofilm surfaces generated by two *Haemophilus influenzae* Hi strains (NTHi and RdKW20 isolates) that had different levels of biofilm formation. In this study, NTHi biofilm in vitro growth was first analysed over a large spot size (~8 mm) using an IR benchtop spectrometer. A *Pseudomonas aeruginosa* positive control (PAO1) was also analysed because the ability of PAO1 to grow biofilm on a CaF_2 disc surface has been previously assessed (Cheung *et al.*, 2007). Then, an IR microscope was used to analyse the biofilm with two different spatial resolutions of 100 μm and 2.7 μm. Infrared hyperspectral images were produced to study the two dimensional (2D) spatial distribution of biofilm chemical functional groups. Data from these images were analysed by various multivariate approaches. The integral of the IR spectrum encompassing the protein and carbohydrates regions (1790 cm^{-1} to 950 cm^{-1}) were used to evaluate relative biofilm production by the test organisms. The integration ranged from 8.13 for the NTHi, to 4.28 and 6.47 for RdKW20 and PAO1 respectively. Changes in the intensity of these regions and variation of the ratio between proteinceous and polysaccharide material within the 2D spectral array of the cellular and slime parts of all isolate

biofilms were spatially visualised. Principle component analysis (PCA) of the spectral data, selected from high growth area and low growth areas of the biofilm formed by the two *Haemophilus influenzae* isolates, confirmed that the cellular aggregates and extracellular polymeric substances (EPS) in the high growth areas of the RdKW20 biofilm chemically clustered with the thin growth areas (EPS only) formed by NTHi A1 biofilm. Multivariate analyses of the IR hyperspectral images were used to identify specific spectral clusters and visualise the spatial distribution of proteins and carbohydrates as major components of the biofilm. Variation in the biofilm coverage by NTHi, when formed *in vitro*, correlated with the spatial distribution of functional groups, demonstrated the presence of chemically heterogeneous biofilm.

5.1. Introduction

In general, the chemical components of biofilm are composed of substances from the bacterial cell wall and genetic material of the bacterial cell (Donlan and Costerton, 2002). The composition and structure of biofilm are believed to be formed by a stress response to environmental changes, and is due to specific mutations in the genetic information of the bacterial cells (Donlan and Costerton, 2002). The polysaccharide component of biofilm has a potential role in the adhesion and antigenic reaction of bacterial cells in the form of cellular and extracellular substances (Vu *et al*., 2009) in addition to capsular polysaccharides that may play a role in biofilm formation for some bacteria (Di Xia *et al*., 2014, Andersson *et al.*, 2009). Biofilms with extracellular polymeric substances contain exopolysaccharide as a main 'cement' for the biofilm (Sutherland, 2001, Costerton *et al.*, 1999). In Gram-negative bacteria, polysaccharide is a major component of the cell wall and is composed of lipopolysaccharide. NTHi (which are non-capsulated *Haemophilus influenzae* species) are believed to be lacking O-antigens that link to the inner core of the lipopolysaccharide, and NTHi possesses lipooligosaccharides instead. These lipooligosaccharides react with sialic acid to attach to the host epithelial cells (Jurcisek and Bakaletz, 2007, Swords *et al.*, 2004, Langereis and Hermans, 2013). Therefore NTHi aggregation of cells and maturation of biofilm is a chemically different process characterised by the presence of oligosaccharides which have fewer glycoforms than polysaccharides. Thus the variability of NTHi strains in relation to biofilm formation may be associated with the chemical components that NTHi biofilm possess during biofilm production and, secondly, the EPS chemical components which may be unique in NTHi biofilm.

FTIR spectroscopy is a non-invasive analytical method that is used here to examine the biofilm functional groups. This method functions by analysing the absorption of infrared light that correlates with specific molecular functional group vibrational modes. The amount of IR light absorbed by the molecular structure can be quantified and IR intensities correlate with the concentration of functional groups according to the Beer- Lambert law (Lin-Vien *et al.,* 1991). Absorbance at a given wavenumber can be obtained by the Beer-Lambert equation $A = \varepsilon \times l \times c$ where (ε) is the molar absorbance coefficient, (*l*) is the pathlength and (c) is the concentration of the component in the sample. According to the IR absorbance, a plot of absorbance versus wavenumber (cm^{-1}) yields an IR spectrum (described in Chapter 1 section 1.2.1). IR spectra show all the major chemical functionalities present in the biofilm, which in this case is a very complex mixture. There are five spectral regions that are dominated by different functional groups for the bacterial cell chemical components: lipids, proteins, nucleic acids and carbohydrate (Burgula *et al.*, 2007). Infrared spectra of the microbiological material were collected in transmission mode using an IR-transparent CaF_2 disc on which the biofilm was grown. Along with the quantitative measurement of the IR spectral regions, spatial distribution of the chemical component information by FTIR microscopy was applied to the mature biofilm grown by the NTHi isolate. The characterisation of the overall chemical composition of NTHi biofilms provides a holistic description of the macromolecule(s) for the cell aggregates and (EPS) of NTHi biofilm over a small scale (10 mm). Quantitative characterization over an area of 8 mm diameter for NTHi mature biofilm by FTIR has not been performed to date. The incorporation of 2D IR imaging shows the spatial distribution of chemical functional groups and enhances our knowledge about the chemical distribution of carbohydrates, proteins and lipids in NTHi biofilms.

Application of FTIR imaging for microbiological samples has been slow to develop, but is promising. It has been applied to classify and identify bacterial cells and measure metabolic changes during the formation of different phenotypic processes and biofilm maturation (Naumann, 2006). FTIR spectroscopy now has potential for studying biofilm maturation, components and recalcitrance to antibacterial treatment (Wolf *et al.*, 2002, Lu *et al.*, 2012b, Paquet-Mercier *et al.*, 2014). Using an IR microscope with a focal plane array detector, images can be obtained with a particular setup of pixel size ≈ 2.7 μm. This high resolution imaging is a novel approach to study the IR features of molecular distribution within biological tissues, including biofilm (Serra *et al.*, 2007). Multivariate analysis of the spectral data, such as principal components analysis (PCA), can help to analyse the complex spectra obtained from biological samples. Basically, PCA decomposes the spectra into 'principal components' (PCs) that summarizes the spectral data matrix, and reduces the data to a few PCs that describe the majority of the spectral variance. PCs appear in descending order, each successive one of which describes less and less variance (described in Chapter 1 section 1.2.4.2.1).

Mature biofilm (after 24 h) that is formed by other microorganisms showed increased carbohydrate to protein ratio compared with the ratio value of the early stages of bacterial growth (Serra *et al.*, 2007). Serra and co-workers (2007) showed that the IR bands for carbohydrate absorption in mature biofilm increased at a higher rate than the protein bands, such as amide II band. From Chapter 2, variability of the *in vitro* formation of biofilm by different NTHi strains was confirmed using a crystal violet-staining assay. We hypothesise here that the ratio of some chemical functional groups, such as the carbohydrate to protein ratio, could vary between the high biofilm

producing NTHi strain and the low biofilm producing strain similar to biofilm formed by other species studied by FTIR spectroscopy (Serra, *et al* 2007, Quilès and Humbert, 2014). Analysis of the carbohydrate and protein regions from IR absorbance may indicate the level of biofilm formation (Humbert *et al.*, 2011). Exploring the variation of these spectral regions and the spatial distribution of carbohydrate and protein regions may provide an estimate of how the NTHi biofilm varies in formation over an area from 0.1 to 10 mm. The biofilm chemical constituents were estimated by IR spectral information of the regions of biofilm growth on the surface at a spot size ≈ 8 mm and obtaining individual spectra. Then, IR data was obtained using an IR microscope with a spot size of about 100 μm and down to 2.7 μm for high resolution. Chemical analysis of EPS produced from different microorganisms has been reported in other studies of biofilm which confirmed that spectroscopic markers include polysaccharides, lipopolysaccharides and protein (Bosch *et al.*, 2006).

The aims of this study were to investigate potential differences in biofilm chemical composition formed by two different *Haemophilus influenzae* strains, and to apply unsupervised multivariate analysis to the FTIR microspectroscopy data in order to identify the spatial distribution of specific chemical markers in NTHi biofilm.

5.2. Methods

5.2.1 Bacterial samples growth and culture conditions

An NTHi clinical isolate (NTHi A1) that was confirmed previously in Chapter 2 to have high biofilm production, and a standard isolate (RdKW20) with low biofilm production were chosen as the model *H. influenzae* strains for this study. The *Pseudomonas aeruginosa* strain, PAO1, also known as a high biofilm producer, was

selected as the positive control organism. The bacterial cells were harvested from overnight incubated chocolate agar and inoculated into sBHI broth and incubated for 18 h at 37ºC and 5% CO_2.

5.2.2 Biofilm formation assay

Bacterial biofilms were prepared using a protocol developed for the MTP biofilm assay as reported in Chapter 2. Microtitre plates (Costar 24 well plate, Corning Incorporated, USA) were inoculated with 2 ml of standardised bacterial broth to about $1X10^7$ CFU/ml. A sterile CaF_2 window (10 mm diameter, Crystran Limited, UK) was performed in two steps. First, CaF_2 window were cleaned using 70% ethanol then autoclaved in steam pressure 120ºC for 15 min. This CaF_2 window was inserted into each well then incubated for 24 hours at 37ºC and 5% CO_2. After incubation, the CaF_2 discs were washed off three times with water and let dry for half an hour at room temperature before IR analysis as described by Naumann (2006). These experiments were repeated (n=10) for the FTIR microspectroscopy methods.

5.2.3 FTIR spectroscopy data collection

Transmission mode FTIR spectra were recorded on a Vertex 70 spectrometer (Bruker Optik, Germany) with a liquid nitrogen-cooled mercury-cadmium-telluride (MCT) detector. Spectra were collected from 3900 cm^{-1} to 800 cm^{-1}. Hyperspectral images were recorded with a Bruker Hyperion 3000 microscope (Bruker Optik, Germany) coupled with a liquid nitrogen-cooled MCT detector with spectral range 4000 cm^{-1} to 820 cm^{-1} then with a focal plane array (FPA) 64×64 detector with spectral range 3800 cm^{-1} to 950 cm^{-1}. Spectral resolution for all transmission spectra acquisition and hyperspectral images was 4 cm^{-1}. The samples were measured under continuous

purged dried air to reduce the interference of water vapour from the atmosphere with 128 scans of the sample and the background using a blank CaF_2 disc. This method was carried out for all ten replicates of biofilm grow on CaF_2 discs for each of the three bacterial strains.

5.2.3.1 Hyperspectral mapping using single point detector

Hyperspectral images using a single point were recorded using a 15× objective lens with numerical aperture =0.4 attached with microscopy camera (Infinity1, Lumenera, Canada). The step size of the hyperspectral image was 100 µm and the sampling area range 2×2 mm. The aperture size was about 160 µm. Hyperspectral images were obtained for three of the ten biofilm preparations from NTHi A1 and RdKW20.

5.2.3.2 Hyperspectral mapping using single point detector FPA detector

A FPA detector (64×64) was used to produce hyperspectral images with a fixed pixel size of 2.73 µm within a sampling area of 680 µm. A total of 1024 scans were recorded for background and sample. One FPA image is 64×64 pixels with an approximate area of 175×175 um. Recording 4×4 of these images was performed to create a larger image. This was carried out one selected biofilm preparation from NTHi A1 and RdKW20.

5.2.4 Raman Spectroscopy

A Renishaw In Via® Raman microspectrometer (Renishaw, UK) was used for spectral acquisition of the biofilm. A 532 nm excitation laser was used in streamline mode recording a spectral region of 668 cm^{-1} to 3147 cm^{-1} with a grating of 1200 l/mm. A 50× objective lens with numerical aperture of 0.75 was used and the laser power was adjusted to 2.4 mW at the sample with a 120 s exposure time. The spot size for the

laser was 1.3 μm with step size 1μm. The mapping size then was about 47×40. This was performed on one biofilm preparation of NTHi A1.

5.2.5 Spectral manipulation and evaluation

Spectral pre-processing was performed using the OPUS 7.2 software (Bruker Optik, Germany). Atmospheric compensation and averaging of the spectral data was performed for all individual spectra (n=10) using the OPUS atmospheric compensation and averaging functions. Peak area integration was calculated as an average of the ten spectral acquisitions by measuring the peak area above a baseline generated between two wavenumber points. The quantification of these areas was performed using the OPUS software in addition to the ratio for these integrations. The spectral ranges were cut for both one single spectrum recording and for the hyperspectral images to the bands of intensities 3000 cm^{-1} to 2769 cm^{-1} and 1750 cm^{-1} to 950 cm^{-1}. Integration of the peaks for the hyperspectral images was performed by the integration function and peak ratios were applied to several peaks by using the trace ratio function within the software. Data were analysed using the student t-test with Microsoft Excel®. P value of <0.05 was considered statistically significant.

Spectral pre-processing was performed for multivariate analysis of the 2D IR hyperspectral images with atmospheric compensation in the form of 2^{nd} derivatives (Savitzky-Golay algorithm with 13 smoothing points) and vector normalisation. For Raman spectra, data pre-processing was performed using cosmic ray removal and noise filter with 12 PCs by using WiRe 4.1 software (Renishaw, UK). The 2^{nd} derivatives were performed to the Raman map to analyse the spectral data with multivariate analysis.

5.2.5.1 Multivariate analysis for the hyperspectral images

From selected images of the 160 × 160 μm pixel size images obtained from NTHi A1 and RdKW20 biofilms, twenty spectra were selected for further analysis. From each image, ten spectra were selected from spots with high biofilm growth and ten from spots with low biofilm growth which were determined from creating an integration image at 1750 cm^{-1} to 950 cm^{-1} region and then select the individual spectra.

These spectra were imported into UnscramblerX® software version 10.1 (CAMO software, Norway) for principal component analysis (PCA), after pre-processing steps were performed for the twenty spectra as described in the previous section. For this PCA model, two spectral ranges were selected: from 3000 cm^{-1} to 2769 cm^{-1} and 1752 cm^{-1} to 952 cm^{-1}.

Cluster analysis of the hyperspectral data from the same selected images was performed using the OPUS® software (Bruker Optik, Germany) and then applying a standard method (Euclidean distance then Wards algorithm). Dendrograms were produced from the clustering analysis and three to five cluster images were produced using this method. The selection of the number of clusters for the clustering images were according to the number of distance separations between clusters that were formed by the dendrograms.

These steps were also performed using the Cytospec v.1.4.03 software (Cytospec®, Germany). Hierarchical cluster analysis (HCA) was performed with data pre-processed using the Euclidean method and Ward's algorithm. Each cluster was colour

coded to display the component separation within the dendrogram and the spatial distribution in the image.

PCA was also performed on the pre-processed data within the 2000 cm^{-1} to 950 cm^{-1} range using OPUS software or Cytospec and selecting the region from 2000 cm^{-1} to 950 cm^{-1}.

For the pre-processed Raman data hierarchical cluster analysis (HCA) was performed with data using the Euclidean method and Ward's algorithm. Each cluster was colour coded to display the component separation within the dendrogram and the spatial distribution in the image. These steps were performed using Cytospec v.1.4.03 software (Cytospec®, Germany).

5.2.6 Optical microscopic images

All isolates analysed in this study were examined optically with 10× objective, NA= 0.3 using a Leica microscope (Leica, UK) attached with video camera (Philips SPC1030NC webcam, UK).

5.2.7 Scanning Electron microscope (SEM)

The samples were fixed overnight with 2.5% glutaraldehyde in phosphate-buffered saline (PBS) then the CaF_2 discs were rinsed three times for ten minutes with PBS prior to dehydration with graded ethanol. The discs were then immersed into 20%, 40%, 60%, 70%, 80%, 90% and 100% ethanol for 20 min for each grade. Then the discs were dried at room temperature and mounted onto aluminium stubs and sputter

coated with gold. The biofilm was examined using Hitachi SU-70 scanning electron microscope (SEM) (Hitachi High Technologies, Japan).

5.2.8 Statistical analysis

The mean and standard deviation of the integrated peaks of the spectra and one-way analysis of variance for the ratio between peaks were obtained using Microsoft Excel 2010.

5.3. Results and discussion

The main focus of this study was to explore the spectral data for the NTHi biofilms grown *in vitro* acquired by FTIR spectroscopy, obtained as overall individual spectra and as hyperspectral images. In order to firstly visualise the biofilm growth over the surface of the CaF_2 discs, the biofilms were analysed by optical light microscopy (Fig. 1a and 1b). For NTHi A1, shown in Fig. 1a, the numbers of cells clusters with a smaller number of individual cells and coverage of biofilm material were less patchy than the RdKW20 low biofilm producer (Fig. 1b) which has shown clear dispersed individual cells over the surface of CaF_2 disc. The SEM image in Fig. 1c, shows the clusters of aggregate cells with an approximate size of 10 μm and deposits of materials is that thought to be EPS. Fig. 1d shows individual cells which are dispersed in this smaller scale (10 μm). These images confirm that the NTHi isolate form more biofilm material than isolate RdKW20, which is consistent with the crystal violet assay results previously reported in Chapter 2 (section 2.3.1).

Biofilms were grown and analysed with FTIR spectroscopy and microspectroscopy within 22-24 h incubation of the initial inoculum. The growth of sessile cells and formation of EPS were allowed to form for the analysis. Studies of biofilm with FTIR showed that chemical fingerprints and major chemical group variation can be related to aggregates cells (sessile cells) that form within the slime of the biofilm between 8 h and 24 h growth (Quilès and Humbert, 2014).

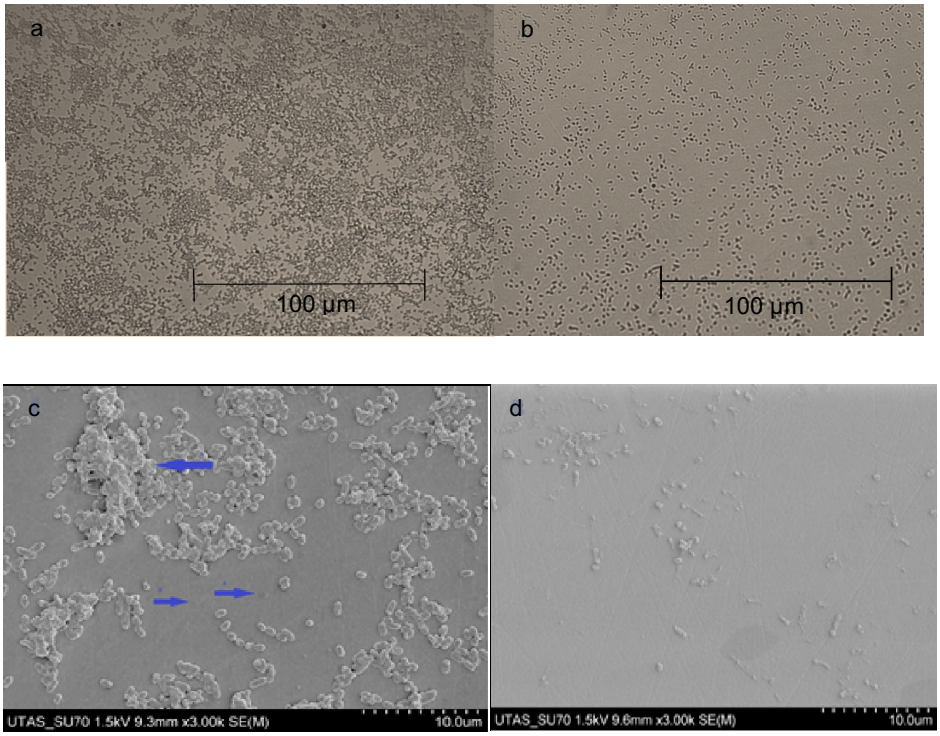

Figure 1. (a) NTHi A1 and(b) RdKW20 biofilm optical images (×10). SEM images within 10 µm scale (c) NTHi A1 where blue arrows shows slime material deposited on the CaF_2 discs and clusters of bacterial cells aggregation that secreted the slime. (d) RdKW20 with less cellular aggregates.

5.3.1 Chemical analysis for FTIR spectra of NTHi biofilm

IR spectra from each bacterial isolate were obtained across each sample (n=10) then the average of these spectra for each isolate was calculated to give a representative spectrum. The averaged spectra for each isolate are presented in Fig. 2.

A CaF_2 disc incubated with broth only without isolate inoculum was analysed by using the same method of FTIR to investigate if there were any nutrient residuals remaining after the cleaning and washing methods of the discs that could overlap with the biofilm IR spectra. This analysis showed that there was no major IR spectra contribution from washed CaF_2 discs formed by the sBHI broth.

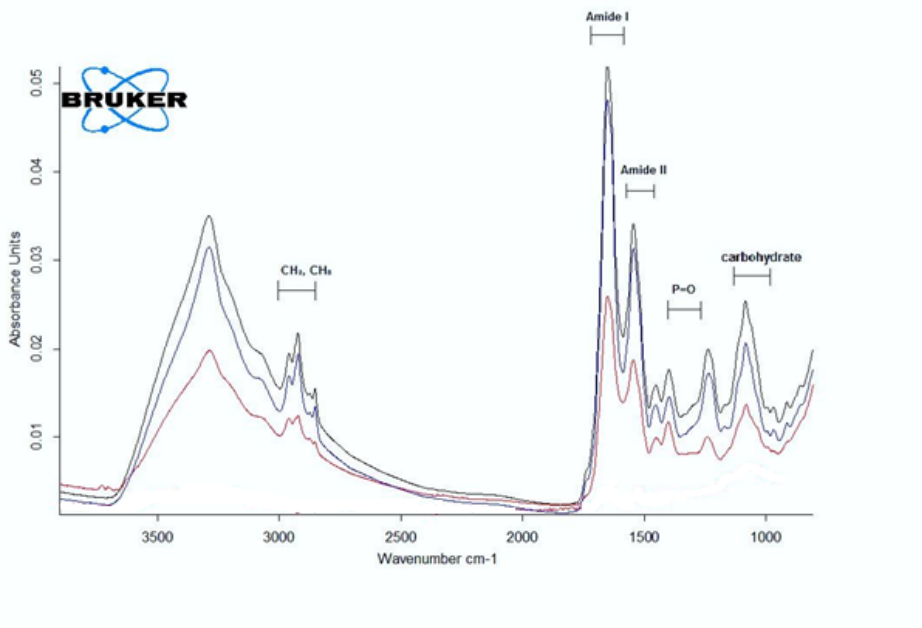

Figure 2. The average of IR spectra for five regions of biofilm intensity bands for NTHi A1 (blue), RdKW20 (red) and PAO1 (black).

The averages of the individual spectra describe the chemical information of the whole biofilm growth over surface area of 10 mm (measured by IR within 8mm spot size). These highlighted regions in the spectra representing functional groups were; lipid bands which were evaluated from the CH_2, CH_3 functional group that are located in the CH stretching region from 3000 to 2830 cm^{-1}; protein contents from the area of amide I from 1730 to 1590 cm^{-1} and amide II from 1590 to 1490 cm^{-1}; nucleic acid region from 1280 cm^{-1} to 1190 cm^{-1} and DNA/RNA containing region 1490 cm^{-1} to 1000 cm^{-1} and Amide III and the carbohydrate band for the polysaccharide profile from 1140 cm^{-1} to 950 cm^{-1}.

Fig. 3 shows the CH stretching bands in region of wavenumber from 3000 cm^{-1} to 2700 cm^{-1}. This region is influenced by functional groups of membrane fatty acids

which is dominated by C-H stretching of $–CH_3$ and $>CH_2$ (Alvarez-Ordonez *et al.*, 2011).

Fig. 4 shows two peaks of amide group belonging to proteins and peptide. The very intense peak is the amide I which provide information on protein structure. This peak in wavenumber from 1700 cm^{-1} to 1600 cm^{-1} provides changes in α-helix and β sheet structure of protein secondary structure (Kong and Yu, 2007, Alvarez-Ordonez *et al.*, 2011). Amide II peak appears next to amide I at wavenumber from 1590 cm^{-1} to 1490 cm^{-1}. This peak dominated to the changes in proteins at NH stretching in the molecule of secondary amide –C (=O)NH-R (Lin-Vien *et al.*, 1991).

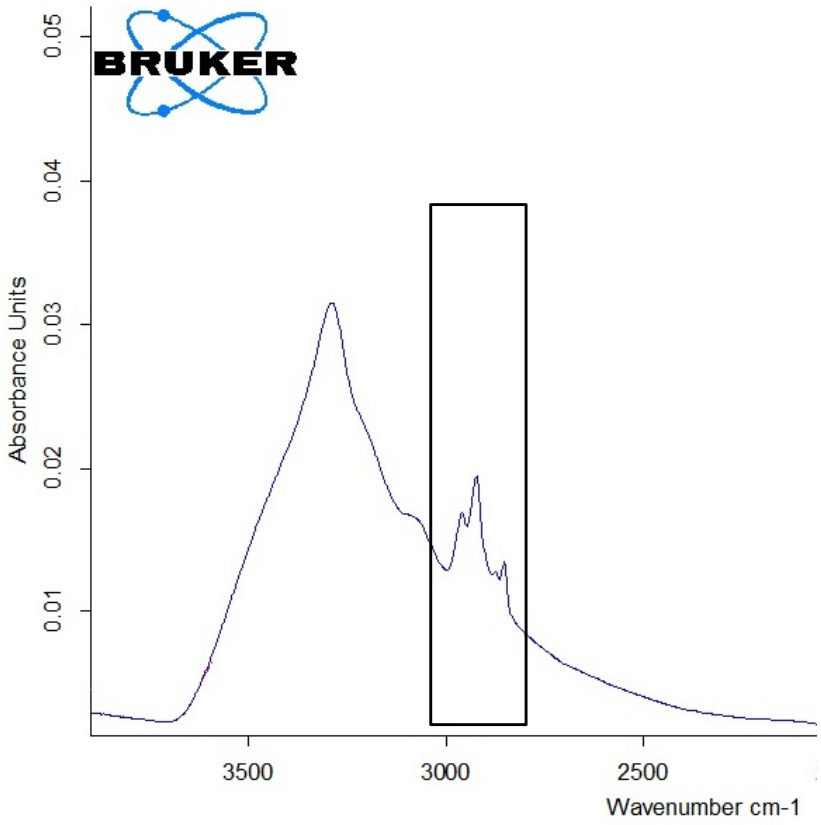

Figure 3. CH stretching band in wavenumbers from 3000 cm^{-1} to 2700 cm^{-1}. These two peaks includes CH_2 and CH_3 functional groups mainly for lipids in biofilm.

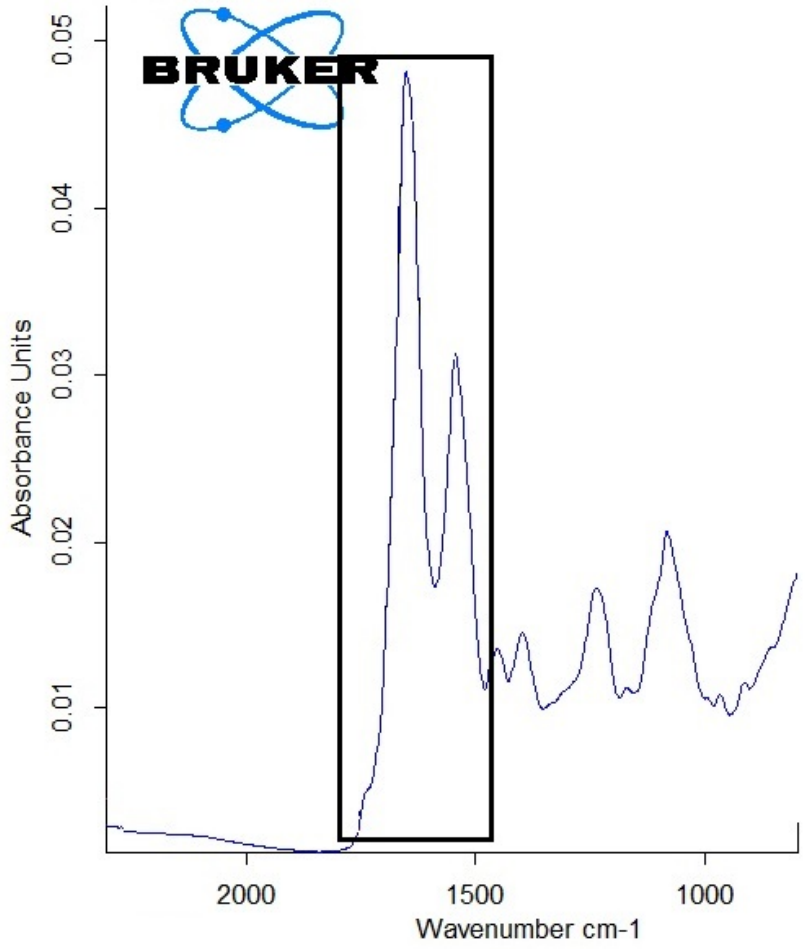

Figure 4. Amide I and amide II bands in wavenumbers from 1730 cm^{-1} to 1590 cm^{-1} and from 1590 cm^{-1} to 1490 cm^{-1}.

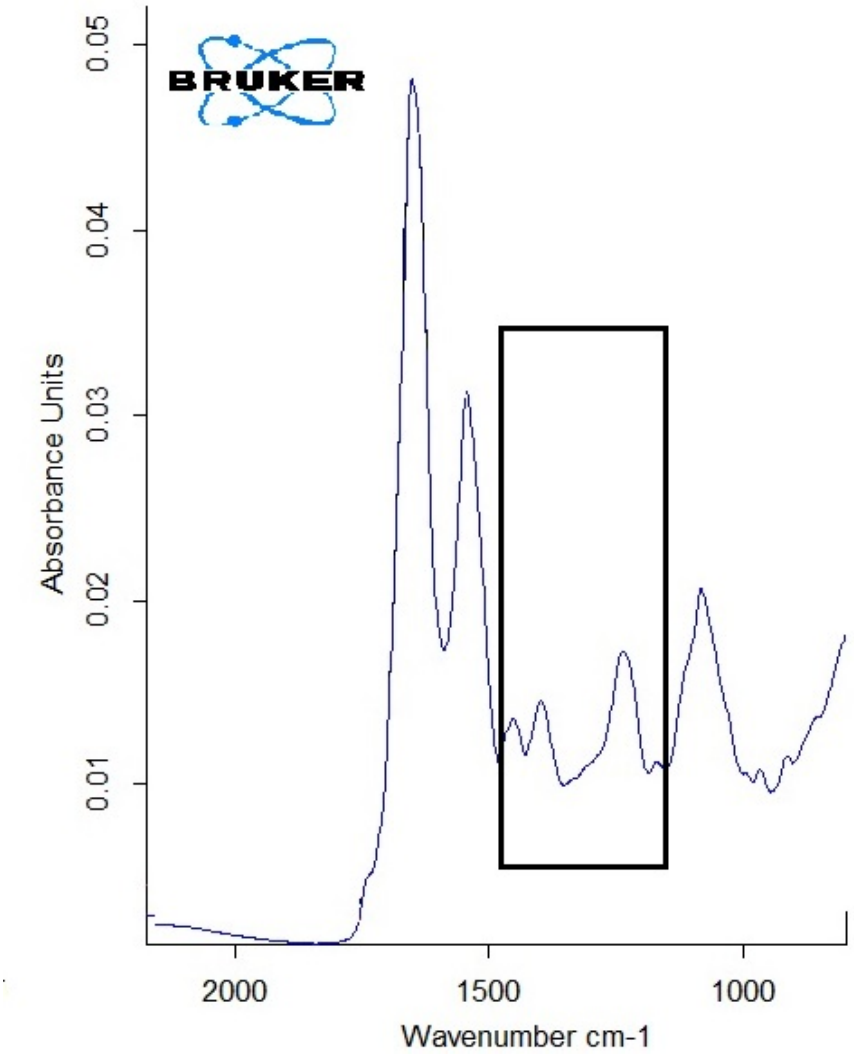

Figure 5. Three or more peaks overlapped and influenced by protein (amide III), fatty acids and phosphate compounds (P=O). Region from 1490 cm^{-1} to 1200 cm^{-1}.

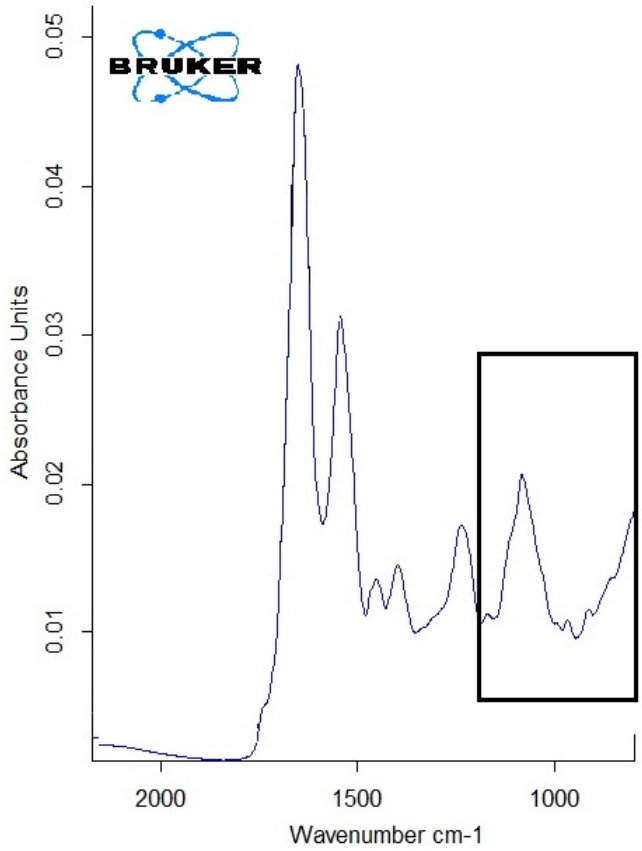

Figure 6. Complex carbohydrate peaks from 1200 cm^{-1} to 950 cm^{-1}.

The region from 1490 cm^{-1} to 1200 cm^{-1} has a number of peaks (Fig. 5) influenced by complex functional groups. Changes in this region are attributed to changes in proteins (mainly amide III), fatty acids and phosphate carrying compound (P=O) (Alvarez-Ordonez *et al.*, 2011). Fig. 6 shows the region between 1200 cm^{-1} to 950 cm^{-1}. This region is dominated by the symmetric vibrational mode of C-O-C and C-O-P stretching of occurrence for carbohydrate in the bacterial cell wall and some due to phosphodiester bond in nucleic acids (Alvarez-Ordonez *et al.*, 2011, Naumann, 2006).

Analysing the spectral integration value for bands from 1795 cm^{-1} to 950 cm^{-1} region is mainly considered to be a biofilm evaluation marker to distinguish between the ability to form biofilm in three isolates. Integration of this region which includes proteins and carbohydrate bands illustrates biofilm-type-specific profiles between isolates. The values of this integration for NTHi A1, RdKW20 and PAO1 were quantified and show 8.13, 4.28 and 6.47 respectively. According to Beers law (described in section 5.1), ε is constant, c (concentration) may be constant (100% biofilm) but may be variable if the density of biofilm is different across the biofilm and l (path length) that also is variable. On average (over the 8mm) the NTHi biofilm had double the thickness compared to the RdKW20 biofilm. These values are in the same trend as biofilm density measured by the crystal violet method which is reported in Chapter 2 that categorise NTHi A1 and PAO1 as high biofilm producer and RdKW20 as low biofilm producer. The spectroscopic analysis by integrating the region 1790 cm^{-1} to 950 cm^{-1} was established in previous FTIR spectroscopic analysis of biofilm as a key biochemical marker for changes in biofilm specific components (Holman *et al.*, 2009). Our hypothesis here is that the formation of biofilm with EPS by the NTHi strain has similar overall chemical characteristics as other species biofilm such as *Bordetella pertussis, Streptococcus pneumoniae* and *Pseudomonas aeruginosa* (Bosch *et al.*, 2006, Nivens *et al.*, 2001, Donlan *et al.*, 2004).

Individual integration values of the different spectral regions for the three-biofilm samples are illustrated in Table 1. The most intense band in the IR spectra is the amide I peak (1700 to 1600 cm^{-1}) with a mean integration value and SD of 2.024 ±0.97 for NTHi A1 which is similar to PAO1 (2.19 ±1.04). This band has shown low integration value in RdKW20 biofilm (0.98 ±0.72) with $P<0.001$ compared to the

other two isolates. This pattern between NTHi A1 biofilm and PAO1 biofilm ($P>0.05$) was also identified for the CH stretching, amide II and P=O bands of nucleic acids. These integration values are correspondently lower in RdKW20 biofilm ($P<0.05$). Specifically the amide II band area has been previously reported to be indicative of biofilm growth after more than 24h (Serra *et al.*, 2007, Quilès and Humbert, 2014).

Table 1. Mean (± SD) of integration values (n=10) for each integrated region obtained from mean IR spectra of biofilm from three bacterial isolates. Each region is associated with chemical functional groups that are characteristic of biofilm. Fatty acids (CH stretching 3000 cm^{-1} to 2830 cm^{-1}), proteins (Amide I 1730 cm^{-1} to 1590 cm^{-1}), proteins (Amide II (1590 cm^{-1} to 1490 cm^{-1}), DNA/RNA (P=O band and amide III 1280 cm^{-1} to 1190 cm^{-1}, 1490 cm^{-1} to 1000 cm^{-1}) and carbohydrates (1140 cm^{-1} to 950 cm^{-1}).

Isolates	CH stretching	Proteins (Amid I)	Proteins (Amide II)	DNA/RNA from P=O band and amide III	Carbohydrates
NTHi A1 biofilm	0.55 ±0.26	2.03 ±0.97	0.73 ±0.35	0.28 ±0.13	0.65 ±0.28
RdKW20 biofilm	0.26 ±0.22	0.98 ±0.72	0.35 ±0.25	0.09 ±0.08	0.34 ±0.25
PAO1(positive control)	0.58 ±0.29	2.19 ±1.04	0.73 ±0.33	0.33 ±0.161	0.97 ±0.46

PAO1 biofilm has the largest carbohydrates bands integration value and is significantly lower in NTHi A1 biofilm and RdKW20 biofilm ($P<0.05$). PAO1 is a well-known biofilm forming species and FTIR analysis of biofilm development on CaF_2 discs has shown constant formation of polysaccharide and proteins (Cheung *et al.*, 2007). In the current study, production of a carbohydrate enriched matrix is related to the biofilm architecture and considered as a marker for biofilm maturation for NTHi A1 biofilm despite the fact that carbohydrate band value here is less than PAO1 biofilm. Carbohydrate bands have high integration values which have reported for other biofilm in previous studies (Humbert *et al.*, 2011, Quilès and Humbert, 2014, Donlan *et al.*, 2004). By comparing PAO1 biofilm with NTHi biofilm values of carbohydrate and protein integrations bands area 0.97 and 0.67 and 2.19 to 2.02 respectively, NTHi biofilm display the presence of proteins and polysaccharides.

In the current study, the biofilms were dried at room temperature prior to measurement by transmittance FTIR spectroscopy, therefore, the water vibrational mode may have less effect on amide I bands than that observed with previous biofilm studies. It is well documented that water also absorb in the region of proteins (1700 to 1515 cm^{-1}) and water content may vary in biofilm with time and during spectral acquisition (Donlan *et al.*, 2004, Kong and Yu, 2007). Amide I and amide II are always related to each other and the intensity of amide II is usually half to one third of the amide I band (Donlan *et al.*, 2004).

Relative changes between carbohydrate bands and protein bands (amide I and II) were assessed from the ratio of integration value for the three biofilms in Table 2. The ratio of the band integrations for carbohydrates and amide I in this analysis are quite different ($P>0.05$) for NTHi A1 biofilm, RdKW20 biofilm and in PAO1 biofilm. Individual spectra of the biofilm here for mature NTHi A1 biofilm and RdKW20 biofilm (22-24 h) show no major difference for amide I compared to carbohydrate. The carbohydrate to amide II ratio show high values (1.34±0.15) for PAO1 biofilm but slight lower values for RdKW20 biofilm (1.01 ±0.36) ($P<0.05$) and the lowest ratio between these three biofilm was for NTHi A1 biofilm (0.87±0.08) indicating that NTHi biofilm has a relative higher amide II value.

Table 2. Average of the ratio between spectral integration for the five assigned bands of FTIR spectral acquired from the three biofilms grown on CaF_2.

Isolates	CH/carbohy-drate	CH/amide I	Carbohydrate /amide I	Carbohydrate /amide II	amide I/ P=O and amide III	Carbohydrate /P=O and amide III
NTHi A1 biofilm	0.81± 0.08	0.26 ±0.02	0.46± 0.18	0.87 ±0.08	7.29±0.32	2.40 ±0.23
RdKW20 biofilm	0.74 ±0.23	0.25 ±0.06	0.37 ±0.14	1.01 ±0.36	10.6 ±1.97	3.82 ±1.39
PAO1 (positive control)	0.59 ±0.03	0.26 ±0.05	0.45 ±0.04	1.34 ±0.15	6.69 ±0.44	2.97±0.27

Amide II seems higher in NTHi A1 biofilm than RdKW20 biofilm and PAO1 comparing to carbohydrate. This ratio may indicate relative changes of the –NH stretching in secondary protein structure involved in biofilm structure compared to the C-O-C and C-O-P stretching of the bacterial cell walls. This carbohydrate to amide II ratio may illustrate the contribution of the cell adhesion and production of sugar components in the PAO1 biofilm and RdKW20 biofilm. Relative changes in the integration between the carbohydrate region and amide I and II region has shown to be correlated to a mature biofilm feature (Serra *et al.* 2007).

The ratio for CH stretching to amide I show very similar values for all the three isolates. The difference in lipid contents relative to amide I is the same in all three biofilms. However, CH stretching to carbohydrate bands show similar ratio for NTHi A1 and RdKW20 biofilms but low in PAO1 biofilm ($P<0.05$). It seems that CH stretching dominated by lipid in the biofilm was greater in NTHi A1 and RdKW20 biofilm than in PAO1 in relation to carbohydrate. Pink *et al.* (2004) interpreted CH stretching region in PAO1 biofilm which dominated after 20 h of incubation (Pink *et al.*, 2004). The CH stretching region seems not dominated in our study and it appears in low value of integration and relative to carbohydrate for PAO1 biofilm compared to NTHi biofilm.

The ratio of amide I to P=O and amide III bands show similar values for NTHi A1 and PAO1 biofilms but was significantly higher for RdKW20 biofilm ($P<0.05$), see Table 2. This ratio indicates that amide I has shown differences over the biofilm for NTHi A1 and PAO1 biofilms which are less than RdKW20 biofilm. RdKW20 biofilm may have less cellular aggregates than NTHi A1 and PAO1. P=O changes within

nucleic acids contents and no difference for amide III appear dominant in RdKW20. The ratio between amid I to amide III and P=O peaks could provide information of the variance of protein production within NTHi biofilm. The region between 1490 cm^{-1} to 1190 cm^{-1} may report on some of the protein and nucleic acid differences involved in biofilm production of the three different biofilms. Calculation of the ratio between amide I peak to amide III and P=O region may quantify the accumulated protein and nucleic acids at the surface growth of NTHi biofilm. Fewer aggregates of cells in RdKW20 biofilm were examined in optical and SEM images which may lower the amount of active changes of P=O in nucleic acids.

Ratio of carbohydrate bands to P=O shows some variation over the value of the three different biofilms. Carbohydrate to amide III and P=O ratio may be related to the molecular activity of proteins cellular synthesis. The RdKW20 produces less biofilm material which means cellular components form higher level of proteins and lower levels of carbohydrate in parallel to the results of Wu *et al*. group (2014). NTHi biofilm with only cellular components of the biofilm fraction show higher ratio of proteins comparing to carbohydrate (Wu *et al.*, 2014).

Obtaining the individual spectra of the biofilm material that grows on the surface of the CaF_2 disc for both biofilm producers by using transmittance IR is an advantage over other traditional methods as it may apply analyse macromolecules over a surface area (8 mm).

5.3.2 Analysis of the two areas of biofilm

Pseudo-colour images of the hyperspectral data were created from the integration values of the region from 1795 cm^{-1} to 950 cm^{-1} for both NTHi A1 and RdW20 and are displayed in Fig. 7 and 8. The numerical value for each pixel in these images represents the integration value of IR spectra from 1795 cm^{-1} to 950 cm^{-1}. The colour illustrated in Fig. 7 NTHi A1 represents the integrations value from 9.23 to 24.0 and for Fig. 8 RdKW20 from 1.45 to 13.8 going from dark blue to white. The heat map represents these values in the form of colour as given in the colour scale in the figure. Beer-Lambert law determines that absorbance of the region from 1795 cm^{-1} to 950 cm^{-1} correlates to the path length (thickness of the sample) if the absorptivity (one band) and concentration were fixed. In order to analyse the spectral data from different thickness areas of the biofilm, spectra were extracted from the hyperspectral image by visually selecting spots of two areas of the growth.

These two areas of growth were also clearly distinguished from light microscopic and SEM images Fig. 1a & b for both NTHiA1 and RdW20 for the high growth areas and low growth areas evident in these heat maps. Each spot selected from the two area of NTHi A1 and RdKW20 biofilm represents one spectrum. In Fig. 7b two spectra are displayed to show the difference of intensities between the spectrum from thick area and the spectrum from thin area. Fig. 8b shows the two spectra from two selected spots from thick area and thin area of RdKW20 biofilm.

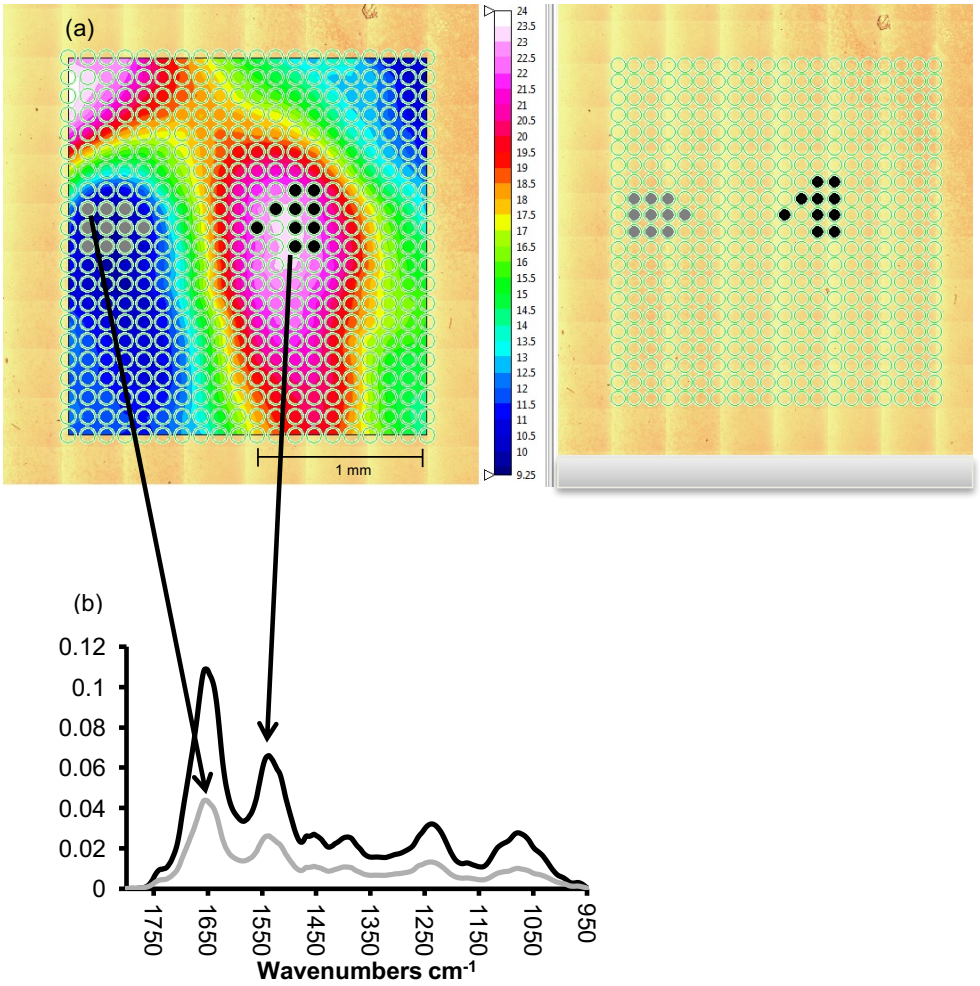

Figure 7. Left: False colour map displaying integration from1790 cm^{-1} to 950 $cm^{-}1$ for NTHi biofilm. Right: spot selection for extracted spectra, black spots are the high biofilm growth and grey spots are the low growth. (b) Typical spectra for black and grey selected spots.

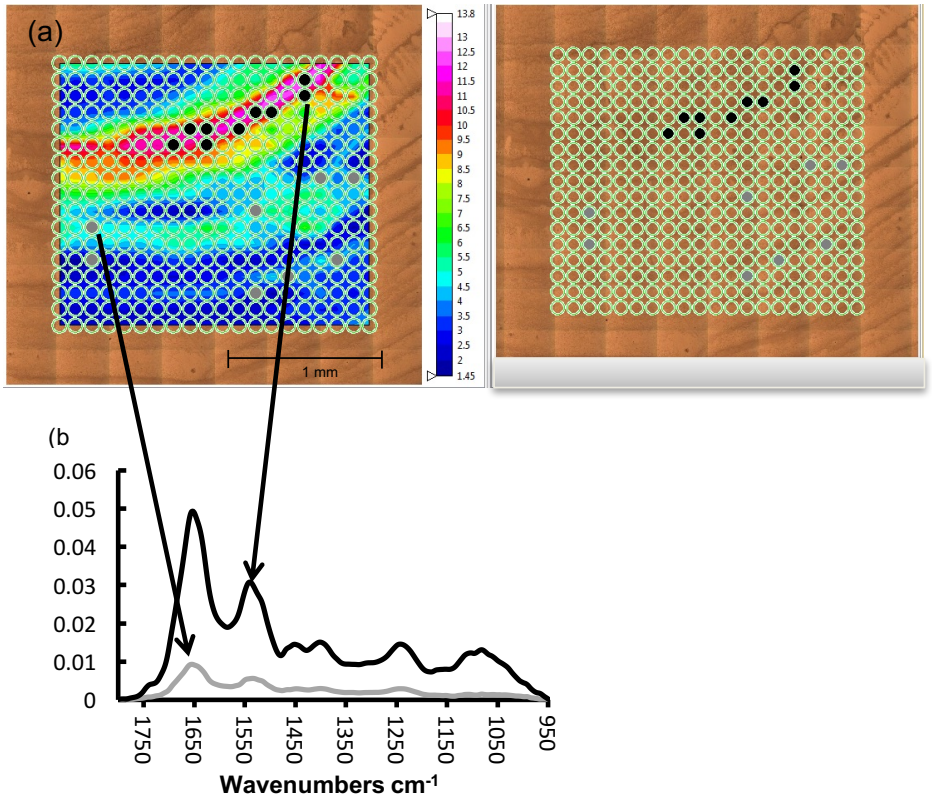

Figure 8. Left: false colour map displaying integration from1790 cm^{-1} to 950 cm^{-1} for RdKW20 biofilm. Right: spot selection for extracted spectra, black spots are the high biofilm growth and grey spots are the low growth. (b) Typical spectra for black and grey selected spots.

To investigate the main variation of these two areas in the two biofilm NTHi A1 and RdKW20), the twenty spectra for each biofilm were pre-processed using 2nd derivatives and PCA analysis performed as unsupervised analysis to show the chemical variation of these spectra. Fig. 9a shows the twenty spectra are clustered together in PC1 versus PC2 score plots. These scores plots of PC1 versus PC2 were generated from principle component analysis of the pre-processed data. The 2nd derivatives are used for this PCA analysis to initially explore the chemical differences between the spectra and to consider the high and thin area of the sample extracted. PC1 explains 99% of the total variance and clearly distinguished the high growth area from the low growth areas of both isolates (Fig. 9a). The thick area of RdKW20 with

black colour displays similar scores in PC1 to the thin area of the NTHi A1 with red colour in Fig. 9a. The thin of NTHi A1 biofilm shows distinct and different scores value to the NTHi A1 (blue colour) of thick area in PC1 and but similar scores value in PC2. Similarly, PC2 scores for the thin area for RdKW20 biofilm (green colour) show similar score value of NTHi A1 biofilm. These score suggest that some spectral features represented by the score can be distinguished from PC1 and other feature with PC2. These spectral features can be investigated more from the corresponding loading graph of the PCs.

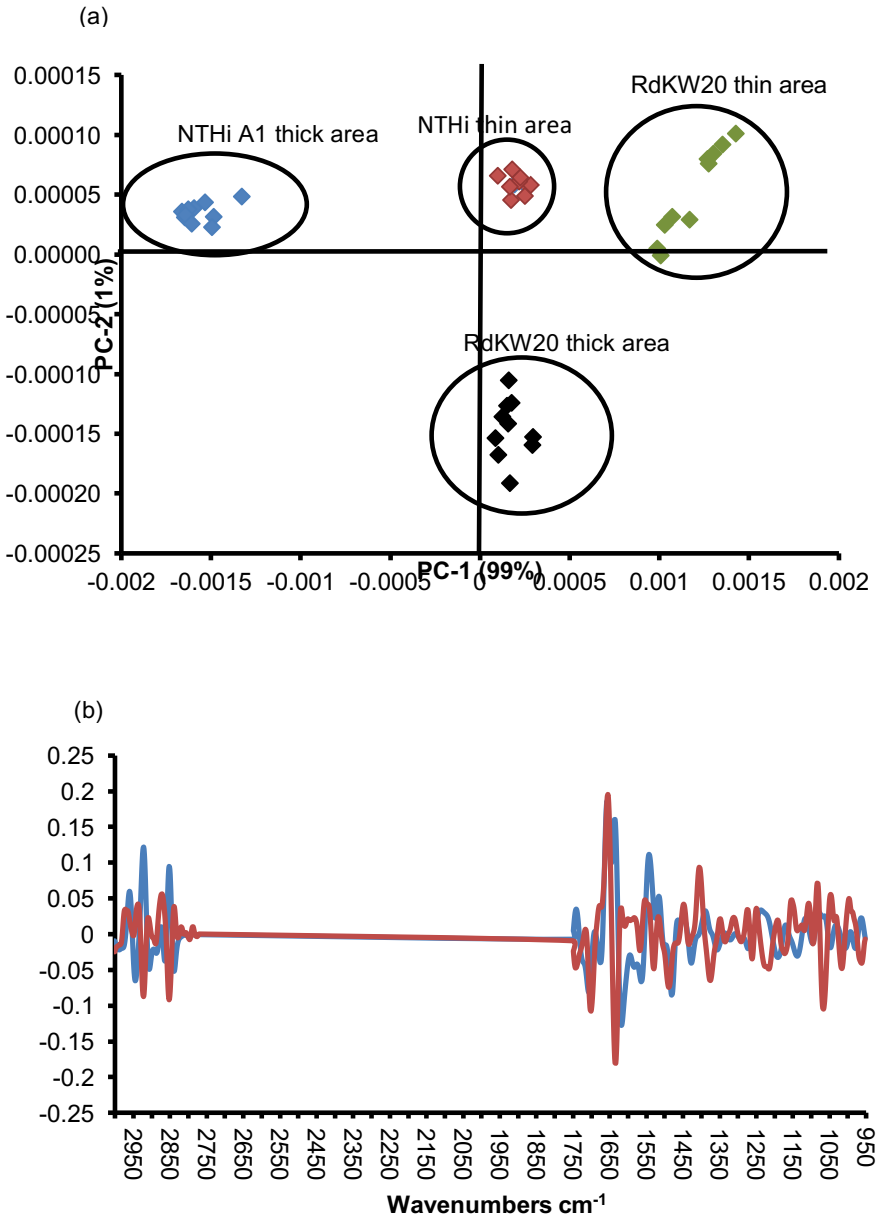

Figure 9. (a) Score plot of PC1 versus PC2 show the NTHi (high biofilm producer) thick area in (blue) thin area in (red). RdW20 (low biofilm producer) thick area (black) thin area (green). (b) loading graph of PC1 for the pre-processed that shows 99% of the variation.

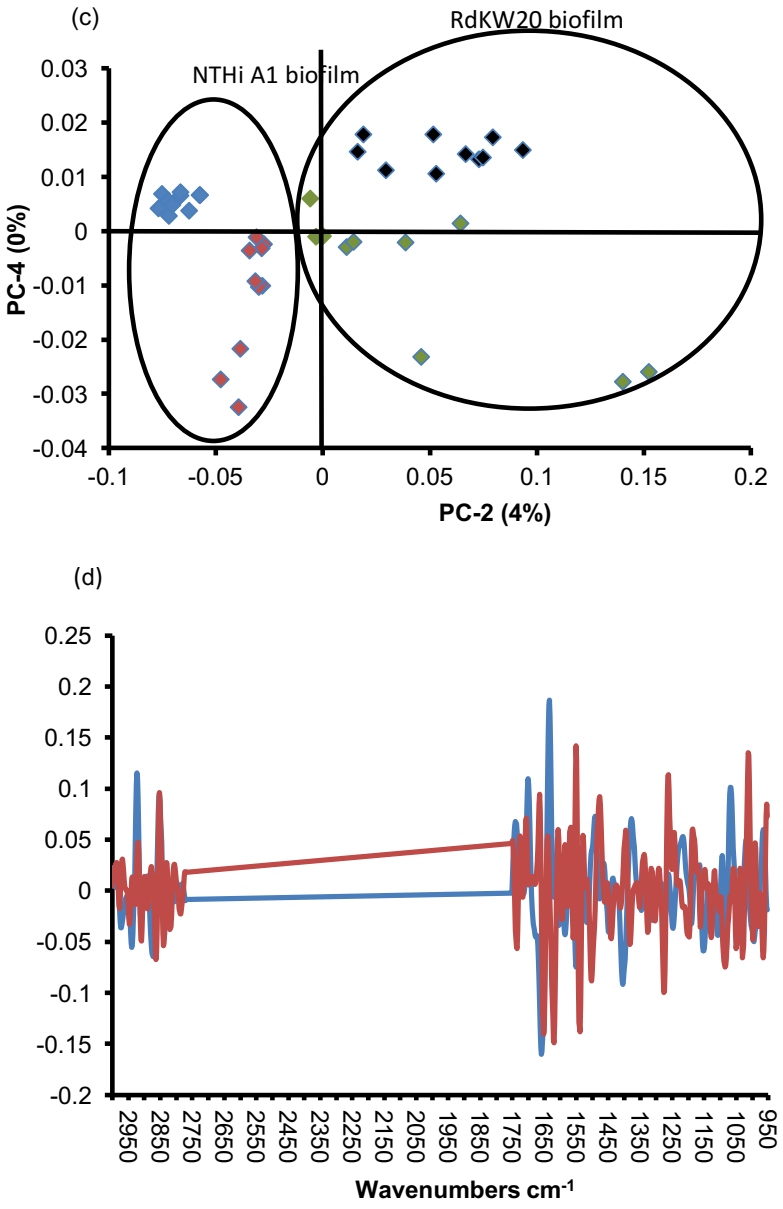

Figure 9. (c) Score plot of PC2 versus PC4 shows the NTHi (high biofilm producer) thick area in (blue) thin area in (red). RdW20 (low biofilm producer) thick area (black) thin area (green). (d) PC2 and PC4 of the 2nd derivatives and 13 smoothing points which normalised by vector normalisation.

The loading graph in Fig. 9b highlights the main chemical variance, mainly PC2 in the protein intensity region and the carbohydrate region. In the loading graph, the protein region of 1706 cm^{-1} shifted in PC2 to 1702 cm^{-1} and there was peak shift from

1658 cm^{-1} in PC1 to 1635 cm^{-1} in PC2. These points show peaks dominated by the difference of α-helical structure in C=O in amide I. The score are reversely affected by the loading graph in peak shift at amide II bands from 1542 cm^{-1} to 1531 cm^{-1}. PC2 show more variances in lipid bands area. The observed pattern of intensity bands assigned to the carbohydrate region are illustrated by PC2 mainly at 1083 cm^{-1} and 1068 cm^{-1} confirmed that one of the differences between the biofilm region is located at (C-O) bonds and showed by PC2 only. The difference between the spectra extracted from two different biofilm in this analysis show variability in proteins (amide I and amide II) and carbohydrates. These two assignments specifically reported change for other biofilm forming species (Quilès and Humbert, 2014). This analysis for the two assignments (protein and carbohydrate) gives us an indication of the biofilm growth difference in the two biofilm (NTHi A1 and RdWK20). Protein changes may indicate the development of biofilm in NTHi A1 which has been reported previously to be related to alterations of bacterial protein in response to surface growth (Quilès and Humbert, 2014). The differences between the two biofilms in the carbohydrate band area may be an indication of the production and accumulation of glycogen which is found in both planktonic cells and sessile cells but with more generally found in sessile cells (Quilès and Humbert, 2014).

Another PCA analysis using an additional pre-processing step (2^{nd} derivative with vector normalisation) on these two pseudo-colour integrated images indicated that some variation of the chemical components are independent of the density of the biofilm growth over the disc and therefore independent from the variability of the biomass of biofilm material. PC2 (4% of variance) versus PC4 (0.2% variance) plot scores (Fig. 9c) showed clear chemical classification differences. PC2 separated the

two different biofilms independent from growth whereas PC4 separated the growth but not the biofilms.

The PC1 score explains 95% of the variance but does not distinguish between the spectral groups from different areas of each sample. The loading graph of PC2 to PC4 displayed in Fig. 9d, illustrate change in the intensity for amide I peaks. Scores were reversely affected by the loading graph which was observed in PC2 at 1680 cm^{-1} and 1657 cm^{-1} and by PC4 peak differences in 1635 cm^{-1} and 1621 cm^{-1}, amide II bands at 1551 cm^{-1} in PC2 and 1538 cm^{-1} in PC4. Amide III and phosphate bands at 1406 cm^{-1}, 1483 cm^{-1}, 1153 cm^{-1} and 1084 cm^{-1}. The amide I peak differences observed in the loading graph is known to be due to differences in the intensity band for α-helix as reported in Kong and Yu (2007). PC2 showed mainly changes in biofilm growth over the surface between the two biofilm. These differences observed particularly in amide I 1657 cm^{-1} and amide II 1551 cm^{-1} which suggests modification in protein profile. Some nucleic acid alteration possibly due to growth of cells was observed from peaks 1406 cm^{-1}, and 1153 cm^{-1}. Some indication of the carbohydrate storage from the peak at 1084 cm^{-1} was also seen. These changes in the amide I bands represent a change in bacterial protein profile in response to surface associated bacterial growth (Quilès and Humbert, 2014). Some variances were observed in the lipid bands area due to CH stretching bands 3000cm^{-1} to 2830 cm^{-1} in both PC2 and PC4. The observed pattern of intensity assigned to the carbohydrate region mainly peaks at 1049 cm^{-1} in PC2, 1087 cm^{-1} in PC4 and 1012 cm^{-1} in both PCs confirmed that one of the differences between the biofilm region is due to (C-O) bonds. Changes assigned to the bands at 1084 cm^{-1} which describes glycoside bonds (due to C-OH stretching and C-O ring vibration) and

have been observed in many spectral bands of biofilm formed by different bacterial species (Nivens *et al.*, 2001, Serra *et al.*, 2007, Quilès and Humbert, 2014).

5.3.3 Analysis of the hyperspectral images for NTHi biofilm

IR hyperspectral data was qualitatively analysed by using one of the hyperspectral images of NTHi A1 and RdKW20 biofilm were replicates give similar results. The hyperspectral data was recorded with spot size (160 μm) and step size 100 μm. Changes occurring in bacterial cell biology were highlighted spatially for individual biofilms, performing integration ratios and multivariate analyses were undertaken for the hyperspectral images. The integrated carbohydrate region of NTHi A1 is illustrated Fig. 10a as a heat map with colour scale and shows spatial carbohydrate distribution within the biofilm with integration values from 0.37 to 1.34. As discussed in section 5.3.1, integration of the carbohydrate region between 1140 cm^{-1} to 950 cm^{-1} shown in Fig. 10a includes many carbohydrate bands allowing evaluation of the main sugar components. Fig. 10b. depicts a chemical map generated by integrating the area under the band absorption from 1730 cm^{-1} to 1590 cm^{-1} which was the area attributed for amide I bands including α-helix and β-sheet which are sensitive to changes in protein secondary structure (Kong and Yu, 2007).

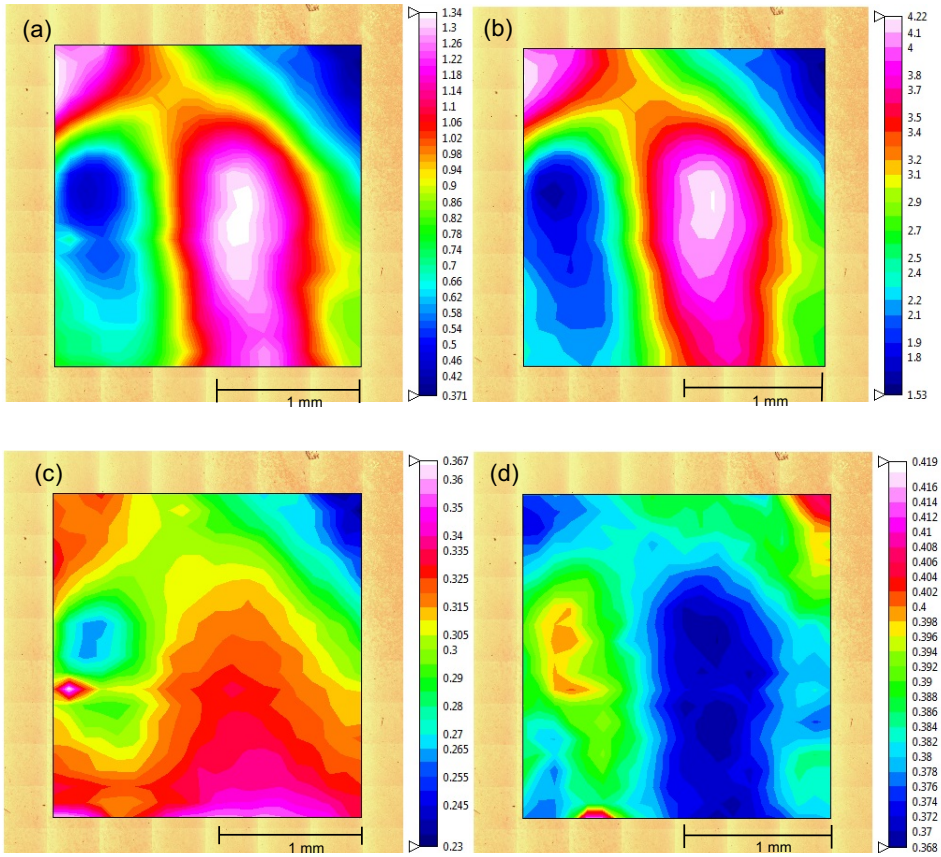

Figure 10**.** IR hyperspectral mapping for the NTHi (A1) high biofilm producer shows (a) carbohydrate peak integration from 1140 to 950 cm^{-1}. (b) amide I peak integration from 1730 to 1590 cm^{-1} . (c) carbohydrate to amide I ratio. (d) CH stretching to amide I ratio.

To investigate how these two components related to biofilm grow on the CaF_2 disc, ratios of the two components could provide an overview of the dominant bands over the tested area of NTHi A1 biofilm. Heat maps were visualised in a colour 2D hyperspectral image using the ratio of integration values of the functional regions in the spectra. Fig. 10c shows the ratio of carbohydrate to amide I as a high intensity range in the heat colour map from 0.305 to 0.367, the region of high carbohydrate can be seen in a semicircular shape with dimensions of 1.5×1.3 mm which is almost two thirds of the analysed area. However, from this range (0.305-0.367), it shows that relative differences between carbohydrate and amide I over the area is low. This result

may indicate that biofilm formed by NTHi A1 has no major differences in relative carbohydrate to amide I ratios. However, the integration map Fig. 10a and b, implies that NTHi biofilm has some spatial distribution differences for amide I in comparison to carbohydrate within the scale of 2 mm. The ratio was chosen because it can be used to investigate the spatial distribution and homogeneity of mature biofilm.

The integral ratio of the C-H stretching bands to the amide I region Fig. 10d may provide some indication of the lipid to protein profiles. This ratio shows minor variation across the measured area from 0.368 to 0.419. The CH stretching band with low intensity relative to the amide I in Fig. 5d. shows a circular shape of approximately 0.9×1.5 mm. The ratio was highest where there was less dense biofilm. This indicates there is more lipid in the low dense area relative to proteins.

The infrared pseudo- colour map created from integrating the carbohydrate region (Fig. 11a) of RdKW20 illustrates the areas of biofilm material with carbohydrate which is different to the NTHi A1 biofilm in terms of chemical composition. For amide I, Fig. 11b depicts a higher intensity of amide I mostly within the area of high growth biofilm. From Fig. 11c and d, the ratio of carbohydrate to amide I (0.02-0.278) and lipid to amide I (0.255-0.418) can be seen. The areas of low colour intensity (from green to blue) of the two ratio maps have thin area biofilm formed on the disc that is thought to be due to less EPS than the NTHi A1. The carbohydrate to protein ratio range from 0.2 to 0.278 within the thick biofilm area was higher than in the area with thin area of biofilm which ranged from 0.03 to 0.14. This pattern in carbohydrate to protein ratio was also reported in a biofilm study with different bacterial species (Bosch *et al.*, 2006). The variability of biofilm growth by RdKW20 in the current

study showed that less EPS was formed by the cells as spatial protein distribution was relatively high in the thin area of RdKW20 biofilm.

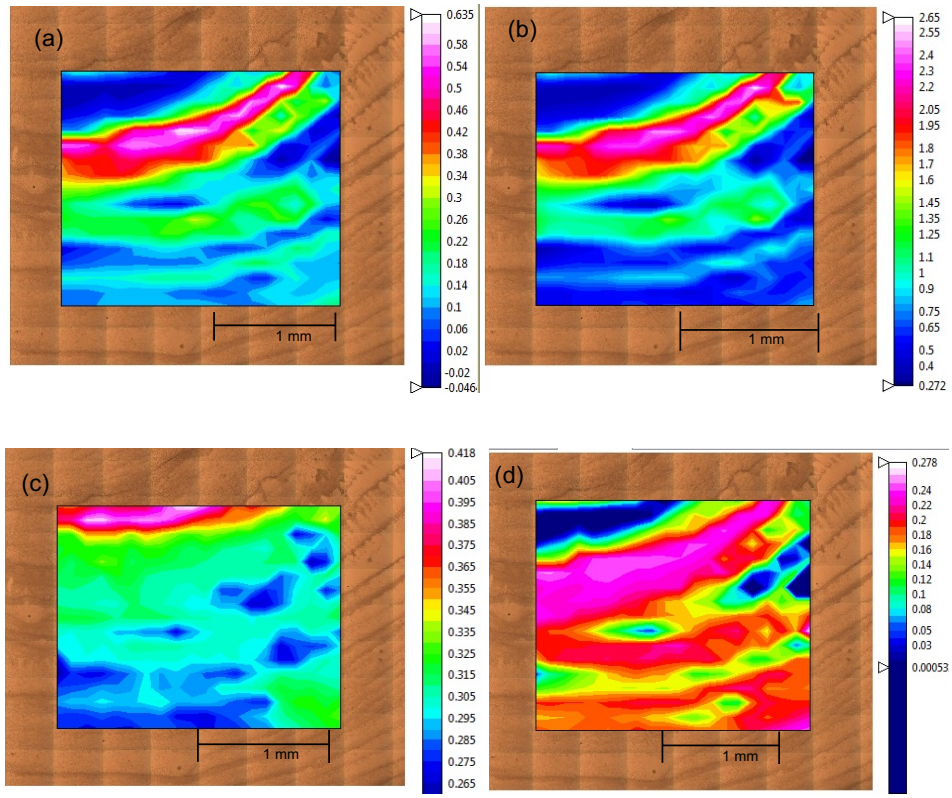

Figure 11. IR hyperspectral mapping for the RdW20 low biofilm producer shows (a) Carbohydrate peak integration 1140 to 950 cm^{-1}. (b) amide I peak integration from 1730 to 1590 cm^{-1}. IR Hyperspectral mapping for the RdW20 low biofilm producer with (c) CH stretching to amide I ratio and (d) carbohydrate to amide I ratio.

The results from the integration ratios of the two biofilm producers indicated notable differences between carbohydrate and protein with regard to spatial distribution. This is also in agreement with the finding of the study by Wu *et al.* (2014) who identified the chemical contents of NTHi biofilm extracellular matrix contained a mixture of polysaccharides and proteinaceous material when they examined the spectra obtained by FTIR. It was reported that NTHi biofilm lacks an EPS and consists largely of

proteinaceous material by comparing FTIR spectra of the NTHi biofilm with EPS and EPS free NTHi biofilm (Wu *et al.*, 2014).

Unsupervised multivariate analysis of the biofilm spectral data is a simple and robust statistical method, which is widely employed to highlight FTIR spectral similarities and differences in biological samples (Chalmers and Griffiths, 2002). In particular, unsupervised PCA analysis of the hyperspectral data, using the pre-processing procedures described earlier in section 5.3.2, can highlight different areas within the biofilm based on chemical information (Hughes *et al.*, 2013, Wang and Mizaikoff, 2008). Performing the unsupervised analysis using cluster analysis and principal component analysis can highlight the functional group differences such as amide I in the protein region and glycogen in the carbohydrate region of the biofilm.

Hierarchical cluster analysis was performed with pre-processed spectral data by converting the data to 2^{nd} derivatives and unit vector normalisation illustrated in Fig. 12. These analyses were performed with chosen 2^{nd} derivatives which seem to be more applicable to normalise the data. Smoothing point up to 13 was chosen to lower the effect of noise for the spectral data which then normalised by vector normalisation. The cluster analyses were performed on the pre-processed hyperspectral data then the number of clusters were chosen based on the dendrogram separation of data.

The green and blue clusters of biofilm are highlighted in the amide I intensity heat maps Fig. 10a as an oval shape which corresponds to the area of high growth of biofilm. Hierarchical clustering has been used in the classification of features within

chemical groups in other microbiological studies for the identification of altered features that classify bacterial strains and species (Naumann, 2006). A dendrogram was generated using a cluster analysis of the NTHi A1 biofilm and is illustrated in Fig. 12b. From the vertical axis in the dendrogram, the clusters that ranged from 0 to 1.3 distance value were distinctively separated into two main groups. This dendrogram signified several chemical group clusters in two main clusters, subdivided into a further two subdivisions with another two minor-subdivision.

In Fig. 12c. the average spectra (2^{nd} derivatives) of each cluster show the differences between clusters. Differences (integration value ± 10 or 5 value) were found in amide I peak at 1657 ± 10 cm^{-1} and 1635 ± 5 cm^{-1}, amide II peak at 1541 ± 10 $cm^{-1}$and 1514 ±5 cm^{-1}, nucleic acid region and amide II peak at 1385 ± 6 cm^{-1} and 1230 ± 6 cm^{-1} lastly carbohydrate peak at 1076 ± 8 cm^{-1}. Specifically changes in peak 1657 ± 10 cm^{-1} and 1635 ± 5 cm^{-1} were described in the previous PCA analysis which were related to amide I sensitive changes of protein secondary structure.

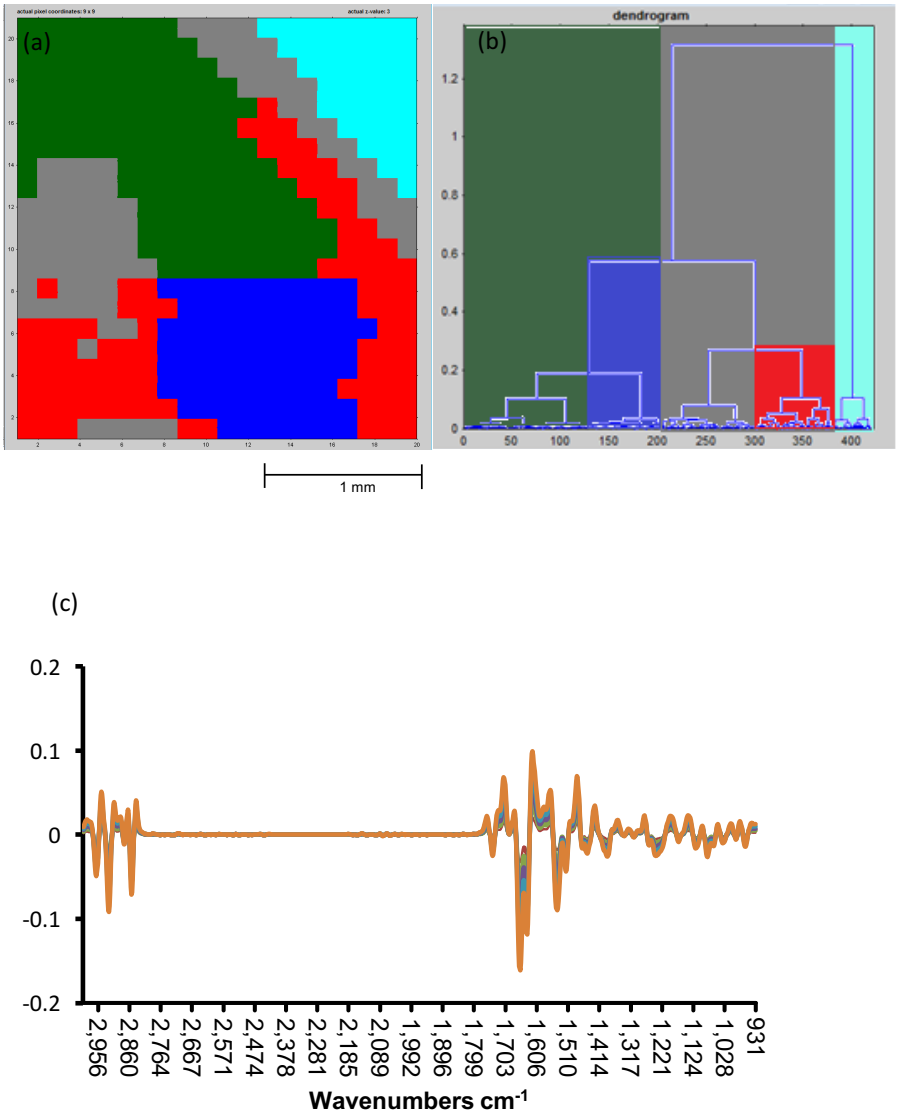

Figure 12. (a) Five clusters by HCA (b) dendrogram of the HCA of 2nd derivatives with 13 smoothing points and vector normalisation of the NTHi A1 high biofilm producer 2D IR hyperspectral image which illustrates the larger the separation between clusters, indicated by connecting lines, the lower the similarity of the spectra. (c) the average spectra for each cluster converted to 2nd derivatievs.

For the RdKW20 biofilm (Fig. 13), cluster analysis was performed with the pre-processed hyperspectral data. A dendrogram of this cluster analysis illustrated Fig. 13b below shows two main clusters which ranged in vertical distance from 0 to 8 distance value. The larger cluster subdivided into two at distance value of 3.4. This

dendrogram illustrates some similarity of the clusters distance between high biofilm producer and low biofilm producer in the spatial distribution of the functional groups, however, the distance of separation for the low biofilm producer was larger (≈6-fold). Average spectra for the clusters in Fig. 13 as 2nd derivatives illustrate peak changes over the clusters for the amide I bands at 1702 cm^{-1} to 1699 cm^{-1}, from 1664 cm^{-1} to 1657 cm^{-1} and 1637 cm^{-1}, and amide II peak from 1544 cm^{-1} to 1539 cm^{-1}. There were some slight changes for the glycogen band of the carbohydrate region in 1020 cm^{-1} (peak shift from 1020 cm^{-1} to 1033 cm^{-1}) between the average clusters. This difference in carbohydrate between the clusters may indicate variability of glycogen biosynthesis in the area covering the disc. The variability between growth rates of biofilm formed on CaF_2 disc illustrated as clusters may be related to the differences in cellular aggregation adhesion. Glycogen band intensities were higher than the amide I band in the area of thick growth biofilm which is a marker for sessile bacteria that has been observed in biofilm formation with other bacterial species (Quilès and Humbert, 2014, Nivens *et al.*, 2001, Bosch *et al.*, 2006).

There was some correlation between clusters in the dendrogram of the RdKW20 biofilm shown in the green and blue area which is similar to part of the chemical map for amide I and CH stretching regions in the heat map of these two integrals. Fig. 11 illustrated RdKW20 biofilm with lower carbohydrate which is displayed in the same region clustered in dendrogram and compatible with the pattern of the chemical map for carbohydrate in Fig. 11 that ranged between 0.001 to 0.25.

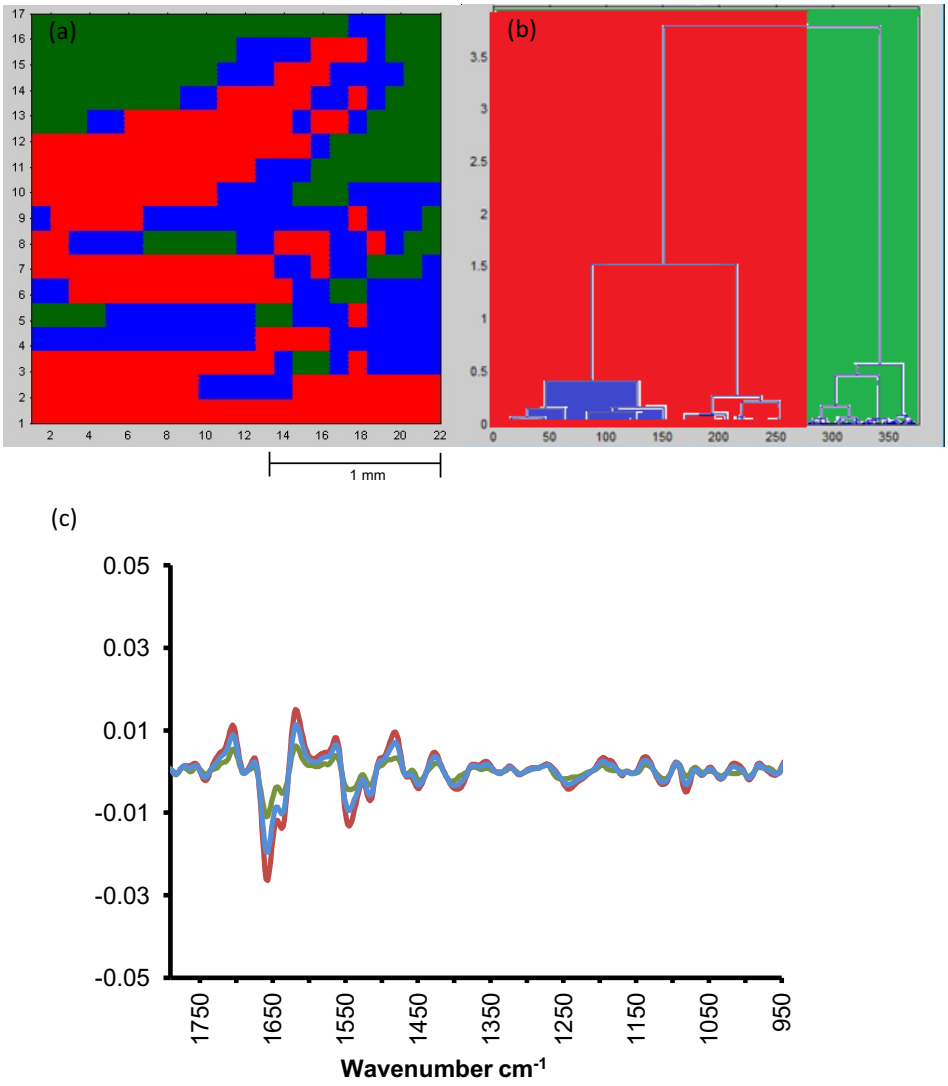

Figure 13. 2D IR hyperspectral image of the RdW20 low biofilm producer illustrates (a) three clusters by HCA (b) dendrogram of the HCA of 2nd derivatives with 13 smoothing points and vector normalisation (c) the average spectra for each cluster converted to 2nd derivatives.

PCA analysis was also performed on the on the IR hyperspectral data. This PCA analysis was different to the first PCA analysis performed on the extracted spectra from selected spots in section 3.2. The PCA in section 3.2 compared spectral data from different biofilms and their different growth areas, without using any of their

spatial information. PCA in this section was performed on a single biofilm to investigate if clustering does occur in a spatial sense of the hyperspectral image. This hyperspectral image shows distribution of the score value of a particular PC and is observed with pseudo-colour hyperspectral image in Fig. 14a and b with an extreme score value in red and low score value in blue. PCs were selected based on the segregation of different regions of biofilm images. The loading graphs of the PC1 and PC2 were examined to find the most variation in molecular features. Fig. 14c, the PCs highlight molecular and conformational changes in the spectral region of amide I.

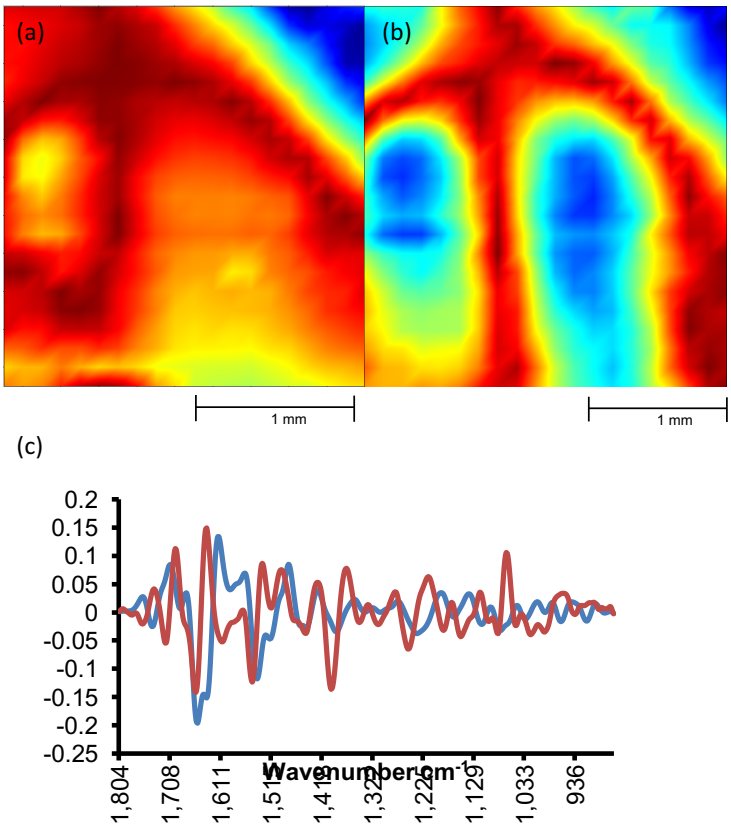

Figure 14. (a) PC1 and (b) PC2 from PCA of the region 1790 cm^{-1} to 950 cm^{-1} for the NTHi A1; (c) loading graph for PC1 and PC2.

Features in the loading graph demonstrate the variation between PC1 (95%) and PC2 (5%). PC2 loading graph of the NTHi A1 biofilm in Fig. 14c shows that amide I bands (a) have variance with minor peak shifts from 1658 cm^{-1} to 1661 cm^{-1}. This peak is sensitive to the changes within the α-helix of the protein secondary structure (Kong and Yu, 2007) and it was frequently noticed with changes in the multivariate analysis for this chemical map. Another peak shift is noticed in the amide II peak from 1553 cm^{-1} to 1550 cm^{-1} of the C-N stretching mode. The two peaks within amide I and amide II region were also reported previously specifically for denaturation on amino nitrogen atoms (Lin-Vien *et al.*, 1991). Difference in the intensity at 1087 cm^{-1} may be related to P=O stretching of phosphate groups (Fang *et al.*, 2011) that is suggested to be as a result of changes in phosphate group within the biofilm. Other studies have also suggested that changes in this band area may related to the bacterial cell membrane and nucleic acids (Quilès and Humbert, 2014).

PCA analysis for the RdKW20 biofilm producer shows an explained variance for PC2 and PC5 (Fig. 15a and b). The pseudo-colour image of PC2 show a high score value red area which was found to be a different area than that highlighted in PC5. Loading graph Fig. 15c shows some variation for PC2 and PC5 located in reversely affected peaks. PC2 shows a *β*-sheet peak shift from 1628 cm^{-1} to 1620 cm^{-1} (Kong and Yu, 2007). PC5 also shows strong peptide amide I and amide II bands near 1653 cm^{-1} and 1545 cm^{-1} related to features of the α-helix structure (Thi and Naumann, 2007). Two changes of the intensity at 1498 cm^{-1} and 1407 cm^{-1} reveal a difference in the intensity of the asymmetrical and symmetrical stretching bands of carboxylate groups. There are some differences of band intensity in the carbohydrate region at 1029 cm^{-1} related to specific carbohydrates namely glycogen (Quilès and Humbert, 2014). These

changes in the intensity within hyperspectral data indicated differences in the amount of polypeptide and polysaccharide compounds within this biofilm growth which were also noticed with HCA average clusters presented as 2nd derivatives for RdKW20 biofilm.

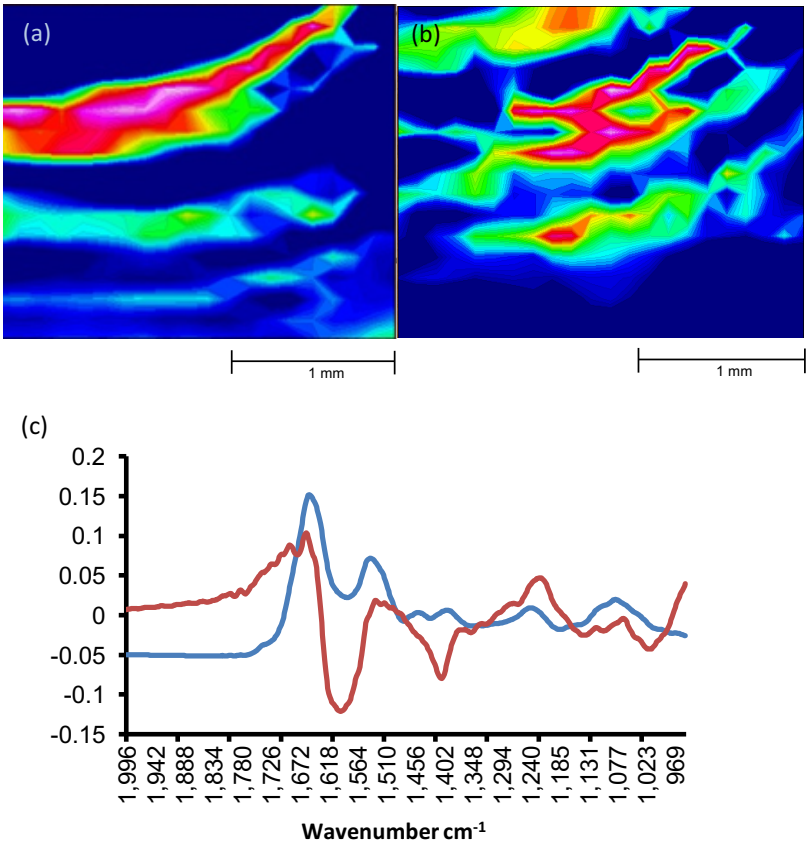

Figure 15. (a) PC2 and (b) PC5 from PCA of the region 1790 cm^{-1} to 950 cm^{-1} for the RdW20 low biofilm producer illustrates the chemical variation of the thin growth part of the biofilm image. (c) loading graph of PC2 (red) and PC5 (blue) for low biofilm producer.

For the multivariate analysis, it is worth mentioning that the signal to noise ratio (SNR) in the low biofilm producer images were problematic which may have been be due to the low thickness of the biofilm. Some of the three hyperspectral image replicates were disregarded because of the variance in low thickness biofilm and

water vapour in the atmosphere. Low sample material may produce noise that affects the spectral resolution. Noise is an issue for multivariate analysis; spectral pre-processing such as 2nd derivatives increases the noise level which can only be counteracted by increasing smoothing points. In the pre-processing of biofilm hyperspectral data, 13 smoothing points were used because too many smoothing points will lower the spectral resolution which is needed to detect certain spectral features. For raw spectral analysis such as integration the data from 2nd derivatives is sufficient, however, for multivariate analyses where 2nd derivate are used noise would be a bigger issue.

The chemical differences between thick and thin growth of biofilm obtained from the ratio plot, PCA and HCA plots of both NTHi A1 and RdKW20 show variation in aggregate of cells and EPS. These variations were displayed clearly in the integration of the NTHi A1 biofilm hyperspectral data which were corresponded to PCA plots and the clustering analysis. This difference is mainly correlated to the protein profile at 1730 cm^{-1}, 1658 cm^{-1}, 1635 cm^{-1} and 1541 cm^{-1} over carbohydrate profile. The variation between these two components may indicate the overproduction of protein which formed by NTHi bacterial cells to form biofilm. RdKW20 biofilm shows also differences at the high and low biofilm growth indicated from PCA. However, the protein and carbohydrate profiles were both varied and carbohydrate profile at 1020 cm^{-1} specifically highlighted by the multivariate analysis which indicate the accumulation of glycogen may have some impact on the biofilm formation of RdKW20.

5.3.4 Analysis of FPA array imaging for NTHi A1 biofilm

An FPA detector was used to investigate the differences within a biofilm at smaller resolution. A hyperspectral image of the NTHi A1 biofilm, showing the integration from 1730 to 1590 cm^{-1} (amide I and amide II peaks) within a smaller area which was chosen to cover 4×4 FPA images where the total image area is 706 ×706 μm^2 and each pixel is about 2.73 μm × 2.73 μm, is illustrated in Fig. 16. This image displays the chemical heterogeneity of the biofilm after 24 h incubation. The spatial distribution of the amide I band integration values are illustrated in Fig. 16a and are ranged from 1.66 to 4.55, with the higher values shown white and red and the lower in blue. The small circular shapes of high intensity are thought to be caused by the cell aggregates that form the extracellular matrix as seen in SEM image Fig. 1. A single FPA image (≈175 μm ×175 μm, 64 ×64 pixels) was chosen for further analysis (Fig. 17) as multivariate analysis for larger data sets is not currently possible with the OPUS software.

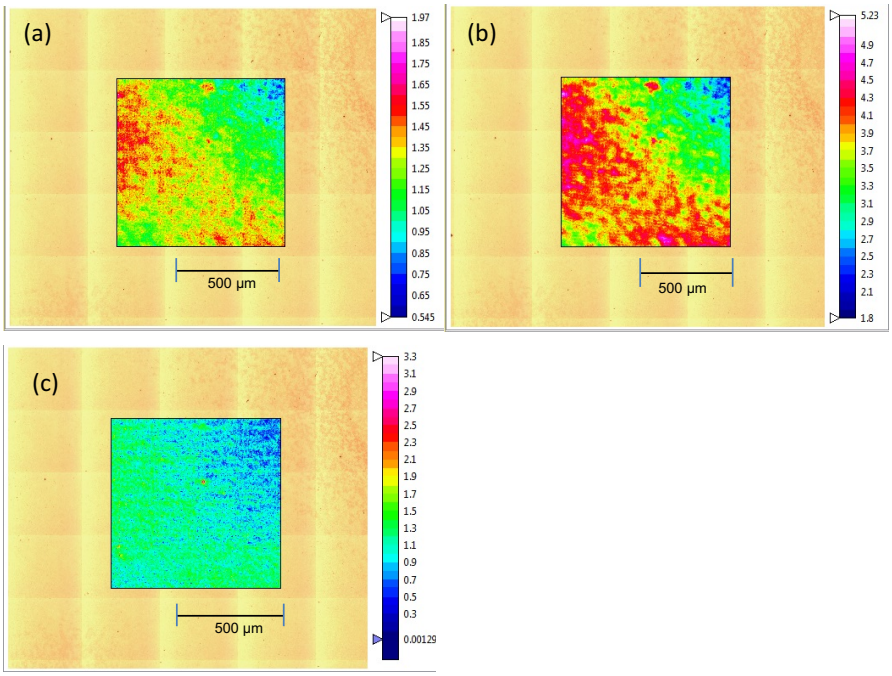

Figure 16. IR hyperspectral FPA data for the NTHi A1 shows intensity integration for (a) amide I 1730 cm^{-1} to 1590 cm^{-1}, (b) amide II 1590 cm^{-1} to 1490 $cm^{-1}$and (c) carbohydrate 1140 cm^{-1} to 950 cm^{-1}.

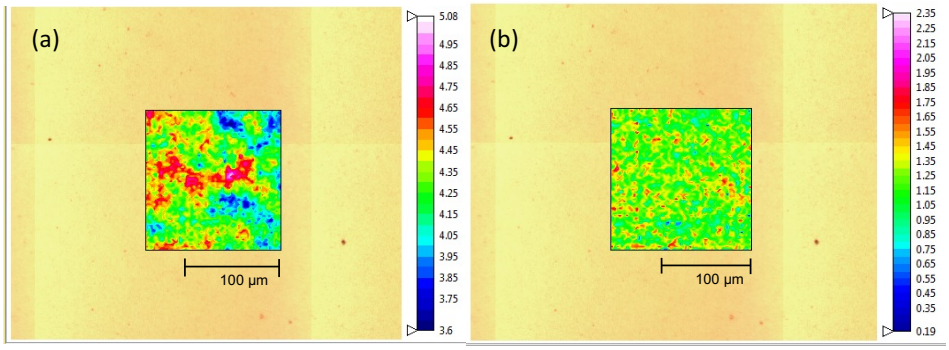

Figure 17. Intensity of peak integration for (a) amide I and (b) carbohydrate from the FPA image cropped to a single FPA image (175 µm × 175 µm).

HCA of this cropped data (≈175 µm ×175 µm) is shown in Fig. 18. The dendrogram illustrated in Fig. 18b. shows two main clusters and two subgroups for each cluster. The main differences in the 2nd derivatives of these clusters are in the regions of amide I and amide II (Fig. 18c). The intensity differences are observed as peak shift in

1540, 1579, 1658, 1689, 1739 and 1785 cm^{-1}. The clusters shown in Fig. 18a. also resemble the spatial distribution of the carbohydrate to amide I integration ratio image which suggests that the main clusters are associated with the changes of the amide I distribution across this area of the biofilm. The peaks at 1658 and 1689 cm^{-1} report the changes in α-helix and β-sheet respectively (Kong and Yu, 2007). These particular peaks within amide I and amide II area can be assigned to phenotype changes that are associated with the biofilm growth due to some protein up-regulation and down-regulation (Quilès and Humbert, 2014). Another peak at 1739 cm^{-1} is known for phospholipid and has been reported for surface colony growth (Thi and Naumann, 2007).

Due to the thickness issues with the biofilm sample, the signal to noise ratio was not sufficient to undertake multivariate analysis for this FPA hyperspectral data of RdKW20 biofilm.

To our knowledge, this is the first time that NTHi biofilm samples have been invistigated by this approach highlighting differences in the carbohydrate, proteins and lipid spatial distribution of high and low biofilm formation.

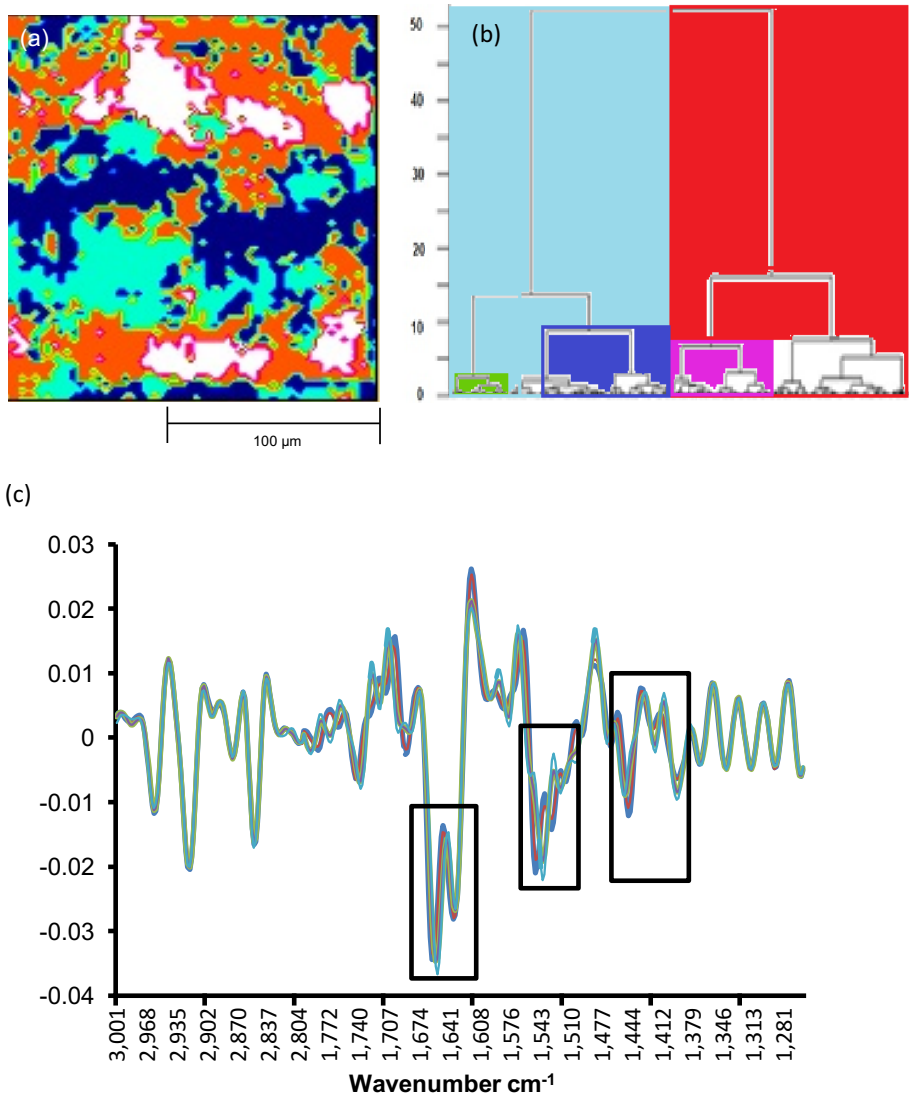

Figure 18. Cluster analysis of pre-processed hyperspectral image for the small spot area within the FPA image (175 µm ×175 µm). (a) four clusters by HCA; (b) dendrogram of the HCA of 2nd derivatives with 13 smoothing points and vector normalisation of the NTHi A1 high biofilm producer 2D IR hyperspectral data. (c) the average spectra for each cluster converted to 2nd derivatives.

5.3.5 Raman mapping for the NTHi A1 biofilm producer

NTHi A1 was investigated using Raman spectroscopy and Fig. 19 shows the map area that analysed as described before. In Fig. 20a, a typical Raman spectra for the NTHi A1 biofilm shows a high noise level despite using a long time acquisition time (120

s). The laser power could not be increased due to sample damage at higher power so the Raman map was recorded with an acquisition time of 120s. For map data a noise filter can be applied, using PCA analysis which greatly reduces the noise level to give data suitable for further analysis Fig. 20b.

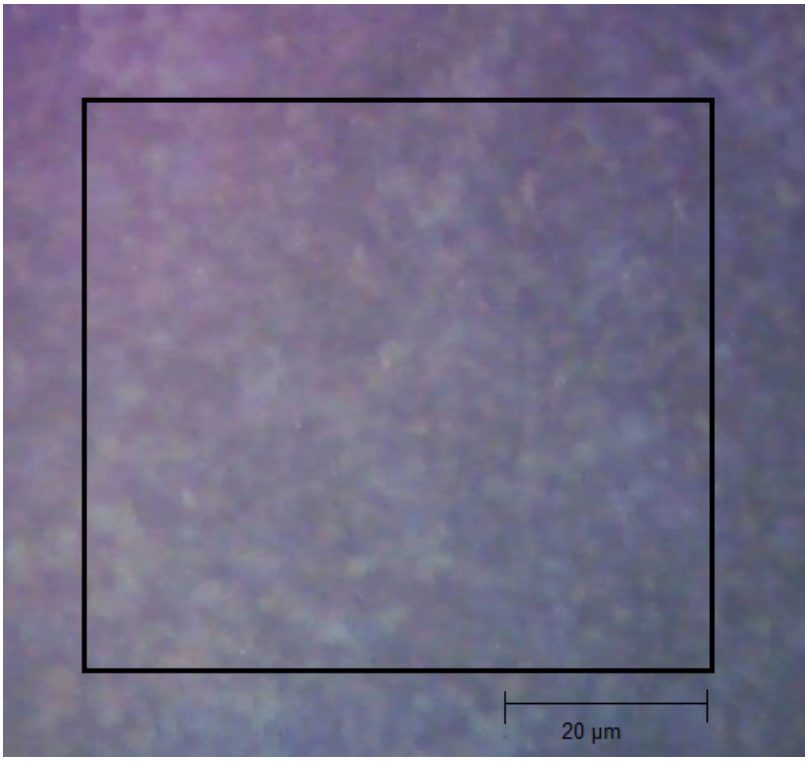

Figure 19. Mapping area of NTHi A1 biofilm investigated suing Raman spectroscopy.

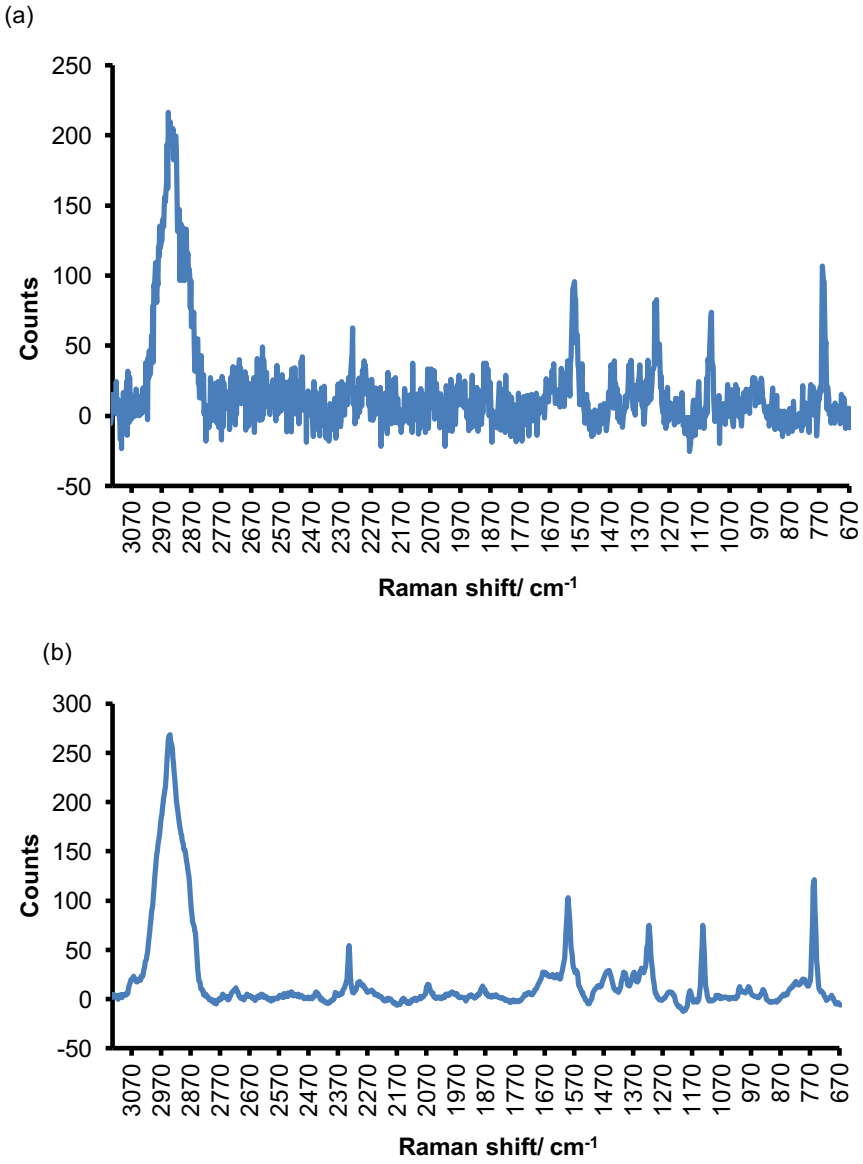

Figure 20. (a) One typical Raman spectra for the NTHi A1 biofilm without noise filter. (b) One typical Raman spectra for the NTHi A1 biofilm with noise filter.

Raman mapping for the NTHiA1 biofilm was analysed using hierarchical clustering procedure and is shown in Fig. 21. The Cluster image shows the different chemical features highlighted by the clusters where the yellow spots are thought to be due to sample damage caused by the laser as they bear the signature of graphite like material and the pink cluster resembles nutrient deposits. The blue clusters (light and dark

blue) exhibit similar spectra to each other but different than the yellow and pink clusters and are thought to be from the biofilm highlighting two different areas.

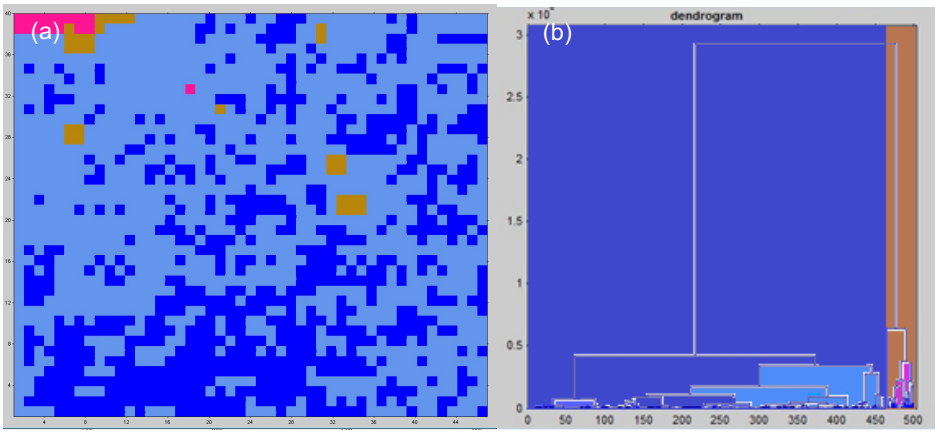

Figure 21. (a) HCA image for the four clusters and (b) Dendrogram of the HCA for the Raman mapping for NTHi A1 biofilm

Fig. 22 shows four average spectra generated from the four clusters. Brown and pink clusters were thought to be not related to biofilm. The blue clusters present the typical biofilm signature with the peak at 753 cm^{-1} depicting nucleic acids, the peak at 1124 cm^{-1} the polysaccharide region, the peak at 1300 cm^{-1} representing the amide III region with contributions from proteins, unsaturated fatty acids in lipids, peak at 1564 cm^{-1} in amide II region and lipids at 2322 cm^{-1} and 2916 cm^{-1}. The difference between these two blue clusters is only shown at intensity of lipid region (2322 cm^{-1} and 2916 cm^{-1}). The other region seems to be similar between these two blue clusters which may indicate that distribution of lipid may change over the biofilm but has no significance on the other biofilm regions. These average spectra suggest that the distribution of proteins and polysaccharides in this NTHi biofilm is similar to other reported Raman map studies of biofilm (Ivleva *et al.*, 2010 and Lu *et al.*, 2012a). Protein concentration in 24 h biofilm was reported to be 2.6 fold than in suspended

cells which may explained microorganism density increase during biofilm formation (Kives *et al.*, 2006, Ivleva *et al.*, 2009).

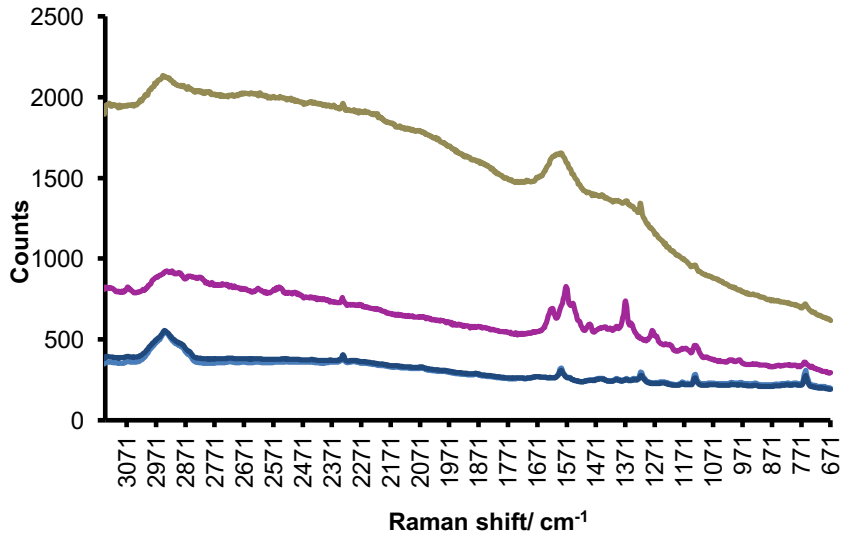

Figure 22. Average Raman spectra from HCA cluster analysis for NTHi A1 biofilm sample.

A second derivative was applied to the Raman spectra for a hierarchical cluster analysis and the average spectra are displayed in Fig. 23. This spectral transformation to 2nd derivative reveals similar peaks at 755 cm^{-1} which is related to the DNA/RNA base region (Lu *et al.*, 2012a). Some spectral difference were also observed in the amide III peak region around 1132 cm^{-1} and fatty acids at 1300 cm^{-1} that reflect properties of the major components of biofilm EPS (Lu *et al.*, 2012a, Chao and Zhang, 2012). Another peak displayed at 1589 cm^{-1} relates to bacterial growth and nucleic acids.

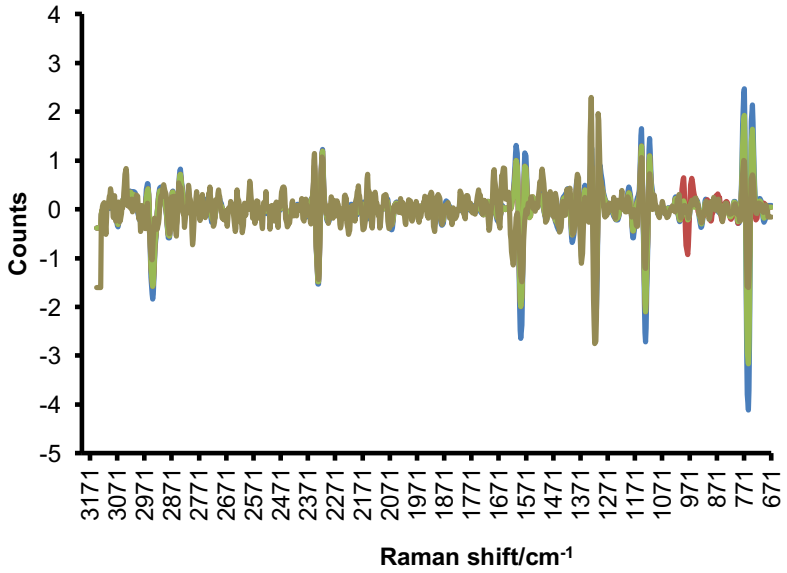

Figure 23. Average of 2nd derivatives from HCA cluster analysis of the NTHi A1 biofilm sample.

This clustering of Raman map spectra demonstrates the spatial distribution of protein secondary structure, polysaccharide and DNA/RNA of the biofilm surface which confirms the heterogeneity of this NTHi biofilm. Data preprocessing techniques such as second derivative transformations prior to cluster analyses for Raman scattering spectra can reveal useful information for overlapping peaks.

In this section, the analysis of Raman spectroscopy images was performed for the NTHi A1 biofilm to explore the differences in Raman band features. The acquisition of good quality data for mapping was found to be less efficient compared to the FTIR spectroscopy study due to the long acquisition time needed to obtain data that has an acceptable signal to noise ratio. An advantage of Raman spectroscopy is the ability to map at a 1 μm spatial resolution which potentially could allow for a more detailed study at that resolution. Due to the disadvantages of Raman spectroscopy for this

work the main focus remained on the analysis by FTIR. Different excitation wavelength for the Raman analysis were also investigated however longer wavelength lasers such as 633 nm, 785 nm and 830 nm induced a strong fluorescence signal in addition to any Raman signal. This can produce strong background and swamp the Raman bands of the biological samples. In addition higher laser power at 532 nm excitation may also cause photo damage (Carter *et al.*, 2009). To avoid this, lower energy with short wavelength for the laser excitation (e. g. 532 nm, with 10% power) was an efficient approach to avoid inducing of fluorescence in our case. However even with this (10%) energy, the Raman mapping for this NTHi A1 biofilm sample was problematic and produced slight photodamage in small areas of the sample.

Enhancements of Raman spectroscopy to dramatically improve signal to noise ratios are possible such as surface-enhanced Raman spectroscopy (SERS) (Ivleva *et al.*, 2010) which requires the use of roughened metal surface as a substrate. Tip-enhanced Raman spectroscopy (TERS) combines SERS with scanning probe microscopy provides spectral and structural information of the tiny amount of the probe molecule. The enhancement properties of TERS dependent on many factors such as tip size and shape, substrate material and the tip-substrate distance (Yang *et al.*, 2009). TERS could provide high spatial resolution of the sample. In this work, SERS and TERS were not attempted and the focus remained with FTIR spectroscopy.

5.4 Conclusion

In conclusion, the outcomes of this work provide compelling evidence that indicate that the sessile cells and EPS contain distinctive chemical feature in NTHi biofilm that differ among high and low biofilm formation. The analysis of biofilm by FTIR spectra gives a new method for quantifying biofilm formation by integrating both the proteins and carbohydrate regions. This way high and low biofilm could be quantified and segregated which was in agreement to the previous staining method reported in Chapter 2. PCA analysis of the FTIR data provides an excellent approach to chemically distinguish between biofilm growth formed on CaF_2. The two biofilms formed by NTHi A1 and RdKW20 have compositional variability when formed on CaF_2. The multivariate analysis of hyperspectral mapping and imaging data demonstrated the spatial distribution of the different chemical components of the NTHi biofilms. The sessile cells spectral features showed specific differences for the amide I band such as β-sheet conformational changes and carbohydrate differences in glycogen bands. FPA-FTIR microspectroscopy can be a sensitive approach to identify the compositional changes across the biofilm growth over CaF_2 discs and provides high spatial resolution of carbohydrate to protein content distribution (<3 μm). This may guide investigations into of chemical features of biofilm candidates and assist with the detection of NTHi biofilm during infection or drug susceptibility studies.

5.5 References

Alvarez-Ordonez, A, Mouwen, D, Lopez, M, & Prieto, M, 2011. 'Fourier transform infrared spectroscopy as a tool to characterize molecular composition and stress response in foodborne pathogenic bacteria'. *Journal of Microbiological Methods,* 84**,** 369-378.

Andersson, S, Dalhammar, G, Land, C J & Rajarao, G K, 2009. 'Characterization of extracellular polymeric substances from denitrifying organism Comamonas denitrificans'. *Applied Microbiology and Biotechnology,* 82**,** 535-543.

Bosch, A, Serra, D, Prieto, C, Schmitt, J, Naumann, D & Yantorno, O, 2006. 'Characterization of Bordetella pertussis growing as biofilm by chemical analysis and FT-IR spectroscopy'. *Applied Microbiology and Biotechnology,* 71**,** 736-747.

Burgula, Y, Khali, D, Kim, S, Krishnan, S, Cousin, M, Gore, J, Reuhs, B. & Mauer, L, 2007. 'Review Of Mid-Infrared Fourier Transform Infrared Spectroscopy Applications For Bacterial Detection'. *Journal of Rapid Methods & Automation in Microbiology,* 15**,** 146-175.

Carter, E. A, Tam, K K, Armstrong, R S & Lay, P A 2009. 'Vibrational spectroscopic mapping and imaging of tissues and cells'. *Biophysical Reviews,* 1**,** 95-103.

Chalmers, J M & And Griffiths, P R 2002. 'Classification Methods'. *Handbook of Vibrational Spectroscopy.* John Wiley & Sons Ltd, Chichester.

Chao, Y & Zhang, T, 2012. 'Surface-enhanced Raman scattering (SERS) revealing chemical variation during biofilm formation: from initial attachment to mature biofilm'. *Analytical and Bioanalytical Chemistry,* 404**,** 1465-1475.

Cheung, H Y, Chan, G L, Cheung, S H, Sun, S Q & Fong, W F, 2007. 'Morphological and chemical changes in the attached cells of Pseudomonas aeruginosa as primary

biofilms develop on aluminium and CaF2 plates'. *Journal of Applied Microbiology,* 102**,** 701-710.

Costerton, J W, Stewart, P S & Greenberg, E P, 1999. 'Bacterial biofilms: a common cause of persistent infections'. *Science,* 284**,** 1318-1322.

Di Xia, F, Mallet, A, Caliot, E, Gao, C, Trieu-Cuot, P & Dramsi, S, 2014. 'Capsular polysaccharide of Group B Streptococcus mediates biofilm formation in the presence of human plasma'. *Microbes and Infection*.

Donlan, R, Piede, J, Heyes, C, Sanii, L, Murga, R, Edmonds, P, El-Sayed, I & El-Sayed, M, 2004. 'Model system for growing and quantifying Streptococcus pneumoniae biofilms in situ and in real time'. *Applied and environmental microbiology,* 70**,** 4980-4988.

Donlan, R M & Costerton, J W, 2002. 'Biofilms: survival mechanisms of clinically relevant microorganisms'. *Clinical Microbiology Reviews,* 15**,** 167-193.

Fang, L, Wei, X, Cai, P, Huang, Q, Chen, H, Liang, W & Rong, X, 2011. 'Role of extracellular polymeric substances in Cu (II) adsorption on Bacillus subtilis and Pseudomonas putida'. *Bioresource Technology,* 102**,** 1137-1141.

Holman, H Y N, Miles, R, Hao, Z, Wozei, E, Anderson, L M & Yang, H, 2009. 'Real-time chemical imaging of bacterial activity in biofilms using open-channel microfluidics and synchrotron FTIR spectromicroscopy'. *Analytical Chemistry,* 81**,** 8564-8570.

Hughes, C, Iqbal-Wahid, J, Brown, M, Shanks, J H, Eustace, A, Denley, H, Hoskin, P J, West, C, Clarke, N W & Gardner, P, 2013. 'FTIR microspectroscopy of selected rare diverse sub-variants of carcinoma of the urinary bladder'. *Journal of Biophotonics,* 6**,** 73-87.

Humbert, F, Saadi, S, Quilès, F & Hani, K, 2011. 'In situ assessment of antibacterial activity of dermaseptine S4 derivatives against Pseudomonas fluorescens nascent biofilms by using ATR-FTIR spectroscopy'. *development,* 2**,** 4.

Ivleva, N P, Wagner, M, Horn, H, Niessner, R & Haisch, C, 2009. 'Towards a nondestructive chemical characterization of biofilm matrix by Raman microscopy'. *Analytical Bioanalytical Chimestry,* 393**,** 197-206.

Ivleva, N P, Wagner, M, Horn, H, Niessner, R & Haisch, C, 2010. 'Raman microscopy and surface enhanced Raman scattering (SERS) for in situ analysis of biofilms'. *Journal of Biophotonics,* 3**,** 548-556.

Ivleva, N P, Wagner, M, Szkola, A, Horn, H, Niessner, R & Haisch, C, 2010. 'Label-Free in Situ SERS Imaging of Biofilms'. *The Journal of Physical Chemistry B*.

Jurcisek, J A & Bakaletz, L O, 2007. 'Biofilms Formed by Nontypeable Haemophilus influenzae In Vivo Contain both Double-Stranded DNA and Type IV Pilin Protein'. *Journal of Bacteriology,* 189**,** 3868-3874.

Kives, J, Orgaz, B & Sanjosé, C, 2006. 'Polysaccharide differences between planktonic and biofilm-associated EPS from Pseudomonas fluorescens B52'. *Colloids and Surfaces B: Biointerfaces,* 52**,** 123-127.

Kong, J & Yu, S, 2007. 'Fourier transform infrared spectroscopic analysis of protein secondary structures'. *Acta Biochimica et Biophysica Sinica,* 39**,** 549-559.

Langereis, J D & Hermans, P W, 2013. 'Novel concepts in nontypeable Haemophilus influenzae biofilm formation'. *FEMS Microbiology letters,* 346**,** 81-89.

Lin-Vien, D, Colthup, N B, Fateley, W G & Grasselli, J G, 1991. *The Handbook of infrared and Raman characteristic frequencies of organic molecules*, Elsevier.

Lu, X, Samuelson, D R, Rasco, B A & Konkel, M E 2012a. 'Antimicrobial effect of diallyl sulphide on Campylobacter jejuni biofilms'. *Journal of Antimicrobial Chemotherapy***,** dks138.

Lu, X, Weakley, A T, Aston, D E, Rasco, B A, Wang, S & Konkel, M E, 2012b. 'Examination of nanoparticle inactivation of Campylobacter jejuni biofilms using infrared and Raman spectroscopies'. *Journal of Applied Microbiology,* 113**,** 952-963.

Naumann, D, 2006. 'Infrared spectroscopy in microbiology'. *Encyclopedia of Analytical Chemistry*.

Nivens, D E, Ohman, D E, Williams, J & Franklin, M J, 2001. 'Role of alginate and its O acetylation in formation of Pseudomonas aeruginosa microcolonies and biofilms'. *Journal of Bacteriology,* 183**,** 1047-1057.

Paquet-Mercier, F, Safdar, M, Parvinzadeh, M & Greener, J, 2014. 'Emerging Spectral Microscopy Techniques and Applications to Biofilm Detection.

Pink, J, Smith-Palmer, T, Beveridge, T & Pink, D, 2004. 'An FTIR study of Pseudomonas aeruginosa PAO 1 biofilm growth and dispersion. An improved ATR method for studying biofilms: the C–H stretch spectral region'. *Biofilms,* 1**,** 157-163.

Quilès, F & Humbert, F, 2014. 'On the production of glycogen by Pseudomonas fluorescens during biofilm development: an in situ study by attenuated total reflection-infrared with chemometrics'. *Biofouling***,** 1-10.

Serra, D, Bosch, A, Russo, D M, Rodríguez, M E, Zorreguieta, Á, Schmitt, J, Naumann, D & Yantorno, O, 2007. 'Continuous nondestructive monitoring of Bordetella pertussis biofilms by Fourier transform infrared spectroscopy and other corroborative techniques'. *Analytical and Bioanalytical Chemistry,* 387**,** 1759-1767.

Sutherland, I W, 2001. 'Biofilm exopolysaccharides: a strong and sticky framework'. *Microbiology,* 147**,** 3-9.

Swords, W E, Moore, M L, Godzicki, L, Bukofzer, G, Mitten, M. J & Voncannon, J, 2004. 'Sialylation of Lipooligosaccharides Promotes Biofilm Formation by Nontypeable Haemophilus influenzae'. *Infection and Immunity,* 72**,** 106-113.

Thi, N N & Naumann, D, 2007. 'Investigating the heterogeneity of cell growth in microbial colonies by FTIR microspectroscopy'. *Analytical and Bioanalytical Chemistry,* 387**,** 1769-1777.

Vu, B, Chen, M, Crawford, R J & Ivanova, E P, 2009. 'Bacterial extracellular polysaccharides involved in biofilm formation'. *Molecules,* 14**,** 2535-2554.

Wang, L & Mizaikoff, B, 2008. 'Application of multivariate data-analysis techniques to biomedical diagnostics based on mid-infrared spectroscopy'. *Analytical and Bioanalytical Chemistry,* 391**,** 1641-1654.

Wolf, G, Crespo, J G & Reis, M A, 2002. 'Optical and spectroscopic methods for biofilm examination and monitoring'. *Reviews in Environmental Science and Biotechnology,* 1**,** 227-251.

Wu, S, Baum, M M, Kerwin, J, Guerrero, D, Webster, S, Schaudinn, C, Vandervelde, D & Webster, P, 2014. 'Biofilm specific extracellular matrix proteins of nontypeable Haemophilus influenzae'. *Pathogens and disease*.

Yang, Z, Aizpurua, J & Xu, H, 2009. 'Electromagnetic field enhancement in TERS configurations'. *Journal of Raman Spectroscopy,* 40**,** 1343-1348.

Chapter 6

FTIR analysis of NTHi biofilm after antibiotic challenge

Abstract

The transmission mode of Fourier transform infrared (FTIR) spectroscopy was used to compare spectra of the high biofilm producer NTHi A1 and low biofilm producer RdKW20 treated with four antibiotics. The growth of biofilms after application of selected antibiotics from β-lactams, fluoroquinolone and macrolide classes at both subinhibitory and inhibitory concentrations as well as at two different degrees of biofilm formation were determined on new and existing biofilm. The samples showed reproducibility within replicates with regard to an observed enhancement in the formation of biofilm material for those treated with the β-lactam agents, amoxicillin and cefotaxime. Hyperspectral image data of the amoxicillin treated samples provided a robust investigation which showed that the FTIR profile of NTHi biofilm protein profile specifically increased in relation to carbohydrate bands. PCA score plots and loading graphs illustrate the main IR bands that characterise NTHi A1 biofilm treated with AMX. From the FTIR spectroscopy analysis, the spatial distribution of the amide I and II bands that dominate the biofilm chemical components in NTHi biofilm was not observed in treated RdKW20 biofilm even with increased biomaterial.

6.1. Introduction

Nontypeable *Haemophilus influenzae* (NTHi) biofilm is attracting more attention due to an association with resistance to *β*-lactam antibiotics and to the persistence of infections treated with this drug (Takei *et al.*, 2013, Wu *et al*., 2014). NTHi is considered as one of the more common pathogens that cause infection in the respiratory tract. Previous studies on NTHi biofilm have investigated variations in its formation and pathogenic relationship *in vitro* (Puig *et al.*, 2014) and as addressed previously in Chapter 3. There may be a significant link between these biofilm growth variations and the variation of cellular behaviour characteristics according to some intercellular or extracellular environment. These alterations may be related to some chemical and genetic attributes which influenced by the extracellular environment. These attributes may alter the distribution of the chemical composition of these isolates. For example, antibiotic treatment could cause some biofilm variation which may increase antibiotic resistance and ability to form antibiotic tolerant biofilms (Sill and Tsang, 2008).

NTHi infection has become more difficult to treat with the first choice of drug (amoxicillin) in acute otitis media (AOM) caused by NTHi biofilm (Moriyama *et al.*, 2009). NTHi infection has been found to be persistent in the site of infections such as otitis media (OM) and lung of chronic obstructive pulmonary disease (COPD) in spite of being susceptible to *β*-lactam at MIC (Takei *et al*., 2013). The persistent nature within the biofilm community and mechanisms of communication between biofilm components differ from planktonic bacterial cells. Due to many mechanisms, such as sessile cells with EPS, bacteria are afforded greater protection from antibiotics (Davies, 2003). Some studies of NTHi infection provide evidence that

fluoroquinolone and macrolides have a more favourable effect on NTHi biofilm than other antibiotics used to treat NTHi infection (Takei *et al*., 2013). However, to date, little research has been conducted on NTHi biofilms treated with different antibiotics.

The characterisation of biological samples using vibrational spectroscopy may enable discrimination between cellular behaviour within normal and abnormal situations. In brief, for microbiological studies, FTIR has become a promising tool to non-invasively examine macromolecular modification in an holistic approach within the microbial cells and to assist in identification and classification of microorganisms (Lasch and Naumann, 2000). Conventional diagnostic tools and standard assay could not deliver sufficient detailed information rapidly which is discussed in detail in Chapter 1. FTIR can also be applied to examine the influence of some exogenous molecules. These exogenous molecules including treatment agents can interact and may interfere with the molecular constitution of the microbial samples. The effects of these interactions could potentially enable to a better understanding of the distribution of chemical components interactions within complex samples such as biofilm (Lu *et al*., 2012b).

FTIR spectroscopy as a tool to study holistic chemical composition has been used for biofilm samples developed for in situ assessments of antibacterial activity on *Pseudomonas fluorescens* biofilm (Humbert *et al.*, 2011) and antimicrobial effect of diallyl sulphide on *Campylobacter jejuni* biofilm (Lu *et al.,* 2012a). With FTIR spectroscopy, chemical information from sessile cells and polymeric matrix data formed on the surface can be used with a precision of up to 2.5 μm as described in detail in Chapter 5 (5.3.3 and 5.3.4) of accuracy to demonstrate biofilm composition

(Serra *et al*., 2007, Bosch *et al.*, 2006, Lu *et al.*, 2012a). In Chapter 5, FTIR microspectroscopy was used and described in detail with regard to studying the spatial distribution of biofilm by obtaining spectral mapping data of a sample, which has enabled the collection of spatially-resolved spectra filling the gap of information in data from the morphological based microscopically studies (Paquet-Mercier *et al.*, 2014).

FTIR spectroscopy, including hyperspectral mapping, will help to better understand the relationships between the macromolecules that construct main components of biofilm like lipids, proteins, phosphate groups and polysaccharides. The IR spectral variation between two isolates, that have a different level of biofilm formation, was discussed in the previous chapter. In this chapter, the potential influence of four classes of antibiotics on the spectral bands and hyperspectral images that provide holistic information about the NTHi biofilm components were investigated for lipids, proteins and carbohydrate spectral areas for the two *Haemophilus influenzae* isolates. The current study focuses only on the chemical compositional attributes of the biofilm as the study of genetic information is beyond the scope of this project. The NTHi biofilm is investigated in regard to chemical distribution of functional groups by using hyperspectral images of biofilm formed *in vitro* with treatment with sub-MIC and MIC of β-lactams, fluoroquinolone and macrolide antibiotics. The influence of two levels of concentration of these antibiotics, that inhibited planktonic cell growth, full-inhibiting concentration at MIC, and sub-MIC (sub-inhibiting concentration) on NTHi biofilm was examined using infrared microspectroscopy.

6.2. Methods

6.2.1 Bacterial samples and biofilm growth

The isolates described previously in Chapter 5 NTHi clinical isolate (NTHi A1), and a standard isolate (RdKW20) were studied in this chapter with same incubation and handling conditions described earlier.

6.2.2 MIC determination and antibiotic preparations

MICs were determined using Etest® and the antibiotic solutions at MIC and sub-MIC concentrations were prepared from stock solutions previously reported in detail in Chapter 4.

6.2.3 Biofilm-antibiotic MTP assay

Bacterial biofilms were prepared using the protocol developed for the MTP biofilm assay as reported in Chapter 2. Briefly, microtitre plates were inoculated with 2 ml of standardised bacterial broth to about $1X10^7$ CFU/ml. CaF_2 discs (10 mm diameter, Crystran Limited, UK) was inserted into five wells, one for each well that inoculum broth with the antibiotics added and one window for the control well.

Two plates were prepared, one plate for sub-MIC concentration of each antibiotic (AMX, CIP, AZM and CTX) then incubated for 24 h at 37ºC and 5% CO_2. After incubation, the CaF_2 discs were washed off three times with water and left to dry for half an hour at room temperature before IR analysis as described in Chapter 5.

The second plate was inoculated with the broth and CaF_2 discs were inserted into wells (four CaF_2 discs, one for each antibiotic), the biofilms were allowed to grow for

24 h before adding antibiotics. After 24h incubation without any antibiotic agent, the inoculum inside the wells with CaF_2 discs was removed aseptically by pipettes and an equivalent MIC concentration for each antibiotic (AMX, CIP, AZM and CTX) in 2 ml of fresh broth was then added as a replacement then incubated for another 24 h at 37ºC and 5% CO_2. After incubation, the CaF_2 discs were washed off three times with water and let dry for half an hour at room temperature. This procedure was replicated three times for NTHi A1 biofilm and three times for RdKW20 biofilm.

6.2.4 FTIR spectroscopy data collection

Transmission mode FTIR spectra were recorded on a Vertex 70 spectrometer (Bruker Optik, Germany) for spectra collected from 3900 cm^{-1} to 800 cm^{-1} as described in Chapter 5. Hyperspectral images were recorded with a Bruker Hyperion 3000 microscope (Bruker Optik, Germany) which is also described in detail in Chapter 5 (section 5.2.3) This method was carried out for three replicates of biofilm grown on CaF_2 discs for NTHi A1 biofilm and RdKW20 biofilm in two different concentrations for each antibiotic (AMX. CIP, AZM and CTX).

6.2.5 Spectral manipulation and evaluation

Spectral pre-processing was performed using the OPUS 7.2 software (Bruker Optik, Germany). Atmospheric compensation then averaging of spectra were performed for all spectra (n=3) obtained as individual IR spectra of the biofilm grown on CaF_2 discs with 8 mm spot size and peak area integration was calculated as described in Chapter 5 (section 5.2.5). The spectral ranges were cut for both one single spectrum recording and for the hyperspectral images as in Chapter 5 (section 5.2.5). Data were analysed

using Student's T-test with Excel® Microsoft. P value of <0.05 was considered statistically significant.

Spectral pre-processing was performed for multivariate analysis of the 2D IR hyperspectral images with atmospheric compensation in the form of 2nd derivatives (Savitzky-Golay algorithm with 13 smoothing points) and vector normalisation.

6.2.6 Multivariate analysis for the hyperspectral images

From a selected image obtained from NTHi A1 untreated and treated with MIC and sub-MIC of AMX and RdKW20 biofilms untreated and treated with MIC of AMX, ten spectra were extracted from each data set. These spectra were processed as described in the Chapter 5 (section 5.2.5.1). For this PCA model, two spectral ranges were selected; from 3000 cm^{-1} to 2769 cm^{-1} and 1752 cm^{-1} to 952 cm^{-1}.

Cluster analysis of the hyperspectral data from selected images was performed using the OPUS software and dendrograms were produced from the clustering analysis with similar procedure to that described in Chapter 5 (section 5.2.5.1). These steps were also performed using the Cytospec v.1.4.03 software (Cytospec®, Germany).

6.3. Results and discussion

6.3.1 IR spectra for the treated biofilm

The average IR spectra for the NTHi A1 biofilm growth on CaF_2 (8 mm) following treatment with antibiotics are illustrated in Fig. 1 It seems that individual spectra of the biofilm with sub-MIC of AMX (red) show no major differences in the overall intensity than the mature biofilm treated with MIC of AMX (blue) and compared to untreated biofilm (black).

The spectra obtained from RdKW20 biofilm with sub-MIC of AMX in Fig. 2 shows a comparatively low intensity to the untreated biofilm, as the biofilm formation may be supressed by the AMX. However, the spectra of mature biofilm treated with MIC of AMX has higher intensity which is even greater than for the NTHi A1 mature biofilm that is considered to be a high biofilm producer, as described in the crystal violet results displayed in Chapter 4 (sections 4.3.3 and 4.3.5).

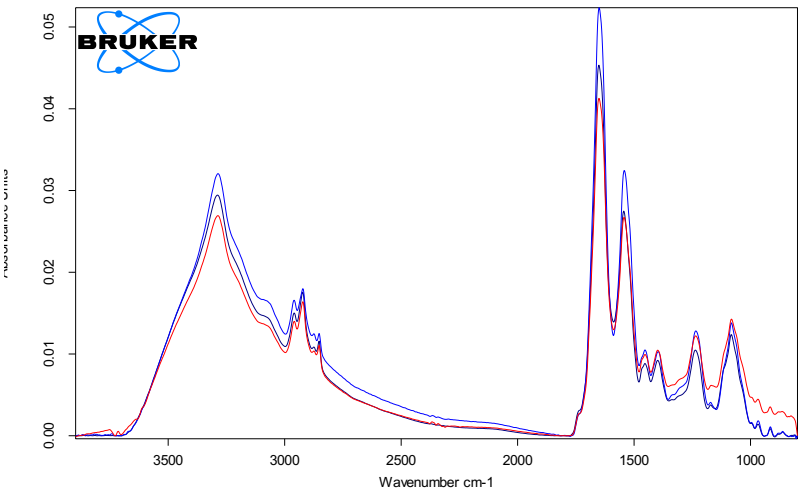

Figure 1. The average FTIR spectra obtained from the CaF_2 discs (n=3) with growth of NTHi A1 biofilm at two concentrations of AMX: mature biofilm exposed to MIC (red); developing biofilm exposed to sub-MIC (blue) and untreated biofilm (black).

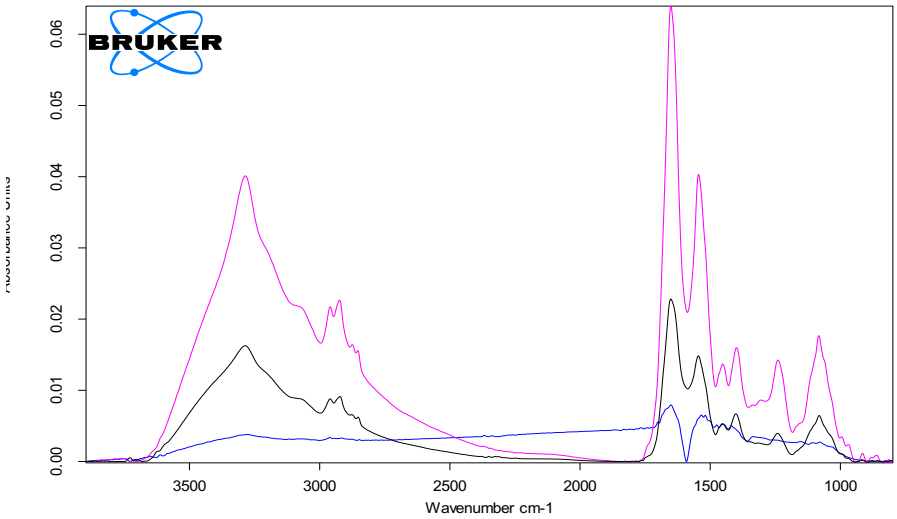

Figure 2. The average FTIR spectra obtained from the CaF_2 discs (n=3) with growth of RdKW20 biofilm at two concentrations of AMX: mature biofilm exposed to MIC (pink); developing biofilm exposed to sub-MIC (blue) and untreated biofilm (black).

The integration values of the specific IR bands are summarised for each antibiotic at two given concentrations, sub-MIC in Table 1 and MIC in Table 2. These integration values illustrate differences in four different regions of the FTIR spectra that are characteristic of lipids, proteins, nucleic acids and carbohydrates that constitute the biofilm similar to the analysis of the FTIR spectra in Chapter 5 (section 5.3.1).

Table 1. Integration of specific bands from average spectra for biofilm after treatment of developing biofilm (24 h) with sub-MIC antibiotics, for NTHi A1 and RdKW20. Fatty acids (CH stretching 3000 cm^{-1} to 2830 cm^{-1}), proteins (amide I 1730 cm^{-1} to 1590 cm^{-1}), proteins (amide II (1590 cm^{-1} to 1490 cm^{-1}), DNA/RNA (P=O band and amide III 1280 cm^{-1} to 1190 cm^{-1}, 1490 cm^{-1} to 1000 cm^{-1}) and carbohydrates (1140 cm^{-1} to 950 cm^{-1}).

	NTHi A1 biofilm					**RdKW20 biofilm**				
	control	AMX	CTX	CIP	AZM	control	AMX	CTX	CIP	AZM
CH stretching	0.55	0.50	0.24	0.12	0.37	0.26	0.03	0.21	0.27	0.24
Amide I	1.94	2.60	1.11	0.68	1.72	0.98	0.43	1.04	1.19	1.10
Amide II	0.73	1.04	0.47	0.30	0.62	0.35	0.25	0.44	0.48	0.42
P=O band and amide III	0.27	0.36	0.14	0.06	0.29	0.10	0.00	0.09	0.11	0.15
Carbohydrates	0.62	0.73	0.31	0.14	0.73	0.34	0.04	0.27	0.39	0.41

The values obtained for the NTHi A1 biofilm show an increase of about 34% for amide I and 42% for amide II after treatment with AMX and CTX compared with the integration values for the same bands in the control. Using Beer-Lambart law (described in Chapter 5 section 5.1), the increase in the integration value can be attributed to the path length or the density in same thickness of the biofilm (concentration) as the molar absorption coefficient can be assumed to be constant.

Similarly, the integration of the carbohydrate bands increased in the sample treated with sub-MIC of AMX. Treatment with the other antibiotics presented integration values lower than the control. The effect of AMX at sub-MIC level resulted in some increase of the integration value for the amide I, II, P=O and amide III and carbohydrate bands. These differences between treated and untreated NTHi A1 biofilm suggest that thickness of biofilm material increased in treated biofilm. Thus it causes an increase of the integration values for the dominant macromolecules after AMX treatment.

For RdKW20 biofilm in Table 1, AMX treated biofilm showed a lower integration value for each band and AMX seemed to have the greatest effect on inhibiting the growth as higher integration values indicate higher growth. The other antibiotic (CIP, AZM and CTX) showed a slight increase of the integration value for the amide I, II and carbohydrate bands compared to the untreated 24 h biofilm.

Table 2. Integration of specific bands from average spectra for biofilm after treatment of developing biofilm (24 h) with MIC antibiotics, for NTHi A1 and RdKW20. Fatty acids (CH stretching 3000 cm^{-1} to 2830 cm^{-1}), proteins (amide I 1730 cm^{-1} to 1590 cm^{-1}), proteins (amide II (1590 cm^{-1} to 1490 cm^{-1}), DNA/RNA (P=O band and amide III 1280 cm^{-1} to 1190 cm^{-1}, 1490 cm^{-1} to 1000 cm^{-1}) and carbohydrates (1140 cm^{-1} to 950 cm^{-1}).

	NTHi A1 biofilm					**RdKW20 biofilm**				
	control	AMX	CTX	CIP	AZM	control	AMX	CTX	CIP	AZM
CH stretching	0.63	0.51	0.85	0.49	0.42	0.17	0.64	0.61	0.27	0.16
Amide I	2.45	1.92	3.40	1.79	1.46	0.69	3.01	2.74	1.17	0.66
Amide II	0.92	0.75	1.30	0.71	0.55	0.25	1.14	1.05	0.46	0.24
P=O band and amide III	0.33	0.27	0.45	0.25	0.21	0.075	0.36	0.31	0.12	0.07
Carbohydrates	0.75	0.58	1.03	0.56	0.50	0.23	0.90	0.81	0.45	0.20

From the data presented in Table 2, it can be seen that the NTHi A1 biofilm after treatment with AMX, CIP and AZM at the MIC showed a lower integration value for all bands compared to the value of these bands for untreated 48 h biofilm. NTHI A1 biofilm treated with a MIC level of CTX display an increased value of all bands compared to untreated biofilm. The largest relative increase is shown for the integration value of amide I (38%) whereas the increase for the other bands was 29% to 37%. NTHi A1 was observed in Chapter 4 (section 4.3.1) as sensitive to CTX. This may suggest that the MIC of CTX on established biofilm increases the resistance which then increase dominant macromolecules in biofilm especially with amide I.

The RdKW20 biofilm with AMX and CTX in Table 2 show similar patterns of increased integration values compared to the untreated 48 h biofilm. The main increase in integration values compared to the untreated 48 h biofilm appeared across all bands. In the RdKW20 biofilm, the MIC level of CIP appears to slightly increase the value of integration for all bands as well but this increase is less significant than the increase of the value with AMX and CTX. This finding is different to the treated NTHi A1 biofilm which showed increased values of all bands with MIC of CIP and

different to the sub-MIC results for CIP. Depending on the aspect of sensitivity to CIP in Chapter 4 (section 4.3.1), RdKW20 has shown sensitivity to CIP. Whereas, established biofilm increased integration values after applying CIP at the MIC which may suggest that biofilm material and cells have some resistance and show increased growth.

Table 3. Average of the ratio between spectral integration for the five assigned bands of FTIR spectral acquired from the two *H. influenzae* strains: NTHi A1 biofilm and RdKW20; untreated, after treatment of sub-MIC of AMX on developing biofilm and treatment of mature biofilm with MIC of AMX.

			Developing biofilm with sub-MIC		**Mature biofilm treated by MIC**	
	Control for NTHi A1	Control for RdKW20	NTHi A1 biofilm	RdKW20 biofilm	NTHi A1 biofilm	RdKW20 biofilm
CH/carbohydrate	0.81	0.74	0.70	2.08	0.83	0.70
CH/ Amide I	0.26	0.25	0.20	0.08	0.25	0.21
Carbohydrate/amide I	0.46	0.37	0.28	0.17	0.30	0.30
Carbohydrate /amide II	0.87	1.01	0.70	0.47	0.79	0.79
Amide I/ P=O and amide III	7.29	10.62	7.18	222	6.95	8.45
Carbohydrate /P=O and amide III	2.40	3.82	2.02	14.01	2.68	2.54

The ratios were calculated and the results are presented in Table 3. As discussed in Chapter 5 (section 5.3.1), the integration ratios for NTHi A1 biofilm and RdKW20 biofilm were calculated to show the relative variation of IR bands to each other. In this current Chapter, the same integration ratio method has been employed to investigate the changes in these ratios from untreated biofilm (control) to treated biofilm with MIC and sub-MIC of AMX.

For the developing biofilm with sub-MIC, the carbohydrate band region of NTHi A1 biofilm showed a decreased ratio in relation to amide I, II, III and P=O when

compared to the control. The ratio of amide I to P=O and amide III also showed a slightly lower value than for the untreated biofilm. Interestingly, these ratios did not show any major difference between mature and developing biofilm treated with the two concentrations. These results may indicate that there are no differences between sub-MIC and MIC treated NTHi A1 biofilm in terms of the ratio between the carbohydrate region and the protein profile. It may suggest that protein profile is dominant in NTHi A1 biofilm treated with sub-MIC and MIC of AMX.

For RdKW20 biofilm, sub-MIC of AMX showed a major increase in the ratio of amide I to P=O and amide III compared to untreated biofilm. This may be related to the low number of bacterial cells material containing nucleic acids. These cells were inhibited to grow after sub-MIC level of AMX as this strain has been confirmed as sensitive to AMX in Chapter 4 (section 4.3.1). An increase is shown in the CH stretching band to carbohydrate ratio from 0.74 compared to untreated biofilm 2.08, which indicates relatively higher lipid than carbohydrate. Carbohydrate to amide III and P=O ratio also increased from 3.82 to 14.01, similar to the amide I to P=O and amide III ratio from 10.62 to 222. These increases are due to less bacterial cell material growth on the disc.

However, mature biofilm treated with the MIC of AMX showed ratios similar to the mature NTHi A1 biofilm ratios but slightly increased for amide I to P=O and amide III. This suggest that the protein profiles are dominant in both mature NTHi A1 biofilm and mature RdKW20 biofilm treated with AMX with only differences in the lower value of P=O and amide III which is related to less bacterial cell material (growth) on the disc.

Table 4. Integration of average spectra from bands area of proteins and carbohydrates regions from 1790 cm^{-1} to 950 cm^{-1} for two *H. influenzae* strains (a) NTHi A1 biofilm and (b) RdKW20 biofilm before and after treatment of AMX on developing biofilm with sub-MIC antibiotics, or treatment of mature biofilm (48 h) with the MIC of antibiotics (MIC).

	control		**AMX**		**CTX**		**CIP**		**AZM**	
Protein and carbohydrate regions	24 h	48 h	sub-MIC	MIC	sub-MIC	MIC	sub-MIC	MIC	sub-MIC	MIC
(a) NTHi A1 biofilm	8.43	11.1	9.6	8.22	3.34	13.2	1.12	8. 2	3.48	8.12
(b) RdKW20 biofilm	4.52	3.36	0.46	12.6	3.69	10.1	4.88	5.53	3.49	1.92

To compare the degree of biofilm formation between the two strains with two AMX treatments, a marker for the changes in the biochemical composition was used. This was the integration of the spectra over the 1790 cm^{-1} to 950 cm^{-1} region, as illustrated in Table 4. The analysis of this region was demonstrated previously by Holman *et al.* (2009) for changes that occur in *E. coli* biofilm after addition of some agents and was considered as a marker for biofilm changes within this region 1790 cm^{-1} to 950 cm^{-1}.

There was no major difference in the NTHi A1 biofilm integration value, shown in Table 4a for AMX for both developing biofilm with sub-MIC and mature biofilm with MIC compared to the control. However, the developing biofilm with sub-MIC for CIP (1.12), AZM (3.48) and CTX (3.34) showed very low integration values compared to the untreated biofilm after 24 h (8.43). Compared to untreated 48 h biofilm, there was only the mature biofilm treated with the MIC of CTX that showed higher integration values (13.2) than 48 h biofilm (11.1). The other antibiotics showed lower integration values of the mature biofilm when treated with MIC. These results confirm that NTHi A1 treated with AMX shows some biofilm growth even though NTHi A1 shows resistance to AMX.

Sub-MIC antibiotic treatment of developing RdKW20 biofilm resulted in integration values that were similar to control values, except in the case of AMX. AMX treatment substantially reduced the integration value to 0.46 compared with control, 4.52 which means that RdKW20 is not enhanced by AMX in sub-MIC of AMX or other antibiotics.

Treatment of mature biofilm with the MIC of AMX and CTX resulted in higher integration values (12.4 and 10.1 respectively) than control (3.36). Similarly, treatment with CIP increased the integration value to a lesser degree (5.53) but treatment with AZM decreased the integration value (1.92). These results were also confirmed previously in Fig. 2 and Table 1 and 2 in which RdKW20 mature biofilm was enhanced with MIC of AMX.

In Chapter 4, a crystal violet assay was used to assess the NTHi isolate's ability to form biofilm in presence of the MIC and sub-MIC level of antibiotics. A significant increase of the biofilm material was demonstrated in AMX through the staining of biofilm formed inside the wells as shown in Chapter 4 (Fig. 5b). It is clear that crystal violet staining of biofilm material provides a semi-quantitative assessment for the biomaterial as it stains all biofilm material without discrimination between differences in specific chemical components.

AMX treated biofilm may have some mechanism to induce biofilm formation even with the evidence of cell lysis. FTIR spectral integral and ratios of the bacterial biofilm chemical can identify changes in composition and distribution of protein and carbohydrate contents after the biofilm treated with antibiotics, and may lead to better

understanding of biofilm development. Previously in some of the *β*-lactam antibiotics studies with NTHi biofilms it was confirmed that biofilm mass increases when NTHi bacterial cells were exposed to subinhibitory concentrations (Wu *et al.*, 2014). In this Chapter, NTHi biofilms demonstrate an increase of biofilm after the addition of sub-MIC to initial inoculum which is the isolate that showed resistance to AMX according to the breakpoint of MIC obtained in Chapter 4 (section 4.3.1). It also forms more biofilm from existing biofilm after addition of a MIC of cefotaxime in which the NTHi isolate is shown to be sensitive (Table 1 in section 4.3.1).

To summarise the results of these average spectral acquisition of the treated NTHi A1 biofilm and RdKW20 biofilm, NTHi A1 with sub-MIC (12.5% MIC) of AMX substantially increased biofilm growth as indicated by high integration values for new biofilm formation. Formation of biofilm material after exposure to sub-MIC levels of AMX demonstrated increases in biofilm density across the whole CaF_2 image. Other antibiotics had no effect, including the other *β*-lactam cefotaxime. MIC on existing biofilm (24 h incubated biofilm) integration bands showed cefotaxime substantially increased biofilm when added on 24 h biofilm. Other antibiotics had no effect.

There may be a gradient of antibiotic concentration across the biofilm, such that even when the cell/biofilm system is exposed to inhibitory concentrations of antibiotic. Many of the cells will only experience exposure to sub-inhibitory concentrations. This type of exposure might favour adaptive stress responses where the bacterial population undergoes changes in metabolic activity to minimise the effect of the antibiotic. For example, this might be the induction of a mucoid phenotype and the generation of additional biofilm matrix components. Alternatively, the response may not be beneficial to the bacterial population, but may be a negative effect on

metabolism such as protein synthesis inhibition with antibiotics such as the macrolides. Stress response gene induction in biofilm cells can antagonise the effect of antibiotics and may regulate interacting signals in some enzymes that contribute to protein synthesis or regulation of membrane permeability (Fux, et al, 2005). Observation of the effect of these antibiotics on NTHi biofilm on inducing or decreasing biofilm material such as protein to carbohydrate ratio would offer option to overcome tolerance.

For RdKW20 sub-MIC (20% MIC) antibiotics did not increase integration values for newly formed biofilm. With MIC on existing biofilm, both β-lactams substantially increased biofilm integration values when added to 24 h biofilm. In a previous examination (Chapter 4) of antibiotics' treatment effects on NTHi biofilm using a crystal violet staining assay, AMX treated biofilm demonstrated a potential increase of biofilm growth ($P<0.05$) due to AMX exposure of new and established biofilms.

While the summarised spectral integration values, shown in Tables 1, 2 and 4, give an indication of quantitative differences within the chemical groups, these quantitative values do not provide detailed information of the chemical differences of the biofilm between the different treatments and untreated biofilms in terms of the spatial distribution of the functional groups. For this, the samples were also investigated using microscopic IR mapping. Further investigation with other complementary technique may be required.

6.3.2 Analysis of 2D hyperspectral data

6.3.2.1 Hyperspectral data analysis for NTHi A1 biofilm

Further investigations were conducted on the spatial distribution of the chemical spectral bands for the 2D IR hyperspectral images of AMX treated biofilm. Integration of the bands for amide I and carbohydrate were obtained for NTHi A1 treated with sub-MIC of AMX, and these are presented in Fig. 3. FTIR hyperspectral images in Fig. 3a from the NTHi A1 biofilm formed after exposure of sub-MIC of AMX showed amide I integration values ranging from 0.86 to 7.8. Carbohydrate integration values in Fig. 3b were from 0.04 to 2.24. These two hyperspectral integration images show a similarity in terms of the visual distribution of these chemical features. Compared to the untreated 24 h biofilm from Chapter 5 (section 5.3.2), the integration values for amide I and carbohydrate bands was lower than the treated biofilm with sub-MIC of AMX.

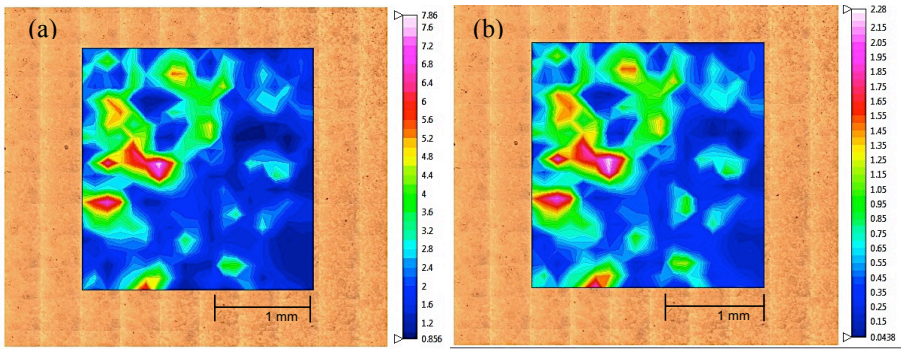

Figure 3. False colour map of hyperspectral data of NTHi A1 biofilm treated with sub-MIC of AMX during development showing (a) amide I integration (b) carbohydrate integration.

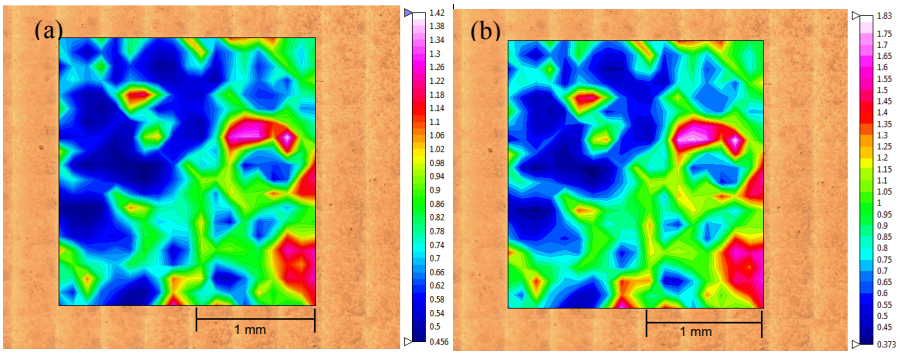

Figure 4. (a) CH stretching/amide I ratio for the NTHi A1 biofilm grown after sub-MIC level of AMX. (b) carbohydrate to amide I ratio for the NTHi A1 biofilm producer grown after sub-MIC level of AMX.

The distribution of the ratio of CH stretching to amide I in Fig. 4a ranged between 1.42 to 0.456 and for carbohydrate to amide I ranged between 1.83 to 0.373. These two ratios seem mostly similar in terms of the intensity values and the visual distribution of the chemical feature. The regions of high amide values in Fig. 3a are also the areas where comparatively more amide compared to CH stretching in Fig. 4a. This means when there is an increase in biofilm production, comparatively more amide presence than CH.

In the presence of MIC of AMX, the FTIR hyperspectral imaging analysis using the amide I integration Fig. 5a shows that the amide I increased over the biofilm region range that was mapped by FTIR. The most intense level of amide I absorption was 23.7 which is much higher than the maximum amide I integration of the control (1.88). The carbohydrate band integration heat map in Fig. 5b. shows an increased value of intensity which is a 10x difference in maximum intensity from 0.31 to 5.7.

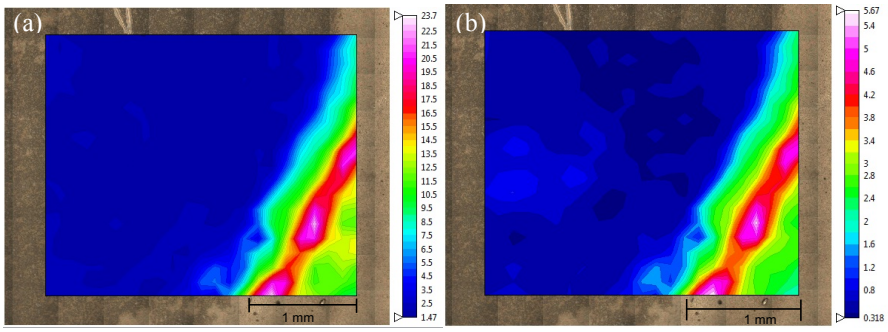

Figure 5. False colour map of hyperspectral data of NTHi A1 biofilm after treatment of established biofilm with MIC of AMX showing (a) amide I integration and (b) carbohydrate integration.

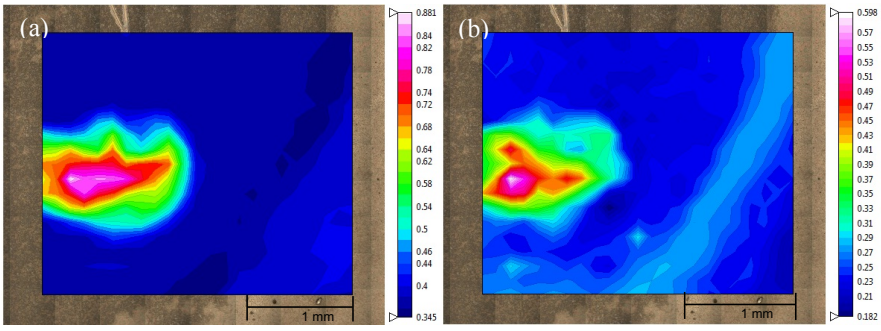

Figure 6. (a) CH stretching/amide I ratio for NTHi A1 biofilm producer isolate MIC of AMX on established biofilm; (b) carbohydrate/amide I ratio hyperspectral data for NTHi A1 isolate after applying MIC of AMX on established biofilm.

Specifically, with CH stretching to amide I and carbohydrate to amide I ratios, Fig. 6a and b illustrate the variations within these regions despite the increase of the biofilm thickness. The CH stretching to amide I ratio ranged from 0.345 to 0.881 within a 2 mm area. The carbohydrate to amide I ratio showed an intensity range from 0.18 to 0.59 for the biofilm growth surface after addition MIC of AMX. The visual chemical features of high intensity shown by the red colour in Fig. 5 have different spatial distribution patterns than the ratio images in Fig. 6. These ratios illustrate the variability of the chemical component distribution, which may be due to the

disruption of AMX on the biofilm formation process as the MIC is added onto biofilm. These hyperspectral integration and ratio images for mature biofilm with MIC are quantitatively different compared to developing biofilm after sub-MIC. The increase of amide I in MIC treated biofilm integration values and ratios are shown mostly as the main difference between sub-MIC and MIC.

The analysis of the treated NTHi A1 biofilm reveals that the bacterial cells exposed to MIC of AMX developed a thicker and more homogeneous biofilm. The results from the analysis of the integration of the amide I and carbohydrate bands for sub-MIC and MIC of AMX show an increase of the amide I integration compared to untreated biofilm which implies that these biofilms contain a larger protein component. The ratio between carbohydrate to amide I has no significant difference in treated NTHi A1 biofilm with sub-MIC over the area of biofilm, however, this ratio image for MIC treated biofilm shows a decreased value. The MIC treated biofilm illustrate that carbohydrate bands become less dominant in biofilm chemical component in relation to amide I (in protein profile).

6.3.2.2 Multivariate analysis of NTHi A1 biofilm hyperspectral data

6.3.2.2.1 Hierarchical cluster analysis for NTHi A1 biofilm

Cluster analysis was performed on pre-processed hyperspectral data similar to the cluster analysis performed in Chapter 5 (section 5.3.3). The cluster analysis of the sub-MIC treatment of the NTHi A1 with AMX shows the dendrogram in Fig. 7 with less distance between the cluster group similarity (two main clusters separated at 2.5 distance unit of similarity). These two main cluster groups divided into two other main groups of less than 1 distance unit. This means that the features that separated the groups have a high degree of similarity and no major distinguished feature

recognised by this dendrogram. Depending on the dendrogram, five clusters represent the main separation distances and show lack of any pattern. However, three clusters are distributed over the map as small shapes on the bottom half of the image. The average spectra displayed as 2nd derivatives for each cluster showed a high degree of matching spectral features to each other. It was difficult to identify a spectral feature of peak differentiation over these average spectra.

On the other hand, the cluster analysis for NTHi A1 with MIC of AMX shows two large distinct clusters in the dendrogram in Fig. 8b, separated subsequently into three main groups divided at 200 distance unit to two major groups and subdivided into further groups starting at 140 distance unit. The two large clusters in the images in Fig. 8a are divided into three subdivisions which is illustrated by the colours dark blue, red and white. The region of the large dark blue cluster is describing the same high carbohydrate to lipids ratio as in Fig. 6. The average spectra of the 2nd derivative for the four clusters are shown in Fig. 8c. and show that the main differences between the clusters was within carbohydrate bands (1163 cm^{-1} and 1105 cm^{-1}) and a minor decrease in intensity at amide I and II peaks. The difference in carbohydrate bands suggests that these two distinct areas in the biofilm have some inconsistency in carbohydrate components and the area with lower carbohydrate is dominated by amide I and amide II. This may indicate that in this NTHi biofilm treated with MIC of AMX is dominated specifically by amide I ,II and carbohydrate bands namely glycogen (Quilès and Humbert, 2014).

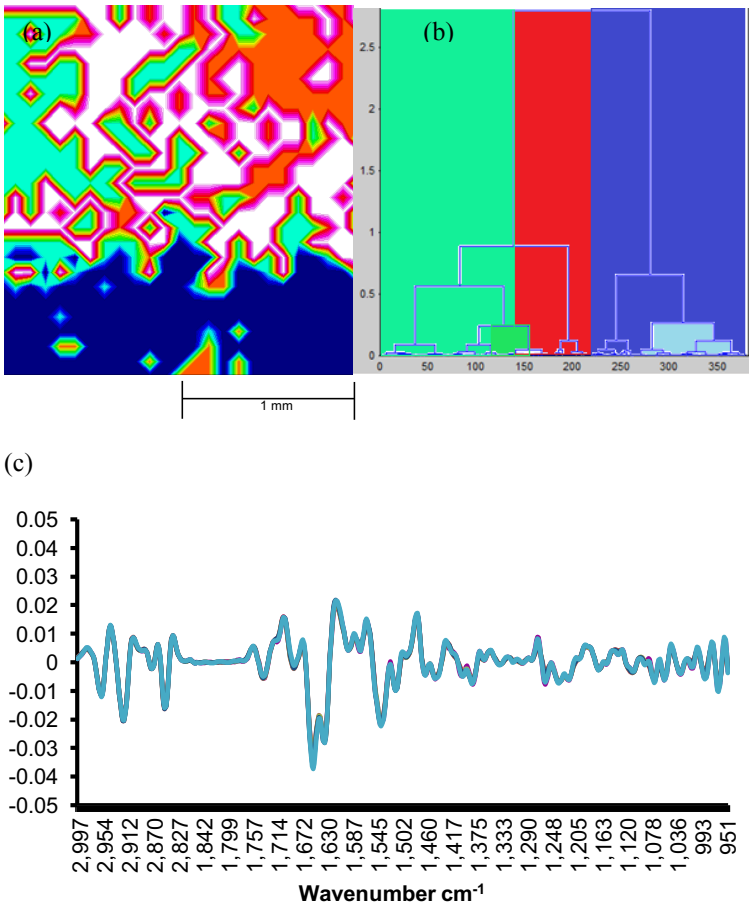

Figure 7. Cluster analysis of the 2nd derivatives and vector normalisation of NTHi A1 biofilm grown after sub-MIC level of AMX. a false colour map (a) showing the spatial distribution of clusters generated from the unsupervised analysis of the pre-processed biofilm hyperspectral data; (b) dendrogram clusters formed by the unsupervised analysis of the pre-processed hyperspectral data and (c) average of 2nd derivative for each cluster.

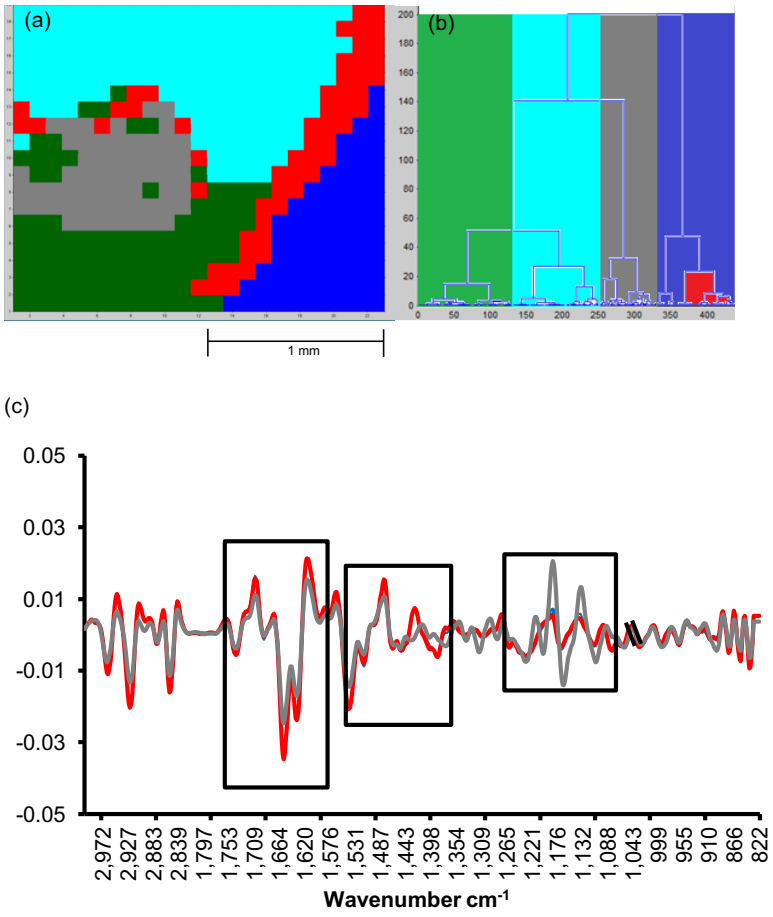

Figure 8. Cluster analysis of the 2nd derivatives and vector normalised IR hyperspectral data of the NTHi A1 biofilm from MIC for AMX. A false colour map (a) showing the spatial distribution of clusters; (b) dendrogram clusters formed by the unsupervised analysis of the pre-processed biofilm hyperspectral image and (c) average of 2nd derivative for each cluster.

6.3.2.2.2 PCA analysis for NTHi A1 biofilm hyperspectral image

A false colour map of the scores from the PCA analysis of the hyperspectral data of the NTHi A1 biofilm treated with sub-MIC of AMX is shown in Fig. 9. The score plot of this PC shows that the main variation of the spectra are in the high intensity area of the same region with amide I and carbohydrate which have the highest integration value as seen in Fig. 3. This PC score plot show differentiated colour based on variation within amide I and carbohydrate spectra.

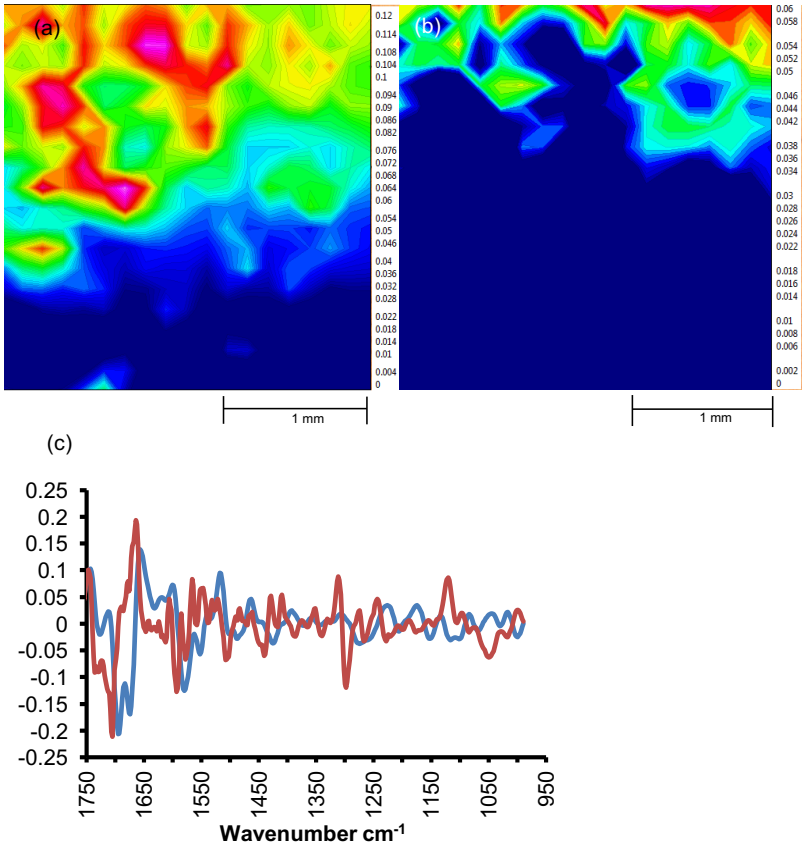

Figure 9. PCA for NTHi A1 biofilm formation after sub-MIC of AMX. (a) PC1 (b) PC2 of the analysis and (c) loading graph for the PC1 and PC2.

These features that are illustrated in PC2 are shown in the carbohydrate and amide I integration (Fig. 3a & b) with the integration value of 0.3 which means that carbohydrate is less dominant in this area in relation to amide I. The loading graph in for PC1 and PC2 in Fig. 9c shows slight peak differences from 1704 $cm^{-1}$to 1693 cm^{-1} and from 1662 cm^{-1} to 1670 cm^{-1} in the amide I band region. In the amide II region there is another slight difference in 1591 cm^{-1} to 1577 cm^{-1} and difference in the intensity of the peaks at amide III and P=O region from 1309 cm^{-1} and 1295 cm^{-1}. The carbohydrate regions show slight differences in the intensity which appear in the peaks 1118 cm^{-1} and 1049 cm^{-1}.

PC4 for the NTHi A1 biofilm treated with MIC of AMX in Fig. 10 shows the main chemical variance in the hyperspectral data. The scores plot of this PC shows the spatial distribution of the spectral variation with different intensity colours based on PC which is mostly within amide I and carbohydrate spectra. However, the scores plot of PC 7 highlights different areas which were lower and displayed in blue colour. The loading graph in Fig. 10. c shows slight peak differences from PC4 and PC7 at 1680 cm^{-1} to 1683 cm^{-1} and from 1637 cm^{-1} to 1600 cm^{-1} in the amide I bands region. In amide II region there was a difference in the intensity from 1409 cm^{-1} to 1400 cm^{-1}. The carbohydrate region show slight peak shift which appears in the peaks 1087 cm^{-1} to 1064 cm^{-1} and 1062 cm^{-1}.

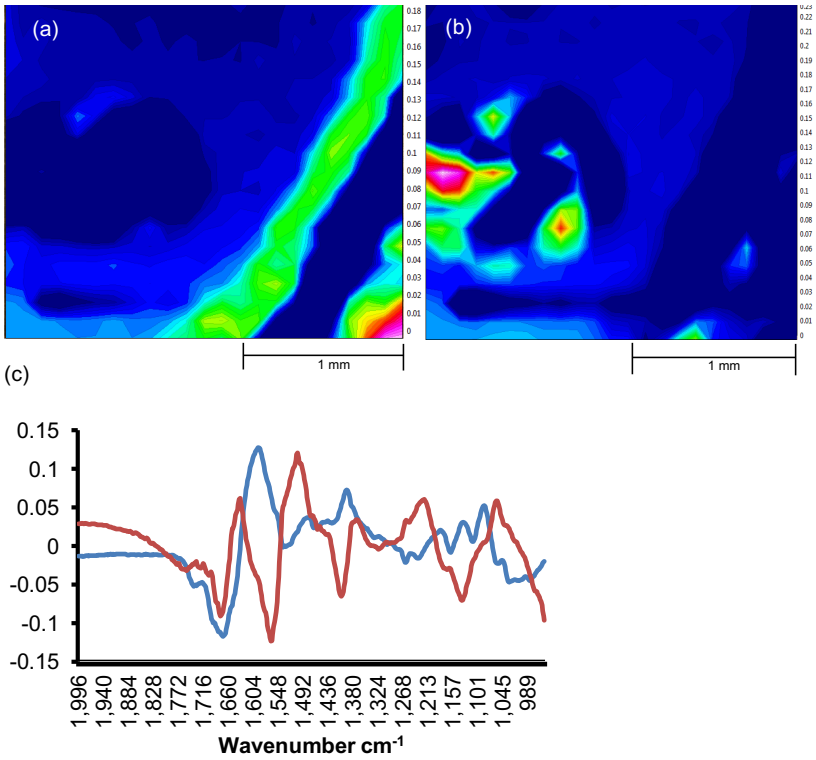

Figure 10. PCA Scores plot of PC4 (a) and PC7 (b) of NTHi A1 with MIC of AMX.; (c) loading graph of PC4 and PC7 for high biofilm isolate with AMX-MIC.

The integration values for the amide I, II and carbohydrate bands specifically increase in sub-MIC treated with AMX. This may suggest that the biofilm is formed after incubation with AMX which influences the bacterial cell protein content secreted and distributed over the CaF_2 disc. The biofilms stimulated in the mature biofilm (existing biofilm) after addition of MIC, had a different spatial distribution of the protein profile (amide I) than other macromolecules especially carbohydrate.

Considering all data from the results of the individual average spectra and results from hyperspectral integration and ratio images from section 3.2, this data contradicted the findings by Wu *et al*. (2014) who found that carbohydrate content is up-regulated and

protein down-regulated in response to *β*-lactams at subinhibitory concentrations (Wu *et al.*, 2014). Protein content in the biofilm was previously thought in another study to exist in a high ratio due to lysed cells that are secreted by the sessile cells which are adhered onto biofilm matrices (Hoffman and Decho, 1999). Past studies of biofilm FTIR spectra considered the high intensity of amide II as a marker for biofilm biomass which is formed in the early stages of biofilm (≈3h) (Humbert *et al.*, 2011). This observation could not be confirmed in this current study as the biofilm examined here was incubated and analysed after 24h incubation.

Applying the MIC level of AMX may have some impact on the cellular behaviour and lead to the formation of more sessile cells. The main variability between treated and untreated NTHi A1 is illustrated by the higher amide I and II to carbohydrate band ratio. In this work, AMX treated biofilm has been analysed which may have some mechanism to induce biofilm formation even with some evidence of cell lysis. Carbohydrates are thought to be one of the main chemical components for the biofilm EPS and the spectral bands of this region may be considered as a marker for biofilm changes formed from other bacterial species (Bosch *et al.*, 2006, Serra *et al.*, 2007). Paradoxically, up-regulated carbohydrate production in biofilm was suggested to occur after exposure to antibiotics such as *β*-lactam (Wu *et al.*, 2014). The analysis of the hyperspectral data for NTHi A1 biofilm treated with AMX in the current Chapter indicates that excess of protein is higher than carbohydrate. Sub-inhibitory concentration (sub-MIC) and MIC level of AMX have different effects on the NTHi biofilm formed on the CaF_2 by examining the ratio of integrated bands and PCA analysis of the extracted spectra from hyperspectral data. It also may be an indication

of the production of various types of protein at different concentrations of AMX treatment.

In this Chapter, only AMX treated samples were selected for the analysis of the hyperspectral data because it is the first choice drug treatment for NTHi infection (Hoberman *et al.*, 2011, Tristram *et al.*, 2007) and can have a clinical impact if there is resistance or an antibiotic tolerant biofilm developed to this *β*-lactam antibiotic (Hall-Stoodley *et al.*, 2006). Although NTHi A1 and RdKW20 have demonstrated a high sensitivity to cefotaxime, it is not necessarily considered to be first-line agent and it is only recommended for failure of other *β*-lactam antibiotics treatment for injection of inpatients (Tristram *et al.*, 2007). For this reason, the analysis here focused only on AMX despite the significance of changes on biofilm after CTX.

The NTHi A1 isolate used in the current study had previously been characterised as possessing a *β*-lactamase negative ampicillin resistant (BLNAR) mechanism of resistance. This mechanism is brought about by an N526K amino acid substitution in penicillin binding protein 3 (PBP3) which is the primary target for *β*-lactams (Tristram *et al.*, 2007). There is no information yet if this protein alteration (N526K) and (BLNR) mechanism of resistance to AMX along with other bacterial proteins such as P5 and Haemophilus adherence and penetration (Hap) (Webster *et al.*, 2006) could be involved in biofilm formation induction. The protein profiles differences that are illustrated in the FTIR spectral integration ratio of amide I to carbohydrate ratio and in PCA and HCA multivariate analysis of hyperspectral data in this chapter may suggest some induction of some bacterial proteins mechanisms of AMX on biofilm formation. This relationship between the AMX (may be other *β*-lactams) inducing the

biofilm formation and protein profile in biofilm chemical components needs further investigation.

6.3.2.3 Hyperspectral image analysis for RdKW20 biofilm

A false colour map of the integration values for the amide I band in Fig. 11 shows range from 1.69 to 3.87, and the carbohydrate band, ranging from 0.375 to 1.06, for the isolate of RdKW20 mature biofilm treated with MIC of AMX. After the addition of MIC of AMX the treated biofilm exhibited a high coverage of biofilm material with lower variation of the amide I (dominated by protein profile) and carbohydrate bands within the biofilm area compared to control.

The integration ratio of the spectral bands showed some differences attributed to the amide I and carbohydrate in Fig. 12. However, variations across the measured area seemed to be minor CH stretching/amide I ratios differences, ranging between 0.28 to 0.31 whereas the ratio of carbohydrate to amide I ranged between 0.21 to 0.33. These ratio plots were both shown to be very consistent in terms of the intensity value range and the similarity of the distributed chemical features with high intensity red in colour.

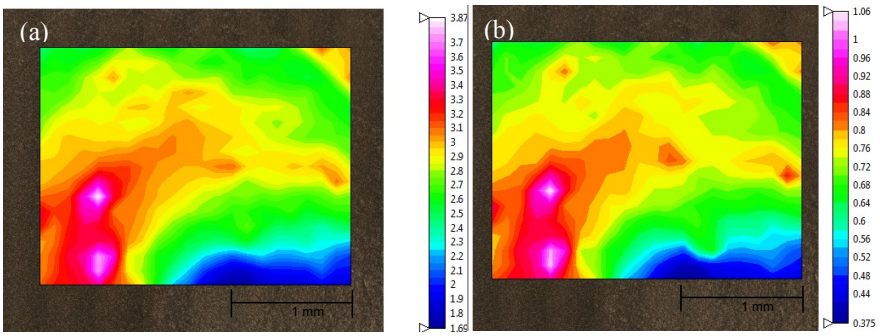

Figure 11. False colour map of hyperspectral data of RdKW20 biofilm after treatment with MIC AMX; (a) amide I integration and (b) carbohydrate integration.

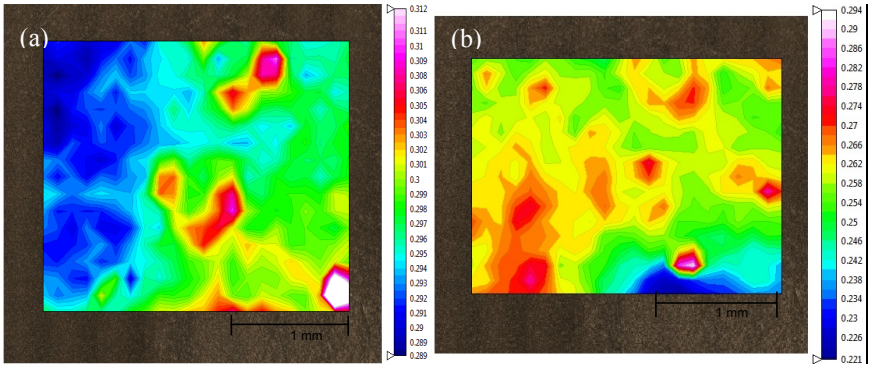

Figure 12. False colour map of hyperspectral data of RdKW20 biofilm after treatment with MIC AMX; (a) CH stretching/ amide I ratio for the low biofilm producer after with MIC AMX and (b) carbohydrate/ amide I ratio for the low biofilm producer biofilm after treatment with MIC AMX.

The treated biofilm exhibited a high coverage of biofilm material after addition of MIC of AMX unlike the untreated RdKW20 biofilm. However, there seemed to be a lower variation of the amide I (dominated by the protein profile) and carbohydrate bands across the analysed sample area as well as no significant variability of the integration ratio between the CH stretching and amide I bands, and the carbohydrate to amide I bands. These findings may suggest that bacterial cells were influenced by AMX to produce biofilm material with a minor impact on specific functional groups

such as carbohydrate bands, which were confirmed in other study to be influenced by AMX (Wu. *et al*. 2014).

6.3.2.3.1 Multivariate analysis for NTHi A1 biofilm hyperspectral data

6.3.2.3.1.2 Hierarchical cluster analysis for RdKW20 biofilm

The Cluster analysis of the hyperspectral data for the RdKW20 biofilm that was treated with MIC for AMX is illustrated in Fig. 13. The dendrogram shows separation of two main groups at 27 distance units then subdivision into further subgroups at 12 and 9 distance units. The cluster maps were constructed using three main group clusters. Clusters seem to mix randomly as the cluster in red colour showed no spectral differences to the other cluster in green colour. This difference had no impact on the spatial distribution of the biofilm within this 2 mm area. The average spectra for these clusters showed low degrees of spectral difference even in the dendrogram where 27 units of separation would suggest that there is a large difference. There is a small degree of variation between intensities at the bands from 1150 $cm^{-1}$to 1050 cm^{-1} which is the area attributed to IR bands for phospholipids and C-O-C, C-O dominated by ring vibrations in various polysaccharides for bacterial cells (Davis, 2010).

From the multivariate analysis for RdKW20 biofilm, HCA illustrates clusters were randomly mixed between the subgroups in Fig. 13 within the second cluster which may indicated how the chemical functional groups overlapped. The inability to demonstrate specific clusters for each functional group within a specific area and no characteristic IR peaks is indicative of how homogeneous in a spatial sense this biofilm has grown.

RdKW20 isolate did not produce enough biofilm material when the sub-MIC level of AMX were introduced to the inoculum thus the signal to noise quality of IR hyperspectral data was not sufficient to perform further analysis.

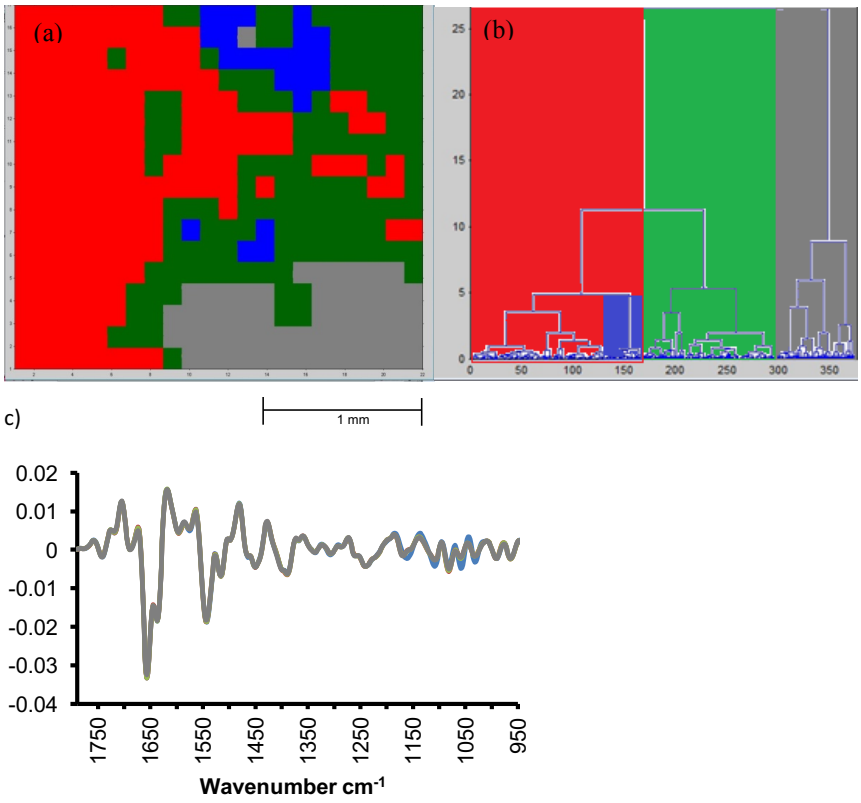

Figure 13. (a) False colour map showing 4 clusters formed by the hierarchical cluster analysis of pre-processed spectral data of the biofilm formed by RdKW 20 biofilm exposed to MIC of AMX; (b) dendrogram clusters formed by the unsupervised analysis of the pre-processed biofilm spectral image formed by a low biofilm producer exposed to MIC of AMX and (c) average of 2nd derivative for each cluster.

6.3.2.3.1.2 PCA analysis for RdKW20 biofilm hyperspectral image

The score plot in Fig. 14 shows PC2 and PC7 obtained after the PCA analysis of pre-processed spectral data for the RdKW20 biofilm treated with MIC of AMX. PC2

shows the main spectral variability which here is mostly based on the spectral region of amide I and carbohydrate.

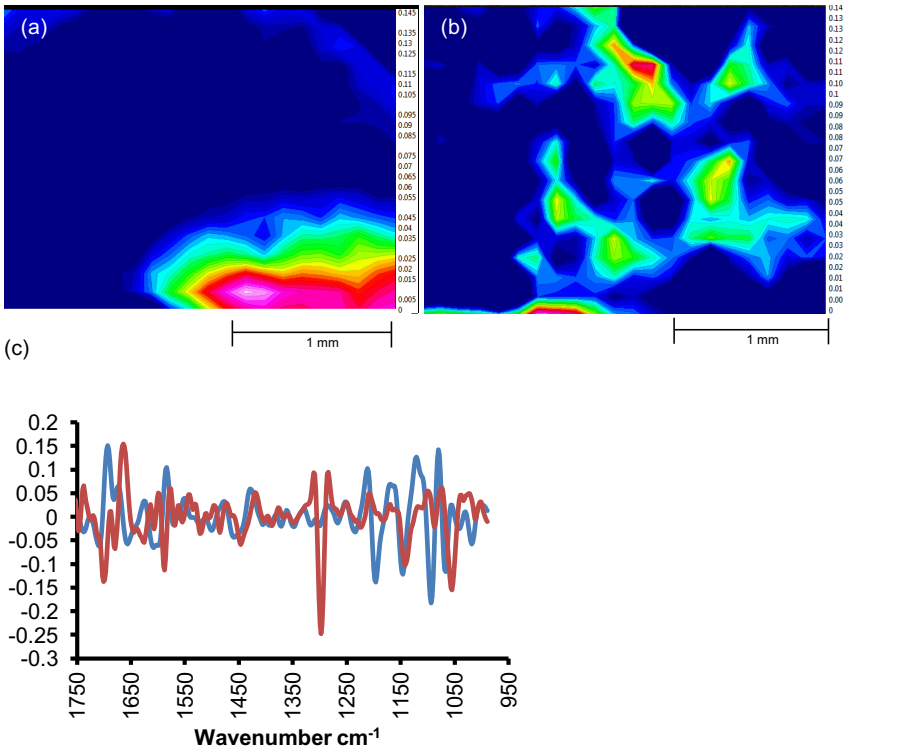

Figure 14. PCA of the RdKW 20 biofilm (a) PC2 and (b) PC7 from PCA unsupervised analysis of the pre-processed of the biofilm spectral image formed by RdKW20 biofilm exposed to MIC of AMX. (c) PC1 and PC7 loading graph.

The intensity features that are illustrated in PC2 (red colour) are the same areas in Fig. 12 that described the carbohydrate to amide I integration ratio with values from 0.22 to 0.25. It may mean that this area is dominated by carbohydrates. However, in Fig. 14, PC7 shows lower score values (blue colour) for the same area with high intensity in PC2. The loading graphs in Fig. 14c shows differences in the intensity between the two PCs from 1699 cm^{-1} to 1691 cm^{-1} and from 1662 cm^{-1} to 1670 cm^{-1} in amide I bands region. In amide II region there is another slight peak shift from 1587 cm^{-1} to

1583 cm^{-1} and strong peak shift at amide III and P=O region from 1309 cm^{-1} and 1297 cm^{-1}. The carbohydrate region showed peak shift which appeared in two peaks; one from 1143 cm^{-1} and 1118 cm^{-1} and from 1093 cm^{-1} to 1078 cm^{-1}. The later peak shift presents the main variable between treated and untreated biofilm which strongly suggests variability in glycogen component over the selected biofilm area.

6.3.2.4 Analysis of the extracted spectra from hyperspectral image

From the hyperspectral data, 10 individual spectra with the region from 1795 cm^{-1} to 950 cm^{-1} were randomly extracted for both NTHi A1 treated by AMX, at sub-MIC and MIC and RdW20 treated by AMX at MIC. Along with these 10 spectra that were extracted from these three hyperspectral images along with 10 spectra extracted previously from both untreated NTHi A1 biofilm and RdKW20 biofilm in Chapter 5 (section 5.3.2). The aim for this analysis was to have an investigation of the spectral differences between treated and untreated biofilm. The same pre-processing technique performed in Chapter 5 (section 5.3.2) was used for the spectra extracted here.

The random selection of the spectra of the treated samples does not take into account the coverage of biofilm into account. Another hypothesis that needed investigation was that antibiotics may have a low impact on discriminating the treated biofilm from untreated biofilm compared to the chemical variation that appear inter-strains (NTHi A1 and RdKW20 biofilm).

A 2D score plots of three different PCs from the PCA analysis shown in Fig. 15. PC1 shows that spectra from untreated NTHi A1, RdKW 20 biofilm with MIC and treated NTHi A1 biofilm are grouped together. The treated NTHi A1 with sub-MIC and

RdKW20 treated with MIC are hardly clustered in PC1 dimension. However, by looking at PC2 dimension plots, it is difficult to see any clusters that differentiate untreated biofilm from both isolates to treated biofilm and it appears the clusters for each category were internal. PC2 may cluster internal chemical features within each isolate and differentiate it within the spots selected and does not discriminate the isolates from each other. PC3 show the major discrimination between RdKW20 biofilm, both treated and untreated, and NTHi A1 biofilm, of treated and untreated.

The loading graph for PC1 is displayed in blue in Fig. 16 and shows specific peak from the spectra selected from untreated and treated biofilm. Protein region variable intensity is present in amide I at 1703 cm^{-1} and in 1657 cm^{-1} peaks. There is also a peaks highlighted in the amide I bands at 1637 cm^{-1} and 1622 cm^{-1}. There are some differences observed in amide II with peak intensity differences at 1547 cm^{-1}, 1516 cm^{-1}, 1479 cm^{-1} and 1470 cm^{-1}. The results may indicate changing of secondary structure of proteins towards α-helix and β-pleated sheet between these different treated and untreated biofilms. Protein differences may indicate the development of biofilm in NTHi A1 which has been reported previously to be related to alterations of bacterial protein in response to surface growth (Quilès and Humbert, 2014). These variations of biofilm growth may be related to the biofilm response to treatment with AMX.

The carbohydrate regions do not seem to play a significant role for PC1 as the loading graph displays low values here. There is some variance demonstrated in lipid band area of the methylene groups of CH stretching bands (3000-2830 cm^{-1}) in PC1 and PC3 but not with PC2.

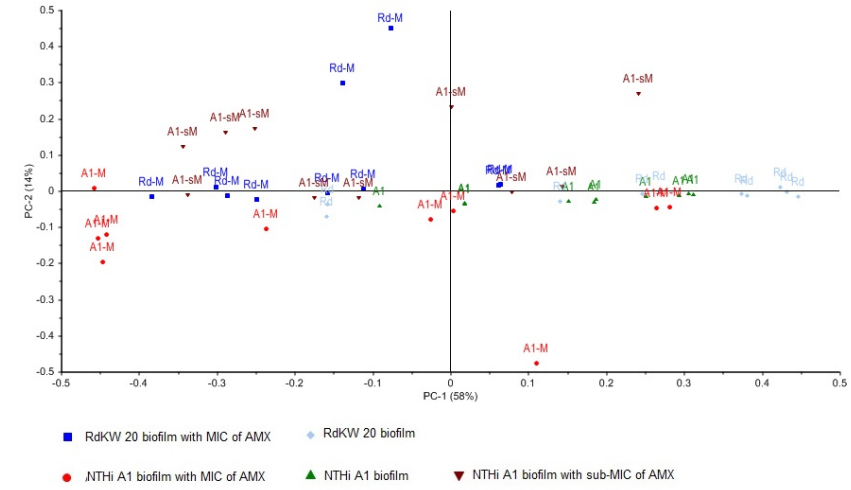

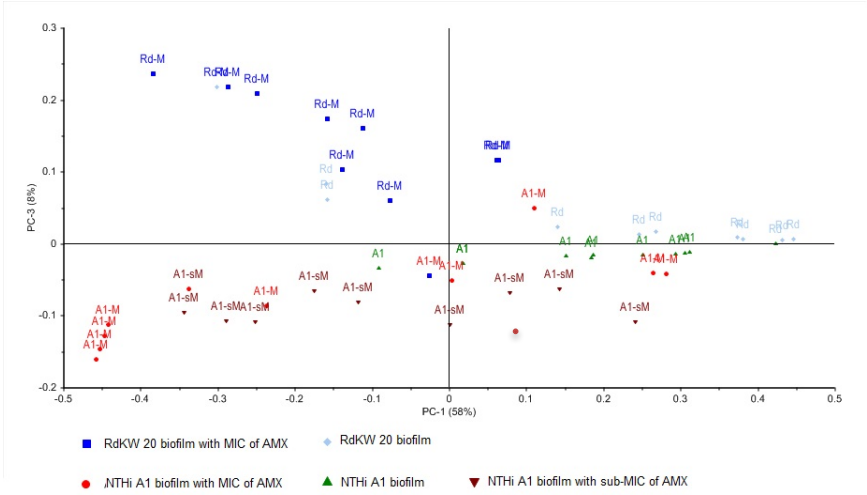

Figure 15. Score plotting of the PCA; (a) PC1 vs PC2 and (b) PC1 vs PC3 from PCA analysis of the spectral pre-processed data from the extracted spectra from areas of untreated NTHi A1 and RdW20 biofilm, and treated biofilm at MIC and sub-MIC AMX.

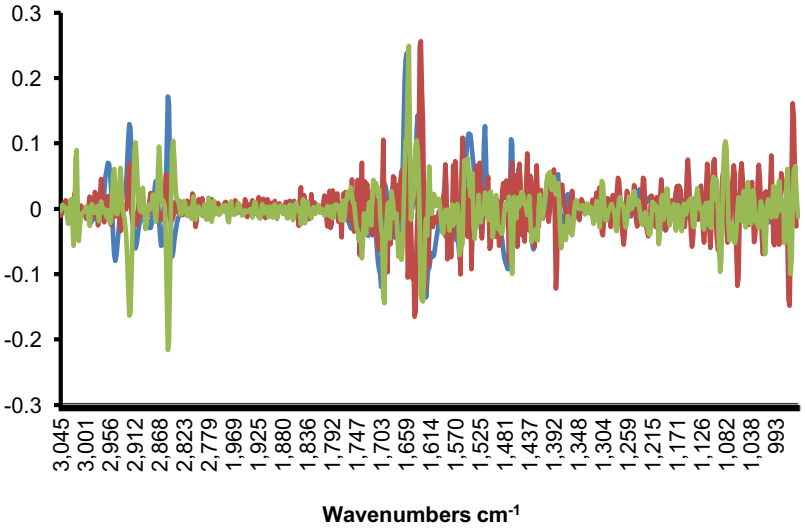

Figure 16. Loading graphs of 2nd derivatives of PC1 (blue), PC2 (red) and PC3 (green) from the spectra selected from areas of untreated NTHi A1 and RdW20 biofilm and treated biofilm at MIC and sub-MIC AMX.

The loading graph for PC3, displayed in green in Fig. 16, shows the significance of the protein region for this PC in amide I at 1699 cm^{-1}, 1653 cm^{-1},1632 cm^{-1} peaks. In amide II peaks, there are some differences observed at 1552 cm^{-1} and 1468 cm^{-1}. These differences in biofilm protein profile may be also related to the biofilm response to treatment with AMX. In this PC loading graph, another spectral feature appears in the carbohydrate band which was not seen in the PC1 loading graph. Two peaks demonstrated by PC2 at 1063 cm^{-1} and PC3 at 1093 cm^{-1}.

NTHi A1 treated with AMX at MIC illustrated distinctive chemical features and cluster as one group. The corresponding loading graph shows that the main areas of variability between the cluster groups are in the protein profile. However, PC3 shows further discrimination at the carbohydrate band. This PC may be the only one to show

individual clustering of each group. The loading graphs of this PCA were examined to determine the spectral features as a guide for discrimination of FTIR spectra that were extracted from the hyperspectral images of AMX induced biofilm and untreated samples. This PCA analysis also revealed that biofilms treated at sub-MIC with AMX have different chemical features than biofilms treated at MIC with AMX.

6.4 Conclusion

FTIR spectroscopy methods used in this study show differences in the NTHi A1 biofilm biomass and RdKW20 biofilm after treatment with antibiotics at two different concentrations. FTIR hyperspectral images were investigated and used for studying the chemical impact of antibacterial treatments on bacterial cells and tendency behaviour to form more biofilm mass for NTHi. FTIR microspectroscopy results demonstrated an increase in the protein profile in relation to carbohydrates of NTHi A1 after exposure to a MIC of AMX. From the FTIR microspectroscopy data analysis, the outcomes show a high accuracy and sensitivity to detect specific chemical compositions which may play a major role in development of NTHi biofilm. These results support the view that analysis using FTIR hyperspectral imaging with multivariate analysis of the bacterial biofilm can identify changes in composition and distribution of protein and carbohydrate contents after the biofilm treated with antibiotics, and may lead to better understanding of biofilm treatment.

6.5 References

Bosch, A, Serra, D, Prieto, C, Schmitt, J, Naumann, D & Yantorno, O, 2006. 'Characterization of Bordetella pertussis growing as biofilm by chemical analysis and FT-IR spectroscopy'. *Applied Microbiology and Biotechnology,* 71**,** 736-747.

Davis, R M, 2010. 'Fourier Tansform Infrared (FT-IR) Spectroscopy: A Rapid Tool for Detection and Analysis of Foodborne Pathogenic Bacteria'. *Journal of Microbiological Methods,* 84, 369-378.

Fux, C, A, Costerton, J, W, Stewart, P, S, & Stoodley, P, 2005. 'Survival strategies of infectious biofilms'. Trends in microbiology, 13(1), 34-40.

Hall-Stoodley, L, Hu, F Z, Gieseke, A, Nistico, L, Nguyen, D, Hayes, J, Forbes, M, Greenberg, D P, Dice, B & Burrows, A, 2006. 'Direct detection of bacterial biofilms on the middle-ear mucosa of children with chronic otitis media'. *The Journal of the American Medical Association,* 296**,** 202-211.

Hoberman, A, Paradise, J L, Rockette, H E, Shaikh, N, Wald, E R, Kearney, D H, Colborn, D K, Kurs-Lasky, M, Bhatnagar, S & Haralam, M A, 2011. 'Treatment of acute otitis media in children under 2 years of age'. *New England Journal of Medicine,* 364**,** 105-115.

Hoffman, M & Decho, A W, 1999. 'Extracellular enzymes within microbial biofilms and the role of the extracellular polymer matrix. *Microbial Extracellular Polymeric Substances*. Springer Berlin Heidelberg, 217-230.

Humbert, F, Saadi, S, Quilès, F & Hani, K, 2011. 'In situ assessment of antibacterial activity of dermaseptine S4 derivatives against Pseudomonas fluorescens biofilms by using ATR-FTIR spectroscopy'. *Science against Microbial Pathogens:*

Communicating Current Research and Technological Advances. Badajoz: Formatex Research Center, 2, 889-95.

Lu, X, Samuelson, D R, Rasco, B A & Konkel, M E, 2012a. 'Antimicrobial effect of diallyl sulphide on Campylobacter jejuni biofilms'. *Journal of Antimicrobial Chemotherapy***,** dks138.

Lu, X, Weakley, A T, Aston, D E, Rasco, B A, Wang, S & Konkel, M E, 2012b. 'Examination of nanoparticle inactivation of Campylobacter jejuni biofilms using infrared and Raman spectroscopies'. *Journal of Applied Microbiology,* 113**,** 952-963.

Lasch, P, Naumann, D, 2000. 'Infrared spectroscopy in microbiology'. *Encyclopedia of Analytical Chemistry*.

Moriyama, S, Hotomi, M, Shimada, J, Billal, D S, Fujihara, K & Yamanaka, N, 2009. 'Formation of biofilm by Haemophilus influenzae isolated from pediatric intractable otitis media'. *Auris Nasus Larynx,* 36**,** 525-531.

Paquet-Mercier, F, Safdar, M, Parvinzadeh, M & Greener, J, 2014. 'Emerging Spectral Microscopy Techniques and Applications to Biofilm Detection'. *Microscopy: advances in scientific research and education.*638-649.

Puig, C, Domenech, A, Garmendia, J, Langereis, J D, Mayer, P, Calatayud, L, Liñares, J, Ardanuy, C & Marti, S, 2014. 'Increased Biofilm Formation by Nontypeable Haemophilus influenzae Isolates from Patients with Invasive Disease or Otitis Media versus Strains Recovered from Cases of Respiratory Infections'. *Applied and Environmental Microbiology,* 80**,** 7088-7095.

Serra, D, Bosch, A, Russo, D M, Rodríguez, M E, Zorreguieta, Á, Schmitt, J, Naumann, D & Yantorno, O, 2007. 'Continuous nondestructive monitoring of Bordetella pertussis biofilms by Fourier transform infrared spectroscopy and other corroborative techniques'. *Analytical and Bioanalytical Chemistry,* 387**,** 1759-1767.

Sill, M L & Tsang, R S, 2008. 'Antibiotic susceptibility of invasive Haemophilus influenzae strains in Canada'. *Antimicrobial Agents and Chemotherapy,* 52**,** 1551-1552.

Takei, S, Hotomi, M & Yamanaka, N, 2013. 'Minimal biofilm eradication concentration of antimicrobial agents against nontypeable Haemophilus influenzae isolated from middle ear fluids of intractable acute otitis media'. *Journal of Infection and Chemotherapy***,** 1-6.

Tristram, S, Jacobs, M R & Appelbaum, P C, 2007. 'Antimicrobial resistance in Haemophilus influenzae'. *Clinical Microbiology Reviews,* 20**,** 368-389.

Webster, P, Wu, S, Gomez, G, Apicella, M, Plaut, A G & Geme Iii, J W S, 2006. 'Distribution of bacterial proteins in biofilms formed by non-typeable Haemophilus influenzae'. *Journal of Histochemistry & Cytochemistry,* 54**,** 829.

Wu, S, Li, X, Gunawardana, M, Maguire, K, Guerrero-Given, D, Schaudinn, C, Wang, C, Baum, M M & Webster, P, 2014. 'Beta-Lactam Antibiotics Stimulate Biofilm Formation in Non-Typeable Haemophilus influenzae by Up-Regulating Carbohydrate Metabolism'. *Public Library of Science one,* 9**,** e99204.

7.1 General conclusion

This study has confirmed production of biofilm material inside the wells of microtitre plates (MTP) and demonstrated the variability of NTHi biofilm formation *in vitro*. Although MTP based measurement of *in vitro* biofilm formation is common for NTHi, little has been previously described about the analytical performance of the MTP method. Using an overnight broth culture as the basis for inoculation of the MTP, standardisation to a pre-determined absorbance does not increase precision compared to standardisation to a pre-determined dilution. However, the use of a suspension of growth from solid agar was shown to decrease precision. The use of BF/FG, where the biofilm measurement was normalised to the final amount of growth in the MTP did not increase precision compared to using BF as a standalone outcome measure. Storage of isolates at -80^{o}C for up to 12 months did not significantly alter the ability of isolates to produce biofilm *in vitro*, and this is an important finding given the frequency in which stored isolate collections are used for retrospective phenotypic studies, including biofilm production.

When this MTP assay was applied to a collection of clinical NTHi isolates from various body sites and collection of both NTHi and *H. haemolyticus* (non-pathogenic) from the nasopharynx of non-diseased individuals, significant variation in the ability to form biofilm was seen in isolates within all groups. However, there was no difference in the ability to form biofilm across groups, with the exception of “eye” isolates, which were uniformly low biofilm producers. The mechanism was not further investigated, but deserves further study. This was the first study that has examined and compared the biofilm formation of pathogenic and non-pathogenic *Haemophilus* isolates including NTHi and *H. heamolyticus*.

The formation of biofilm by a high biofilm producing NTHi isolate tested along with a low biofilm producer RdKW20 after addition of various antibiotic agents showed that the MTP assay with standardisation of the inoculum can be used to test the influence of antibiotics at two different concentrations (sub-MIC and MIC). This study illustrated that existing NTHi biofilm production can be enhanced by amoxicillin at MIC to form biofilm with the NTHi strain which initially showed high biofilm production and resistance to amoxicillin. Whereas other classes of antibiotics tended to decrease biofilm production. This indicates that biofilm production may be related to antibiotic resistance. This study also showed that sub-MIC of amoxicillin influenced biofilm formation for RdKW20 and confirmed more biofilm material was produced *in vitro* despite the sensitivity of this isolate to amoxicillin. This suggests that RdKW20 may develop resistance to amoxicillin and produce biofilm.

IR spectra of biofilm were recorded for the NTHi and RdKW20 biofilm isolates. These data add to the growing literature demonstrating the abilities of FTIR microspectroscopy for biofilm research. The chemical information obtained from spectra distinguished between high and low biofilm from one individual spectral acquisition and spectral integration over the region from the wavenumbers 1790 cm^{-1} to 950 cm^{-1}. These spectral data acquisition procedures can give a direct quantitative measure of overall biofilm production. Chemical ratios between protein profiles to carbohydrate were also obtained for the individual spectra of biofilm and from hyperspectral data which showed an increase in amide I which may indicate the contribution of some cellular protein structures present in biofilm.

Multivariate analysis of the hyperspectral data performed in this study demonstrated that this is a suitable and promising approach to discriminate between chemical changes that occur within biofilm. Principal component analysis (PCA) showed chemical differences specifically in the area of NTHi biofilm with different thickness and distinguished between the biofilms. This analysis showed that the thick biofilm was chemically distinct from the thin biofilm, with most of the difference relating to the amide I and II region.

The hyperspectral data of NTHi treated with MIC and sub-MIC of amoxicillin presented here have confirmed a finding from the previous staining assay that amoxicillin substantially increased NTHi biofilm growth as indicated by the high integration value for new and established biofilm formation. For RdKW20, IR integration value showed that amoxicillin enhanced the formation of biofilm only when applied to established biofilm at the MIC.

Even with the resistance to amoxicillin that was evident in the NTHi isolate, our study showed that amoxicillin at certain concentrations can specifically increase biofilm material as well as the protein profiles in relation to carbohydrate content and lipid in new and mature biofilm formed by NTHi. These results were determined by examining the ratio of integrated bands and PCA analysis of the extracted spectra from hyperspectral data. The production of various type of protein at different concentrations of amoxicillin may be related to amoxicillin resistance mechanisms by this NTHi isolate. This study showed that NTHi isolates produced variable amounts of biofilm as demonstrated both by chemical staining of the whole biofilm material and FTIR spectroscopy investigation of chemical components over an area of 2 mm. FTIR

spectroscopy has approved to be a powerful tool to analyse both chemical differences in a small area within the biofilm and between biofilms that are treated with antibiotics and untreated biofilm. FTIR offers significant potential as a tool to further elucidate biofilm production mechanisms.

Appendix

Isolate ID		Mean of biofilm formation	±SD
	Eye isolates		
1	Ci2	0.12	±0.07
2	Ci5	0.14	±0.02
3	Ci29	0.27	±0.14
4	Ci51	0.04	±0.08
5	Ci 113	0.32	±0.09
6	ci 130	0.29	±0.08
7	Ci 126	0.21	±0.07
8	J83	0.37	±0.08
9	J130	0.66	±0.11
10	ci 94	0.26	±0.24
	CF isolates		
11	CF 3	0.26	±0.11
12	CF 6	0.57	±0.19
13	CF10	0.53	±0.11
14	CF16	0.66	±0.18
15	CF20	0.19	±0.10
16	CF23	0.69	±0.09
17	CF 29	1.57	±0.13
18	CF 41	1.03	±0.21
19	CF 63	1.22	±0.46
20	CF51	0.35	±0.12
	Ear isolates		
21	L76	0.12	±0.02
22	L79	1.19	±0.44
23	L139	1.27	±0.23
24	L143	1.04	±0.14
25	L146	1.31	±0.11
26	Ci58	1.36	±0.28
27	Ci 121	0.88	±0.08
28	Ci 1	1.43	±0.42
29	Ci 24	0.48	±0.09
30	Ci 35	0.77	±0.03
	LRT isolates		
31	Ci 3	0.86	±0.16
32	Ci 9	0.58	±0.16
33	Ci 13	0.51	±0.11
34	Ci 30	0.55	±0.40
35	Ci 23	0.04	±0.02
36	Ci 36	1.74	±0.31
37	Ci 11	0.05	±0.01

38	Ci 16	1.72	±0.09
39	Ci 43	0.12	±0.08
40	Ci 50	0.16	±0.06
	Normal flora		
41	NF3	1.40	±0.70
42	NF38	0.96	±0.09
43	BWoct 21	1.24	±0.36
44	NF 7	1.20	±0.09
45	NF 30	0.29	±0.05
46	NF 37	0.25	±0.05
47	Bwoct 1	0.39	±0.05
48	Bwoct 4	0.71	±0.47
49	Bwoct 8	1.37	±0.33
50	Bwoct 11	0.92	±0.16
	Haemophilus haemolyticus (Hh)		
51	L4	0.02	±0.03
52	L7	1.76	±0.35
53	L23	1.49	±0.59
54	CF 14	0.03	±0.02
55	BW 1	0.06	±0.02
56	BW 15	0.21	±0.07
57	BW 20	0.06	±0.07
58	BW 21	0.65	±0.17
59	BW 5	0.04	±0.03
60	CF 25	0.87	±0.09